HELLENIC REPUBLIC

National and Kapodistrian University of Athens

EST. 1837

Impact of earthquakes in Greece from the antiquity up to now: Database development and space-time distribution with GIS tools

By

Ioanna Triantafyllou

Athens, February 2021

HELLENIC REPUBLIC

National and Kapodistrian University of Athens

EST. 1837

Impact of earthquakes in Greece from the antiquity up to now: Database development and space-time distribution with GIS tools

By

Ioanna Triantafyllou

Athens, February 2021

Copyright (c) 2021 Ιωάννα Τριανταφύλλου. Με την επιφύλαξη παντός δικαιώματος.

Απαγορεύεται η αντιγραφή, αποθήκευση και διανομή της παρούσας εργασίας, εξ ολοκλήρου ή τμήματος αυτής, για εμπορικό σκοπό. Επιτρέπεται η ανατύπωση, αποθήκευση και διανομή για σκοπό μη κερδοσκοπικό, εκπαιδευτικής ή ερευνητικής φύσης, υπό την προϋπόθεση να αναφέρεται η πηγή προέλευσης και να διατηρείται το παρόν μήνυμα. Ερωτήματα που αφορούν τη χρήση της εργασίας για κερδοσκοπικό σκοπό πρέπει να απευθύνονται προς τη συγγραφέα.

Οι απόψεις και τα συμπεράσματα που περιέχονται στην παρούσα εργασία εκφράζουν τη συγγραφέα και δεν πρέπει να ερμηνευτεί ότι εκφράζουν τις επίσημες θέσεις του Ε.Κ.Π.Α. (Ν. 5343/1932 202 παρ. 2).

ADVISORY COMMITTEE

E. Lekkas (Professor, National and Kapodistrian University of Athens)

I. Kassaras (Ass. Professor, National and Kapodistrian University of Athens)

I. Koukouvelas (Professor, University of Patras)

EXAMINATION COMMITTEE

E. Lekkas (Professor, National and Kapodistrian University of Athens)

I. Kassaras (Ass. Professor, National and Kapodistrian University of Athens)

I. Koukouvelas (Professor, University of Patras)

M. Stavropoulou (Ass. Professor, National and Kapodistrian University of Athens)

E. Skordilis (Professor, Aristotle University of Thessaloniki)

A. Ganas (Research Director, National Observatory of Athens)

M. Baptista (Professor, Polytechnic Institute of Lisbon)

SUBJECT AREA: Seismicity, Earthquake Impact, Tsunami Impact

KEYWORDS: earthquake catalogues, magnitude comparison, magnitude determination, casualties from earthquakes, building damage, earthquake impact database, tsunami impact database, impact mapping, tsunami risk assessment

ACKNOWLEDGEMENTS

Undertaking this PhD Thesis has been a truly life-changing experience for me and it would not have been possible to make it without the support and guidance that I received from several organizations and many people.

The research performed in the frame of my Thesis has been supported partially by the Hellenic Foundation for Research and Innovation (HFRI) under the HFRI PhD Fellowship grant (Fellowship Number: 490), the EU-FP7 research project ASTARTE (Assessment, Strategy And Risk Reduction for Tsunamis in Europe; grant agreement no: 603839, 2013-10-30), and the research project "Environmental, Disaster and Crisis Management Strategies" of the Dept. of Geology and Geoenvironment, National and Kapodistrian University of Athens (NKUA). Chapter 8 of the Thesis is also a contribution to the European Cooperation in Science and Technology COST project AGITHAR (Accelerating Global science In Tsunami HAzard and Risk analysis).

I am grateful to Prof. E. Lekkas (Dept. of Geology and Geoenvironment, NKUA) for his constant and restless support, guidance and encouragement during the execution of my Thesis in the last four years. Many thanks are also due to the Ass. Professor I. Kassaras (Dept. of Geology and Geoenvironment, NKUA) and to Prof. I. Koukouvelas (Dept. of Geology, University of Patras) for their help and advice. Suggestions for the improvement of the final text expressed by the other members of the Examination Committee proved quite useful; I thank all of them.

Many thanks are directed to Prof. A. Kijko, Director of the Natural Hazard Centre, University of Pretoria, South Africa, who provided his software and helped me with many advises regarding the probabilistic tsunami risk assessment. I also thank a lot Dr. A. Smith of the same Centre for the very useful exchange of opinions on the same topic.

Many thanks are also due to Prof. S. Tinti, Dr A. Armigliato and Dr F. Zaniboni (University of Bolonia), Dr T. Novikova, Dr M. Charalampakis and MSc A. Fokaefs (Institute of Geodynamics, National Observatory of Athens) as well as to Dr S. Mavroulis, MSc M. Gogou and Mr M. Thravalos for their collaboration in parts of this research

Dr Gerassimos Papadopoulos, Research Director at the Institute of Geodynamics, National Observatory of Athens, helped me a lot with several issues related to dealing with earthquake catalogues, magnitude comparisons and tsunami study.

I warmly thank all the colleagues from the Dept. of Geology and Geoenvironment, NKUA, as well as from the Institute of Geodynamics, National Observatory of Athens, for their kind help and friendship. The list is too long and, therefore, I don't mention them by name since I'm afraid to miss someone.

My warm thanks also go to my family members for their constant encouragement and support throughout my studies.

ΠΕΡΙΛΗΨΗ

Από πληθώρα δημοσιεύσεων, αλλά και από την εμπειρία των τελευταίων δεκαετιών, προκύπτει ότι οι σεισμοί στην Ελλάδα έχουν διαχρονικά επιφέρει πολυποίκιλες αρνητικές επιπτώσεις, τόσο στο ανθρωπογενές όσο και στο φυσικό περιβάλλον Στην παρούσα διατριβή επιτεύχθηκαν δύο βασικοί στόχοι: (1) οργανώθηκε για πρώτη φορά μια Ελληνική Βάση Δεδομένων Επιπτώσεων από Σεισμούς-Greek Earthquake Impact Database (GEIDB), και (2) διερευνήθηκαν πρότυπα χωροχρονικής μεταβολής των επιπτώσεων και η εξάρτησή τους από τις παραμέτρους σεισμικότητας και την μακροσεισμική ένταση των σεισμών.

Σε αυτό το πλαίσιο, η συνολική έρευνα που πραγματοποιήθηκε περιλάμβανε τρεις διαφορετικές φάσεις: (1) Η πρώτη φάση έχει αφιερωθεί στη συλλογή των «βέλτιστων» δεδομένων σεισμικότητας τόσο για την ενόργανη (1900-2020) όσο και για την ιστορική περίοδο. (2) Η δεύτερη φάση περιλάμβανε τη συλλογή και την εξέταση μεγάλου αριθμού πηγών δεδομένων για τις σεισμικές επιπτώσεις και την οργάνωση της GEIDB καθώς και τον προσδιορισμό κατάλληλων Μέτρων Σεισμικών Επιπτώσεων (Earthquake Impact Metrics, EIMs). Ως συμπλήρωμα της GEIDB, οργανώθηκε η Ελληνική Βάση Δεδομένων Επιπτώσεων από Τσουνάμι (Greek Tsunami Impact Database, GTIDB). (3) Χρησιμοποιήθηκαν στατιστικές μέθοδοι και εργαλεία GIS για τη διερεύνηση και χαρτογράφηση της χωροχρονικής μεταβολής των EIMs και των πιθανών παραγόντων από τους οποίους ελέγχονται.

Η διατριβή διαρθρώνεται σε εννέα κεφάλαια. Το πρώτο είναι μια εισαγωγική ανασκόπηση του γεωδυναμικού καθεστώτος και της σεισμικότητας της περιοχής της Ελλάδας. Από μια πρώτη στατιστική ανάλυση των γνωστών επιπτώσεων, από την αρχαιότητα μέχρι και το 2020, προέκυψε ότι μόνο από το 1800 μ.Χ. τα δεδομένα έχουν ικανοποιητική πληρότητα. Για το λόγο αυτό η GEIDB οργανώθηκε για την περίοδο 1800-2020.

Για την επιλογή των «βέλτιστων» εστιακών παραμέτρων των σεισμών που εισήχθησαν στη GEIDB, αναπτύχθηκε σειρά ερευνητικών εργασιών, τα αποτελέσματα των οποίων αξιοποιήθηκαν για την επιλογή αυτή. Αρχικά έγινε ανάλυση πληρότητας των διαφόρων καταλόγων σεισμών, που είναι διαθέσιμοι για την περίοδο 1800-2020, με σύγχρονες παραμετρικές και μη παραμετρικές μεθόδους (Κεφάλαιο 2). Στη συνέχεια αξιοποιήθηκαν, για πρώτη φορά, δεδομένα για τα πλάτη των σεισμικών καταγραφών των σεισμογράφων τύπου Agamennone, που λειτουργούσαν στη χώρα στην περίοδο 1901-1910, και επαναπροσδιορίστηκαν τα μεγέθη 52 ισχυρών επιφανειακών και ενδιάμεσου βάθους σεισμών με M~5 και άνω (Κεφάλαιο 3). Στο Κεφάλαιο 4 έγινε σύγκριση των μεγεθών και των εστιακών βαθών των σεισμών στους διάφορους καταλόγους της περιόδου 1911-2020. Στην οργάνωση της GEIDB είναι αφιερωμένο το Κεφάλαιο 5. Κατάλληλα Μέτρα των Σεισμικών Επιπτώσεων (EIMs) επιλέχθηκαν στο Κεφάλαιο 6, ενώ στο Κεφάλαιο 7 διερευνήθηκαν οι διάφοροι παράγοντες που ενδεχομένως ελέγχουν τις επιπτώσεις των σεισμών. Το Κεφάλαιο 8 αναφέρεται στις επιπτώσεις που προκλήθηκαν από τα τσουνάμι στην περιοχή της Ελλάδας και στην οργάνωση της GTIDB που αποτελεί συμπλήρωμα της GEIDB. Η εκτίμηση της επικινδυνότητας (ή διακινδύνευσης, risk) από τσουνάμι προσεγγίστηκε με δύο διαφορετικές μεθόδους: (1) μέθοδος ακραίων σεναρίων και (2) πιθανοτική μέθοδος μέγιστης πιθανοφάνειας (maximum likelihood) με αξιοποίηση μη πλήρων και πλήρων αρχείων. Το Κεφάλαιο 9 αφιερώνεται στα συμπεράσματα, στα οποία καταλήξαμε σε καθένα από τα προηγούμενα κεφάλαια της διατριβής, και σε ορισμένες προτάσεις και συζήτηση για περαιτέρω έρευνα.

Η GEIDB είναι οργανωμένη σε μορφή Access και περιλαμβάνει δεδομένα επιπτώσεων για 248 σεισμούς στην Ελλάδα στην περίοδο 1800-2020, τις εστιακές παραμέτρους και την ένταση των σεισμών και αρχείο βιβλιογραφίας. Τα δεδομένα επιπτώσεων περιλαμβάνουν πληροφορίες για

βλάβες και μερικές ή ολικές καταρρεύσεις κτιρίων, για θανάτους και τραυματισμούς ανθρώπων και για τσουνάμι, που έγιναν στην Ελλάδα στην ίδια περίοδο, δεδομένου ότι τα τσουνάμι προκαλούν τις δικές τους επιπτώσεις. Τα δεδομένα επιπτώσεων συλλέχθηκαν από μεγάλο όγκο περιγραφικών καταλόγων, βιβλίων, Σεισμολογικών Δελτίων του Εθνικού Αστεροσκοπείου, επιστημονικών δημοσιεύσεων, τεχνικών εκθέσεων και μελετών, αδημοσίευτων αρχείων, και δημοσιευμάτων του Τύπου. Οι πληροφορίες καταχωρήθηκαν στην GEIDB μόνο μετά από μια διαδικασία ελέγχου αξιοπιστίας και διόρθωσης. Επιπλέον, μελετήθηκαν σε βάθος οι επιπτώσεις τριών σεισμών που παρέμεναν λίγο γνωστοί (Άθως 1905, Κως 1926 και 1933) και τριών πρόσφατων σεισμικών επεισοδίων με τη διεξαγωγή υπαίθριων παρατηρήσεων (Κεφαλονιά, 2014, Κως 2017, Σάμος 2020).

Η διερεύνηση προτύπων μεταβολής των EIMs έδειξε ότι οι θάνατοι και οι τραυματισμοί ανθρώπων, και οι βλάβες κτιρίων οφείλονται κυρίως σε σεισμούς με εστίες στην κεντρική και νότια ηπειρωτική χώρα και στα νησιά του κεντρικού Ιονίου. Οι θάνατοι μειώνονται με το χρόνο, ενώ ο λόγος επιβίωσης (τραυματισμοί/θάνατοι) αυξάνεται. Επίσης, ο λόγος βλαβών (επισκεύασιμα/μη επισκευάσιμα κτίρια) αυξάνεται με το χρόνο. Αν και αυτά τα EIMs δεν συσχετίζονται καλά με το μέγεθος και την ένταση των σεισμών, προκύπτει ότι η ένταση ελέγχει το ανώτατο πλήθος των θάνατων, τραυματισμών, επισκευάσιμων κα μη επισκευάσιμων κτιρίων. Τα αποτελέσματα αυτά δίνουν την προοπτική επιχειρησιακής αξιοποίησης για τη μείωση της σεισμικής διακινδύνευσης.

ABSTRACT

The impact of the earthquakes on the human communities and on the natural environment is multifold and comes as a direct or indirect result of the earth's shaking. The present thesis is a contribution towards two main objectives: (1) to organize for the first time an earthquake impact database in Greece, and (2) to investigate the spatio-temporal distribution of the earthquake impact and how it possibly depends on various factors, such as seismicity parameters, macroseismic intensity, time of the day, season, and others.

In this frame, the overall research performed included three distinct phases: (1) The first phase has been devoted to the compilation of the "best" *seismicity data sets* for both the instrumental (1900-2020) and the historical time periods; (2) The second phase comprised the collection and examination of a large number of earthquake impact data sources and the organization of the *Greek Earthquake Impact Database (GEIDB)* as well as the determination of appropriate *Earthquake Impact Metrics (EIMs)* based on the data availability and on the international experience in this field; as a supplement to GEIDB, the *Greek Tsunami Impact Database (GTIDB)* has been organized; (3) Finally, statistical methods and GIS tools have been used to investigate, map and examine statistically possible variations patterns of the several *EIMs* selected for the casualties, both fatalities and injuries, and for the building damage.

The overall thesis is structured in nine chapters. Chapter 1 reviews the geodynamic and seismotectonic setting of the Greek region. What follows is the analysis of seismicity catalogues available for that region, an issue which is needed for the next chapters anyway. Based on the descriptive and parametric catalogue by Papazachos and Papazachou (2003), which is a reference work, we performed a first statistics about the impact data collected for earthquakes occurring from the 6th century BC up to recently. We found that the reporting rate of destructive earthquakes ($MMI_o \geq VIII$) remained nearly constant in the time interval from 1800 up to 2001. For this reason the time interval 1800-2020 has been selected as the reference period for the examination of the earthquake impact in Greece.

To investigate the dependence of the earthquake impact on seismicity parameters, e.g. earthquake epicenters, focal depths and magnitudes, the "best" seismicity parameters should be selected. Therefore, in Chapter 2, modern methods have been used to examine the level of completeness of the various earthquake catalogues utilizing the statistical z-map toolbox. The results provide a clear picture of the completeness of several Greek earthquake catalogues covering the entire reference period 1800-2020.

In Chapter 3 a methodology has been developed to re-determine magnitudes of 52 shallow and intermediate-depth earthquakes of M~5 and over. To this purpose, trace wave amplitudes recorded by five Agamennone-type seismographs that operated in Greece in that period, and published in the Bulletins of the National Observatory of Athens (NOA), have been utilized for the first time to re-calculate magnitudes calibrated over surface-wave magnitudes determined at the Institute of Geodynamics, NOA, from post-1910 records in Mainka and Wiechert seismographs. This has been achieved thanks to that the three types of seismographs (Agamennone, Mainka and Wiechert) shared the common feature of being instruments of intermediate natural period, i.e. ~3.5-6.0 s.

In Chapter 4 statistical methods have been used to compare magnitudes and focal depths inserted in various earthquake catalogues available for the time period 1911-2010.

Chapter 5 is devoted to the organization, format, internal structure and content of the *Greek Earthquake Impact Database (GEIDB)*, while in Chapter 6 several *Earthquake Impact Metrics (EIMs)* have been introduced. Then, in Chapter 7 statistical and GIS tools were used to examine and map the variation in space and time of the several EIMs as well as their correlation with seismicity parameters, i.e. earthquake origin time, epicentral location, focal depth, and magnitude, as well as with macroseismic intensity.

In Chapter 8 we focused our interest to the impact caused by tsunamis in the Greek region. However, the organization of tsunami impact data sets has been rather neglected so far, since only a few preliminary results have been presented. Therefore, we organized the *Greek Tsunami Impact Database (GTIDB)* which has a structure similar to that of the GEIDB and it should be considered as a supplement to it. Although this database covers the entire period from the antiquity up to the present time, in this thesis we are interested for the part of the GEIDB that covers the reference period 1800-2020.To show how tsunami impact data could be useful for the tsunami risk assessment two different approaches have been applied. The first is the extreme scenario method applied to the coastal zone of the test-site of Heraklion city, Crete. The second approach is a probabilistic method which utilizes incomplete data sets and is based on the maximum likelihood estimation of the hazard parameters. This approach was applied utilizing tsunami intensity data from Heraklion, from the city of Rhodes and from the area of Aegion in Corinth Gulf, Central Greece.

Chapter 9 is devoted to a summary of the conclusions reached at in each one of the previous chapters of the thesis as well as on some suggestions and discussion for further research.

TABLE OF CONTENTS

ACKNOWLEDGEMENTS 7
ΠΕΡΙΛΗΨΗ 8
ABSTRACT 10
TABLE OF CONTENTS 12
LIST OF FIGURES 16
LIST OF TABLES 25
INTRODUCTION 28
CHAPTER 1. GEODYNAMICS AND SEISMIC ACTIVITY OF THE GREEK REGION - AN OVERVIEW OF SEISMICITY CATALOGUES 33
1.2 Main geotectonic features and seismicity of the Greek region 33
1.3 Major developments in seismicity recording 35
1.3.1 A short overview 35
1.3.2. Earthquake catalogues for the instrumental period (1900-2020) 36
1.3.3 Seismicity catalogues for the historical period (6th century BC-1899 AD) 39
1.4 Determination of the study reference time period 40
1.4.1 Reporting of destructive earthquakes: a first statistics 41
1.4.2 Reporting of earthquakes that caused environmental effects 42
1.4.3 Reporting of earthquakes impact: first concluding remarks 43
1.5 Research strategy for the selection of seismicity parameters 43
1.5.1 Historical period (AD 1800-1899) 44
1.5.2 Early instrumental period (1900-1910) 44
1.5.3 Instrumental period (1911-2020) 44
1.6 Summary of Chapter 1 44
CHAPTER 2. COMPLETENESS ANALYSIS OF GREEK SEISMICITY CATALOGUES: 1800-2020 45
2.1 Introduction 45
2.2 Methods for catalogue completeness analysis 45
2.3 Completeness analysis of historical catalogues (1800-1899) 46
2.3.1 Data 46
2.3.2 Completeness analysis 47
2.4 Completeness analysis of Greek instrumental catalogues 49
2.4.1 Data 49
2.4.2 Completeness analysis 50
2.4.3 Results 50
2.5 Summary of Chapter 2 55

CHAPTER 3. EARLY INSTRUMENTAL SEISMICITY (1900-1910): REDETERMINATION OF MAGNITUDES FROM RECORDS IN AGAMENNONE SEISMOGRAPHS 56
3.1 Introduction 56
3.2 Method 57
3.3 Data 59
3.3.1 Instrumental records 59
3.3.2 Macroseismic data 63
3.4. Procedure and results 63
3.4.1 Correlation of "Agamennone amplitude" with M_{AUTH} 63
3.4.2 Magnitude determination from Agamennone records 64
3.4.3. Shallow earthquakes: correction of magnitude misfits 66
3.5 Summary of Chapter 3 67
CHAPTER 4. INSTRUMENTAL SEISMICITY (1900-2020): COMPARISON OF CATALOGUES 68
4.1 Introduction 68
4.2 Magnitude comparison 68
4.2.1 Data and procedures 68
4.2.2 $M_{ISC\text{-}GEM}$ / M_{AMR} comparison 68
4.2.3 $M_{ISC\text{-}GEM}$ /M_{UOA} comparison 70
4.2.4 $M_{ISC\text{-}GEM}$ / M_{AUTH} comparison 71
4.2.5 M_{UOA} / M_{AUTH} comparison 73
4.3 Focal depth comparison 74
4.3.1 Data and procedures 74
4.3.2 $h_{ISC\text{-}GEM}$ / h_{UOA} comparison 75
4.3.3 $h_{ISC\text{-}GEM}$ / h_{AUTH} comparison 75
4.3.4 h_{UOA} / h_{AUTH} comparison 76
4.4. Summary of Chapter 4 77
CHAPTER 5. THE GREEK EARTHQUAKE IMPACT DATABASE (GEIDB) 78
5.1 Introduction 78
5.2 Global review 78
5.2.1 Compilations of earthquake impact data 78
5.3 The Mediterranean and Balkans region 80
5.4 Review for Greece 81
5.4.1 Catalogues, books and studies 81
5.4.2 Databases and data compilations 83
5.5 Collection of Earthquake Impact Data for Greece 84
5.5.1 Definitions and explanatory remarks 84

5.6 Sources of earthquake impact data 86
5.6.1 Scientific publications 86
5.6.2 Institutional bulletins and archives 89
5.6.3 Electronic databases 89
5.6.4 Press articles and reports 89
5.7 Data filtering procedure 89
5.8 Format, structure and content of the GEIDB 91
5.9 The Quick-Look Seismicity Section (QLSS) 93
5.9.1 Format 93
5.9.2 Seismicity parameters 93
5.10. The Quick-Look Impact Section (QLIS) 94
5.11. The Impact Metadata Section (IMS) and the References File (RF) 95
5.11.1 The Impact Metadata Section (IMS) 95
5.11.2 The References File (RF) 95
5.12 Case studies 95
5.12.1 The 30 October 2020 earthquake in Samos Island 95
5.12.2 The 25 February 1933 and 20 July 2017 earthquakes in Kos Island: a comparative study 96
5.12.3 Earthquake of 8 February 1926, Kos Island 100
5.12.4 Earthquake (M_w=7.24) and tsunami of 8 November 1905, Athos peninsula 102
5.13. A short statistics of the GEIDB 104
5.14 Summary of Chapter 5 105
CHAPTER 6. EARTHQUAKE IMPACT METRICS 106
6.1 Introduction 106
6.2 Earthquake impact metrics and their variation patterns 106
6.2.1 A global overview 106
6.2.2 Earthquake impact variation in Greece 109
6.3 Selection of Earthquake Impact Metrics (EIMs) 113
6.4 Summary of Chapter 6 115
CHAPTER 7. VARIATION PATTERNS OF EARTHQUAKE IMPACT METRICS IN GREECE 116
7.1 Introduction 116
7.2 Variation patterns of EIMs for casualties 116
7.2.1 A first statistics 116
7.2.2 Casualties from shallow earthquakes 117
7.2.3 Casualties from intermediate-depth earthquakes 121
7.2.4 Dependence of casualties on earthquake magnitude 122

7.2.5 Dependence of casualties on macroseismic intensity 124
7.2.6 Seasonal and diurnal variation of the mortality and morbidity 129
7.3 Variation patterns of EIMs for buildings damage 133
7.3.1 A first statistics 133
7.3.2 Spatial distribution of the damaging and destructive earthquakes 133
7.3.3 Dependence of building damage on earthquake magnitude and intensity 137
7.3.4 Variations of the damage ratio DR 141
7.4 Summary of Chapter 7 142
CHAPTER 8. THE GREEK TSUNAMI IMPACT DATABASE (GTIDB) AND TSUNAMI RISK ASSESSMENT 144
8.1 Introduction 144
8.2 Content and structure of the GTIDB 146
8.2.1 Parameters of Tsunami Sources 147
8.2.2 Tsunami Data 148
8.2.3 Tsunami impact data and metadata 148
8.2.4 Tsunami impact statistics 149
8.3 Tsunami case studies 149
8.3.1 The tsunami caused by the earthquake (M_w=7.24) of 8 November 1905, Mt Athos 149
8.3.2 The tsunami caused by the Samos earthquake (M_w=7.0) of 30 October 2020 153
8.4 Tsunami hazard and risk assessment: a short review 158
8.4.1 Discrimination of hazard and risk 158
8.4.2. Tsunami magnitude and intensity 159
8.4.3 Methods for the tsunami hazard and risk assessment 160
8.5. The extreme scenario approach – Heraklion (Crete) test-site 161
8.5.1 Introductory remarks 161
8.5.2 The test site 161
8.5.3 Work Flow 162
8.5.4 Vulnerability assessment with the DAMASCHE GIS tool 164
8.5.5 Estimation of the cost expected from the tsunami impact to buildings 166
8.6 Probabilistic Tsunami Risk Assessment (PTRA) from incomplete data files 168
8.6.1 Maximum likelihood Probabilistic Tsunami Risk Assessment (PTRA) 168
8.6.2 Maximum likelihood PTRA in Greek test-sites: tsunami data 171
8.6.3. Maximum likelihood PTRA in Greek test-sites: results and sensitivity analysis 172
8.7 Summary of Chapter 8 176
9. CONCLUSIONS AND DISCUSSION 177
REFERENCES 180
Appendix 206

LIST OF FIGURES

Figure A. Work flow-chart of the present thesis…….32

Figure 1.1. Main geotectonic features in the eastern Mediterranean region (adapted from Papazachos and Papazachou, 2003)……...34

Figure 1.2. Main geotectonic features in the region of Greece (adapted from Bocchini, 2018)…….35

Figure 1.3. Frequency distribution of earthquakes occurring in Greece from the 6th century BC up to AD 2001; frequency is counted in 50-year time intervals……41

Figure 1.4. Frequency distribution of earthquakes that occurred in Greece from the 6th century BC up to AD 2001 and caused various types of ground failures; frequency is counted in 50-year time intervals……..43

Figure 2.1. Modern techniques which are in use for the assessment of the completeness magnitude, Mc, according to the tutorial by Mignan and Woessner (2012): FMD=Frequency-Magnitude Distribution…….46

Figure 2.2. Magnitude $M_{w(PP)}$ against $M_{w(SH)}$ for the historical earthquakes occurring in the Greek region in the time period 1800-1899. Solid line shows the best-fit regression; r=correlation coefficient; red dashed line represents $M_{w(PP)}=M_{w(SH)}$……47

Figure 2.3. Magnitude-frequency distribution for the historical (AD 1800-1899) catalogues by Papazachos et al. (2000) (left) and by SHEEC (right)…….48

Figure 2.4. Magnitude frequency for the historical (AD 1800-1899) catalogues by Papazachos et al. (2000) (left) and by SHEEC (right)…….48

Figure 2.5. Cumulative number of seismic events against time for the historical (AD 1800-1899) catalogues by Papazachos et al. (2000) (left) and by SHEEC (right). Stars illustrate dates of large magnitude (≥7.5) events: 1810, 1856 and 1863……..48

Figure 2.6. Time variation of magnitude of completeness, Mc, of the AUTH (left) and UOA (right) catalogues. Mc was estimated with the MAXC method and bootstrap calculation for the time interval of 1900-2009. The sample size used is 250 events; number of samples in bootstrap is 10……51

Figure 2.7. Magnitude-frequency distribution (left) and magnitude frequency (right) for the ISC-GEM catalogue for the period 1905-1910. Mc=5.8 was found with the MAXC method..……80

Figure 2.8. Seismicity rate (left) and magnitude distribution with time (right) for the ISC-GEM catalogue for the period 1905-1910. Stars show large earthquakes (M>7). Star illustrates high magnitude event……..53

Figure 2.9. Magnitude-frequency diagram (left) and magnitude distribution (right) for the UOA catalogue for the period 1900-1910. Mc=5.4 was found with the MAXC method……53

Figure 2.10. Seismicity rate (left) and magnitude distribution with time (right) for the UOA catalogue for the period 1900-1910. Stars show large earthquakes (M>7). Stars illustrate high magnitude events……..54

Figure 2.11. Magnitude-frequency diagram (left) and magnitude distribution (right) for the AUTH catalogue for the period 1900-1910. Mc=5.0 was found with the MAXC method……55

Figure 2.12. Seismicity rate (left) and magnitude distribution with time (right) for the AUTH catalogue for the period 1900-1910. Stars show large earthquakes (M>7). Stars illustrate high magnitude events……55

Figure 3.1. Monthly frequency distribution of the seismicity in the AUTH catalogue for the time period 1900-1910. The frequency peak during 1904 reflects the occurrence of sequences of very strong earthquakes, e.g. in Samos Isl., SE Aegean Sea, and in SW Bulgaria. Statistics was performed with the use of the z-map toolbox……57

Figure 3.2. Locations of the Agamennone seismograph stations (squares) operated from 1900 to 1910. Epicenters of the shallow (dots) and intermediate-depth (triangles) earthquakes listed in Table 3.3, along with the respective numbers, are also plotted……60

Figure 3.3. A typical page of the seismological Bulletin of NOA for the year 1906……..61

Figure 3.4. Amplitude, Av, recorded by the Agamennone instrument at ATH station against M_{AUTH} magnitude for shallow and intermediate-depth earthquakes shown by circles and triangles, respectively (data in Table 3.3)……...64

Figure 3.5. Agamennone magnitude, M_A, against magnitude M_{AUTH} for shallow (circles) and intermediate-depth (triangles) earthquakes for the period 1900-1910……65

Figure 4.1. Magnitudes M_{AMR} plotted against $M_{ISC-GEM}$; r=correlation coefficient……69

Figure 4.2. Magnitude difference $\delta M=M_{ISC-GEM}-M_{AMR}$ plotted against M_{AMR}……..69

Figure 4.3. Magnitudes $M_{ISC-GEM}$ (black triangle) and M_{AMR} (gray circle) plotted against time…….70

Figure 4.4. Magnitudes M_{UOA} plotted against $M_{ISC-GEM}$; r=correlation coefficient……70

Figure 4.5. Magnitude difference $\delta M=M_{ISC-GEM}-M_{UOA}$ plotted against M_{UOA}; r=correlation coefficient. No good correlation exists between δM and M_{UOA}……...71

Figure 4.6. Magnitudes $M_{ISC-GEM}$ (black triangle) and M_{UOA} (gray circle) plotted against time……..71

Figure 4.7. Magnitudes M_{AUTH} plotted against $M_{ISC-GEM}$; r=correlation coefficient……...72

Figure 4.8. Magnitude difference $\delta M=M_{ISC-GEM}-M_{AUTH}$ plotted against M_{AUTH}; r=correlation coefficient……...72

Figure 4.9. Magnitudes $M_{ISC-GEM}$ (black triangle) and M_{AUTH} (grey circle) plotted against time…....72

Figure 4.10. Magnitudes M_{AUTH} plotted against M_{UOA}; r=correlation coefficient……73

Figure 4.11. Magnitude difference $\delta M=M_{UOA}-M_{AUTH}$ plotted against M_{UOA}; r=correlation coefficient. M_{UOA} and δM are not correlated……..73

Figure 4.12. Magnitudes M_{AUTH} (black circle) and M_{UOA} (grey triangle) plotted against time……74

Figure 4.13. Plot of focal depth h_{UOA} against focal depth $h_{ISC-GEM}$. The issue of the fixed focal depths is noted in the text……75

Figure 4.14. Plot of focal depth h_{AUTH} against focal depth $h_{ISC-GEM}$. The issue of the fixed focal depths is noted in the text……76

Figure 4.15. Plot of focal depth h_{AUTH} against focal depth h_{UOA}. The issue of the fixed focal depths is noted in the text……76

Figure 5.1. Flow chart of the procedure followed for the earthquake impact data compilation…….86

Figure 5.2 Damage in a two storey building in Ayios Dimitrios, Cephalonia Island, after the 26 January 2014 (M_w=6.0) earthquake (left) and after the 3 February 2014 (M_w=5.9) earthquake (right) (photos credit, I. Triantafyllou)……...88

Figure 5.3. Information flow regarding casualties reportedly caused in Chalki Island due to the 18 October 1843 earthquake……91

Figure 5.4. Basic structure of the GEIDB……..92

Figure 5.5. Extracts from the Quick-Look parts 1, 2 and 3 of the GEIDB…….92

Figure 5.6. External and internal damage at the Church of Christ in Ano Vathy, Samos, after the earthquake (M_w=7.0) of 30 October 2020 (photos credit, I. Triantafyllou)……96

Figure 5.7. The study area. Key: star=earthquake epicenter; solid circles= Kos and Rhodes cities; stars= epicenters of earthquakes mentioned in the text: 1926, 1933 and 2017 stand for the earthquakes of 26 June 1926, 23 April 1933 and 20 July 2017, respectively; 26(1), 26(2) and 26(3) represent the 8 February 1926 earthquake epicenter estimated by Comninakis and Papazachos (1982), Kárnik (1969), Galanopoulos (1981), Ambraseys and Adams (1998), respectively. 26(1) is the preferred solution as dISC-GEMussed in the text. The area of Gökova Gulf is a graben dominated by two main faults, the south-dipping Gökova fault at the north and the north-dipping Datça fault at the south (e.g. Kurt et al., 1999; Altunel et al., 2003; Karasözen et al., 2018; Ocakoğlu et al., 2018). Hatched lines show tectonic faults. Solid triangle in inset shows the location of Baliaga village mentioned in the text……..97

Figure 5.8. Macroseismic and environmental (in parenthesis) intensities assigned at various localities of Kos Isl. in relation to the 1933 earthquake. Macroseismic intensities are according to the MM and EMS-98 scales while environmental intensities were estimated from the ESI-07 scale. Key: KE=Kefalos, KA=Kardamena, PY=Pyli, AS=Asfendiou, VO=Vorinas, KC=Kos City, TH=Therma, CL=Cape Louros. In Antimachia (AN) MM/EMS-98 intensity was estimated in relation due to the 8 February 1926 earthquake too…….....99

Figure 5.9. Localities in Kos city where ground failures were observed in relation to the 1933 earthquake (Port 1 and Bella Vista) and the 2017 earthquake (Port 1, Port 2, Kos Castle and Marina)……...99

Figure 5.10. A masonry building that survived the 1933 earthquake in the historical center of Kos city. The partial collapse of the upper floor with the 2017 earthquake killed two persons…….100

Figure 5.11. Eastern Kos: Tsunami inundation zone after the 2017 earthquake. Run-up of maximum 0.8 m, 1.0 m and 1.5 m is illustrated by green, yellow and red, respectively. Seismic intensities assigned at various localities of eastern Kos Isl. in relation to the 2017 earthquake are also illustrated. Intensity estimates in MM and ESI-07 scales are shown…….……100

Figure 5.12. Macroseismic intensities in 12-grade MM scale felt at sites in mid epicentral distances due to the Mt Athos earthquake (large star) of 8 November 1905. For intensity documentation and numbering of sites see Table A1. Symbol key: AFZ=Athos Fault Zone (white line, redrafted from Roussos and Lyssimachou, 1991), NAT=North Aegean Trough. Small stars show the epicenters of the 18 Jan.1982 (M_w6.56) and 6 Aug. 1983 (M_w6.65) earthquakes mentioned in the section of Discussion; earthquake focal parameters are from the ISC-GEM (2018) catalogue……103

Figure 5.13. Macroseismic intensities in the 12-grade MM scale felt at sites of Mt Athos peninsula due to the 8 Nov. 1905 earthquake. For intensity documentation and numbering of sites see Table A1; star=earthquake epicenter. Earthquake parameters are from the ISC-GEM (2018) catalogue...104

Figure 5.14. Main co-seismic ground failures reported in association to the 1905 Athos earthquake (star). Key for localities: Iv=Iviron Monastery, GL= Great Lavra Monastery, Ka=Kafsokalivion Monastery, Ah=Ayia Anna hermitage. The tsunamis reported offshore Ka and GL were in association to the 1905 and 1585 earthquakes, respectively……104

Figure 5.15. Frequency of the three main attributes inserted in the GEIDB……105

Figure 6.1. Relation between the total number of victims and the total amount of monetary losses according to Ohta et al. (1986). Greece possesses a relatively low position in this relationship……107

Figure 6.2. Relation of the number of fatalities to the number of buildings damaged in earthquakes (Coburn and Spence, 1992). The position of the Corinth 1981 and Kalamata 1986 earthquakes is relatively low in this relationship……..108

Figure 6.3. Epicenters of all the earthquakes that during the period AD 1800-2020 caused impact of any kind considered in GEIDB, i.e. building damage or destruction, and/or human losses (fatalities and/or injuries)……..…114

Figure 7.1. Spatial distribution of the epicenters of shallow, fatal earthquakes occurring in Greece from 1800 up to 2020…….…...118

Figure 7.2. Epicenters of shallow earthquakes that caused injuries in Greece from 1800 up to 2020……..118

Figure 7.3. Casualties caused in Greece by single, shallow earthquakes occurring from 1800 up to 2020. The extremely high numbers corresponding to the Chios island earthquake of 3 April 1881 are out of scale……119

Figure 7.4. Time variation of the survival ratio, R, in the time period 1800-2020; r=correlation coefficient……120

Figure 7.5. Epicenters of intermediate-depth earthquakes that caused at least one fatality (a) and at least one injury (b) from 1800 up to 2020……121

Figure 7.6. Number of casualties, N, caused in Greece by single, intermediate-depth earthquakes from 1800 up to 2020……..…..122

Figure 7.7. Variation of the fatalities number, Fa, with the earthquake magnitude, M, for the time period 1800-2020. Key: circle=shallow earthquake, triangle=intermediate-depth earthquake. Best-fit regression line is for intermediate-depth earthquakes; r=correlation coefficient. M/Fa correlation for shallow earthquakes is very weak…….……123

Figure 7.8. Variation of the injuries number, In, with the earthquake magnitude, M, for the time period 1800-2020. Key: circle=shallow earthquake, triangle=intermediate-depth earthquake. Best-fit regression line is for intermediate-depth earthquakes; r=correlation coefficient. M/In correlation for shallow earthquakes is very weak…….……123

Figure 7.9. Variation of the fatalities number, Fa, with the maximum intensity, I_o, in the time period 1800-2020. Key: solid circle=shallow earthquake, red triangle=intermediate-depth earthquake…..124

Figure 7.10. Correlation between the number of fatalities, Fa, and the intensity, I_o, for shallow earthquakes that occurred in the time interval 1800-2020. Key: solid and dashed lines represent the

best-fits to all data (relation 7.3) and to the upper bound Fa values (relation 7.6), respectively; round dot line is the relation (6.4) found by Papazachos and Papazachou (2003).....125

Figure 7.11. Correlation between the number of fatalities, Fa, and the maximum intensity, I_o, for shallow earthquakes that occurred in the time interval 1900-2020. Key: solid and dashed lines represent the best-fits to all data (relation 7.4) and to the upper bound Fa values (relation 7.7), respectively…….……..126

Figure 7.12. Correlation between the number of fatalities, Fa, and the maximum intensity, I_o, for shallow earthquakes that occurred in the time interval 1960-2020. Key: solid and dashed lines represent the best-fits to all data (relation 7.5) and the upper bound best fit to I_o values of 5, 8, and 9 (relation 7.8), respectively……....126

Figure 7.13. Correlation of the injuries number, In, with the intensity, I_o, in the time period 1800-2020. Key: solid circle=shallow earthquake, red triangle=intermediate-depth earthquake…….127

Figure 7.14. Correlation of the injuries number, In, with the intensity, I_o, for shallow earthquakes in the time interval 1800-2020. Key: solid and dashed lines represent the best-fits to all data (relation 7.9) and to upper bound In values (relation 7.12), respectively; rounded dot line is the relation (6.5) found by Papazachos and Papazachou (2003)……..128

Figure 7.15. Correlation of the injuries number, In, with the intensity, I_o, for shallow earthquakes in the time interval 1900-2020. Key: solid and dashed lines represent the best-fits to all data (relation 7.10) and to upper bound In values (relation 7.13), respectively……..128

Figure 7.16. Correlation of the injuries number, In, with the intensity, I_o, for shallow earthquakes in the time interval 1960-2020. Key: solid and dashed lines represent the best-fits to all data (relation 7.11) and to upper bound In values (relation 7.14), respectively……..129

Figure 7.17. Seasonal distribution of the numbers of fatalities (red) and injuries (blue) in the time period 1800-2020……..……130

Figure 7.18. Seasonal distribution of the numbers of fatalities (red) and injuries (blue) in the time period 1800-2020 excluding data from the 1881 and 1953 extreme events……..130

Figure 7.19. Seasonal distribution of the numbers of fatalities (red) and injuries (blue) in the time period 1900-2020……..131

Figure 7.20. Seasonal distribution of the numbers of fatalities (red) and injuries (blue) in the time period 1900-2020 excluding the 1953 extreme event……131

Figure 7.21. 24-hr distribution of the numbers of fatalities (red) and injuries (blue) in the time period 1900-2020. Local Greek time has been considered……..132

Figure 7.22. 24-h distribution of the numbers of fatalities (red) and injuries (blue) in the time period 1900-2020 after removing the earthquake event of 12 August 1953. Local Greek time has been considered……132

Figure 7.23. Spatial distribution of the shallow (circle) and intermediate-depth (triangle) earthquakes that caused repairable building (RB) damages in Greece in the time interval 1800-1959. Numbers of RB are represented with different colors in the Legend. Symbol size increases with the increase of magnitude class……134

Figure 7.24. Spatial distribution of the shallow (circle) and intermediate-depth (triangle) earthquakes that caused repairable building (RB) damages in Greece in the time interval 1960-2020. Numbers of RB are represented with different colors in the Legend. Symbol size increases with the increase of magnitude class……135

Figure 7.25. Spatial distribution of the shallow (circle) and intermediate-depth (triangle) earthquakes that caused unrepairable building (UB) damages in Greece in the time interval 1800-1959. Numbers of UB are represented with different colors in the Legend. Symbol size increases with the increase of magnitude class……136

Figure 7.26. Spatial distribution of the shallow (circle) and intermediate-depth (triangle) earthquakes that caused unrepairable building (UB) damages in Greece in the time interval 1960-2020. Numbers of UB are represented with different colors in the Legend. Symbol size increases with the increase of magnitude class……136

Figure 7.27. Spatial distribution of the damage ratio, DR, for shallow (circle) and for intermediate-depth (triangle) earthquakes in Greece in the time interval 1800-2020. Values of DR are represented with different colors in the Legend. Symbol size increases with the increase of magnitude class…..137

Figure 7.28. Correlation between the number of RB per event and the earthquake magnitude, M, for the period 1800-2020. RB for shallow shocks is not correlated with M. A weak M/RBint correlation was found for intermediate-depth events (dashed line). The RBmax upper bound (gray circles) is well controlled by M (round dot line). Key: circle=shallow event, triangle=intermediate-depth event; gray circle=upper bound RB points for shallow events. RBint=RB for intermediate-depth events; RBmax=RB for upper bound points; r=correlation coefficient……138

Figure 7.29. Correlation between the number of UB per event and the earthquake magnitude, M, for the period 1800-2020. UBsh for shallow shocks is weakly correlated with M (solid line). A good M/UB correlation was found for intermediate-depth events (dashed line). The UBmax upper bound (gray circles) is well controlled by M (round dot line). Key: circle=shallow event, triangle=intermediate-depth event; gray circle=upper bound UB points for shallow events. RBint=RB for intermediate-depth events; RBmax=RB for upper bound points; r=correlation coefficient…….138

Figure 7.30. Correlation between the number of RB per event and the intensity, I_o, for the period 1800-2020. RBsh for shallow shocks is very weakly correlated with I_o (solid line). A weak M/RBint correlation was found for intermediate-depth events (dashed line). The RBmax upper bound (round dot line) and the RBmin lower bound (long dash dot line) (gray circles) are both very well controlled by I_o. Key: circle=shallow event, triangle=intermediate-depth event; RBsh=RB for shallow events; RBint=RB for intermediate-depth events; RBmax=RB for upper bound points; RBmin=RB for lower bound points; r=correlation coefficient……139

Figure 7.31. Correlation between the number of UB per event and the intensity, I_o, for the period 1800-2020. UBsh for shallow shocks is weakly correlated with I_o (solid line). A better I_o/RBint correlation was found for intermediate-depth events (dashed line). The RBmax upper bound (round dot line) (gray circles) is well enough controlled by I_o. Key: circle=shallow event, triangle=intermediate-depth event; RBsh=RB for shallow events; RBint=RB for intermediate-depth events; RBmax=RB for upper bound points; r=correlation coefficient……140

Figure 7.32. Correlation between the number of RB per event and the intensity, I_o, for the period 1960-2020. RBsh for shallow shocks is weakly correlated with Io (solid line). The RBmax upper bound (round dot line) and the RBmin lower bound (long dash dot line) (gray circles) are both very well controlled by I_o. Key: circle=shallow event, RBsh=RB for shallow events; RBmax=RB for upper bound points; RBmin=RB for lower bound points; r=correlation coefficient……..140

Figure 7.33. Correlation between the number of UB per event and the intensity, I_o, for the period 1960-2020. RBsh for shallow shocks is well correlated with I_o (solid line). The UBmax upper bound (round dot line) and the UBmin lower bound (long dash dot line) (gray circles) are both very well controlled by I_o. Key: circle=shallow event, UBsh=UB for shallow events; UBmax=UB for upper bound points; UBmin=UB for lower bound points; r=correlation coefficient……...141

Figure 7.34. Correlation between the damage ratio, DR, per event and the intensity, I_o, for the period 1960-2020. DRsh for shallow shocks (circles) is weakly correlated with I_o (solid line) but the correlation is better for intermediate-depth earthquakes (DRint) (triangles). The DRmax upper bound (round dot line) is very well controlled by Io; r=correlation coefficient……...142

Figure 7.35. Gradual increase of DR for shallow shocks in the time period 1960-2020; r=correlation coefficient. The correlation is not very good……142

Figure 8.1. Tsunamigenic zones, defined from documentary sources, and their relative tsunami potential classification. WMS, western Mediterranean Sea; GC, Gulf of Cádiz; AB, Alboran Basin; EMS, Eastern Mediterranean Sea; AS, Aegean Sea; ADS, Adriatic Sea; MS, Marmara Sea; BS, Black Sea. Zonation key: 1, East Alboran Sea/North Algerian Margin Sea; 2, Liguria and Côte d'Azur; 3, Tuscany; 4, Aeolian islands; 5, Tyrrhenian/Calabria; 6, Eastern Sicily and Messina Straits; 7, Gargano Promontory; 8, East Adriatic Sea; 9, West Hellenic Arc; 10, East Hellenic Arc; 11, Cyclades; 12, Corinth Gulf; 13, Maliakos Bay; 14, East Aegean Sea; 15, North Aegean Sea; 16, Marmara Sea; 17, Cyprus; 18, Levantine Sea; 19, Bulgaria; 20, Crimea; 21, East Black Sea; 22, South West Iberia (after Papadopoulos et al., 2014a)……...145

Figure 8.2. Excerpt of the GTIDB for the time period 1800-2020……147

Figure 8.3. Earthquake and other sources that produced impactful tsunamis in Greece in the time period 1800-2020: Bathymetry data are from EMODNET. GS means gravity slide…….…..148

Figure 8.4. The tsunami was reported from the southern end of the Mt Athos peninsula and the surrounding. The two possible landslide source areas are marked in red (Scar 1) and in blue (Scar 2) (in collaboration with the UNIBO tsunami team, Triantafyllou et al. 2020a)……..150

Figure 8.5. Upper panel: Initial sliding mass assumed for case S1 (area within the purple boundary inside the scar area delimited by the red line, and slide thickness given in the yellow-red scale). Predefined Center of Mass (CoM) trajectory and lateral boundaries are drawn as black and grey curves, respectively. The final deposit thickness is represented by the different scales of green, from light to dark. Lower panel: blocks' CoM velocity vs. Time (in collaboration with the UNIBO tsunami team, Triantafyllou et al. 2020a)……...151

Figure 8.6. Maximum water elevation for scenario S1. The red line marks the Scar 1 boundary. The black boundary evidences the sliding surface (in collaboration with the UNIBO tsunami team, Triantafyllou et al. 2020a)……...…..152

Figure 8.7. Virtual tide gauges at the points 1, 2, 3 and 4 to the west of Scar 1, and synthetic tide gauge records obtained for the tsunami generated by landslide scenario S1. Grey area represents the sliding surface (in collaboration with the UNIBO tsunami team, Triantafyllou et al. 2020a)……153

Figure 8.8. Map showing the record of the tsunami generated by the Samos 30 October 2020: solid triangle shows tide-gauge station, 1=Bodrum, 2=Kos, 3=Kos-Marina, 4=Plomari, 5=Syros, 6=Kasos, 7=Heraklion; red triangle shows main sites of tsunami observation: Samos Isl., V=Vathy, K=Karlovasi, S=south Samos; Ikaria Isl.: I1=Evdilos, I2=Ayios Kirykos, I3=Gialiskari; O1=Komi (Chios Isl.), O2=Scala (Patmos Isl.), O3=Nimporio (Andros Isl.) (for more details see in text); black circles show epicenters of earthquakes mentioned in the text, 2017 (1) and 2017 (2) stand for the 12 June and 20 July earthquakes, respectively; beach-ball shows earthquake focal mechanism, from

moment tensor solution, indicating about WNW- ESE normal faulting (after National Observatory of Athens, https://bbnet.gein.noa. gr/HL/seismicity/mts/revised-moment- tensors). Arrow in inset shows direction of lithospheric plate motion……155

Figure 8.9. Sites of tsunami field-survey in Samos: V1-V6=Vathy town, V7=Gagou beach, V8=Malagari, N1=Kedros, N2=Kokkari, K1-K3=observation sites in Karlovasi town, K4=Ayios Nikolaos; S stands for south Samos coasts, S1=Psili Ammos, S2=Pythagorion Port, S3=Heraion, S4=Kampos. For more details see the text. ……..…156

Figure 8.10. Observation sites V1 to V6 (red triangles) along the Vathy bay east coast and three characteristic tsunami transects A,B,C (white lines) measuring maximum run-up, h, at respective run-in distance, d (for details see in text). ……..……..…157

Figure 8.11. Site V2. Indoor material damage caused by the tsunami attack in the fish restaurant (a). Water mark at h~1.09 m was measured at run-in distance of ~45 m (b) (photos credit, I. Triantafyllou)……..……158

Figure 8.12. The study area of the western segment of Heraklion city (Gazi), Crete Isl., in Google Earth map. The area is characterized by the Yofiros river and the nearby stadium in the eastern side, by the Xeropotamos river and a free of buildings area in the central side and by the motorway running from east to west at the south side (see details in Triantafyllou et al., 2018). ……162

Figure 8.13. Flow chart of the procedures followed to calculate expected losses due to tsunami building damage in terms of absolute monetary cost (Triantafyllou et al., 2018). …….163

Figure 8.14. Tsunami inundation zone and the DEM beyond this zone in the study area (Triantafyllou et al., 2018). ……..……164

Figure 8.15. Mapping of the tsunami inundation zone with water depth (in m) and building damage level per building block as determined from the application of the DAMASCHE GIS tool (Triantafyllou et al., 2018). ……..……..…166

Figure 8.16. Typical illustration of data used for assessment of model recurrence parameters based on prehistoric, historic, and instrumental datasets; vertical dimension expresses event size (e.g. magnitude or intensity). Prehistoric data are subject to uncertainty relevant to the time of occurrence, the exact size of the event, and incompleteness in terms of the probability of detecting an event. Historic data, consisting of the largest observed events, and instrumental datasets are subject to incompleteness and uncertainty relevant to the observed event size, varying levels of certainty regarding the exact location of an event, and varying probabilities of all events above a certain minimum size being observed. Time gaps T_g represent missing event records (figure adapted from Smit et al., 2019).……..……169

Figure 8.17. Flow diagram of the methodological steps followed for the probabilistic tsunami hazard assessment (PTHA) with maximum likelihood estimate (MLE) with the use of incomplete and uncertain tsunami catalogue data sets (figure adapted from Smit et al., 2019). ……170

Figure 8.18. Annual probability of exceedance (left) and return period (right) of tsunami intensity values for the city of Rhodes; tsunami intensity in 12-grade scale..……...…174

Figure 8.19. Probability of exceedance of tsunami intensity values for the city of Rhodes for return periods of 10, 50 and 100 years; tsunami intensity in 12-grade scale. ……..…174

Figure 8.20. Annual probability of exceedance (left) and return period (right) of tsunami intensity values for the city of Heraklion; tsunami intensity in 12-grade scale. ……..……175

Figure 8.21. Probability of exceedance of tsunami intensity values for the city of Heraklion, including paleotsunami data, for return periods of 10, 50 and 100 years; tsunami intensity in 12-grade scale……..175

Figure 8.22. Annual probability of exceedance (left) and return period (right) of tsunami intensity values for the city of Aegion; tsunami intensity in 12-grade scale. ……..…176

Figure 8.23. Probability of exceedance of tsunami intensity values for the city of Aegion, including paleotsunami data, for return periods of 10, 50 and 100 years; tsunami intensity in 12-grade scale. ……176

LIST OF TABLES

Table 1.1. Summary of earthquake catalogues covering the Greek region for the instrumental seismicity period……..…36

Table 1.2. Summary of the most recent historical earthquake catalogues covering the entire Greek area. Key: MMI_o=maximum intensity in MM scale, P=parametric, D=descriptive, sP=semi-parametric……..….40

Table 2.1. Features of the catalogues used in the statistical examinations……..….50

Table 2.2. Magnitude of completeness, Mc, determined with the application of the MAXC, GFT-95% (Mc95) and GFT-90% (Mc90) methods; α and b are parameters in the magnitude-frequency formula (2.1)……...52

Table 3.1. Main characteristics of four catalogues covering the study region (latitude 33^0-43^0N, longitude 18^0-30^0E) for the period 1900-1910. Key: N=number of events, n=shallow earthquakes, i=intermediate-depth earthquakes, M_{min}=minimum magnitude, M_{max}=maximum magnitude, Mc= completeness magnitude as determined in Chapter 2. The AM catalogue is by definition truncated at Mc=6.0 by the author of that catalogue. Magnitudes are in M_w scale; symbol * shows M_s……56

Table 3.2. Constants and other technical characteristics of the Agamennone, Mainka and Wiechert seismographs operated in Greece (Eginitis, 1905, 1910, 1912, Comninakis et al., 1987). Symbol key: φ=geographical latitude, λ=geographical longitude, m=pendulum mass, T=natural period, h=altitude of installation site, V=static magnification, DS=drum speed (mm/min). For CHA Agamennone station no further information is available. Notes: for Mainka horizontal components T=6, V=80 and DS=15 for the period 1911-1956, T=3.5, V=60 and DS=30 for the period 1957-1963; for Wiechert horizontal components T=5.0-9.2, V=160-175 and DS=12-30 for the period 1924-1963; for Wiechert vertical component T=1.6-4.0, V=140-280 and DS=10-30 for the period 1928-1963……...…….59

Table 3.3. Calibrated (M_{ac}) and final (M_A) magnitudes calculated from wave amplitudes recorded at the components A_{NE}, A_{NW} (in mm) of Agamennone seismographs operating in Greece from 1901 to 1910. All records are from the Athens (ATH) station unless otherwise indicated (working names of other stations: CH=Chalkis, CA=Calamata, E=Egion, Z=Zante). Key: n=event number, mo=month, d=day, hr=hour, mi=minute, s=sec; φ^oN, λ^oE=epicentral geographic coordinates, h=focal depth (km), M=magnitude, Δ=epicentral distance (km), M_{ac}=calibrated Agamennone magnitude, M_A=final Agamennone magnitude. Focal parameters from year to M are taken from the AUTH catalogue unless are revised in this study and marked in bold (see text); A_{NE}, A_{NW} are amplitudes recorded at the NE and NW components of Agamennone stations taken from the NOA Bulletins; Δ, M_{ac}, and M_A have been calculated in this study……62

Table 5.1. Information about Global Earthquake Databases (last access, 9 January 2021)……80

Table 5.2. Main attributes of the Greek Earthquake Impact Database (GEIDB)……..……..85

Table 5.3. Summary of the 1933 and 2017 damage seismic intensities (DSIs) and environmental seismic intensities ESI-07s assigned. Key: Fa=fatalities, In=injuries, GF=ground failures, SL=soil liquefaction, LD/RF= landslides/rock falls, HC=hydrological changes, TS=tsunami wave……98

Table 5.4. Focal parameters of the Mt Athos 8 November 1905 earthquake listed in various earthquake catalogues. Key: y=year, m=month, d=day, φ_N^0 and λ_E^0 are geographic latitude north and longitude east, respectively; l.t.=local time, *h*=focal depth, *n*=shallow earthquake, I_o=epicentral intensity in Modified-Mercalli scale, M_s=surface-wave magnitude, M_w=moment magnitude; * indicates magnitude obtained from modeling. Parameter marked by an asterisk has been derived by modeling of macroseismic data. For the earthquake origin time see explanations in the text……102

Table 6.1. Summary of the Earthquake Impact Metrics (EIMs) used……...…134

Table 7.1. EIMs for casualties. Symbol key: Fa=number of fatalities per event, In=number of injuries per event, FaE=number of earthquakes that caused at least one fatality, InE=number of earthquakes that caused at least one injury, AFa=average Fa, AIn=average In, R=In/Fa, R_i= 100 x R, MFa=maximum Fa caused by a single event, MIn=maximum In caused by a single event……117

Table 7.2. Time variation of the numbers of fatalities (mortality) and injuries (morbidity) and of the survival Ratio as well as of their coefficient of variation. In the time segment marked with * the 7 September 1999 extreme event is not included…….120

Table 7.3. Minimum (M_{min}) and maximum (M_{max}) magnitudes of earthquakes that caused casualties in the time period 1800-2020. Key: Fa=number of fatalities, In=number of injuries…….....124

Table 7.4. Minimum (I_{omin}) and maximum (I_{omax}) intensities of earthquakes that caused casualties in the time period from 1800 to 2020. Key: Fa=number of fatalities, In=number of injuries……127

Table 7.5. EIMs for buildings damaged or destroyed. Symbol key: RB=total number of repairable buildings, UB=total number of unrepairable buildings, RBE=number of earthquakes that caused repairable buildings, UBE=number of earthquakes that caused unrepairable buildings, ARB=average number of repairable buildings per earthquake event, AUB=average number of unrepairable buildings per earthquake event, MRB=maximum RB caused by a single event, URB=maximum UB caused by a single event, ADR=average damage ratio……..133

Table 8.1. Building damage level as a function of the water depth (in m) in the inundation zone (Gardi et al. 2009; Valencia et al., 2011). The building classification is according to the construction material types listed in Table 8.2……..……..….165

Table 8.2. Building vulnerability classification (Leone et al. 2011)…….….165

Table 8.3. Calculated cost for reparation of buildings suffering damage level D2 and D3 due to strong tsunami attack in the inundation area of Gazi, west of Heraklion, Crete Isl. We adopted that the ratio of residential/commercial buildings equals 4 and that the average surface of residential and

commercial buildings is 100 m^2 and 80 m^2, respectively. Then, the average building surface is 96 m^2……..…167

Table 8.4. Calculated cost for reconstruction of buildings suffering partial or total collapse (damage levels D4 and D5 combined together) due to strong tsunami attack in the inundation area of Gazi, west of Heraklion, Crete Isl…….…..167

Table 8.5. Tsunami data used for the PTIA in the cities of Rhodes, Heraklion and Aegion. Symbol key: K=tsunami intensity in the 12-grade scale by Papadopoulos and Imamura (2001), SD(K)=standard deviation of K, R=reliability, symbol – means BC…….....171

Table 8.6. Results of the probabilistic tsunami risk assessment in three test sites. Key: K=tsunami intensity (scale by Papadopoulos and Imamura, 2001), λ=tsunami activity rate (events/yr), RP=Return Period (yrs), P=probability of exceedance in T years……..……..……173

INTRODUCTION

The impact of the earthquakes on the human communities and on the natural environment is multifold and comes as a direct or indirect result of the earth's shaking. Direct effects are caused by the earthquakes in human life, buildings, infrastructures and other property as well as in land, e.g. surface fault-traces and ground failures (landslides, soil liquefaction and others) and in the sea (e.g. tsunamis). Indirect effects of the earthquakes include the economic impact, social disruption as well as various negative psychological, political and cultural consequences.

A better understanding of the various impact types caused by earthquakes and the factors that control them is of particular importance for undertaking actions towards the earthquake risk mitigation. However, the study of issues relevant to the earthquake impact is quite challenging for the reason that often no organized impact databases are available. On the other hand, the earthquake impact should be considered in the frame of the geographical area, the time period and the social and economic environment it takes place. The earthquake impact is traditionally expressed in terms of macroseismic intensity, which is an estimate of the earthquake effects measured in appropriate scales, such as the 12-level Modified-Mercalli (MM), the EMS-98 or other relevant scales. The assignment of macroseismic intensity is based mainly on building damage data. On the other hand, the Environmental Seismic Intensity (ESI) scale has been developed in the last years for the intensity assessment on the basis of only the environmental effects of the earthquakes. In either case, however, the macroseismic intensity does not provide raw data about the direct earthquake effects and remains only a metadata attribute regardless the scale used.

Limited progress has been made internationally in organizing earthquake impact databases and in understanding the various factors on which the impact is dependent on. In Greece, the research performed in this field is also limited as compared to seismicity and earthquake engineering studies.

The present thesis is a contribution towards two main objectives: (1) to organize for the first time an earthquake impact database in Greece, and (2) to investigate the spatio-temporal distribution of the earthquake impact and how it possibly depends on various factors, such as seismicity parameters, macroseismic intensity, time of the day, season, and others. Of interest here is the direct earthquake impact, i.e. the one caused directly by the ground shaking. However, the indirect impact of earthquakes, e.g. social, economic and other consequences, which are not directly due to the ground shaking, is not of interest to this study. In this frame, the overall research performed included three distinct phases: (1) The first phase has been devoted to the compilation of the "best" *seismicity data sets* for both the instrumental (1900-2020) and the historical time periods; (2) The second phase comprised the collection and examination of a large number of earthquake impact data sources and the organization of the *Greek Earthquake Impact Database (GEIDB)* as well as the determination of appropriate *Earthquake Impact Metrics (EIMs)* based on the data availability and on the international experience in this field; as a supplement to GEIDB, the *Greek Tsunami Impact Database (GTIDB)* has been organized; (3) Finally, statistical methods and GIS tools have been used to investigate, map and examine statistically possible variations patterns of the several *EIMs* selected for the casualties, both fatalities and injuries, and for the building damage. A special investigation concerns the tsunami risk assessment based on data inserted in the GTIDB and approached with two different methods: (1) an extreme scenario approach and (2) a maximum likelihood probabilistic approach.

The overall thesis is structured in nine chapters, the description of the content of which follows (Fig. 1).

Chapter 1 reviews the geodynamic and seismotectonic setting of the Greek region. This is not, however, an easy task due to the very large number of relevant studies published particularly in the last about 50 years, i.e. after the establishment in the 1960's of the New Global Tectonics including the Theory of Lithospheric Plates. Therefore, Chapter 1 is not an exhaustive review but highlights the most important points of the geodynamic setting of the area leaving room for a more detailed examination of the various seismicity catalogues which are available for the region of Greece. The analysis of seismicity catalogues is needed for the next chapters anyway. Based on the descriptive and parametric catalogue by Papazachos and Papazachou (2003), which is a reference work, we performed a first statistics about the impact data collected for earthquakes occurring from the 6th century BC up to recently. We found that the reporting rate of destructive earthquakes ($MMI_o \geq VIII$) remained nearly constant in the time interval from 1800 up to 2001. On the contrary, before 1800 this rate drops, which is an evidence of incomplete reporting for destructive earthquakes in Greece. For this reason the time interval 1800-2020 has been selected as the reference period for the examination of the earthquake impact in Greece. At the same time it was found that the minimum earthquake magnitude that caused some kind of impact in Greece is ~5. Since the Greek territory has historically changed through time and for reasons of standardization, we selected to examine the earthquake impact in the area which is covered by the current territory of the country.

To investigate the dependence of the earthquake impact on seismicity parameters, e.g. earthquake epicenters, focal depths and magnitudes, the "best" seismicity parameters should be selected. As regards the instrumental period of seismicity (1900-2020), it has been found (Chapter 1) that there are several catalogues available which have been organized by following different procedures for hypocentral and magnitude determinations. This implies that these catalogues cover different time segments and are of different levels of completeness. However, the year 1911 has been a turning point in the seismicity monitoring in Greece thanks to the installation (November 1910) and operation of a reliable seismograph of Mainka type at the Athens (ATH) station of the National Observatory of Athens. Therefore, 1911 has been quoted as the beginning of the instrumental era of Greek seismicity (Båth, 1983). Since 1924 a Wiechert-type seismograph operated also at the ATH station.

In Chapter 2, modern methods have been used to examine the level of completeness of the various earthquake catalogues utilizing the statistical z-map toolbox. The methods used are the non-parametric Maximum Curvature (MAXC) method, and the Mc95 and Mc90 techniques relying on the parametric method of Goodness-of-Fit Test (GFT). The results provide a clear picture of the completeness of several Greek earthquake catalogues covering the entire reference period 1800-2020.

In the very early instrumental era of seismicity (1900-1910) the available catalogues are more incomplete as compared to the post-1910 period while significant magnitude differences can be found in the various catalogues for several earthquakes. For this reason, in Chapter 3 a methodology has been developed to re-determine magnitudes of 52 shallow and intermediate-depth earthquakes of M~5 and over. To this purpose, trace wave amplitudes recorded by five Agamennone-type seismographs that operated in Greece in that period, and published in the Bulletins of the National Observatory of Athens (NOA), have been utilized for the first time to re-calculate magnitudes calibrated over surface-wave magnitudes determined at the Institute of Geodynamics, NOA

(Papazachos and Comninakis, 1971, 1972), from post-1910 records in Mainka and Wiechert seismographs. This has been achieved thanks to that the three types of seismographs (Agamennone, Mainka and Wiechert) shared the common feature of being instruments of intermediate natural period, i.e. ~3.5-6.0 s.

Chapter 4 is devoted to the comparison of magnitudes and focal depths inserted in various earthquake catalogues available for the time period 1911-2010. This examination showed the time variation of the completeness levels as well as the possible magnitude overestimations or underestimations in the various catalogues. On the other hand, a clear picture was obtained about the differences in the focal depth distributions from one catalogue to the other.

In Chapter 5 the organization of the *Greek Earthquake Impact Database (GEIDB)* is described starting with a short review of the international databases available. This is followed by an exhaustive review of the various sources that offer earthquake impact data for the region of Greece for the time period from 1800 to 2020. The various types of data sources include electronic databases (e.g. NOAA, USGS, EM-DAT etc.), books, scientific papers, technical reports, institutional bulletins, unpublished archives and documents as well as press reports. For some strong earthquakes, which occurred in the last years, impact data were collected during post-event field surveys contacted in the aftermath of the events with the participation of the author of the present thesis. The field surveys have been organized by the Institute of Geodynamics of NOA or by the Department of Geology and Geoenvironment, University of Athens, immediately after the earthquakes of Cephalonia 26th January (M_w=6.0) and 3rd February (M_w=5.9) 2014, the tsunamigenic earthquake of Bodrum-Kos (M_w=6.6), 20th July 2017 and the tsunamigenic earthquake of Samos (M_w=7.0), 30th October 2020. On the other hand, some earlier impactful earthquakes needed further examination since they remained little known. These earthquakes are the large (M_w=7.24, ISC-GEM 2018) earthquake of 8 November 1905 in Mt Athos, North Aegean Sea, the strong (M_w=6.5) earthquake in Kos Island on 23 April 1933 and the moderate earthquake (M_s=5.5) of 8 February 1926 in Kos Island. The impact of these events has been examined in depth after finding new documentary sources not used so far in the seismological tradition (Triantafyllou et al, 2020a,b).

The impact data of interest include various attributes, such as building damage or destruction and impact on the population, i.e. fatalities and injuries. From the environmental effects of the earthquakes of interest here are the tsunami waves. The reason is that they also cause serious impact on the human communities. However, the study of other types of earthquake environmental effects, such as ground failures, hydrological changes etc., are beyond the scope of this thesis. Numerical data have been preferably inserted in the GEIDB, otherwise descriptive information has been inserted. Before we insert impact data in the GEIDB a procedure for data filtering was applied separately for each one of the earthquakes. The filtering procedure included a data reliability control through cross-correlation and critical evaluation of the sources collected. This procedure concluded with the adoption, correction or even rejection of certain data sets. The total number of event entries in the GEIDB is as high as 248.

The GEIDB is structured in four main sections: (1) the *Quick-Look Seismicity Section (QLSS),* (2) the *Quick-Look Impact Section (QLIS),* (3) the *Impact Metadata Section (IMS),* and (4) the *References File (RF)*. The QLSS includes the seismicity parameters selected on the basis of the analysis in Chapters 2, 3 and 4 for the period 1900-2020. The analysis of the earthquake catalogues available

for the 19th century indicated that the most appropriate catalogues for the adoption of seismicity parameters are mainly the SHEEC catalogue produced in the frame of the EC-FP7 project SHARE and the catalogue by Papazachos and Papazachou (2003). For the last years of the time period examined the ISC-GEM and GCMT catalogues were as a rule adopted. The QLIS includes in a parametric and/or descriptive way the various impact data for each event, e.g. numbers of fatalities, injuries, buildings damaged but repairable, or unrepairable buildings. The IMS includes for each event the estimated maximum macroseismic intensity. The QLSS, QLIS and IMS of the GEIDB are organized in Access format, while the References File (RF) is in text format.

To investigate the space and time distribution of the earthquake impact as well as its dependence on seismicity parameters, several *Earthquake Impact Metrics (EIMs)* have been selected in Chapter 6. The EIMs adopted include the numbers of fatalities and injuries, the survival ratio, the numbers of repairable and unrepairable buildings, the damage ratio and others. The selection of appropriate EIMs has been based on the data availability in the GEIDB and by taking into account the international experience after a brief review of the relevant literature. Then, in Chapter 7 several statistical and GIS tools were used to examine and map the variation in space and time of the several EIMs as well as their correlation with seismicity parameters, i.e. earthquake origin time, epicentral location, focal depth and magnitude. In addition, we didn't neglect to examine the EIMs correlation with the maximum macroseismic intensity. It is worth noting that it is the first time that such a type of research has been contacted in Greece.

In Chapter 8 we focused our interest to the impact caused by tsunamis in the Greek region. Revised and updated tsunami catalogues for Greece and the entire Mediterranean Sea have been compiled by various authors after a systematic effort that started by the beginning of 1990's within the frame of a series of pan-European research projects (e.g. Tinti and Maramai, 1996, Papadopoulos 2001, Maramai et al., 2014, Papadopoulos et al., 2014a). However, the organization of tsunami impact data sets has been rather neglected so far, since only a few preliminary results have been presented. Therefore, we organized the *Greek Tsunami Impact Database (GTIDB)* which has a structure similar to that of the GEIDB and it should be considered as a supplement to it. Although this database covers the entire period from the antiquity up to the present time, in this thesis we are interested for the part of the GEIDB that covers the reference period 1800-2020. New impact data were collected during post-event field survey, performed under the leadership of Prof. E. Lekkas (Dept. of Geology, University of Athens), immediately after the tsunami caused in the East Aegean Sea area from the large (M_w=7.0) Samos Island earthquake of 30 October 2021 (Triantafyllou et al, 2021).

To show how tsunami impact data could be useful for the tsunami risk assessment two different approaches have been applied. The first is the extreme scenario method applied to the coastal zone of the test-site of Heraklion city, Crete, in the frame of the pan-European EC-FP7 tsunami research project ASTARTE (2013-2017) coordinated by IPMA, Lisbon (project co-ordinator Prof. Maria Ana Baptista). Numerical tsunami modelling of the extreme Minoan tsunami combined with GIS tools led us to estimate the cost for replacement of buildings damaged by the tsunami. The second approach is a probabilistic method which utilizes incomplete data sets and is based on the maximum likelihood estimation of the hazard parameters, already successfully used in the earthquake hazard assessment (e.g. Kijko and Sellevoll, 1989). This concept was introduced in the tsunami hazard assessment taking the wave height as a measure of the tsunami size (Smit et al., 2017). Working in the frame of the tsunami COST Project AGITHAR, we developed further this concept by taking tsunami intensity

instead of tsunami height as a tsunami size metric, thus leading to tsunami risk assessment instead of tsunami hazard assessment. This approach was applied utilizing tsunami intensity data from Heraklion, from the city of Rhodes and from the area of Aegion, Corinth Gulf, Central Greece. The data sets extend not only in the instrumental and the historical period but also in the pre-historical era by utilizing results of paleotsunami investigations with geological methods. The mean repeat times as well as the probabilities of exceedance of certain tsunami intensity values in certain time intervals have been received and compared for the three test-sites.

Chapter 9 is devoted to a summary of the conclusions reached at in each one of the previous chapters of the thesis as well as on some suggestions and discussion for further research.

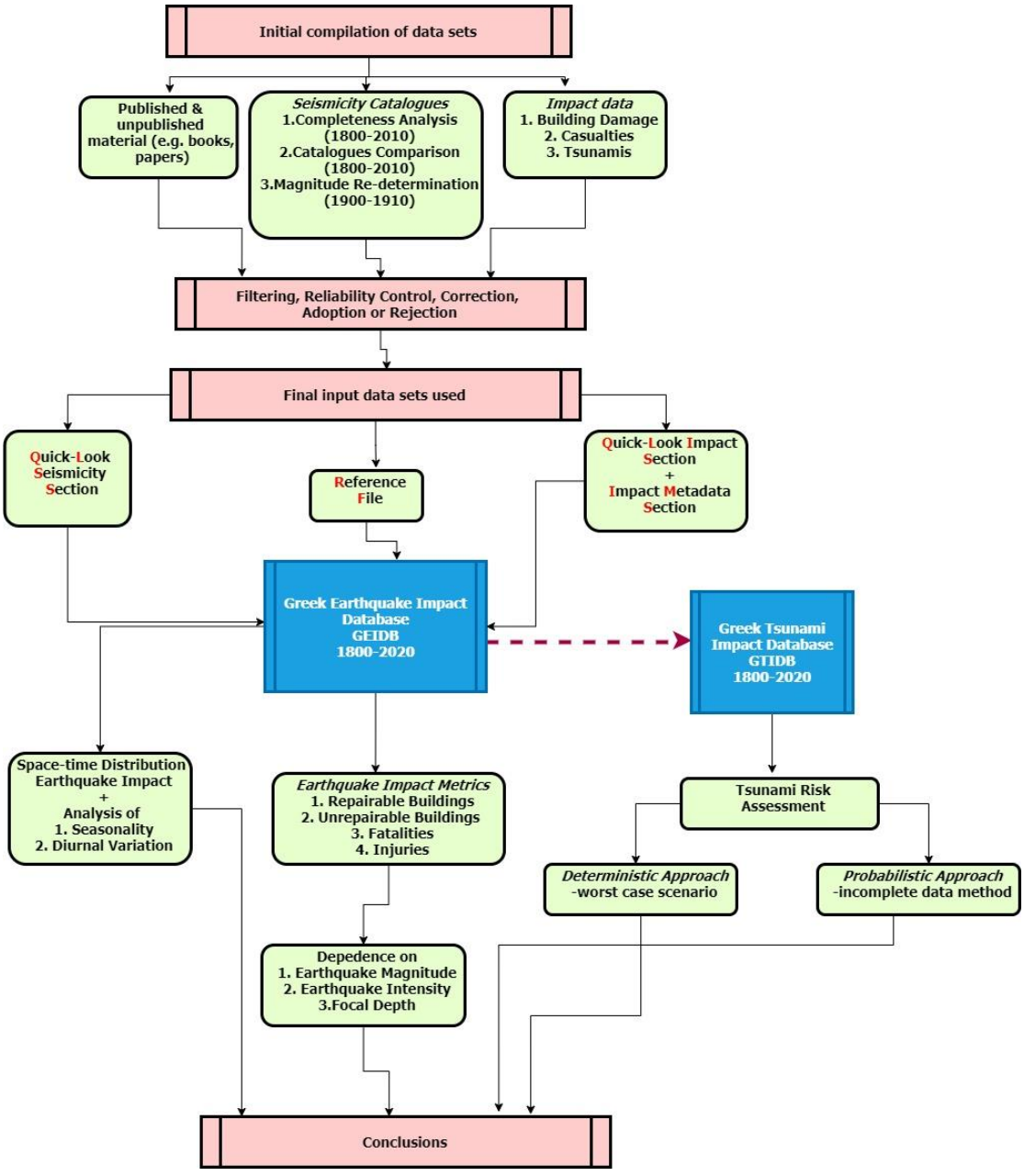

Figure A. Work flow chart of the present thesis.

CHAPTER 1. GEODYNAMICS AND SEISMIC ACTIVITY OF THE GREEK REGION - AN OVERVIEW OF SEISMICITY CATALOGUES

1.1 Introduction

Greece and its surrounding areas, referred to as Greek region for reasons of brevity, is characterized by very high seismicity, likely the highest in the western Eurasia. At the same time, the region is extremely complex from the point of view of tectonic structure and geodynamics.

In this Chapter we present briefly the main geotectonic features and seismicity characteristics of the region and examine the various seismicity catalogues, which are available for both the historical (pre-1900) and the instrumental (1900-2020) time periods. In addition, we perform a first statistics of the earthquakes impact in Greece. Based on these examinations we (1) conclude that the interval from AD 1800 to 2020 is a suitable reference period for the organization of the Greek Earthquake Impact Database (GEIDB), and (2) explain the research strategy decided to follow for the selection of the best seismicity parameters to insert in GEIDB, a topic which is helpful to our analysis in the next Chapters.

1.2 Main geotectonic features and seismicity of the Greek region

In the last about 50 years the main geotectonic and geophysical properties of the region of Greece have been explained well in the frame of the plate tectonics in the eastern Mediterranean (Fig. 1.1). Such properties include the seismicity and earthquake focal mechanisms, the main geomorphological features of tectonic origin as well as the kinematics, geodynamics and volcanism of the region. The relevant literature includes many papers, books and theses and, therefore, we quote here only a few of them: Papazachos and Delibasis (1969), McKenzie (1970, 1972, 1978), Papazachos and Comninakis (1971), Ninkovich and Hays (1971, 1972), Boccaletti et al. (1974), Makris (1976, 1978), Le Pichon and Angelier (1979), Papazachos and Papadopoulos (1979), Papadopoulos (1982), Rotstein (1985), Spakman et al. (1988), Papadopoulos et al. (1986), Papazachos and Nolet (1997), Armijo et al. (2004), Taymaz et al. (1990, 1991), Kahle et al. (1995, 2000), McClusky et al. (2000), Sachpazi et al. (2000, 2016), Laigle et al. (2004), Bohnhoff et al. (2005), Sodoudi et al. (2006), Papanikolaou and Royden (2007), Ganas and Parsons (2009), Hollenstein et al. (2008), Floyd et al. (2010), Reilinger et al. (2006, 2010), Becker and Meier (2010), Shaw and Jackson (2010), Nocquet (2012), Jolivet et al. (2013), Kaviris et al. (2015), Mouslopoulou et al. (2015), Papadimitriou et al. (2015), Kassaras et al. (2016), Evangelidis (2017), Bocchini et al. (2018), Halpaap et al. (2018), Hansen et al. (2019), Le Pichon (2019), Kassaras et al. (2020), Maggini and Caputo (2020).

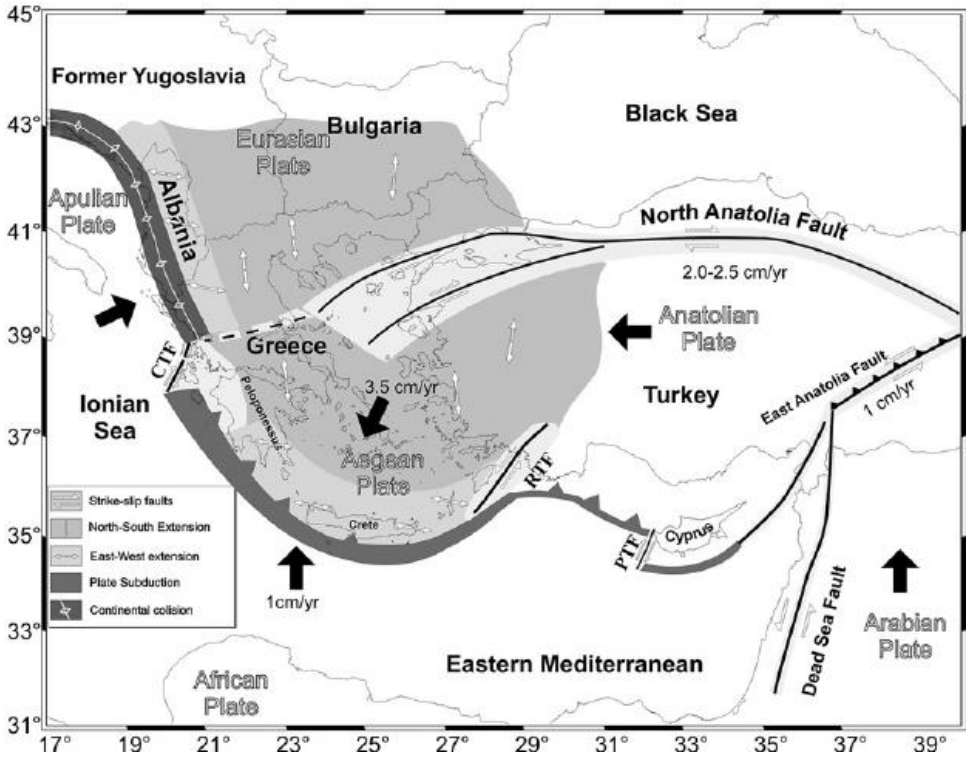

Figure 1.1. Main geotectonic features in the eastern Mediterranean region (adapted from Papazachos and Papazachou, 2003).

The geotectonics in the Greek region are illustrated in Figures 1.1 and 1.2. It is evident that the region is dominated by four main features: (1) the Hellenic Subduction Zone (HSZ), which is associated with compressional field along a system of trenches called the Hellenic Trench, (2) the back-arc area, which extends in the Aegean Sea, in continental Greece, and in western Turkey, and is characterized by ~N-S tensional field, (3) the dextral strike-slip branches of the North Anatolian Fault that interrupt the tensional field in the area of the North Aegean Trough (NAT), and (4) the South Aegean volcanic arc comprising several volcanic centers, three of them being active (Santorini, Nisyros, Methana). The HSZ in its NW and SE terminations turn to transform faults known as CTF (C or K stands for C(K)ephalonia) and RTF (R stands for Rhodes).

Most of the seismic activity in the Greek region is due to tectonic earthquakes. Magnitudes up to ~M8 have been estimated for large earthquakes taking place along the Hellenic subduction zone, such as the 365 and 1303 AD earthquakes of M~8.3 and M~8.0, respectively (see reviews in Papazachos and Papazachou, 2003, Papadopoulos, 2011) (Fig. 1.2). Volcanic earthquakes, usually small but occasionally strong ones (M~6), occur along the active South Aegean volcanic arc, which geographically coincides with the isodepth of ~150 km of the intermediate-depth earthquake foci (Fig. 1.2). Very small earthquakes due to the collapse of underground karst cavities occur frequently in several places of Greece.

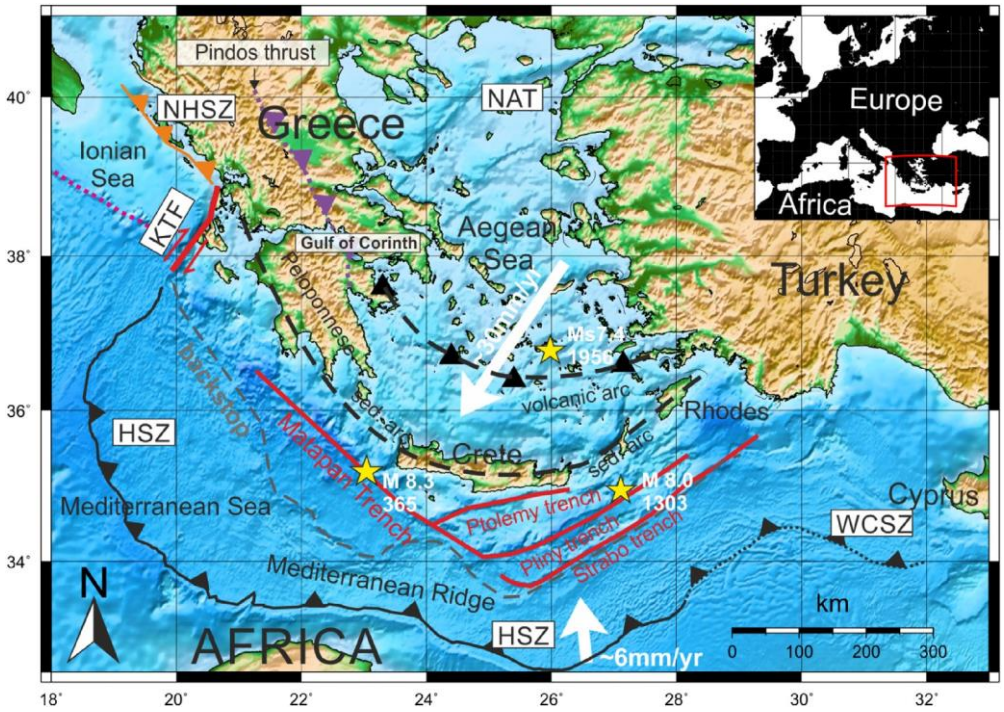

Figure 1.2. Main geotectonic features in the region of Greece (adapted from Bocchini, 2018).

1.3 Major developments in seismicity recording

1.3.1 A short overview

Historical seismicity data for the Greek region are available from the 6th century BC. The first primitive seismograph network installed in Greece comprised five mechanical instruments of Agamennone type, named thanks to G. Agamennone, Professor of Seismology in Rome. The instruments were installed at Athens station (ATH, June 1899) and in other stations in the next few years (Comninakis et al., 1987; more details are given in Chapter 3). Therefore, typically the instrumental period of the Greek seismicity started in 1900 and relevant seismic record data have been published in the Bulletins of the National Observatory of Athens (NOA) since that year. By the end of 1910 a Mainka instrument of intermediate natural period was installed at ATH station. For this reason the year 1911 is a turning point for the monitoring of Greek seismicity and, therefore, it has been quoted as the beginning of the instrumental era of Greek seismicity (Båth, 1983). Since 1911 the earthquake activity in Greece has been systematically recorded for magnitudes over 5.0.

A Wiechert instrument was installed at ATH station and operated since 1924. However, the publication of seismic record data in the Bulletins of NOA was interrupted in the period 1927-1949. This issue is examined and interpreted in Chapter 2 in the frame of the completeness analysis of the seismicity catalogues. The publication of seismic record data was recommenced in 1950. Other seismograph instruments were gradually added and the seismicity record of the region improved drastically particularly after the establishment in 1963 of the national seismograph network at the Institute of Geodynamics of the National Observatory of Athens (NOA) and its operation in the frame of the World-Wide Standardized Seismograph Network (WWSSN). Since that time several gradual improvements led to the modern Hellenic Unified Seismic Network (HUSN, http://www.gein.noa.gr/en/networks/husn). Currently, the HUSN operates under the coordination of NOA with the participation of, and significant contribution from, the geophysical divisions of the

National and Kapodistrian University of Athens, of the Aristotle University of Thessaloniki and of the University of Patras (https://bbnet.gein.noa.gr/HL/real-time-plotting/husn/husnmap).

1.3.2. Earthquake catalogues for the instrumental period (1900-2020)

Several earthquake catalogues covering the instrumental seismicity period have been published for Greece and the surrounding areas. In an extensive review of the seismology in Greece, Båth (1983) reported in details about the various earthquake catalogues published for that region and classified them in three different kinds: (a) catalogues for larger areas, of which Greece forms a part, (b) catalogues covering the Greek region and a fairly long period of time, (c) catalogues covering limited areas within Greece and/or limited periods of time. Although this is an old classification is still valid for the today existing catalogues. For the needs of our study only catalogues combining specifications of the kinds (a) and (b) are suitable since they cover the entire Greek region and are extended at long time intervals. Several catalogues satisfying these specifications exist, some of them being extended versions of previous ones. Specifications of these catalogues are summarized in Table 1.1.

Table 1.1. Summary of earthquake catalogues covering the Greek region for the instrumental seismicity period.

n.	*Reference*	*Area*	*Period*	*Specifications*
1	Gutenberg & Richter, 1954	the World	1904-1952	M>5.5
2	ISS	the World	1918-1963	M>5.5
3	Galanopoulos, 1960	32-43N, 17-30E	1801-1958	$MMI_o \geq VI$ or $M \geq 5$
4	Kárnik, 1969, 1996	Europe-Mediterranean	1901-1971	M>4.5
5	Shebalin et al., 1974	the Balkans	1901-1970	$M \geq 4.0$
6	Galanopoulos, 1981	32-43N, 17-30E	1902-1976	M>5.5
7	Engdahl et al., 1998	the World	1964-1995	M>5.2
8	Ambraseys, 2001	East Mediterranean	1900–1999	$M_S \geq 6.0$, shallow events
9	Burton et al., 2004	33–43N, 18-31E	1900–1999	$M_w \geq 4.0$, 1964-1999
10	Papazachos et al., 2010 (AUTH)	33-43N, 18-30E	1901–2010	$M_w \geq 5.2$, 1911-2010
11	Makropoulos et al., 2012 (UOA)	33-42.5N, 19-30E	1900–2009	M_S, $M_w \geq 5.5$, 1911-2009
12	SHEEC catalogue, 2012	Europe-Mediterranean	1900-2006	M_w>5.2, 1911-2006
13	EMEC catalogue, 2012	Europe-Mediterranean	1900-2006	M_w>5.2, 1911-2006
14	ISC-GEM, 2020	the World	1904-2016	$M_w \geq 5.40$
15	NOA	33-43N, 18-30E	1964-	$M_L \geq 4.5$
16	Global CMT project	the World	1976-	$M_w \geq 5.5$

Catalogues numbered from 1 to 6 in Table 1.1 have not been examined further in our analysis since they were taken into account in the compilation of most recent catalogues. The catalogue by Engdahl et al. (1998) is essentially the ISC-GEM catalogue. For this reason we eventually considered only the catalogues numbered from 8 to 16. In the next lines these catalogues are briefly reviewed.

Ambraseys (2001) catalogue

The catalogue compiled by Ambraseys (2001) for the Eastern Mediterranean region, including Greece, is extended from 1901 to 1998 and contains only shallow events truncated at lower magnitude M_s=6.0. On the other hand, the catalogue by Ambraseys (2001), which will be briefly called "AM catalogue", is homogeneous at large extent as regards magnitude. The reason is that M_s was calculated from bulletin readings of long-period phases for each event examined. In the AM catalogue seismic moment M_o was also listed for each event occurring after 1962 based on various sources, e.g. P/SH modelling or solutions by CMT, today GCMT project. Ambraseys (2001) assumed that $M_s \neq M_w$ and developed the empirical formula (1.1) between M_s and $\log M_o$:

$$\log M_o = 16.07 + 1.5\, M_s, \qquad M_s \geq 6.0 \quad (1.1)$$

This formula is nearly identical to the global relationship found by Hanks and Kanamori (1979):

$$\log M_o = 16.05 + 1.5\, M_s\,, \qquad M_s \geq 6.0 \quad (1.2)$$

Formula (1.1) permits calculation of M_w from M_s and is useful to our further analysis in Chapter 4.

Burton et al. (2004) catalogue

The catalogue by Burton et al. (2004) is rather inhomogeneous since its development relies primarily, during three different time periods, on the studies by Makropoulos and Burton (1981) for 1900–1963, Engdahl et al. (1998, essentially ISC-GEM data) for 1964-1998, and the Institute of Geodynamics of NOA for 1999.

Aristotle University of Thessaloniki (AUTH) catalogue

This earthquake catalogue covers the Mediterranean region, including Greece, for both the instrumental and historical periods. The catalogue is hosted at the website of the Geophysical Laboratory, Aristotle University of Thessaloniki (AUTH; http://geophysics.geo.auth.gr/ss/CATALOGS/seiscat.dat) and, therefore, it is briefly called the "AUTH catalogue". The instrumental part (1900-2010) of the AUTH catalogue is the last extended version of a series of previously published catalogues (e.g., Comninakis and Papazachos, 1986, Papazachos et al. 2000, 2010) and constitutes the result of a long-lasting effort that initially started at the Institute of Geodynamics of NOA with the compilation of a pioneering earthquake catalogue covering the time period 1911-1971 (Papazachos and Comninakis, 1972). The main achievement of that catalogue has been that magnitude, M, of sizable (magnitude ~5 and over) shallow shocks was directly measured from records either by the Wiechert or Mainka instruments installed at the ATH station. M was calculated from a relation proposed by Papazachos and Vasilicou (1966), which is similar to the relation introduced by Gutenberg (1945) for the calculation of surface-wave magnitude, M_s (see details in Chapter 3). Papazachos and Comninakis (1971) proposed a similar formula for the calculation of intermediate-depth earthquakes in Greece. However, for the time period 1900-1910 the AUTH catalogue relies at large extent on the European and Mediterranean earthquake catalogue published by Kárník (1969) and its updated version (Kárník, 1996).

The effort continued at AUTH and new data were utilized to show that the above relations are effective in calculating M_s of strong earthquakes ($6.0 \leq M_s \leq 8.0$) (Kiratzi and Papazachos, 1984, Kiratzi, 1989) and that magnitude M is equivalent to M_w for a wide range of magnitudes ($5.0 \leq M_s \leq 8.0$) (Papazachos, 1989, Papazachos et al. 1997). As a consequence, the routine calculation of magnitudes less than 6.0 has been possible. Around 1980 the operation of the Wiechert and Mainka instruments terminated. Then, M_s was calculated from a conversion relationship found between original ISC-GEM or NEIC magnitudes, M_s, and original local magnitudes, M_L, determined from the Wood-Anderson instrument at ATH station of NOA. In this way, the AUTH catalogue lists magnitudes equivalent to $M_w = M_s$ in its largest part. In the last years magnitude M_w directly calculated has been inserted, when possible.

The website of AUTH lists also a catalogue of earthquakes of M≥2.0 for the time period from 1.1.1995 up to the end of 2020 (last access 31.12.2020).

Catalogue compiled at the University of Athens (UOA)

The catalogue organized by Makropoulos et al. (2012) (http://www.nat-hazards-earth-syst-sci.net/12/1425/2012/nhess-12-1425-2012-supplement.zip), which covers the region of Greece for the time period 1900-2009, was compiled at the University of Athens and, therefore, hereafter will be called "UOA catalogue". This catalogue is an extended version of the ones initially compiled by Makropoulos (1978) and published by Makropoulos and Burton (1981) and Makropoulos et al. (1989). In the UOA catalogue both magnitudes M_s and M_w are listed. For the time period 1900-1963, M_s for an event was calculated only under the condition that ground amplitudes in long-period instruments at Uppsala (UPP) and Kiruna (KIR) stations were available. Then, M_s was calculated as the average of M_s values obtained by using the widely adopted Prague formula. Since 1964, when ISC-GEM commenced to publish m_b magnitude, M_s was calculated from the regression equation obtained from magnitudes M_s and m_b listed in the ISC-GEM catalog:

$$M_s = 1.37m_b(\text{ISC-GEM}) - 1.74 \quad (1.3)$$

Magnitudes M_w were collected from various sources including the GCMT project and M_s/M_w regression relationships developed by Makropoulos et al. (2012). In this way M_w was also inserted for all the events in the catalogue.

SHEEC and EMEC catalogues

The SHARE European Earthquake Catalogue (SHEEC) compiled in the frame of the EU-FP7 SHARE project (Stucchi et al., 2013), as well as the European-Mediterranean Earthquake Catalogue (EMEC, Grünthal and Wahlström, 2012, 2013), for the time period from 1900 to 2006 rely at large extent on the AUTH and UOA catalogues.

ISC-GEM global earthquake catalogue

The catalogue organized jointly by the International Seismological Center and the Global Earthquake Model is a reference global data compilation which is regularly updated (version v.7.0 released on 9 April 2020; http://www.isc.ac.uk/iscgem/; ISC-GEM, 2020) ISC-GEM, 2020) and covers the time period from 1900 (from 1904 for Greece) up to 2016. The ISC-GEM (2020) catalogue and its earlier versions were developed after re-computation of surface-wave magnitudes, M_s, and body-wave magnitudes, m_b, uniformly at large extent and with procedures detailed by Bondar and Storchak (2011), Bondar et al. (2015) and Di Giacomo et al. (2015, 2018). Re-computed magnitudes provided the basis for deriving new non-linear regression models and conversion relationships to moment magnitude, M_w. For the time period up to 1975 M_w proxies were inserted, instead of the re-computed M_S and m_b values, using the derived conversion relationships. However, directly measured M_W values as published by the GCMT project and by a large number of publications were inserted for the post-1975 period. The final magnitude composition in the ISC-GEM catalogue is an improvement in terms of magnitude homogeneity as compared to other catalogues. Although the ISC-GEM catalogue is regularly updated we utilized as working version the one released on 18 June 2018 (v.5.1; hereafter

"ISC-GEM catalogue") which practically is identical with the v.7.0 as regards data referring to the seismicity of Greece.

NOA catalogue

The seismicity database of the Institute of Geodynamics of NOA covers the time window from 1964 up to the present and is updated daily (http://www.gein.noa.gr/el/ seismikotita/katalogoi-seismwn). Local magnitude, M_L, determined from wave amplitudes recorded by the Wood-Anderson instrument at Athens station of NOA is listed in that catalogue. Since 2008, however, local magnitude is calculated from synthetic Wood-Anderson measurements.

GCMT project global earthquake catalogue

The GCMT project global earthquake catalogue (https://www.globalcmt.org/) starts in 1975, extends up to the present, is regularly updated and lists earthquakes of magnitude M_w over ~5.5. The basic methodology and approach is described by Dziewonski et al. (1981), while the most recent description of how the centroid moment tensor (CMT) analyses have been conducted, including a number of significant improvements to the analysis, are provided by Ekström et al. (2012).

From the previous short review we concluded that five catalogues covering the Greek region are extended to a sufficiently long period and, at the same time, do not rely to other catalogues at large extent: (1) the global ISC-GEM catalogue; (2) the catalogue of GCMT project; (3) the AM (Ambraseys, 2001) catalogue of strong earthquakes for the region of Eastern Mediterranean and Middle-East, (4) the UOA catalogue by Makropoulos et al. (2012); (5) the AUTH catalogue by Papazachos et al. (2010). In the catalogue of GCMT project the earthquake magnitudes are in M_w scale. The ISC-GEM and AUTH catalogues list magnitudes in M_w scale or proxy M_w. The catalogue of UOA lists both M_s and proxy M_w, while the AM catalogue lists M_s but one may convert M_s to M_w through formula (1.1).

1.3.3 Seismicity catalogues for the historical period (6th century BC-1899 AD)

Data for the historical period of Greek seismicity can be found in a long list of descriptive and/or parametric earthquake catalogues. The tradition goes back before the 19th century but reviewing such old catalogues is beyond the scope of the present study. Besides, old catalogues have been reviewed by, and taken into account in, more recent publications. In the 19th and 20th centuries worldwide earthquake catalogues containing data for the Greek seismicity include those by Perrey (1844-1873) and Mallet (1850-58) and later by Montesus de Balore (1906), Milne (1912), Sieberg (1932), Montandon (1953) and Rothé (1969).

In the 20th century, published local, national, regional or European catalogues include the ones by Galanopoulos (1960, 1961, 1981), Kárník (1971, 1996), Shebalin et al. (1974), Comninakis and Papazachos (1986), Papazachos and Papazachou (1989, 1997, 2003), Spyropoulos (1997), Guidoboni et al. (1994), Papadopoulos et al. (2000, 2014b), Guidoboni and Comastri (2005), Papazachos and Papazachou (2003), Ambraseys (2009) and Papadopoulos (2011). A recent development has been the release of the last version of the parametric and descriptive Catalogue of Strong Earthquakes in Italy and in the Mediterranean area, termed CFTI5Med (Guidoboni et al., 2019). In addition to being

available on an INGV website (https://doi.org/ 10.6092/ingv.it-cfi5) the full dataset is published in the PANGAEA® Data Publisher (Guidoboni et al., 2018). CFTI5Med stores information on 1,259 earthquakes (98 of which are currently considered false) that occurred in Italy from 461 B.C. to 1997, and 475 earthquakes that occurred in the extended Mediterranean area, including Greece, from 760 B.C. to AD 1500. Essentially, as regards Greece the CFTI5Med lists earthquakes already known from previous publications.

Table 1.2 summarizes specifications of the historical earthquake catalogues published since 1960. The catalogues numbered from 1 to 6 have been taken into account in later publications and catalogues. Spyropoulos (1997) compiled a descriptive catalogue which is relying extensively on the catalogues by Papazachos and Papazachou (1989, 1997). The catalogue by Papazachos et al. (2000) is a more complete version of the parametric part of the catalogue by Papazachos and Papazachou (2003) since the last contains data only for large earthquakes (M≥6.0).

SHARE European Earthquake Catalogue (SHEEC), compiled in the frame of the project SHARE (Stucchi et al., 2013), relies partly on the Papazachos and Papazachou (2003) catalogue, while the European-Mediterranean Earthquake Catalogue (EMEC, Grünthal and Wahlström, 2012, 2013) relies on that catalogue at large extend. The work by Ambraseys (2009) is the most comprehensive descriptive catalogue for the region but it provides earthquake parameters only occasionally. On the other hand, the Papazachos and Papazachou (2003) catalogue remains the only one which is descriptive and parametric for the entire historical period, i.e. from the 6th century BC up to 1899 and is extended in the instrumental period up to 2001.

Based on the previous analysis we suggested that the historical catalogues which are suitable for our further analysis are the ones by Papazachos et al. (2000), Ambraseys (2009) and SHEEC (2012). Papazachos and Papazachou (2003)

Table 1.2. Summary of the most recent historical earthquake catalogues covering the entire Greek area. Key: MMI_o=maximum intensity in MM scale, P=parametric, D=descriptive, sP=semi-parametric.

n.	*Reference*	*Area*	*Time Period*	*Specifications*
1	Galanopoulos, 1960	32-43N, 17-30E	1801-1899	MMI_o≥VI, P
2	Galanopoulos, 1961	32-43N, 17-30E	Prior 1800	MMI_o≥VII, P
3	Kárník, 1971, 1996	Europe-Mediterranean	1801-1900	MMI_o≥VII, DP
4	Shebalin et al., 1974	Balkans	Prior 1900	MMI_o≥VI, P
5	Galanopoulos, 1981	32-43N, 17-30E	Prior 1900	MMI_o≥VII, P
6	Papazachos & Comninakis, 1982	32-43N, 18-30E	Prior 1900	M_{min}≥6.5, P
7	Papazachos & Papazachou 1989, 1997, 2003	32-43N, 18-30E	Prior 1900	M_{min}≥6.0, DP
8	Guidoboni et al., 1994	Mediterranean	Prior 1000	D
9	Spyropoulos, 1997	32-43N, 18-30E	Prior 1900	M_{min}≥6.0, sP
10	Papazachos et al., 2000	32-43N, 18-30E	Prior 1900	M_{min}≥4.5, P
11	Guidoboni and Comastri, 2005	Mediterranean	1000-1500	D, sP
12	Ambraseys, 2009	Mediterranean	Prior 1900	D, sP
13	SHEEC catalogue	Europe-Mediterranean	1000-1899	P
14	EMEC catalogue	Europe-Mediterranean	1000-1899	P
15	CFTI5Med	Mediterranean	Prior 1500	P

1.4 Determination of the study reference time period

One of the main objectives of this study is to organize the Greek Earthquake Impact Database (GEIDB). To analyze the impact of earthquakes, e.g. fatalities or building damage, and examine the

dependence of the various impact metrics on seismicity parameters, in the GEIDB we need to organize not only a section on the earthquake impact data but also a seismicity data section. The determination of the time period covered by the GEIDB and the procedures for the seismicity data set selection among the various seismicity catalogues available are topics examined in the next subsections.

1.4.1 Reporting of destructive earthquakes: a first statistics

To obtain a preliminary view of the completeness of the earthquakes impact reporting in Greece we performed a first statistics based on the publication by Papazachos and Papazachou (2003). The selection of this publication has been made for the reason that it contains not only a seismicity catalogue but also earthquakes impact data, such as descriptions of the earthquake effects in the built and the natural environment, as well as impact metadata is terms of macroseismic intensity. The earthquakes considered in this analysis are the ones that caused maximum macroseismic intensity, I_o, of at least degree VII in the 12-grade Modified-Mercalli (MM) or in the EMS-98 scales.

Figure 1.3 illustrates the frequency of earthquakes occurring from the 6th century BC up to the year AD 2001 and counted in 50-year time intervals. Three earthquake data sets are plotted: (1) all earthquakes, regardless their maximum Modified-Mercalli (MM) intensity, I_o; (2) destructive earthquakes with $MMI_o \geq VIII$; (3) damaging earthquakes with $MMI_o = VII$. The low earthquake frequency reported until the beginning of 15th century indicates highly incomplete earthquake catalogue. After that period, however, the event reporting increased quasi-exponentially. A similar preliminary result was found earlier by Papadopoulos (1988).

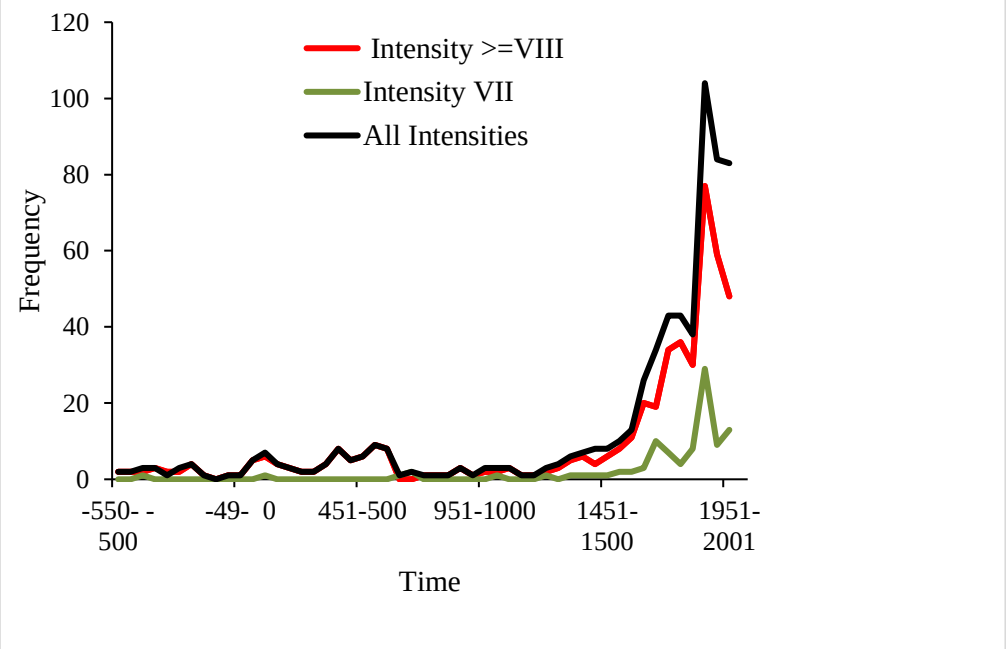

Figure 1.3. Frequency distribution of earthquakes occurring in Greece from the 6th century BC up to AD 2001; frequency is counted in 50-year time intervals.

On the other hand, until about the beginning of the 17th century the earthquake reporting is dominated by destructive events, while the reporting of damaging events is minimal. After that period, however,

the reporting of damaging events increases as well. We found that the mean rate, *d*, of high-impact (destructive) earthquakes is d_1=1.04 events/yr for the 19th century (1800-1899) and d_2=1.09 events/yr for the 20th century (1900-2001). On the contrary, the rate *d* decreases backwards, e.g. d_3=0.7 events/yr was found for the 18th century data. These results indicate that the reporting of destructive earthquakes in the Greek region remained constant in the last two centuries providing evidence that the reporting of such earthquakes is nearly complete since about AD 1800. We also suggested that only very few high-impact earthquakes could have escaped the historical record in the post-1800 time period.

The preliminary statistics of the earthquakes impact in Greece is based on data regarding only strong earthquakes of magnitude M≥6.0 since this is the lowest magnitude threshold considered in the catalogue by Papazachos and Papazachou (2003). From other sources, however, we found that the minimum magnitude of earthquakes that caused even limited impact in Greece is M_{IMP}~5.0. For example, on 31st August 1989 a moderate earthquake (M_w=4.7) caused limited building damage and ground failure in the city of Patras. In Milos Island, two moderate earthquakes occurring on the 11th and 30th September of 1918 with magnitudes M_w=4.9 and M_w=5.2, respectively, caused damage in houses and in churches. More details and additional examples can be found in Chapter 5. This result is consistent with the findings of other authors in other seismogenic regions of the world. As an instance, in China Chen et al. (2005) found M_{IMP}=5.0, while according to Chaoxu et al. (2020) M_{IMP}=4.7.

1.4.2 Reporting of earthquakes that caused environmental effects

Based on the publication by Papazachos and Papazachou (2003) we also investigated the environmental effects of the earthquakes occurring in the Greek region from the 6th century BC up to the year AD 2001. From Figure 1.4 it is evident that the reporting of various types of earthquake-induced environmental effects, such as hydrological changes, soil liquefaction, landslides and other types of ground failures, e.g. surface fault traces, ground fissures and cracks, is vastly incomplete until the 15th century. However, since the 16th century the reporting of earthquake-induced ground failures gradually increases particularly after AD 1800. These results are consistent with the results obtained earlier regarding the reporting of destructive earthquakes as illustrated in Figure 1.3.

From various sources it has been found that the minimum magnitude of earthquakes causing ground failures in the Greek region is M_{IMP}~5.0; see Papadopoulos and Lefkopoulos (1993) and Papathanassiou et al. (2005) for soil liquefaction and Papadopoulos and Plessa (2000) for landslides. This result is consistent with the M_{IMP} found in other seismogenic regions, e.g. in Italy (Martino et al., 2014).

Further examination of the environmental effects of the earthquakes is beyond the scope of this study. Tsunamis, however, is an exception for the reason that historical tsunamis have caused remarkable impact in the Greek region. Therefore, a detailed study has been performed in Chapter 7.

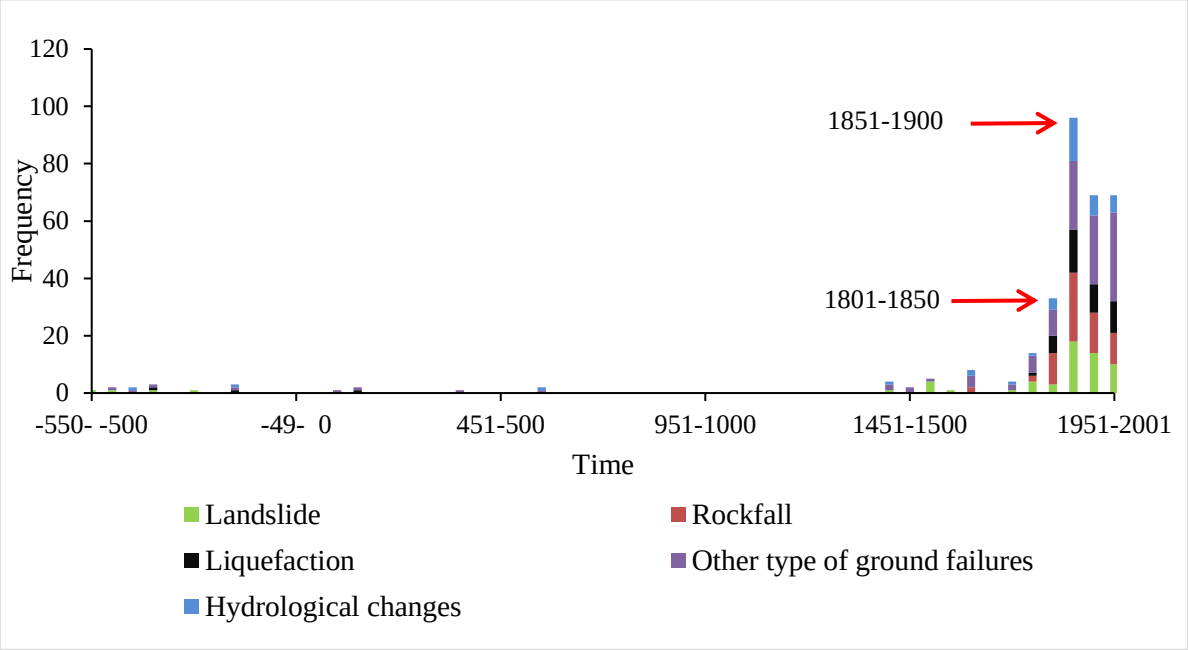

Figure 1.4. Frequency distribution of earthquakes that occurred in Greece from the 6th century BC up to AD 2001 and caused various types of ground failures; frequency is counted in 50-year time intervals.

1.4.3 Reporting of earthquakes impact: first concluding remarks

Since the reporting of destructive earthquakes ($MMI_o \geq VIII$) is nearly complete since about AD 1800 up to the present time, we concluded that the time interval 1800-2020 is a suitable reference period for the organization of the GEIDB. This, however, does not imply that our examination has been restricted to earthquakes of only $MMI_o \geq VIII$. On the contrary, in the GEIDB we inserted earthquakes impact data regardless the magnitude and the maximum intensity of the relevant seismic events. The only restriction criteria adopted are that the earthquakes should have occurred in the Greek region in the post-1799 time interval.

On the other hand, an important issue is the selection of the seismicity parameters for the earthquakes included in the GEIDB. This is issue is quite challenging since several earthquake catalogues are available for both the historical and instrumental periods of seismicity. Therefore, in the next lines we explain briefly the research step undertaken to select seismicity (focal) parameters for the earthquakes which are inserted in the GEIDB.

1.5 Research strategy for the selection of seismicity parameters

Based on the major developments in seismicity monitoring of the Greek region we may distinguish three main seismicity periods during the reference period of 1800-2020: (1) 1800-1899: this is the period of historical earthquake record; (2) 1900-1910: this the early instrumental period of seismicity; (3) 1911-2020, which is the instrumental period of seismicity.

The review of the various earthquake catalogues available for the Greek region showed that five instrumental and three historical catalogues are in principle the most suitable for our further analysis. However, these earthquake catalogues discussed earlier do not cover the same time periods and are characterized by different homogeneity, completeness level and accuracy in different time segments. For these reasons none of the catalogues available could serve the needs of our study for the entire

reference time interval which is extended from AD 1800 to 2020. To meet this challenge, we developed a research procedure to select the "best" data sets for the various time segments of the period under examination. To this aim three different methodological strategies were followed for the three main time periods.

1.5.1 Historical period (AD 1800-1899)

Based on the analysis in section 1.3.3 a statistical comparison has been performed in Chapter 2 among the catalogues by Papazachos et al. (2000) and Papazachos and Papazachou (2003) on one side and the SHEEC catalogue (Stucchi et al., 2013) on the other. The Ambraseys (2009) catalogue is also discussed as regards its parametric part.

1.5.2 Early instrumental period (1900-1910)

The earthquake catalogues available for the early instrumental period of Greek seismicity have been discussed earlier and are those of AM, AUTH, ISC-GEM and UOA. Their specifications have been summarized in Table 1.1. In Chapter 3 a comparison of these catalogues showed important differences in homogeneity and in completeness level. Therefore, we developed a procedure of proxy M_w magnitude redetermination for 52 moderate and strong earthquakes by utilizing, for the first time, Agamennone seismograph records as listed in the Bulletins of NOA. Then, the criteria used to select seismicity parameters for this time period are explained.

1.5.3 Instrumental period (1911-2020)

The selection of seismicity parameters for this time interval is examined in Chapter 4. A first step has been to compare the various catalogues available (AM, AUTH, ISC-GEM, GCMT project, UOA) as regards their completeness level, magnitude differences and focal depth differences with the use of statistical methods (e.g. z-map toolbox). This examination concluded with the determination of the features, i.e. completeness, accuracy and homogeneity, characterizing the various catalogues in certain time segments of the entire period. Then, the criteria used to select seismicity parameters for each time segment are explained.

1.6 Summary of Chapter 1

Seismicity data of the Greek region have been compiled in various parametric and descriptive earthquake catalogues covering both the historical period, which extends from the 6th century BC up to AD 1899, and the instrumental period from 1900 to 2020. The reporting of earthquakes is vastly incomplete until the beginning of the 15th century. Since that time, however, the reporting of the seismic events as well as of the earthquake impact data increases quasi-exponentially. On the other hand, there is evidence that the reporting of high-impact events, i.e. of $MMI_o \geq VIII$, has been nearly complete since AD 1800. Therefore, the time interval from 1800 to 2020 has been selected as the reference period to be considered in the Greek Earthquake Impact Database (GEIDB). For the selection of data for the seismicity section of the GEIDB, different research procedures have been followed for each one of the three main seismicity periods: (1) historical earthquake period (1800-1899); (2) early instrumental period of seismicity (1900-1910); (3) instrumental period of seismicity (1911-2020). These procedures are analyzed in details in Chapters 2, 3 and 4.

CHAPTER 2. COMPLETENESS ANALYSIS OF GREEK SEISMICITY CATALOGUES: 1800-2020

2.1 Introduction

To investigate the best seismicity parameters, which are suitable to insert in the Greek Earthquake Impact Database (GEIDB), the first step has been the performance of a completeness analysis of catalogues available for the Greek region. Both the historical (AD 1800-1899) and the instrumental periods of seismicity (1900-2020) have been analyzed in this Chapter, which starts with a short review of modern techniques in use for catalogue completeness determination. This type of analysis has been performed with the statistical ZMAP MATLAB package, available at http://www.earthquake.ethz.ch/software/zmap (Wiemer, 2001).

2.2 Methods for catalogue completeness analysis

The magnitude of completeness, Mc, in a given earthquake catalogue is meant as the lowest magnitude at which 100% of the events are included. The determination of Mc is not an easy task since Mc depends on several factors. Therefore, various methods to determine Mc in a catalogue have been developed and tested with various seismicity data sets. A comprehensive tutorial about the various peer-reviewed methods to estimate and map Mc has been provided by Mignan and Woessner (2012). According to these authors there are two classes of methods developed for assessing Mc: the catalogue-based and the network-based methods (Fig. 2.1). The computation of Mc with the catalogue-based methods is based on readily accessible parametric catalogue data. On the other hand, the class of network-based methods requires the use of phase-pick or waveform data. In this study the network-based approach is not applicable for a time period as long as 120 years of seismicity. Therefore, our analysis has been based on catalogue-based methods which are straightforward.

Most of the catalogue-based methods assume the validity of the frequency-magnitude distribution, FMD, known as Gutenberg-Richter (1944) or simply G-R law, which is expressed by the formula:

$$\log N = \alpha - b\,M \quad (2.1)$$

N is either the discrete frequency of magnitudes M in each magnitude bin or the cumulative frequency of magnitudes ≥M; α, b are parameters determined by the data, where b is the slope of the FMD line and α expresses the seismicity level. The main distinction between various catalogue-based methods is whether the technique applied is parametric or non-parametric. Parametric techniques are based on fitting the FMD, while non-parametric techniques are based on the evaluation of changes in the FMD, such as possible breaks in the slope.

Among the non-parametric methods, the Maximum Curvature (MAXC) technique (Wyss et al. 1999; Wiemer and Wyss 2000) is a fast and straightforward way to estimate Mc. It consists in defining the point of the maximum curvature by computing the maximum value of the first derivative of the G-R curve. Practically speaking, MAXC matches the magnitude bin with the highest frequency of events in the non-cumulative FMD. On the other hand, the Goodness-of-Fit Test (GFT), proposed by Wiemer and Wyss (2000), is one of the most used among the parametric methods. GFT calculates Mc by comparing the observed FMD with synthetic ones. Mc is defined as the first magnitude bin at

which the residual falls below the horizontal line of the 95% confidence level fit. When the 95% level of fit is not obtained, a 90% level is an alternative. Pros and cons of the various techniques are summarized by Mignan and Woessner (2012).

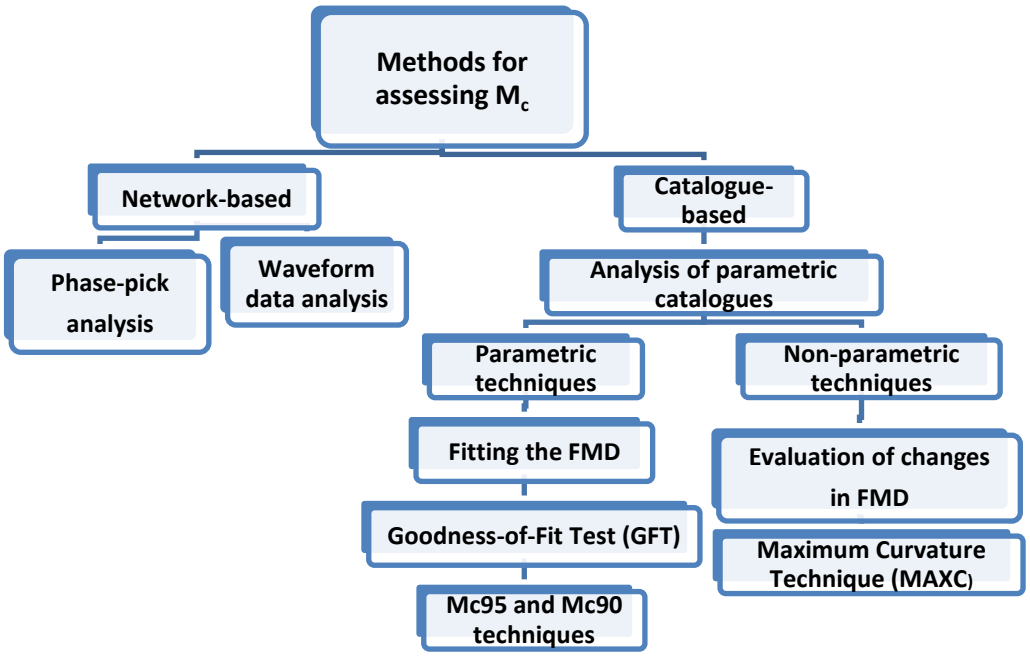

Figure 2.1. Modern techniques which are in use for the assessment of the completeness magnitude, Mc, according to the tutorial by Mignan and Woessner (2012): FMD=Frequency-Magnitude Distribution.

2.3 Completeness analysis of historical catalogues (1800-1899)

2.3.1 Data

Specifications of the main parametric earthquake catalogues that cover the time window AD 1800-1899 are summarized in Table 1.2. From the specifications of these catalogues it was found that in principle the most suitable for further consideration are the parametric catalogues by Papazachos et al. (2000), Papazachos and Papazachou (2003) and SHEEC (Stucchi et al., 2013). On the other hand, the work by Ambraseys (2009) is an extensive descriptive catalogue, which provides earthquake magnitude only occasionally. In addition, only magnitude ranges have been estimated in that catalogue, e.g. magnitude ranges from 5 to 6 or from 6 to 7 and so on. For this reason the parametric part of the Ambraseys (2009) catalogue is not considered further in the present analysis. However, the descriptive part of the catalogue is still quite useful for the collection of earthquake impact data as explained in Chapter 5.

The SHARE European Earthquake Catalogue (SHEEC) compiled in the frame of the EC-FP7 project SHARE (Stucchi et al., 2013), as well as the European-Mediterranean Earthquake Catalogue (EMEC, Grünthal and Wahlström, 2012, 2013), both have used various catalogue sources. In the EMEC catalogue the focal parameters have been extensively adopted by Papazachos and Papazachou (2003). In the SHEEC catalogue earthquake focal parameters, including magnitudes proxy M_w, have been either estimated from Macroseismic Data Points (MDP's) or adopted by Papazachos and Papazachou

(2003). The minimum magnitudes inserted in the SHEEC and the Papazachos and Papazachou (2003) catalogues are 5.38 and 6.0, respectively.

We compared the magnitudes listed in the SHEEC and in the Papazachos and Papazachou (2003) catalogues, $M_{w(SH)}$ and $M_{w(PP)}$, respectively, and found that they are correlated well enough (Fig. 2.2). However, $M_{w(PP)}$ as an average is slightly overestimated with respect to $M_{w(SH)}$ given that the difference $\delta=M_{w(PP)}-M_{w(SH)}$ has been found equal to 0.12 ± 0.24.

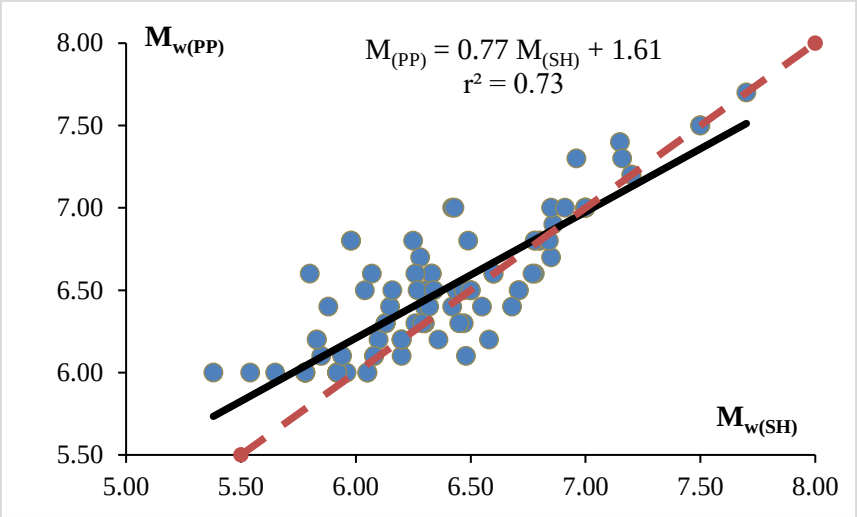

Figure 2.2. Magnitude $M_{w(PP)}$ against $M_{w(SH)}$ for the historical earthquakes occurring in the Greek region in the time period 1800-1899. Solid line shows the best-fit regression; r=correlation coefficient; red dashed line represents $M_{w(PP)}=M_{w(SH)}$.

2.3.2 Completeness analysis

In the catalogue by Papazachos et al. (2000), which lists more events than the Papazachos and Papazachou (2003) one, all the events listed have estimated magnitude. For the time period 1800-1899 the number of events is n=269, the estimated magnitude ranges from 4.6 to 7.7 and the focal depth ranges from 0 to 150 km. In the SHEEC catalogue the number of events with estimated or adopted magnitude is n=135, while the ranges of magnitude and focal depth are identical with those in Papazachos et al. (2000).

Testing for completeness the catalogue by Papazachos et al. (2000) we found that the MAXC solution provides completeness magnitude threshold Mc=4.8 (Fig. 2.3). This is due to that the frequency of magnitude 4.8, which equals to 56, disproportionately exceeds the frequency of other magnitude bins in this catalogue (Fig. 2.4). A consequence is the estimation of a too low b-value of 0.37. We checked the catalogue and concluded that nearly all the events with magnitude of 4.8 are independent, i.e. they are not foreshocks or aftershocks of larger events. Unfortunately, the Mc90 and Mc95 techniques of the GFT method are not applicable due to the low number of events in the catalogue. The distribution of magnitude frequency (Fig. 2.4) implies that Mc around 6 is a more realistic solution. On the other hand, Mc=5.8 was found for the SHEEC catalogue (Fig. 2.3), which is characterized by the highest magnitude frequency at the 5.8 magnitude bin (Fig. 2.4). A more reasonable b-value of 0.74 was estimated.

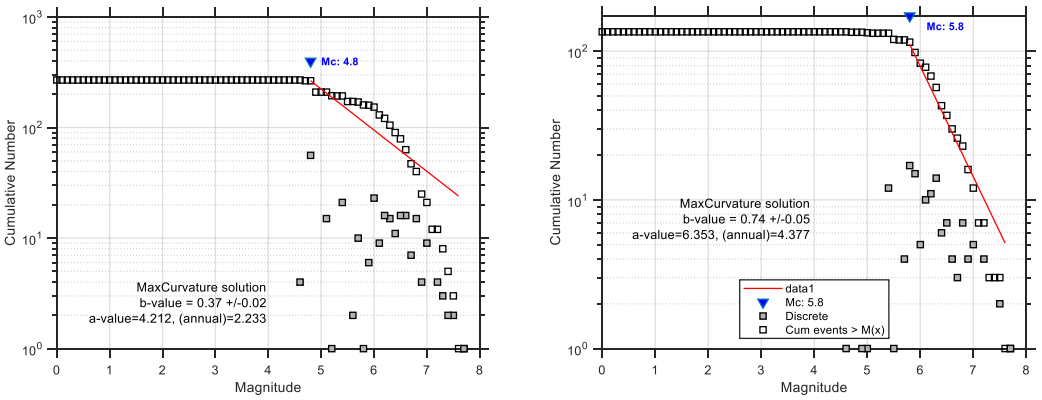

Figure 2.3. Magnitude-frequency distribution for the historical (AD 1800-1899) catalogues by Papazachos et al. (2000) (left) and by SHEEC (right).

A characteristic of both catalogues is the non-linear rate of seismicity as reflected in the diagrams of Figure 2.5. These diagrams show an increase of the events listed in both catalogues during the second half of the 19th century. Namely, the seismicity rate (in events/year) in the Papazachos et al. (2000) catalogue in the first and the second half of the 19th century is r_{1P}=0.96 and r_{2P}=4.4, respectively, while the respective rates in the SHEEC catalogue are r_{1S}=0.7 and r_{2S}=2. This indicates that both catalogues are more complete in the second half than in the first half of the 19th century.

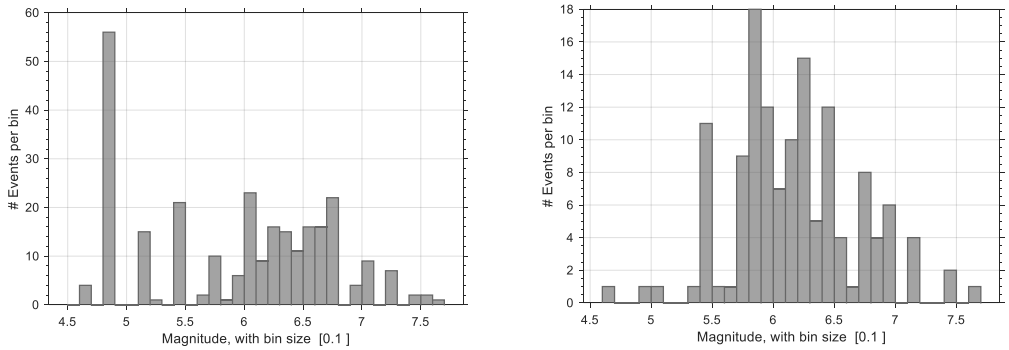

Figure 2.4. Magnitude frequency for the historical (AD 1800-1899) catalogues by Papazachos et al. (2000) (left) and by SHEEC (right).

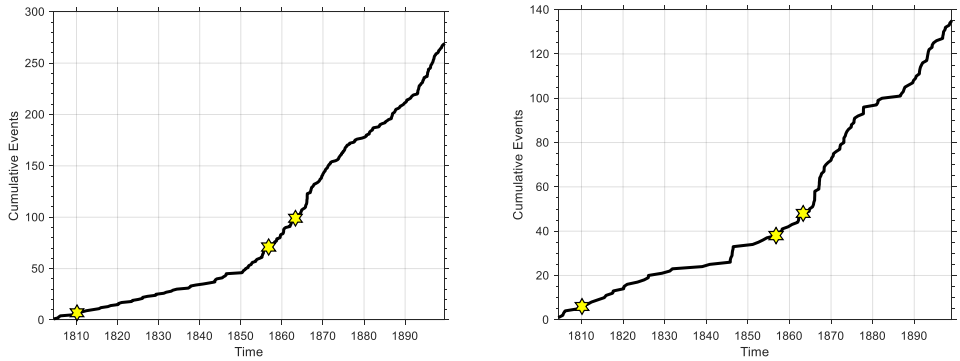

Figure 2.5. Cumulative number of seismic events against time for the historical (AD 1800-1899) catalogues by Papazachos et al. (2000) (left) and by SHEEC (right). Stars illustrate dates of large magnitude (≥7.5) events: 1810, 1856 and 1863.

2.4 Completeness analysis of Greek instrumental catalogues

Various methods, have been applied to investigate the magnitude of completeness of the Greek seismicity in the post-1963 time period based on the NOA catalogue (e.g. D'Alessandro et al., 2011, Deshcherevskii and Sidorin, 2012, Leptokaropoulos et al., 2013, Mignan and Chouliaras, 2014). On the other hand, Makropoulos et al. (2012) and Papazachos et al. (2000, 2010) analyzed the magnitude of completeness for their own catalogues, i.e. UOA and AUTH, respectively. However, this is the first time to use modern techniques for a comparative analysis of the completeness levels of different catalogues covering the Greek region and the entire post-1899 time period.

2.4.1 Data

In Chapter 1 we reviewed the instrumental earthquake catalogues available for the Greek region and concluded that five of them are in principle suitable for our analysis. The reason is that these catalogues cover the entire region (latitude 33^o-43^{o}N, longitude 18^o-30^{o}E) and each one of them extends to a significant time interval without relying extensively on other catalogues. The five catalogues and their respective magnitude scales used are summarized as follows: (1) the global earthquake catalogue of the GCMT project (M_w scale, https://www.globalcmt. org/); (2) the ISC-GEM catalogue, working version v.5.1/2018 (M_w scale http://www.isc. ac. uk/ iscgem/); (3) the AM catalogue (Ambraseys, 2001, M_s scale and a $\log M_o/M_s$ empirical relationship); (4) the UOA-University of Athens catalogue (Makropoulos et al., 2012; M_s and M_w scales, http://www.nat-hazards-earth-syst-sci.net/12/1425/2012 /nhess-12-1425-2012supplement.zip); (5) the AUTH-Aristotelian University of Thessaloniki catalogue (Papazachos et al., 2010; M_w scale, http://geophysics.geo. auth.gr/ss CATALOGS/seiscat.dat).

The global earthquake catalogue of the GCMT is a long-lasting project based on a procedure of regular updating of the catalogue and covering the time interval from 1976 up to the present with earthquakes of magnitude about M_w5.5 and over for the entire period. One of the important features of the GCMT project global catalogue is its homogeneity as regards the magnitude determinations. The basic methodology and approach is described by Dziewonski et al. (1981) while the most recent description of how the CMT analyses have been conducted, including a number of significant improvements to the analysis, are provided by Ekström et al. (2012). The GCMT project catalogue is generally considered as a standard and reliable reference source recognized worldwide. For these reasons, the M_w magnitudes estimated in the GCMT catalogue have been adopted for the 1976-2020 time period.

As a consequence, four catalogues remained for comparison, i.e. AM, ISC-GEM, UOA and AUTH. The characteristics of the four catalogues are summarized in Table 2.1. Since the AM catalogue lists only a small number of events, all of $M_w \geq 6.0$ by default, further completeness analysis was eventually performed for pairs of the rest three catalogues. The analysis, however, have not been restricted to the pre-1976 time period. On the contrary, it was extended to the entire time period covered commonly by each pair of catalogues, e.g. 1905-2009 when comparing ISC-GEM with UOA and so on. The aim is to utilize earthquake samples as large as possible. In all catalogues M_w magnitudes have been compared for reasons of consistency.

Table 2.1. Features of the catalogues used in the statistical examinations.

Catalogue	Number of events	Time period	M_{min}	Focal depth
ISC-GEM	563	1905-2014	M_w=5.4	all depths
UOA	7352	1900-2009	M_w=4.1, M_s=4.0	all depths
AUTH	10786	1900-2010	M_w=4.5	all depths
AM	135	1900-1999	M_s=6.0	shallow≤40 km

2.4.2 Completeness analysis

The completeness level of a seismicity catalogue extended in a long time interval such as the entire instrumental period from 1900 up to 2020, is susceptible to various spatio-temporal heterogeneities. This is due to several factors, which are of two types, geophysical and artificial or human-made. The geophysical factors include transient seismicity changes as well as seismotectonic complexity. Spatio-temporal earthquake clusters, such as aftershock sequences and swarm activities, are usual causes of transient seismicity changes. Seismotectonic complexity is reflected in the different long-term seismicity rates characterizing different tectonic segments. This factor includes also the generation of not only shallow but also of intermediate-depth earthquakes. Shallow earthquakes occur everywhere in the Greek region but the intermediate-depth events are restricted at the southern part of the region as a result of the active lithospheric subduction along the Hellenic arc. On the other hand, the gradual improvement of the seismographic coverage and monitoring procedures of the region since 1911, particularly after 1963, concluded in very important artificial changes in the recorded seismicity. These changes have been caused by the drastic upgrades of the instrumental networks, of the methods used for magnitude and location determinations and of the software used (see short overview in Chapter 1).

To investigate the Mc in the three seismicity catalogues of ISC-GEM, UOA and AUTH we used two different techniques. The first considers the change of Mc with time as a continuous variable by keeping stable the predefined sample size and the percentage of overlapping between samples. This approach revealed better the main artificial factors that affected the monitoring and cataloguing of the Greek seismicity. With the second technique the Mc was estimated for certain discrete time segments of each catalogue. The catalogue time segments were determined on the basis of the main human-made factors that affected the earthquake cataloguing in the region found from the results of the first technique. In both techniques, Mc is calculated with the MAXC and GFT methods, if applicable.

2.4.3 Results

Time variation of Mc

The application of the technique of Mc time variation proved quite unstable with the ISC-GEM catalogue due to the relatively small number of events (n=562) contained in this catalogue. Therefore, this technique was applied only to the AUTH and UOA catalogues. The results obtained with this technique by applying the method MAXC for Mc estimation are illustrated in Figure 2.6. Similar results were obtained with the application of GFT-90% method but the results of MAXC are of better

smoothness. The results obtained are explainable on the basis of not only the procedures used for magnitude determinations in each catalogue but also by human-made factors that affected the seismicity monitoring.

In the AUTH catalogue some remarkable Mc changes are evident (Fig. 2.6). The first is the gradual decrease of Mc after 1911 when the operation of the first reliable seismometer of Mainka type started at ATH station. This trend lasted for about ten years. However, from the mid 1920's the Mc value increased gradually until the end of 1940's, although a two-horizontal component Wiechert-type seismometer was already installed and operated since the year 1924, while one more of similar type but of vertical component instrument was put in operation in March 1928 at ATH station (Comninakis et al., 1987). A possible explanation is that during the period 1922-1949 the country suffered highly unstable conditions due to major political and war conflicts, which affected the collection of seismic records. As a matter of fact, the publication of seismic record data in the Bulletins of NOA, which started in the year 1900, was interrupted during the period 1927-1949. The publication of such data sets was recommenced in 1950. This change is reflected quite well in the abrupt drop of the Mc value since 1950. Besides, the operation at ATH station of a vertical component Critikos-type seismometer in 1954 and of a vertical component Benioff seismometer in 1957 contributed to improve the seismograph monitoring of the region during the decade of 1950's. A further drop of Mc is noted since 1963 following the drastic improvement of the national monitoring network during 1962 in the frame of the WWSSN.

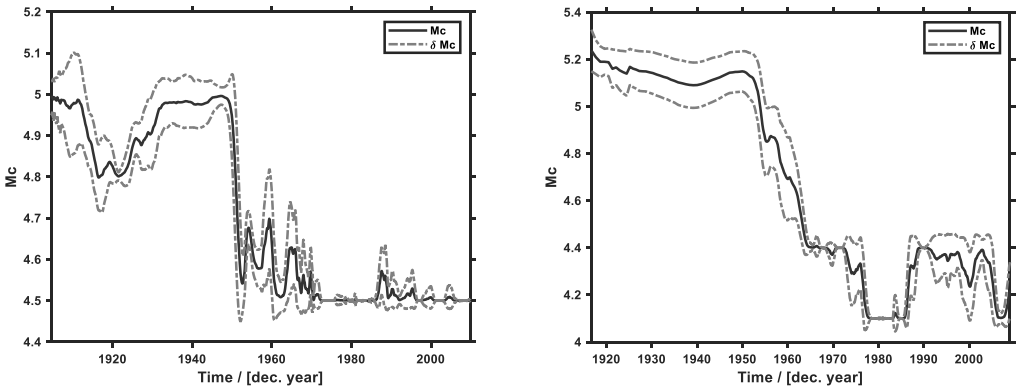

Figure 2.6. Time variation of magnitude of completeness, Mc, of the AUTH (left) and UOA (right) catalogues. Mc was estimated with the MAXC method and bootstrap calculation for the time interval of 1900-2009. The sample size used is 250 events; number of samples in bootstrap is 10.

In the UOA catalogue the abrupt drop of Mc is also evident after 1949 as well as after 1963 (Fig. 2.6). However, the increase of Mc observed in the AUTH catalogue in the 1922-1949 time interval is not evident in the UOA catalogue. Very likely this is due to that the main criterion for inclusion of an event in the UOA catalogue in the period 1900-1963 has been that the event should have been registered by the UPP (Uppsala) and/or (Kiruna) stations, with reported ground amplitudes (see review in Chapter 1). Then, the gradual decrease of Mc from the beginning of the time period examined until about mid 1980's is consistent with the gradual improvements for events registration by those stations and less affected by local station records. Since 1964, however, M_s in UOA catalogue was calculated from the empirical formula (1.3) between M_s and m_b(ISC-GEM). Eventually, M_w for the events of the entire period were calculated from regression relationships between M_{sUOA} and M_w collected from the CGMT project as well as from local sources for the post-1975 period. The interpretation of the Mc increase noted from the end of 1980's until about 2007 is a challenge and may be due to several factors. One reason would be the fact that several stations of

the Greek national seismograph system were off from the end of 1980's until about 1994. Another explanation could be that for the period of 2003-2007 M_w was collected from various sources. The temporary decrease of the number of national stations operating in the years around 1990 is possibly reflected in small Mc fluctuations in the AUTH catalogue too.

Mc in discrete catalogue time segments

The Mc was estimated in discrete time segments of the ISC-GEM, UOA and AUTH catalogues. The catalogue time segments were determined by considering that major improvements in the seismicity monitoring in Greece have been noted in the years 1900, 1911, 1950 and 1964. The Mc estimation was performed with the MAXC method, which proved applicable in all the catalogue segments examined. However, the Mc95 and Mc90 options of the GFT method have been applicable only in some of the segments. The results are summarized in Table 2.2.

Table 2.2. Magnitude of completeness, Mc, determined with the application of the MAXC, GFT-95% (Mc95) and GFT-90% (Mc90) methods; α and b are parameters in the magnitude-frequency formula (2.1).

Catalogue/ M_w min	period	MAXC-Mc	GFT-Mc95	GFT-Mc90	b (MAXC)	A (MAXC)
ISC-GEM / 5.4	1905-1910	5.8	-	-	1.10±0.33	7.423
	1911-1949	5.6	-	5.6	1.05±0.06	8.150
	1950-1963	5.6	-	5.7	1.09±0.12 0.89±0.10	8.075 6.841
	1964-2014	5.7	-		0.85±0.06	6.917
	1900-2014	5.6	-	5.6	0.96±0.04	8.019
UOA / 4.1	1900-1910	5.5	-	5.4	0.88±0.15 0.80±0.12	6.517 6.040
	1911-1949	5.2	5.0	5.0	0.98±0.06 0.91±0.04	7.574 7.181
	1950-1963	4.6	-	4.7	0.88±0.03 0.93±0.04	6.768 7.020
	1964-2009	4.1	4.3	4.1	0.99±0.01 1.15±0.02	7.848 8.585
AUTH / 4.5	1900-1910	5.0	-	4.8	1.02±0.07 0.85±0.04	7.478 6.584
	1911-1949	4.9	5.1	4.7	1.10±0.03 0.98±0.04 0.91±0.02	8.445 7.807 7.475
	1950-1963	4.5	4.5	4.5	1.01±0.03	7.597
	1964-2010	4.5	-	4.5	1.57±0.02	10.957

In the ISC-GEM catalogue Mc=5.8 was found for the time period from 1905 to 1910 (Fig. 2.7). During 1905 the seismicity rate is increased with respect the time interval from 1906 onwards (Fig. 2.7). As we will see later this seismicity trend appears in the other catalogues as well and, therefore, we recall it in the next lines. In the largest part of the catalogue (1911-1963) the Mc drops to 5.6 but Mc value of 5.7 has been found in the recent period of 1964-2014 (Table 2.2).

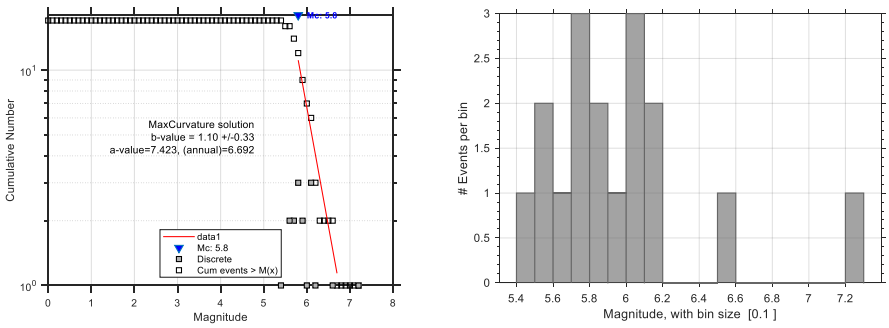

Figure 2.7. Magnitude-frequency distribution (left) and magnitude frequency (right) for the ISC-GEM catalogue for the period 1905-1910. Mc=5.8 was found with the MAXC method.

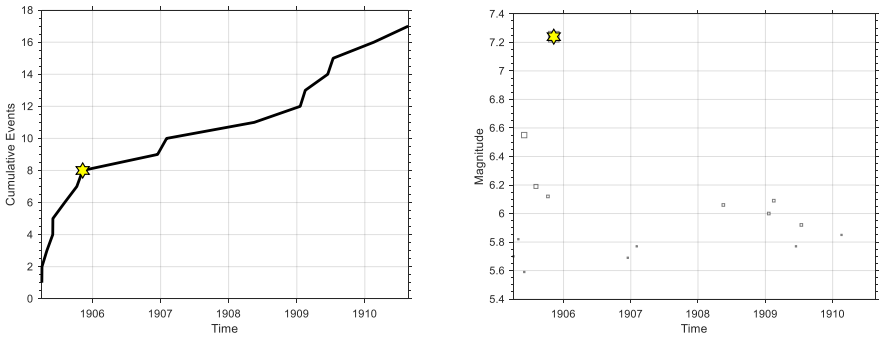

Figure 2.8. Seismicity rate (left) and magnitude distribution with time (right) for the ISC-GEM catalogue for the period 1905-1910. Stars show large earthquakes (M>7). Star illustrates high magnitude event.

The UOA catalogue is characterized by a gradual drop of the Mc (Table 2.2), a change which is generally consistent with the results obtained from the time variation of Mc (Fig. 2.6). In the period 1900-1910 Mc=5.4 was found with the MAXC method (Fig. 2.9). Mc as low as 4.1 characterizes the UOA catalogue time segment of 1964-2009 (Table 2.2).

During the period 1904-1905 the seismicity rate is increased in the UOA catalogue (Fig. 2.10). This is due to that the activity was very high in the years 1904 and 1905 with large magnitude earthquakes occurring mainly in northern Greece. As a matter of fact, during 1904 a seismic sequence with large magnitude events ruptured SW Bulgaria very close to the Greek borders. The largest event occurred on 4 April with M_w=7.4 (UOA). On 1 June 1905 another strong earthquake of M_w=6.4 (UOA) occurred in the Greek-Yugoslavian borders. The 8 November 1905 earthquake (M_w=7.1, UOA), that occurred in Athos peninsula, north Greece, has also been another very large event followed by several aftershocks (see also Chapter 5 and Triantafyllou et al., 2020a). The drop of seismicity since 1906 has been noted in the UOA, ISC-GEM and AUTH catalogues.

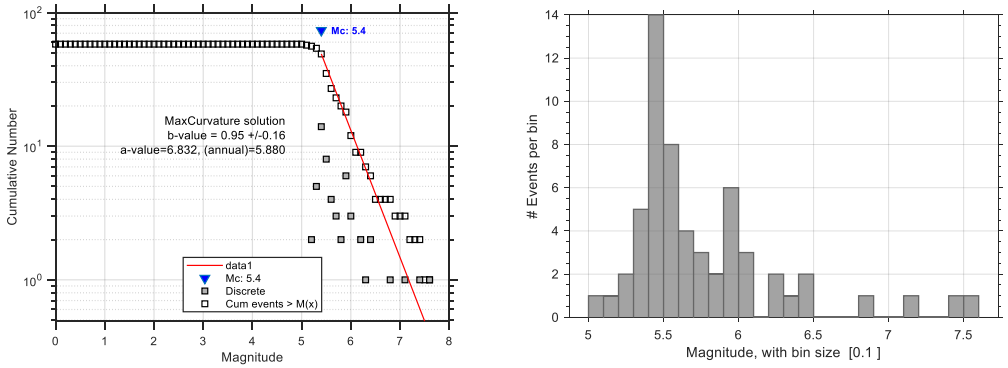

Figure 2.9. Magnitude-frequency diagram (left) and magnitude distribution (right) for the UOA catalogue for the period 1900-1910. Mc=5.4 was found with the MAXC method.

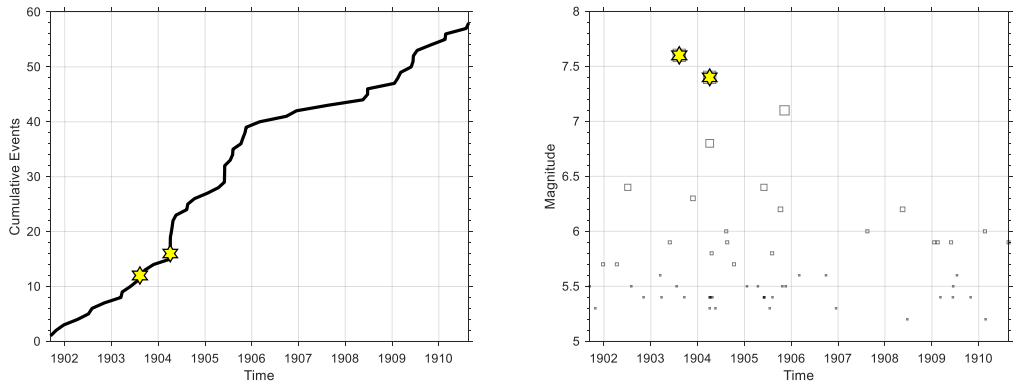

Figure 2.10. Seismicity rate (left) and magnitude distribution with time (right) for the UOA catalogue for the period 1900-1910. Stars show large earthquakes (M>7). Stars illustrate high magnitude events.

In the AUTH catalogue Mc=5.0 was found for the early period 1900-1910 (Fig. 2.11). This is a relatively low value of Mc, which perhaps is attributed to the fact that the AUTH catalogue segment 1900-1910 lists several events adopted from the catalogue of Kárník (1969, 1996). In the later formulae similar to the Prague formula were used to calculate M_s from LR and Sg waves and m_b from body (P and S) waves recorded at remote European stations. Proxy M_w magnitudes inserted eventually in the AUTH catalogue were obtained with the use of empirical global relations developed by Scordilis (2006) for the convertion of M_s and m_b magnitude scales to M_w scale.

In the AUTH catalogue the Mc values found for three discrete time segments of the period 1911-1963 are lower than the respective values found for the UOA catalogue (Table 2.2). This is explainable by that the records of the Mainka and Wiechert seismometers at ATH station have been systematically utilized for that period. The Mc estimated for the period 1964-2009, however, is an exception since magnitude M_w=4.5 is by default the lowest one inserted in the AUTH catalogue as compared to M_w=4.1 in UOA. The seismicity rate increase noted in the UOA and ISC-GEM catalogues during 1904-1905 is also clearly seen in the AUTH catalogue (Fig. 2.12).

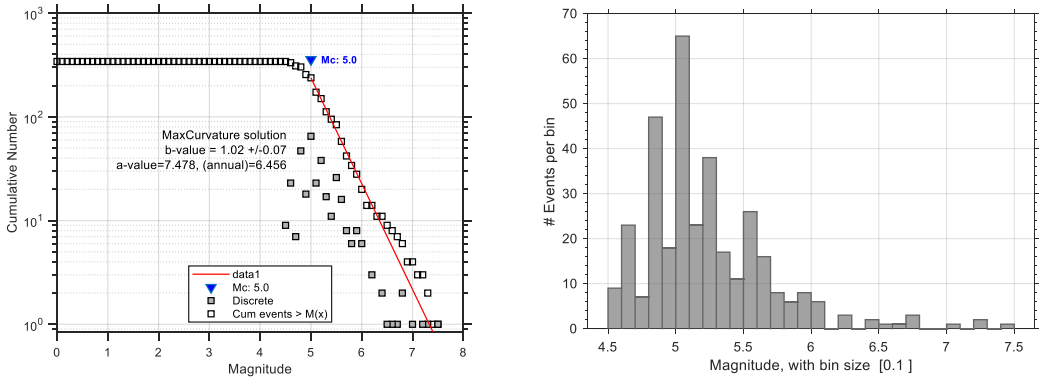

Figure 2.11. Magnitude-frequency diagram (left) and magnitude distribution (right) for the AUTH catalogue for the period 1900-1910. Mc=5.0 was found with the MAXC method.

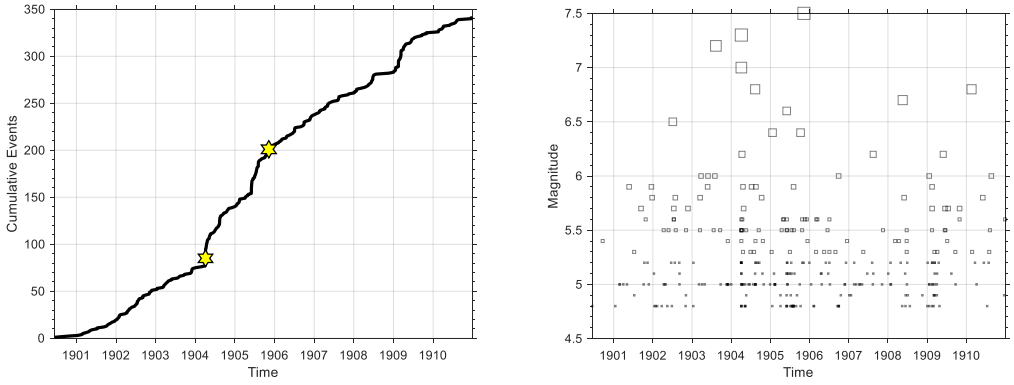

Figure 2.12. Seismicity rate (left) and magnitude distribution with time (right) for the AUTH catalogue for the period 1900-1910. Stars show large earthquakes (M>7). Stars illustrate high magnitude events.

2.5 Summary of Chapter 2

For a large time segment of the ISC-GEM catalogue (1911-1963) Mc=5.6 was found. However, Mc=5.8 and Mc=5.7 was estimated for the intervals 1905-1910 and 1963-2014, respectively. In the ISC-GEM catalogue the Mc changes are not remarkable as compared to the UOA and AUTH catalogues. The reason is that ISC-GEM lists only strong earthquakes. The UOA catalogue is characterized by Mc=5.5 during the time period 1900-1910. Then Mc gradually decreases and becomes equal to 4.1 in the 1963-2009 time interval. The Mc in AUTH catalogue is 5.0 for the time interval 1900-1910. Then Mc drops gradually and remains at the level of 4.5 from 1950 up to 2010 since 4.5 is by default the minimum magnitude in that catalogue.

All catalogues are characterized by an increased seismicity rate in the time intervals of 1904-1905 (1905 for ISC-GEM), 1953-1959 and 1980-1983. The increase rate during 1904-1905 has already been explained as due to the occurrence of several sequences with high magnitude earthquakes. Similar explanations are reasonable for the other two time periods. During the 1950's Greece experienced several sequences of large magnitude earthquakes, such as the ones of 1953 in the Ionian islands, of 1954-1957 in Central Greece and of 1955-1957 in the South Aegean Sea. In the period 1980-1983 earthquake sequences with large magnitude events occurred in Central Greece (1980 and 1981), in the North Aegean Sea (1981-1983) and in the Ionian Sea (1983).

CHAPTER 3. EARLY INSTRUMENTAL SEISMICITY (1900-1910): REDETERMINATION OF MAGNITUDES FROM RECORDS IN AGAMENNONE SEISMOGRAPHS

3.1 Introduction

In this Chapter we analyze the research methods followed, the data sets used and the results obtained towards revisiting earthquake magnitudes for the early instrumental era of seismicity, i.e. from 1900 up to 1910. Earthquakes occurring during this seismicity period are listed in various catalogues, which include those of ISC-GEM, AUTH, UOA and AM. A review on these catalogues can be found in Chapter 1 while a completeness analysis and comparison of the catalogues has been performed in Chapter 2. Table 3.1 summarizes the main characteristics of the four catalogues for the time period 1900-1910. From the completeness analysis in Chapter 2 it is evident that the AUTH catalogue is the most complete one and, therefore, it has been used as a reference catalogue for the present analysis. The magnitude-frequency distribution of earthquakes listed in the AUTH seismicity catalogue are shown in Figure 2.12 while the monthly frequency of earthquakes is illustrated in Figure 3.1.

Table 3.1. Main characteristics of four catalogues covering the study region (latitude 33^0-43^0N, longitude 18^0-30^0E) for the period 1900-1910. Key: N=number of events, n=shallow earthquakes, i=intermediate-depth earthquakes, M_{min}=minimum magnitude, M_{max}=maximum magnitude, Mc= completeness magnitude as determined in Chapter 2. The AM catalogue is by definition truncated at Mc=6.0 by the author of that catalogue. Magnitudes are in M_w scale; symbol * shows M_s.

Catalogue	N	M_{min}	M_{max}	Mc	Time period
AUTH	340 (n + i)	4.5	7.3	5.0	1900-1910
UOA	58 (n + i)	5.0, 5.0*	7.6, 8.0*	5.5	1900-1910
ISC-GEM	21 (n + i)	5.44	7.24	5.8	1905-1910
AM	14 (n)	6.0*	7.24*	6.0	1900-1910

The procedure used to insert magnitudes in the AUTH seismicity catalogue of the time period 1900-1910 was based on the collection of magnitudes from various sources including the catalogue by Kárník (1969) and its updated version (Kárník, 1996). In the catalogues by Kárník (1969, 1996) formulae similar to the Prague formula (see below) were used to calculate M_s from *LR* and *Sg* waves and m_b from body (*P* and *S*) waves recorded at remote European stations. Proxy M_w magnitudes inserted eventually in the AUTH catalogue were obtained with the use of empirical global relations converting M_s and m_b magnitude scales to M_w scale (Scordilis, 2006).

After these procedures the AUTH catalogue is a homogeneous one as regards the conversion of M_s and m_b to M_w for the time segment of 1900-1910. However, it remains inhomogeneous as regards the data sources used. On the other hand, for events which are common in the AUTH catalogue and in other catalogues, i.e. ISC-GEM, UOA, AM, the magnitudes are generally consistent but some important discrepancies exist. For example, for the large event of 8 November 1905 that ruptured the North Aegean Sea close to Mt Athos the magnitudes determined are 7.5, 7.24, 7.24 and 7.1 in AUTH, ISC-GEM, AM and UOA, respectively. Another example is the 18 February 1910 event with magnitudes 6.8 (AUTH), 5.85 (ISC-GEM) and 6.0 (UOA).

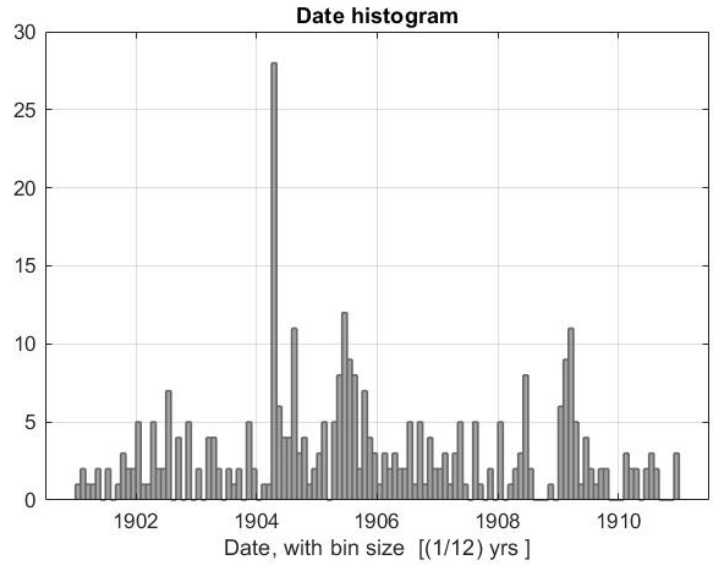

Figure 3.1. Monthly frequency distribution of the seismicity in the AUTH catalogue for the time period 1900-1910. The frequency peak during 1904 reflects the occurrence of sequences of very strong earthquakes, e.g. in Samos Isl., SE Aegean Sea, and in SW Bulgaria. Statistics was performed with the use of the z-map toolbox.

For these reasons, an effort was undertaken to re-determine magnitudes for earthquakes occurring in the 1900-1910 time period. To this aim we utilized records from the five Agamennone-type seismographs of intermediate natural period that operated in Greece in that time period. From macroseismic information the epicenters of a few events have been revised too.

3.2 Method

For the calculation of surface-wave magnitude, M_s, Gutenberg (1945) proposed the formula

$$M_s = \log A + 1.656 \log \Delta + 1.818, \quad (3.1)$$

where A (in μm) is the amplitude of combined horizontal amplitudes of surface waves of period ~20 s and Δ is the epicentral distance in degrees. Formula (3.1) was designed mainly for records at Pasadena station. After this development several equations similar to (3.1) but with different coefficients were developed for other stations (see review in Utsu, 2002a). A major contribution came with the introduction of the widely adopted Prague or IASPEI formula (Vaněk et al., 1962):

$$M_s = \log (A/T)_m + 1.66 \log \Delta + 3.3, \quad (3.2)$$

In Prague formula, $(A/T)_m$ is the combined value of the maximum A/T ratios of horizontal components of the surface waves of period T~20 s and Δ is the epicentral distance in degrees; amplitude A is in μm.

Magnitude, M, equivalent to M_s for earthquakes occurring in Greece in the post-1910 time interval, has been determined under the assumption that the seismic records by the Mainka and Wiechert instruments operating at ATH (Athens) station (Table 3.2) are suitable thanks to their intermediate

natural period. On that basis, Papazachos and Vasilicou (1966) suggested that the magnitude of surface earthquakes (focal depth h<60 km) can be calculated as a function of ground amplitude, *a* (in microns), and epicentral distance Δ (< 600 km) in km from Athens:

$$M = \log a + 1.42 \log \Delta + 0.2, \qquad (3.3)$$

This formula was developed after similar formulas were already tested earlier at the Institute of Geodynamics of NOA (e.g. Galanopoulos, 1961, 1966; see review in Ambraseys, 2001). In formula (3.3) the ground amplitude is taken from the maximum average amplitude recorded at the two horizontal components (NS, EW) of Mainka and/or Wiechert instruments at ATH station. The parameters in formula (3.3) were determined with linear regression utilizing M_s magnitudes calculated from surface- waves of Greek earthquakes recorded at distant stations, such Pasadena and Berkeley. On the other hand, starting from early 1970s, magnitudes of intermediate-depth earthquakes (h>60 km) were calculated from the formula

$$M = \log a + 0.18 (R/100) + 3.2, \qquad (3.4)$$

proposed by Papazachos and Comninakis (1971); where *R* is the hypocentral distance in km and *a* as in (3.3). The validity of *M*, as a magnitude equivalent to M_s and M_w, was shown in a series of publications (Kiratzi and Papazachos, 1984; Papazachos, 1989; Papazachos et al., 2002). Formulae (3.3) and (3.4) remained in use at NOA up to the mid-1980s. For the time period from 1911 to mid-1980s the AUTH catalogue lists M_w magnitudes equivalent to M_s determined by the procedure described above. Other procedures were followed for magnitude determinations after that period but this is not of interest to the present analysis.

Since seismographs of Agamenonne, Mainka and Wiechert types had the common feature of being instruments of intermediate natural period, we put forward the hypothesis that trace wave amplitudes, *A*, in Agamenonne records should correlate with magnitudes M_{AUTH} calculated from Mainka and Wiechert ground amplitudes; M_{AUTH} denotes earthquake magnitude in the AUTH catalogue. Then, it would be possible to utilize ground motion amplitudes *A* for the calculation of an "Agamennone magnitude". Technical features of the Agamennone-type instruments as well as of the Mainka and Wiechert seismographs, installed at ATH station and operating since 1911 and 1924, respectively, are listed in Table 3.2.

Wave amplitude data from Agamennone records were calibrated over surface-wave magnitudes, M_s, inserted in the AUTH catalogue for the post-1910 period and an "Agamennone magnitude" was calculated for 52 moderate and strong earthquakes. In some occasions we were able to improve earthquake epicenters too based on macroseismic information.

Table 3.2. Constants and other technical characteristics of the Agamennone, Mainka and Wiechert seismographs operated in Greece (Eginitis, 1905, 1910, 1912, Comninakis et al., 1987). Symbol key: φ=geographical latitude, λ=geographical longitude, m=pendulum mass, T=natural period, h=altitude of installation site, V=static magnification, DS=drum speed (mm/min). For CHA Agamennone station no further information is available. Notes: for Mainka horizontal components T=6, V=80 and DS=15 for the period 1911-1956, T=3.5, V=60 and DS=30 for the period 1957-1963; for Wiechert horizontal components T=5.0-9.2, V=160-175 and DS=12-30 for the period 1924-1963; for Wiechert vertical component T=1.6-4.0, V=140-280 and DS=10-30 for the period 1928-1963.

Station/ Instrument	**φ(Nº) d:m:s**	**λ(Eº) d:m:s**	**m(kgr)**	**T (s)**	**h (m)**	**V**	**DS**	**Recording status**
Station Athènes (ATH) **Instruments**	37.973	23.717			103.52			
Agamennone			200	5.2-6.0		12	6.4	Very good: June 1900-1910
Mainka			136	3.5-6.0		60-80	15-30	Very good: 1911-1963
Wiechert			1000/ 1300	5.0-9.2/ 1.6-4.0		160-175/ 140-280	12-30/ 10-30	Very good: 1924-1963
Station Chalcis (CHA) **Instrument** Agamennone	38.482	23.584						Interruptions: 1903-1908 No operation: 1909-1910
Station Egion (EGI) **Instrument** Agamennone	38.233	22.072	200	6.5	65	12	5.4	No operation: 1903-1908 Good: interruptions in 1910
Station Zante (ZAN) **Instrument** Agamennone	37.877	20.663	200	4.2	4.45	12	5.3	Occasionally: 1903-1908 Only occasionally:1909-1910
Station Calamata (CAL) **Instrument** Agamennone	37.035	22.096	200	5.8	47.70	12	6	No operation: 1903-1907 Normal operation: 1908 Interruptions: 1908-1910

3.3 Data

3.3.1 Instrumental records

The first seismograph network installed in Greece comprised five mechanical Agamennone-type instruments, named thanks to G. Agamennone, Professor of Seismology in Rome. The instruments were installed in June 1899 at ATH station at the premises of NOA as well as in the cities of Chalkis (June 1900), Calamata (September 1900), Zante (modern Zakynthos, October 1902) and Egion (January 1903) at stations to which we have given the working names CHA, CAL, ZAN and EGI, respectively (Fig. 3.2). Phase data and wave trace amplitudes were collected from the annual *Annales de l' Observatoire National d' Athènes* (NOA Bulletins; Eginitis, 1905, 1910, 1912).

Of particular importance to our study is that the three types of instruments shared the common feature of being of intermediate natural period, which falls in the range 5.2-6.0 s for Agamenonne, 3.5-6.0 s for Mainka and 5.0-9.2 s for Wiechert (horizontal components) instruments (Eginitis, 1910, 1912, Båth, 1983, Comninakis et al. 1987). Due to instrument malfunction problems several Agamennone stations operated with interruptions (Table 3.2). However, the instrument at ATH station operated without important interruption in the entire period of 1900-1910. In the NOA Bulletins record data for the year 1900 are listed for only three earthquakes implying that practically our data set starts from 1901.

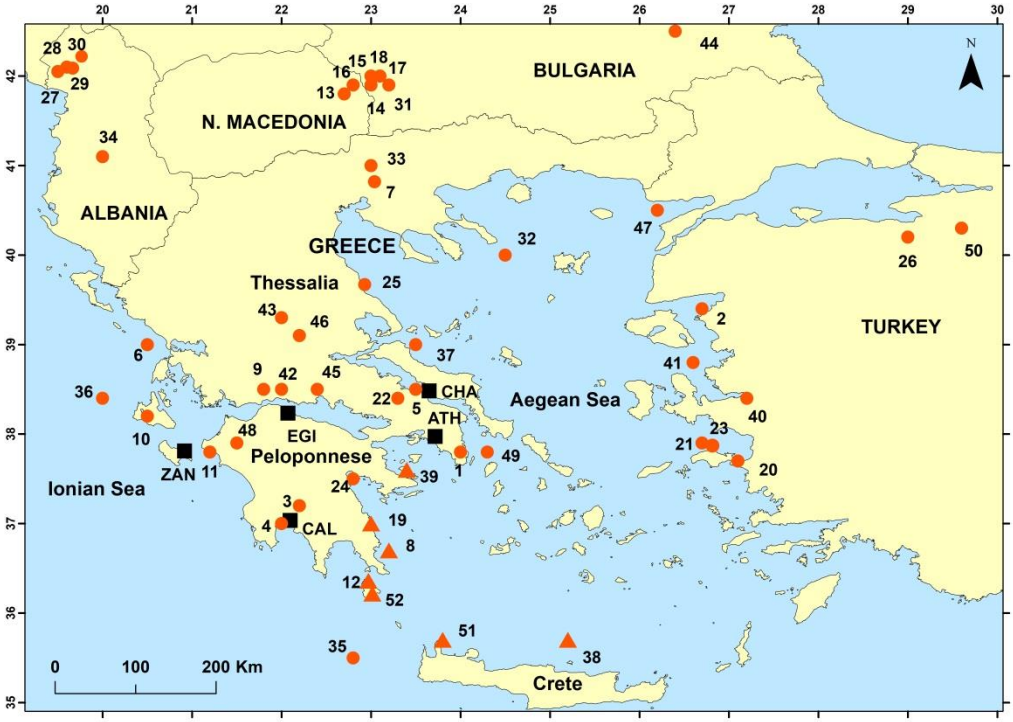

Figure 3.2. Locations of the Agamennone seismograph stations (squares) operated from 1900 to 1910. Epicenters of the shallow (dots) and intermediate-depth (triangles) earthquakes listed in Table 3.3, along with the respective numbers, are also plotted.

Parameters of earthquakes occurring since 1901 onwards and recorded by at least one Agamennone instrument were systematically published in the NOA Bulletins (Eginitis, 1905, 1910, 1912). The parameters included, among others, the event date, the arrival time of the first wave arrival time, the termination time of the pendulum motion and the maximum trace wave amplitude, *A* (in mm), of the record. For sizable earthquakes of magnitude of ~5.5 and over, the geographic name of the epicentral area is frequently listed too. Since 1901 maximum amplitude at one horizontal component was reported. However, from 1904 onwards maximum amplitudes at two horizontal components (NE, NW) were listed. A typical page of the NOA Bulletin of that period is illustrated in Figure 3.3.

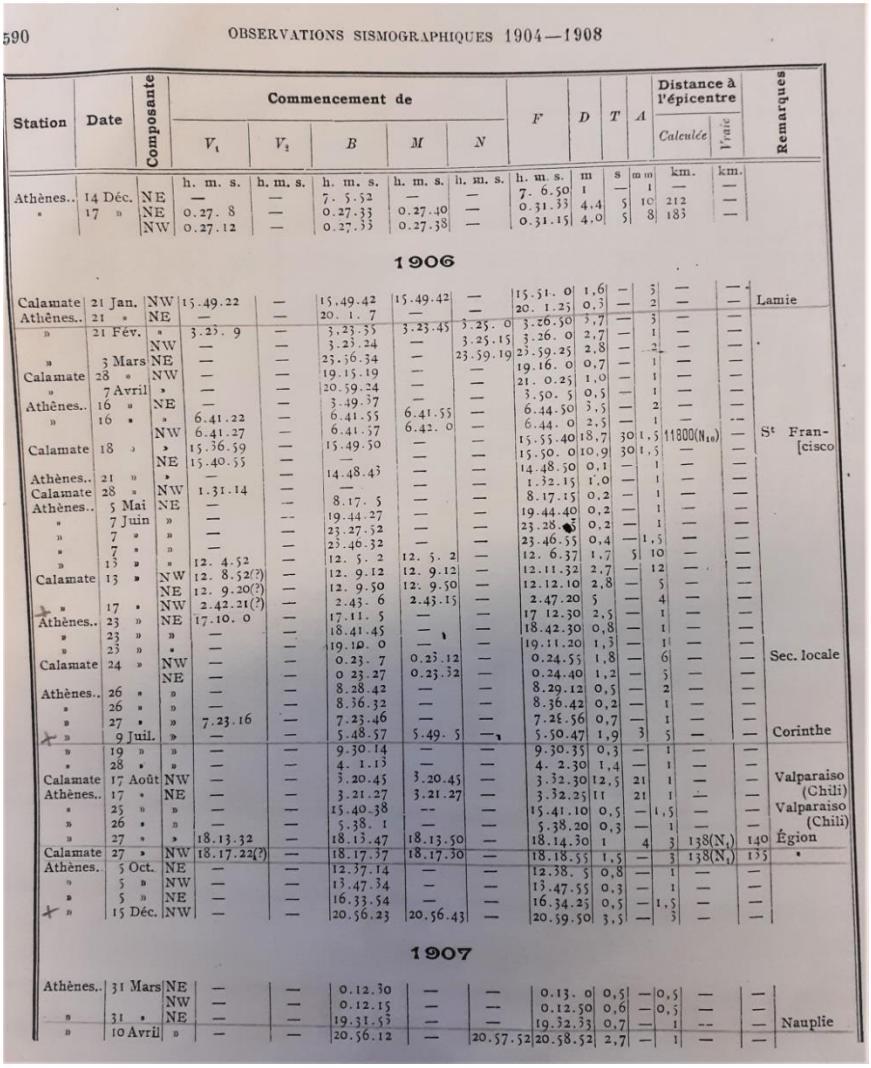

590 OBSERVATIONS SISMOGRAPHIQUES 1904—1908

Station	Date	Composante	Commencement de V_1	V_2	B	M	N	F	D	T	A	Distance à l'épicentre Calculée	Distance à l'épicentre Tracé	Remarques
			h. m. s.	h. m. s.	h. m. s.	h. m. s.	h. m. s.	h. m. s.	m	s	m m	km.	km.	
Athènes..	14 Déc.	NE	—	—	7. 5.52	—	—	7. 6.50	1	—	1	—	—	
»	17 »	NE	0.27. 8	—	0.27.33	0.27.40	—	0.31.33	4.4	5	10	212	—	
		NW	0.27.12	—	0.27.33	0.27.38	—	0.31.15	4.0	5	8	183	—	
1906														
Calamate	21 Jan.	NW	15.49.22	—	15.49.42	15.49.42	—	15.51. 0	1,6	—	5	—	—	Lamie
Athènes..	21 »	NE	—	—	20. 1. 7	—	—	20. 1.25	0,3	—	2	—	—	
»	21 Fév.	»	3.23. 9	—	3.23.55	3.23.45	3.25. 0	3.26.50	2,7	—	3	—	—	
		NW	—	—	3.23.24	—	3.25.15	3.26. 0	2,7	—	1	—	—	
»	3 Mars	NE	—	—	23.56.34	—	23.59.19	23.59.25	2,8	—	2	—	—	
Calamate	28 »	NW	—	—	19.15.19	—	—	19.16. 0	0,7	—	1	—	—	
»	7 Avril	»	—	—	20.59.24	—	—	21. 0.25	1,0	—	1	—	—	
Athènes..	16 »	NE	—	—	3.49.37	—	—	3.50. 5	0,5	—	1	—	—	
»	16 »	»	6.41.22	—	6.41.55	6.41.55	—	6.44.50	3,5	—	2	—	—	
		NW	6.41.27	—	6.41.57	6.42. 0	—	6.44. 0	2,5	—	1	—	—	
Calamate	18 »	»	15.36.59	—	15.49.50	—	—	15.55.40	18,7	30	1,5	11800(N_{10})	—	St Fran-[cisco
		NE	15.40.55	—	—	—	—	15.50. 0	10,9	30	1,5	—	—	
Athènes..	21 »	»	—	—	14.48.43	—	—	14.48.50	0,1	—	1	—	—	
Calamate	28 »	NW	1.31.14	—	—	—	—	1.32.15	1,0	—	1	—	—	
Athènes..	5 Mai	NE	—	—	8.17. 5	—	—	8.17.15	0,2	—	1	—	—	
»	7 Juin	»	—	—	19.44.27	—	—	19.44.40	0,2	—	1	—	—	
»	7 »	»	—	—	23.27.52	—	—	23.28. 5	0,2	—	1	—	—	
»	7 »	»	—	—	23.40.32	—	—	23.46.55	0,4	—	1,5	—	—	
»	13 »	»	12. 4.52	—	12. 5. 2	12. 5. 2	—	12. 6.37	1,7	5	10	—	—	
Calamate	13 »	NW	12. 8.52(?)	—	12. 9.12	12. 9.12	—	12.11.32	2,7	—	12	—	—	
		NE	12. 9.20(?)	—	12. 9.50	12. 9.50	—	12.12.10	2,8	—	5	—	—	
»	17 »	NW	2.42.21(?)	—	2.43. 6	2.43.15	—	2.47.20	5	—	4	—	—	
Athènes..	23 »	NE	17.10. 0	—	17.11. 5	—	—	17 12.30	2,5	—	1	—	—	
»	23 »	»	—	—	18.41.45	—	—	18.42.30	0,8	—	1	—	—	
»	23 »	»	—	—	19.10. 0	—	—	19.11.20	1,3	—	1	—	—	
Calamate	24 »	NW	—	—	0.23. 7	0.23.12	—	0.24.55	1,8	—	6	—	—	Sec. locale
		NE	—	—	0 23.27	0.23.32	—	0.24.40	1,2	—	5	—	—	
Athènes..	26 »	»	—	—	8.28.42	—	—	8.29.12	0,5	—	2	—	—	
»	26 »	»	—	—	8.36.32	—	—	8.36.42	0,2	—	1	—	—	
»	27 »	»	7.23.16	—	7.23.46	—	—	7.25.56	0,7	—	1	—	—	
»	9 Juil.	»	—	—	5.48.57	5.49. 5	—	5.50.47	1,9	3	5	—	—	Corinthe
»	19 »	»	—	—	9.30.14	—	—	9.30.35	0,3	—	1	—	—	
»	28 »	»	—	—	4. 1.13	—	—	4. 2.30	1,4	—	1	—	—	
Calamate	17 Août	NW	—	—	3.20.45	3.20.45	—	3.32.30	12,5	21	1	—	—	Valparaiso
Athènes..	17 »	NE	—	—	3.21.27	3.21.27	—	3.32.25	11	21	1	—	—	(Chili)
»	25 »	»	—	—	15.40.38	—	—	15.41.10	0,5	—	1,5	—	—	Valparaiso
»	26 »	»	—	—	5.38. 1	—	—	5.38.20	0,3	—	1	—	—	(Chili)
»	27 »	»	18.13.32	—	18.13.47	18.13.50	—	18.14.30	1	4	3	138(N_1)	140	Égion
Calamate	27 »	NW	18.17.22(?)	—	18.17.37	18.17.30	—	18.18.55	1,5	—	3	138(N_1)	135	»
Athènes.	5 Oct.	NE	—	—	12.37.14	—	—	12.38. 5	0,8	—	1	—	—	
»	5 »	NW	—	—	13.47.34	—	—	13.47.55	0,3	—	1	—	—	
»	5 »	NE	—	—	16.33.54	—	—	16.34.25	0,5	—	1,5	—	—	
»	15 Déc.	NW	—	—	20.56.23	20.56.43	—	20.59.50	3,5	—	3	—	—	
1907														
Athènes..	31 Mars	NE	—	—	0.12.30	—	—	0.13. 0	0,5	—	0,5	—	—	
		NW	—	—	0.12.15	—	—	0.12.50	0,6	—	0,5	—	—	
»	31 »	NE	—	—	19.31.53	—	—	19.32.33	0,7	—	1	—	—	Nauplie
»	10 Avril	»	—	—	20.56.12	—	20.57.52	20.58.52	2,7	—	1	—	—	

Figure 3.3. A typical page of the seismological Bulletin of NOA for the year 1906.

From the examination of the NOA Bulletins for the period 1901-1910 we found that the list of earthquakes with recorded amplitude *A* is quite long. However, earthquake epicenter was determined only in a very few cases and with considerable uncertainty. We correlated earthquake origin times listed in the NOA Bulletins and in the AUTH catalogue. We found 52 earthquakes in the AUTH catalogue which are listed in the NOA Bulletins along with the respective amplitude *A* recorded in at least one Agamennone station. The shallow (h<60 km) earthquakes are 45 and their magnitude M_{AUTH} ranges from 4.8 to 7.5. The set of the remaining 7 events are intermediate-depth earthquakes (h≥60 km) with M_{AUTH} ranging from 5.8 to 7.2. Focal parameters of the 52 earthquakes along with the respective wave amplitude *A* recorded at Agamennone stations are listed in Table 3.3. Epicentral determinations in the AUTH catalogue were adopted for magnitude re-calculation from amplitude *A*.

Table 3.3. Calibrated (M_{ac}) and final (M_A) magnitudes calculated from wave amplitudes recorded at the components A_{NE}, A_{NW} (in mm) of Agamennone seismographs operating in Greece from 1901 to 1910. All records are from the Athens (ATH) station unless otherwise indicated (working names of other stations: CH=Chalkis, CA=Calamata, E=Egion, Z=Zante). Key: n=event number, mo=month, d=day, hr=hour, mi=minute, s=sec; φ^o_N, λ^o_E=epicentral geographic coordinates, h=focal depth (km), M=magnitude, Δ=epicentral distance (km), M_{ac}=calibrated Agamennone magnitude, M_A=final Agamennone magnitude. Focal parameters from year to M are taken from the AUTH catalogue unless are revised in this study and marked in bold (see text); A_{NE}, A_{NW} are amplitudes recorded at the NE and NW components of Agamennone stations taken from the NOA Bulletins; Δ, M_{ac}, and M_A have been calculated in this study.

n	*year*	*mo d hr mi s*	φ^o_N	λ^o_E	*h*	*M*	A_{NE}	A_{NW}	*Δ*	M_{ac}	M_A
1	1901	11 23 18 30 00	37.80	24.00	0	5.0	2		**290**	**5.4**	**5.4**
2	1901	12 18 03 51 00	39.40	26.70	0	5.9	2		**304**	**5.4**	**5.4**
3	1901	12 24 23 18 00	37.20	22.20	15	5.8	8		**160**	**5.6**	**5.6**
4	1902	2 09 08 17 00	37.00	22.00	0	4.8	1		**160**	**4.7**	**4.7**
5	1902	4 11 18 35 30	38.50	23.50	0	5.5	9		**40**	**4.8**	
5CH							50		**45**	**5.6**	
5CA							3		**145**	**5.1**	**5.2**
6	1902	5 26 11 06 00	39.00	20.50	0	5.5	1		**350**	**5.2**	
6CA							1		**320**	**5.2**	**5.2**
7	1902	7 05 14 56 30	40.82	23.04	0	6.5	32	40	**318**	**6.7**	**6.7**
8	1902	7 29 01 20 00	36.70	23.20	100	5.8	9		**180**	**6.0**	**6.0**
9	1902	8 02 05 38 30	**38.50**	**21.80**	0	5.5	1		**170**	**4.8**	**4.8**
10	1902	11 05 23 50 30	38.20	20.50	0	5.5	8		**280**	**6.0**	**6.0**
11	1903	3 15 19 03 30	37.80	21.20	0	5.5	1		**220**	**4.9**	**4.9**
12	1903	8 11 04 32 54	36.36	22.97	80	7.2	70		**244**	**7.0**	**7.0**
13	1904	4 04 10 02 55	41.80	22.70	0	7.0	100	75	**428**	**7.3**	**7.3**
14	1904	4 04 10 26 00	41.90	23.00	0	7.3	110		**434**	**7.4**	**7.4**
15	1904	4 04 11 09 30	42.00	23.00	0	5.5	1	1	**446**	**5.4**	**5.4**
16	1904	4 10 08 52 46	41.90	22.80	0	6.2	11	8	**438**	**6.3**	**6.3**
17	1904	4 19 18 14 30	42.00	23.10	0	5.9	2		**444**	**5.7**	**5.7**
18	1904	4 25 20 02 00	42.00	23.00	0	5.7	1		**446**	**5.4**	**5.4**
19	1904	7 09 00 50 00	37.00	23.00	100	5.9	7	1	**162**	**5.6**	**5.6**
20	1904	8 11 06 08 30	**37.70**	**27.10**	0	6.8	18	9	**310**	**6.3**	**6.3**
21	1904	8 18 20 07 30	**37.90**	**26.70**	0	5.9	24	18	**255**	**6.3**	**6.3**
22	1904	9 13 09 30 00	38.40	23.30	16	5.5	22	16	**54**	**5.3**	**5.3**
23	1904	10 10 17 40 30	**37.90**	**26.70**	20	5.8	10		**255**	**6.0**	**6.0**
24	1904	12 28 06 15 00	37.50	22.80	0	5.0	11	14	**96**	**5.5**	**5.5**
25	1905	1 20 02 32 30	39.67	22.93	13	6.4	55	54	**200**	**6.6**	**6.6**
26	1905	4 15 05 36 30	40.20	29.00	0	5.5	4	4	**520**	**6.1**	**6.1**
27	1905	6 01 04 42 15	42.05	19.50	0	6.6	30		**566**	**7.0**	**7.0**
28	1905	6 03 05 10 43	42.10	19.60	0	5.6	3	3.5	**568**	**6.0**	**6.0**
29	1905	8 04 05 09 00	42.10	19.60	0	5.9	2		**568**	**5.8**	**5.8**
30	1905	8 28 05 30 00	42.10	19.60	0	4.8	0.5		**568**	**5.2**	**5.2**
31	1905	10 08 07 27 00	41.90	23.20	0	6.4	10		**432**	**6.3**	**6.3**
32	1905	11 08 22 06 30	40.00	24.50	0	7.5	110		**230**	**7.1**	
32CA							77		**385**	**7.2**	**7.2**
33	1905	11 18 00 19 00	41.00	23.00	0	5.6	2		**338**	**5.5**	**5.5**
34	1906	3 03 21 46 30	41.10	20.00	5	5.6	2		**464**	**5.7**	**5.7**
35	1906	6 17 01 11 00	35.50	22.80	0	5.5	4		**290**	**5.7**	**5.7**
36	1906	12 15 19 21 00	38.40	20.00	0	5.4	3		**326**	**5.6**	**5.6**
37	1907	5 15 23 30 00	39.00	23.50	0	5.3	2		**110**	**4.8**	**4.8**
38	1908	5 17 12 30 42	35.70	25.20	80	6.7	25	21	**309**	**6.6**	
38Z							80	62	**445**	**7.4**	
38E							20	25	**400**	**6.8**	**6.9**
39	1908	5 30 15 00 00	37.60	23.40	150	5.8	20		**158**	**6.3**	
39E							20		**197**	**6.4**	
39CA							15		**170**	**6.2**	
39Z							15		**260**	**6.3**	**6.3**
40	1908	6 23 14 18 00	38.40	27.20	0	5.5	2	3	**310**	**5.5**	**5.5**
41	1908	6 23 16 03 00	38.80	26.60	0	5.3	1	1	**268**	**5.0**	**5.0**
42	1909	1 01 21 40 00	38.50	22.00	0	4.8	3	5	**158**	**5.3**	**5.3**
43	1909	1 20 19 57 00	39.30	22.00	33	5.0	1	3	**206**	**5.2**	**5.2**
44	1909	2 15 09 34 30	42.50	26.40	0	5.9	1	1.5	**645**	**5.7**	**5.7**

45	1909	5 30 06 14 30	**38.50**	**22.40**	20	6.2	42	65	**130**	**6.3**	
45E								100	**45**	**5.9**	**6.1**
46	1909	6 15 23 30 30	39.10	22.20	0	5.7	20	18	**176**	**6.1**	**6.1**
47	1909	6 19 17 45 54	40.50	26.20	0	5.5	0.5		**350**	**4.9**	**4.9**
48	1909	7 15 00 34 42	37.90	21.50	3	5.7	39	68	**192**	**6.6**	**6.6**
49	1909	9 22 03 48 00	37.80	24.30	14	5.0	8	7	**58**	**5.0**	**5.0**
50	1909	10 29 17 38 00	40.30	29.60	0	5.7	0.5		**570**	**5.2**	**5.2**
51	1910	2 18 05 09 18	35.70	23.8	90	6.8	43	43	**271**	**6.8**	**6.8**
52	1910	6 03 04 28 00	36.30	23.00	100	5.8	2	2	**219**	**5.4**	
52E							2	3	**255**	**5.6**	**5.5**

3.3.2 Macroseismic data

In some earthquake cases we determined alternative epicentral locations different from those listed in the AUTH catalogue. This has been done with the aim to investigate alternative earthquake magnitude. In these cases epicenters were determined from macroseismic material collected from three sources: (1) NOA Bulletins (Eginitis, 1905, 1910, 1912), (2) temporary press reports, (3) NOA "Book of Earthquakes". The "Book of Earthquakes" is an unpublished manuscript consisting of two volumes covering the time periods from 1893 to 1901 and from 1902 to 1915, respectively. This manuscript includes macroseismic observations collected by a network of local observers affiliated to NOA. Hereafter the two volumes of this book are referred to as Anonymous (1893-1901) and Anonymous (1902-1915). Part of this macroseismic material has been published in the NOA Bulletins. In the examination of macroseismic material the dates are according to the New Style [N.S.] or according to the Old Style [O.S.], if needed. Macroseismic intensities are assigned to the 12-grade Modified-Mercalli (MM) scale.

3.4. Procedure and results

3.4.1 Correlation of "Agamennone amplitude" with M_{AUTH}

Plotting amplitudes Av recorded at Agamennone ATH station for 51 out of 52 earthquakes against corresponding magnitudes M_{AUTH} showed good correlation (Fig. 3.4) for both shallow and intermediate earthquakes and verified our hypothesis. From regression analysis the best-fit curves found for shallow and intermediate-depth earthquakes are

$$Av = 21.504\ (M_{AUTH})^2 - 226.3\ M_{AUTH} + 597.13,\ r^2 = 0.80 \quad (3.5)$$

and

$$Av = 45.767\ (M_{AUTH})^2 - 550.48\ M_{AUTH} + 1662.4,\ r^2 = 0.92 \quad (3.6)$$

The shallow earthquake listed with code number 48 in Table 3.3 is an outlier and, therefore, it has not been taken into account to produce the relation (3.5). This is the 15 July 1909 earthquake (M_{AUTH}=5.7) with estimated epicenter near Chavari village in NW Peloponnese (Fig. 3.2, n. 48). This event was recorded at the Agamennone ATH station with trace wave amplitudes A_{NS}=39 mm and A_{EW}=68 mm, average Av=53.5 mm. It is noticeable that 6 out of 52 earthquakes were recorded not only in ATH station but also in other Agamennone stations.

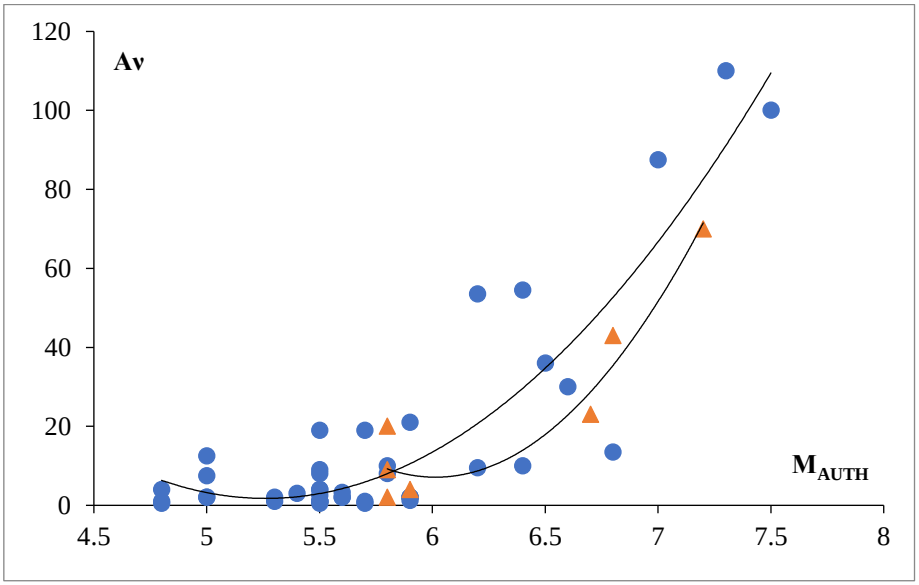

Figure 3.4. Amplitude, Av, recorded by the Agamennone instrument at ATH station against M_{AUTH} magnitude for shallow and intermediate-depth earthquakes shown by circles and triangles, respectively (data in Table 3.3).

For each earthquake event examined, the next three magnitude types were sequentially produced with the procedure adopted: M_a is the initial magnitude calculated from one record in an Agamennone station by applying formulas (3.3) and (3.4) for shallow and intermediate-depth earthquakes, respectively; M_{ac} is the magnitude received after calibrating M_a to M_{AUTH}; the final Agamennone magnitude, M_A, of a single earthquake event is the average of the M_{ac} values received from more than one stations, if available. Otherwise, M_A equals to the single M_{ac} value.

The magnitude misfits, D_a and D_A, have also been calculated for each earthquake event; where D_a is the absolute value of the difference between the magnitudes M_{AUTH} and M_a, D_A is the absolute value of the difference between M_{AUTH} and M_A, i.e. $D_a = \left| M_{AUTH} - M_a \right|$ and $D_A = \left| M_{AUTH} - M_A \right|$.

3.4.2 Magnitude determination from Agamennone records

To calculate M_a for shallow earthquakes, amplitudes A (in mm) from records at ATH station and epicentral distances Δ (in km) based on epicenter coordinates listed in the AUTH catalogue were inserted in formula (3.3). The mean of the difference $D_a = \left| M_{AUTH} - M_a \right|$ was found equal to 1.4±0.4. Then, the calibrated Agamennone magnitude, M_{ac}, was calculated as $M_{ac} = M_a + 1.4$ and eventually the final Agamennone magnitude M_A was received as described above. The M_A/M_{AUTH} correlation is shown in Figure 3.5 and after regression the best-fit line found is expressed by the formula 3.7. The magnitude misfit was found equal to $D_A = 0.3 \pm 0.2$.

$$M_A = 0.37 + 0.93\, M_{AUTH}, \quad r^2 = 0.74 \qquad (3.7)$$

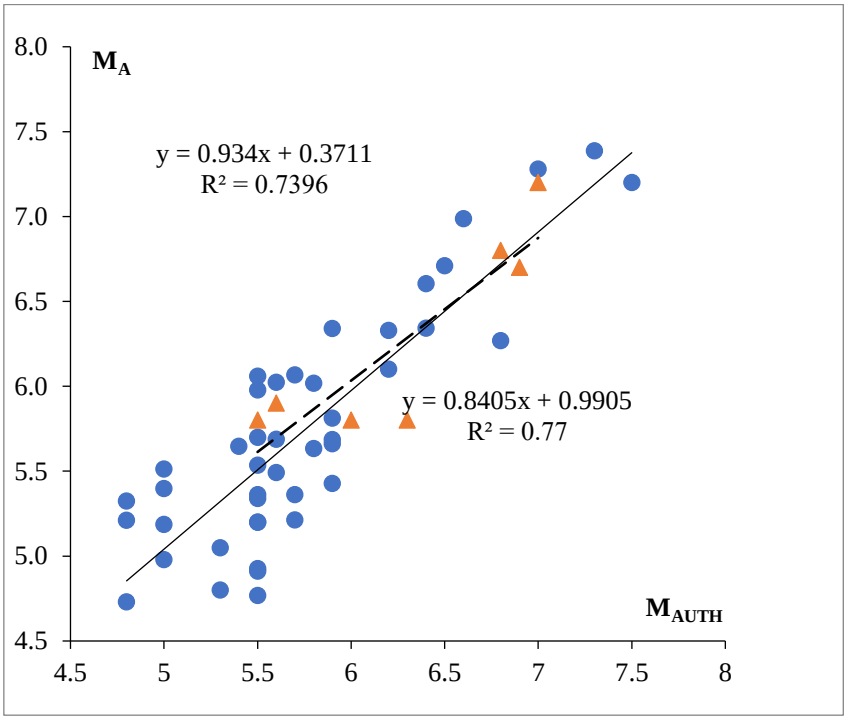

Figure 3.5. Agamennone magnitude, M_A, against magnitude M_{AUTH} for shallow (circles) and intermediate-depth (triangles) earthquakes for the period 1900-1910.

Four out of 45 shallow earthquakes (events 5, 6, 32, 45 in Table 3.4) were recorded not only by the ATH station but also by other stations. In general, for each event consistent magnitudes M_{ac} were calculated from different stations although some inconsistencies were noted. For the earthquake of 11 April 1902 (M_{AUTH}=5.5) we found M_{ac} equal to 4.8, 5.6 and 5.1 for ATH, CHA and CAL stations, respectively; then M_A=5.2. For the earthquake of 26 May 1902 (M_{AUTH}=5.5) we found M_{ac} equal to 5.2 for both the ATH and CAL stations. Magnitude M_{ac} of 7.1 and 7.3 (M_A=7.2) have been calculated for ATH and CAL stations for the large earthquake of 8 November 1905. The M_{AUTH}=7.5 for this earthquake is overestimated not only with respect to the magnitude found here but also as compared to the magnitude M_w=7.26 calculated independently in the ISC-GEM and AM catalogues and to the macroseismic magnitude of ~7 found by Triantafyllou et al. (2020a; see also Chapter 5). For the event of 30 May 1909 (M_{AUTH}=6.2) we found M_{ac} equal to 6.3 and 5.9 for the ATH and EGI stations, respectively, then M_A=6.1. For the event of 19 June 1909 (M_{AUTH}=5.5) we found M_{ac}=4.9 for both the ATH and EGI stations, respectively.

Magnitudes, M_a, of intermediate-depth earthquakes (Table 3.3) have been determined from the formula (3.4) with the adoption of epicentral coordinates from the AUTH catalogue and calculation of hypocentral distances, *R* (km), from the ATH station. M_a was found to correlate well with M_{AUTH}, the magnitude misfit being equal to D_a=1.5±0.3. Then, we calculated calibrated Agamennone magnitude as $M_{ac}=M_a+1.5$ and final Agamennone magnitude M_A with the procedure described earlier for the magnitude determination of shallow earthquakes. The M_A/M_{AUTH} correlation is shown in Figure 3.5. The best-fit linear relation obtained (3.8) is:

$$M_A = 0.99 + 0.84\, M_{AUTH}, \quad r^2 = 0.77 \qquad (3.8)$$

Three out of 7 intermediate-depth earthquakes (n. 38, 39 and 52; Table 3.3) have been recorded not only in ATH station but also in other stations. The magnitudes M_A found from different stations for

each one of the events examined are generally consistent. The magnitude misfit was found equal to D_A=0.2±0.1.

3.4.3. Shallow earthquakes: correction of magnitude misfits

The epicentral distance, *Δ*, is one of the parameters involved in the magnitude determination from Agamennone station records. To calculate *Δ* we adopted epicentral coordinates listed in the AUTH catalogue. In a few cases, however, significant magnitude misfit, D_A, was found. Therefore, from macroseismic information we investigated alternative epicenter solutions that may decrease D_A. If an event was recorded by more than one Agamennone instruments the new epicenter was also controlled by the first arrival times in the Agamennone stations and occasionally by *P*-*S* travel-time curves.
A misfit case regards the earthquake (M_{AUTH}=5.5) that occurred in the northwestern termination of the Corinth Gulf on 2 August 1902. This event caused fissures to the fortress of Rio town and the collapse of three houses in Nafpaktos town (Anonymous, 1899-1913, Press reports [3.8.1904, O.S.], Eginitis, 1905). Based on the macroseismic observations we adopted an epicenter location (38.5^{o}N/21.8^{o}E; Fig. 3.2, n. 9), which is shifted by a few km to the north with respect to that listed in the AUTH catalogue. This selection caused the smallest misfit between the magnitude calculated here (M_A=5.2) and the M_{AUTH}=5.5.

Another misfit case concerns a set of three strong earthquakes (n. 20, 21, 23 in Table 3.3, Fig. 3.2) occurring during the 1904 seismic sequence that was recorded in the eastern Aegean Sea, near Samos Island. The M_{AUTH}=6.8 of the first shock, occurring on 11 August 1904, is overestimated not only as compared to the M_A=6.3 calculated here but also to magnitudes inserted in other catalogues, e.g. M_s=6.2 (Kárník, 1996), M_w=6.1 (Kalafat et al., 2007), M_{wUOA}=6.0. However, more consistent magnitudes are listed in various catalogues (e.g. Kárník, 1996, Kalafat et al., 2007) for the strong aftershocks of 18 August 1904 (M_{AUTH}=5.9) and 10 October 1904 (M_{AUTH}=5.8). The main shock of 11 August 1904 hit the island of Samos causing damage to several buildings and the collapse of about 60 houses in several villages, while 10 persons were killed and 20 injured (Anonymous, 1899-1913, Press reports [16.8.1904, O.S.], Eginitis, 1905). Very likely, the earthquake had its epicenter close to the island. However, no important damage was reported after the strong aftershocks, implying that likely they had epicenters away from the island. For the first earthquake our calculation returned M_A=6.3 for an alternative epicenter solution of 37.7^{o}N/27.1^{o}E (Fig. 3.2, n. 20), which is slightly different from that inserted in the catalogues of AUTH and Kalafat et al. (2007). For the first and second aftershocks, however, we adopted epicentral coordinates 37.9^{o}N/26.7^{o}E and found M_A=6.3 and M_A=6.0, respectively (Fig. 3.2, n. 21 and 23). The three epicenters are well controlled by *P*-*S* travel-time curves.

The 30 May 1909 earthquake (M_{AUTH}=6.2) was recorded by the ATH and EGI Agamennone stations. The earthquake caused damage in several villages at the northwestern Corinth Gulf area. Based on various sources (Anonymous, 1899-1913, Press reports, [June 1909, N.S.], Eginitis, 1912) we assigned epicentral intensity MMI_o=VII-VIII. The most consistent magnitudes of M_A=6.3 for ATH and M_A=5.9 for EGI stations were found for an epicenter located at 38.5^{o}N/22.4^{o}E (Fig. 3.2, n. 45). This epicenter falls within the meizoseismal area but is shifted to the northeast with respect to the AUTH epicenter. The new epicenter is well controlled by *P*-*S* travel-time curves for the most distant ATH station at epicentral distance *Δ*~130 km.

3.5 Summary of Chapter 3

Seismic wave amplitudes recorded by Agamenonne seismographs and published in the NOA Bulletins have been utilized for the first time to redetermine magnitudes of 52 shallow and intermediate-depth earthquakes occurring in the region of Greece from 1901 to 1910. The method is based on calibrating the ground motion amplitudes recorded at Agamenonne stations during the period 1901-1910 on magnitudes determined (Papazachos and Comninakis, 1971, 1972) by Mainka and Wiechert seismograph records for the post-1910 period. The AUTH magnitudes of these earthquakes range from 4.8 to 7.5, while the calculated magnitudes range from 4.7 to 7.4. The method proved successful and opens the way for magnitude calculation from Agamenonne records of smaller events that occurred in the 1901-1910 period.

CHAPTER 4. INSTRUMENTAL SEISMICITY (1900-2020): COMPARISON OF CATALOGUES

4.1 Introduction

In this study we need to compare several catalogues covering the Greek area for the entire instrumental period (1900-2020). After testing for completeness in Chapter 2, the magnitudes and focal depths of the seismicity catalogues for the Greek region are compared with statistical methods. As far as we know this is the first time that such a comparison is attempted. The magnitude redetermination of 52 earthquakes for the period 1900-1910 (Chapter 3) have not been involved in the present analysis.

4.2 Magnitude comparison

4.2.1 Data and procedures

The data used in the present analysis are the catalogues listed in Table 2.1. For reasons of consistency we compared M_w in all catalogues. Therefore, M_s listed in the UOA catalogue has not been used in our analysis. For the same reason we organized a revised version of the AM catalogue as follows. The AM catalogue extends in the time interval from 1900 to 1999 and lists 135 earthquakes all being shallow ($h \leq 40$ km) and of $M_s \geq 6.0$ by default. Magnitudes M_s listed for all the events in the AM catalogue have been calculated from bulletin readings of long-period phases for each event examined. For events occurring after 1961, the AM catalogue provides also seismic moment M_o based on various sources, e.g. P/SH modelling or the GCMT project. Then, from an empirical $M_s/\log M_o$ relationship (formula 1.1) obtained by the author of the AM catalogue (Ambraseys, 2001) we calculated magnitude M_w for the pre-1962 events too. In this way we obtained a revised catalogue, AMR, with magnitudes M_w or proxy-M_w for all the events in the entire time interval 1900-1999 covered by the catalogue.

Magnitudes M_{AMR} inserted in the AMR revised catalogue were compared only with magnitudes, $M_{ISC\text{-}GEM}$, of earthquakes inserted in the ISC-GEM catalogue, for reasons explained later. After comparing the pair $M_{ISC\text{-}GEM}/M_{AMR}$, three pairs of the magnitudes $M_{ISC\text{-}GEM}$, M_{UOA} and M_{AUTH} of the ISC-GEM, UOA and AUTH earthquake catalogues, respectively, were compared. For the comparisons of $M_{ISC\text{-}GEM}/M_{UOA}$ and $M_{ISC\text{-}GEM}/M_{AUTH}$ all the events listed in ISC-GEM have been considered. We recall that in the ISC-GEM catalogue the minimum magnitude inserted is M_w=5.40. In these comparisons, from the UOA and AUTH catalogues all the events that are in common with the ISC-GEM catalogue have been considered, regardless their magnitudes. For the M_{UOA}/M_{AUTH} comparison we considered events with $M_{UOA} \geq 5.0$ and all the corresponding events in the AUTH catalogue regardless their magnitudes.

4.2.2 $M_{ISC\text{-}GEM}$ / M_{AMR} comparison

For the Greek region, the AMR and ISC-GEM catalogues have in common 127 out of 135 events listed in the AMR catalogue. A comparison between $M_{ISC\text{-}GEM}$ and M_{AMR} shows that the magnitudes

in the 127 common events are statistically well correlated (Fig. 4.1). The average magnitude difference $\delta M=M_{ISC\text{-}GEM}-M_{AMR}$ equals to 0.03±0.16. No systematic change of δM is observed with the change of M_{AMR} (Fig. 4.2), although for a few events $M_{ISC\text{-}GEM}$ is overestimated for $M_{AMR}\geq 7.3$ and underestimated for $M_{AMR}\leq 6.0$ (Figs 4.2, 4.3). These results imply very small magnitude differences with larger differences in a few events.

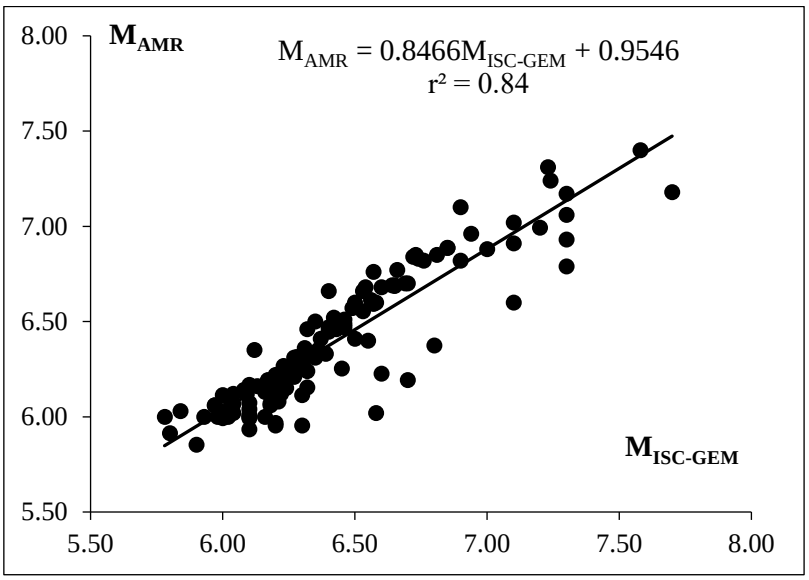

Figure 4.1. Magnitudes M_{AMR} plotted against $M_{ISC\text{-}GEM}$; r=correlation coefficient.

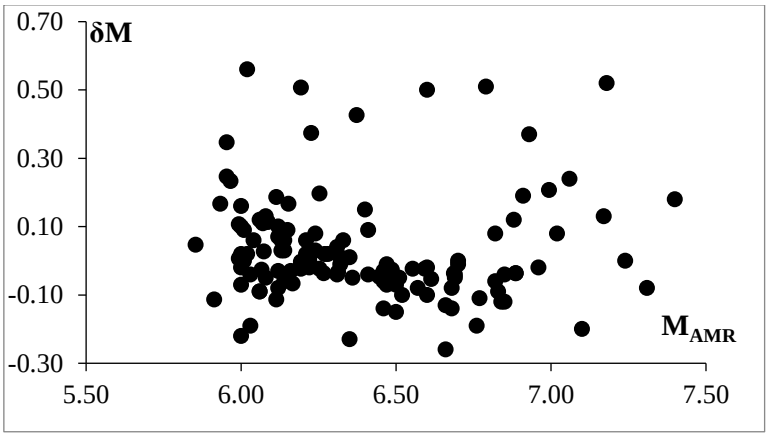

Figure 4.2. Magnitude difference $\delta M=M_{ISC\text{-}GEM}-M_{AMR}$ plotted against M_{AMR}.

The characteristics of the AMR (and AM) catalogue are summarized as follows: (1) includes small number of events, (2) includes only shallow, strong events ($M_s\geq 6.0$), (3) magnitude M_w is available only from 1962 onwards but proxy-M_w can be calculated for the pre-1962 period (already done in AMR catalogue), (4) magnitudes M_{AMR} are well correlated with $M_{ISC\text{-}GEM}$. Based on these characteristics the AM catalogue has not been considered further in the present analysis.

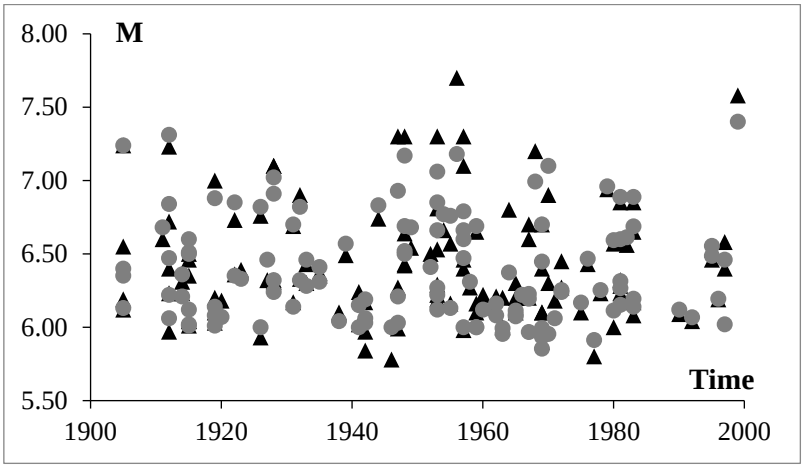

Figure 4.3. Magnitudes $M_{ISC-GEM}$ (black triangle) and M_{AMR} (gray circle) plotted against time.

4.2.3 $M_{ISC-GEM}$ /M_{UOA} comparison

Comparing $M_{ISC-GEM}$/M_{UOA} we found that the two magnitudes are in general correlated well (Fig. 4.4). However, the average difference $\delta M=M_{ISC-GEM}-M_{UOA}$ was found equal to 0.24±0.21, which implies that there is a trend for $M_{ISC-GEM}$ overestimation with respect to M_{UOA}. This is valid particularly for $M_{UOA}<6.1$ where $M_{ISC-GEM}$ is systematically overestimated (Fig. 4.5). For $M_{UOA}\geq 6.1$, however, no systematic change is observed in δM but the absolute values of δM are increased as compared to those for $M_{UOA}<6.1$. The overestimated $M_{ISC-GEM}$ with respect to M_{UOA} for $M_{UOA}<6.1$ is valid for the entire time interval examined but particularly before 1964 (Fig. 4.5). In the upper magnitude bound ($M_{UOA}\geq 7$) $M_{ISC-GEM}$ is as a rule larger than M_{UOA}.

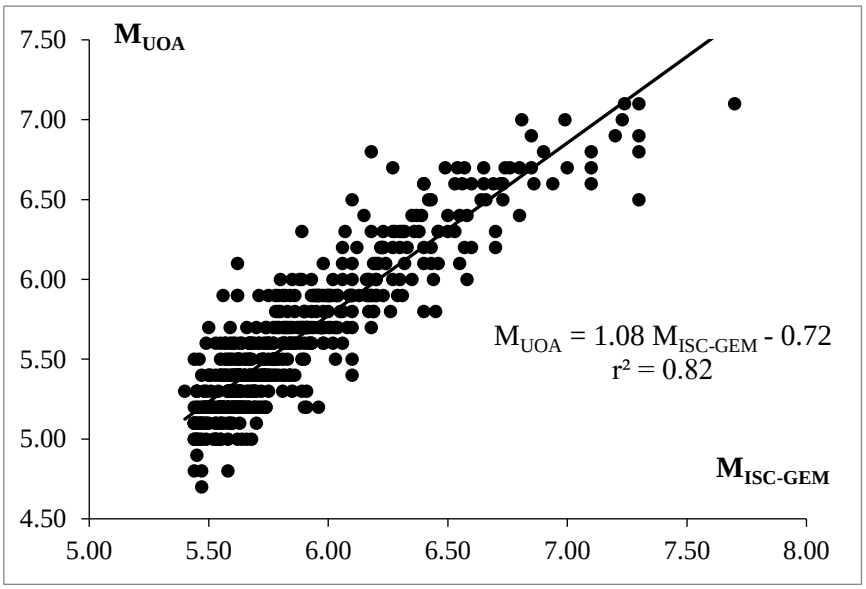

Figure 4.4. Magnitudes M_{UOA} plotted against $M_{ISC-GEM}$; r=correlation coefficient.

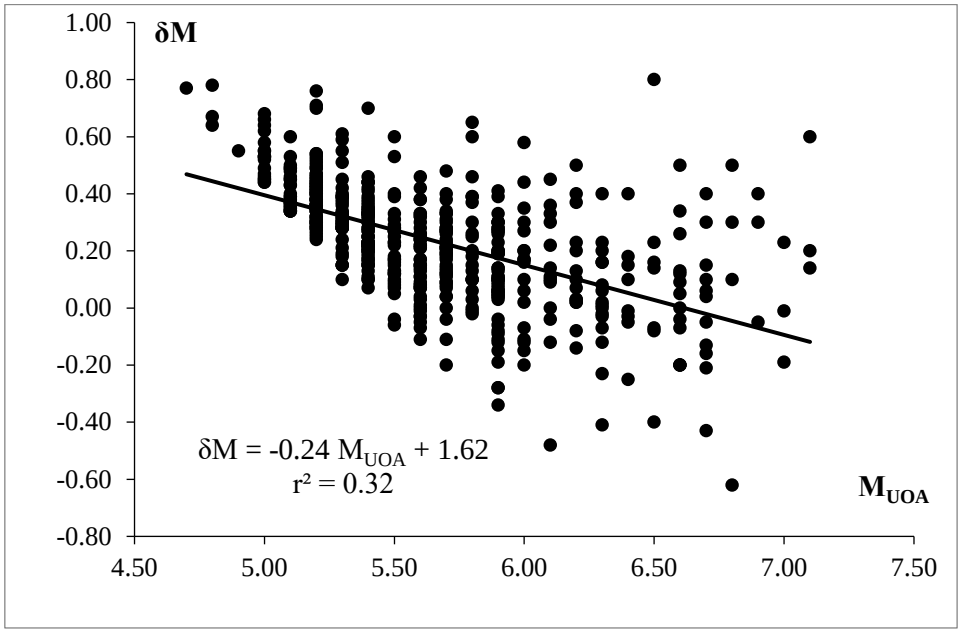

Figure 4.5. Magnitude difference $\delta M=M_{ISC\text{-}GEM}-M_{UOA}$ plotted against M_{UOA}; r=correlation coefficient. No good correlation exists between δM and M_{UOA}.

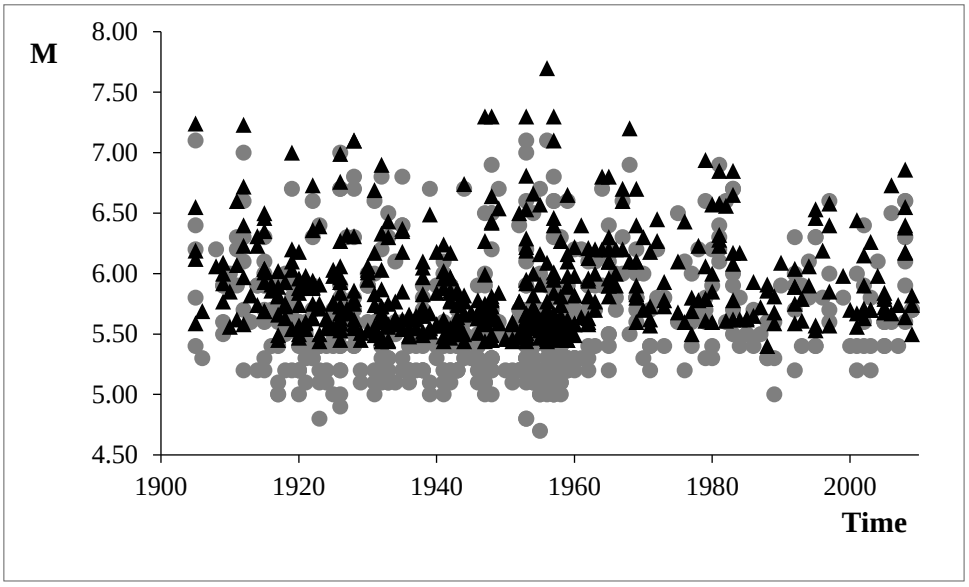

Figure 4.6. Magnitudes $M_{ISC\text{-}GEM}$ (black triangle) and M_{UOA} (gray circle) plotted against time.

4.2.4 $M_{ISC\text{-}GEM}$ / M_{AUTH} comparison

Magnitudes $M_{ISC\text{-}GEM}$ and M_{AUTH} are in general well correlated (Fig. 4.7). The average difference $\delta M=M_{ISC\text{-}GEM}-M_{AUTH}$ was found equal to 0.03±0.23, which although is smaller than the difference $\delta M=M_{ISC\text{-}GEM}-M_{UOA}$, yet it implies that some important magnitude misfits exist. As an instance, δM reached up to -1.03 as regards the event of 4 April 1911 with $M_{ISC\text{-}GEM}$=6.07 (shallow event) and M_{AUTH}=7.1 (intermediate-depth event). On the other hand, δM is gradually decreasing with the increase of M_{AUTH} (Figure 4.8). For magnitudes <5.9, however, M_{AUTH} is underestimated as compared to $M_{ISC\text{-}GEM}$. This is particularly evident for the time interval before 1964 (Fig. 4.9). On the contrary, for M_{AUTH}>5.9, and particularly for $M_{AUTH}\geq$7 there is a trend of M_{AUTH} overestimation, whilst the absolute value of δM is gradually increasing with the increase of magnitude (Fig. 4.8).

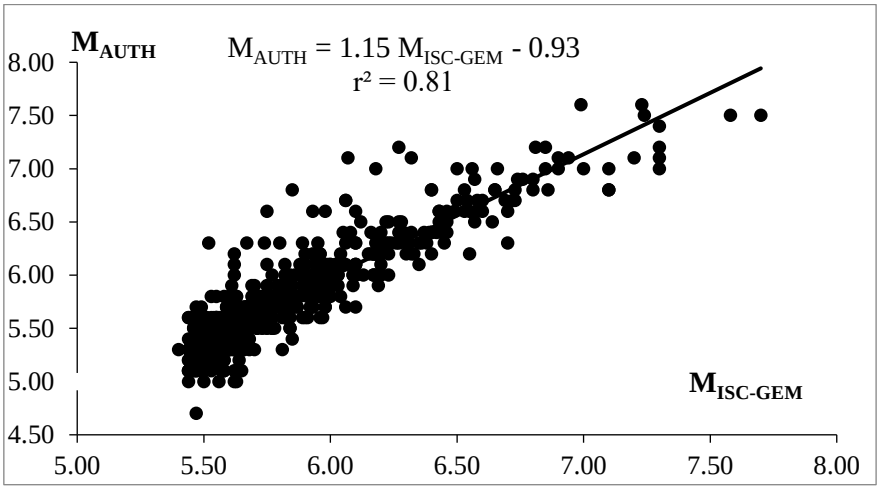

Figure 4.7. Magnitudes M_{AUTH} plotted against $M_{ISC-GEM}$; r=correlation coefficient.

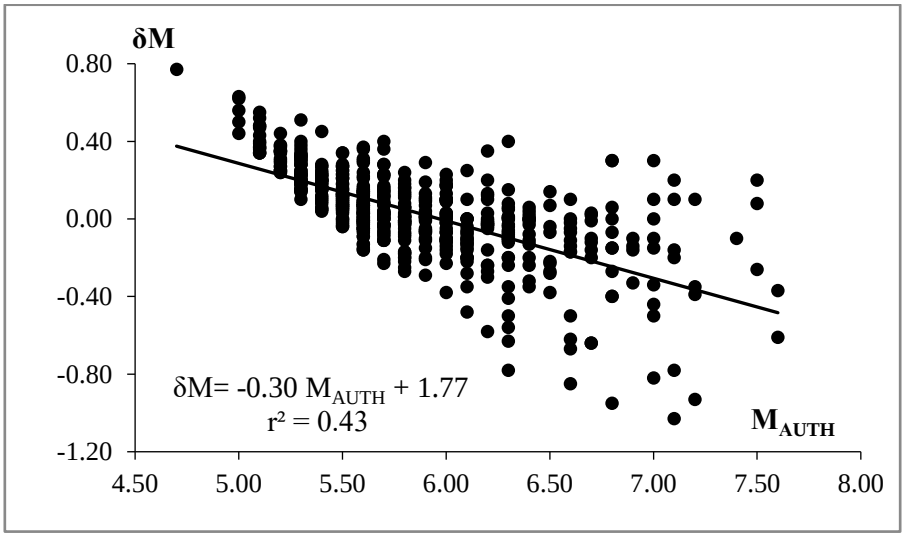

Figure 4.8. Magnitude difference $\delta M=M_{ISC-GEM}-M_{AUTH}$ plotted against M_{AUTH}; r=correlation coefficient.

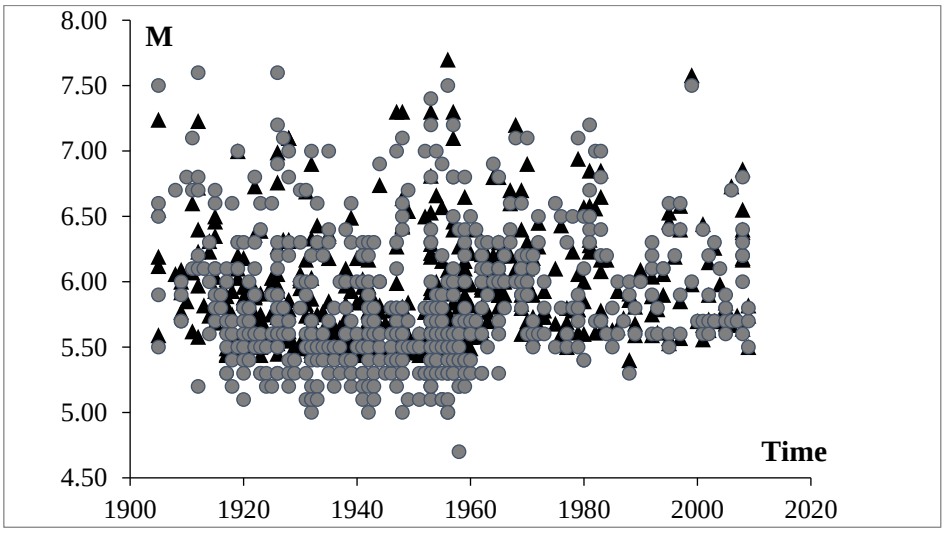

Figure 4.9. Magnitudes $M_{ISC-GEM}$ (black triangle) and M_{AUTH} (grey circle) plotted against time.

4.2.5 M_{UOA} / M_{AUTH} comparison

To compare magnitudes M_{UOA} and M_{AUTH} we collected earthquakes with $M_{UOA} \geq 5.0$ and the corresponding earthquakes from the AUTH catalogue regardless their magnitudes. We found 1501 such events. The M_{UOA} and M_{AUTH} are in general well correlated (Fig. 4.10). However, the difference $\delta M = M_{UOA} - M_{AUTH}$ was found equal to -0.10 ± 0.23. This implies that M_{UOA} is slightly smaller than M_{AUTH} as an average but several events are characterized by important magnitude discrepancies in the two catalogues (Fig. 4.11). In fact, δM values as high as 1.2 are observed for $M_{AUTH} \leq 5.8$. For $M_{AUTH} \geq 5.9$ absolute δM values are decreased and do not exceed 0.7. However, in the upper magnitude bound as a rule it is $M_{AUTH} > M_{UOA}$, which is valid for $M_{AUTH} > 7.0$ until 1963 and for $M_{AUTH} > 6.7$ after 1963 (Fig. 4.12). On the other hand, in the lower magnitude bound ($M_{UOA} \leq 5.5$) M_{AUTH} is systematically underestimated with respect to M_{UOA} after 1950.

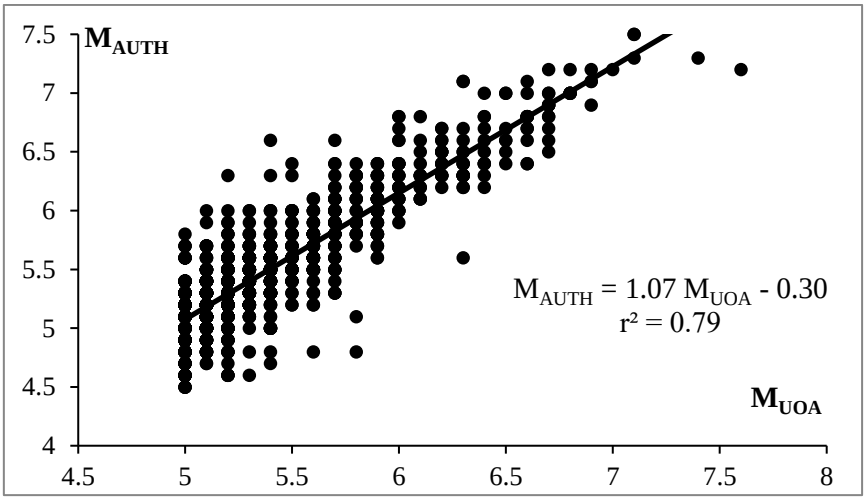

Figure 4.10. Magnitudes M_{AUTH} plotted against M_{UOA}; r=correlation coefficient.

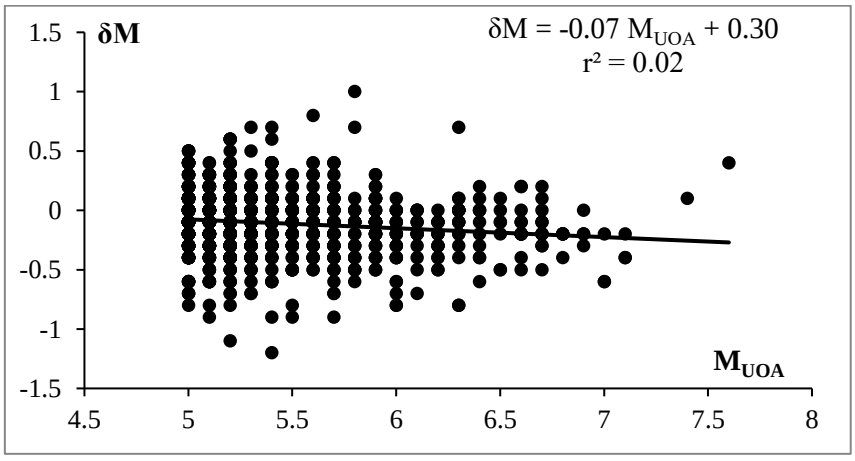

Figure 4.11. Magnitude difference $\delta M = M_{UOA} - M_{AUTH}$ plotted against M_{UOA}; r=correlation coefficient. M_{UOA} and δM are not correlated.

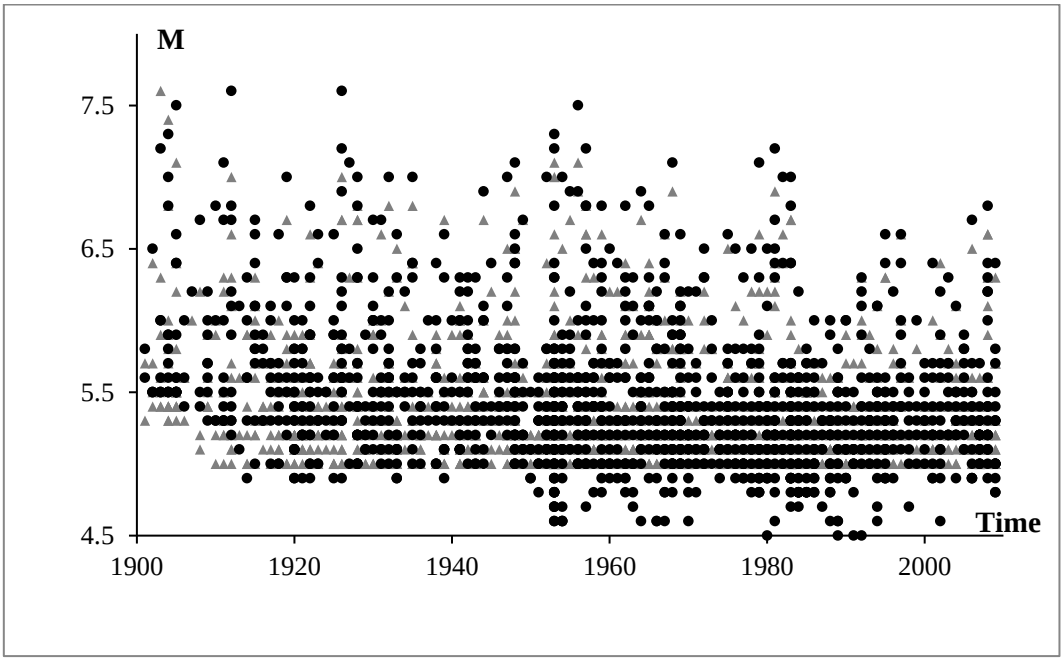

Figure 4.12. Magnitudes M_{AUTH} (black circle) and M_{UOA} (grey triangle) plotted against time.

4.3 Focal depth comparison

4.3.1 Data and procedures

From the catalogues listed in Table 2.1 we compared focal depths $h_{ISC\text{-}GEM}$, h_{UOA} and h_{AUTH} inserted in the catalogues ISC-GEM, UOA and AUTH, respectively. The AM catalogue has not been considered here since it lists only shallow earthquakes, defined as of focal depth $h \leq 40$ km. Besides, that catalogue does not list h value for the earthquakes listed. The focal depths $h_{ISC\text{-}GEM}$, h_{UOA} and h_{AUTH} range from 10 to 152.7 km, from 0 to 215 km and from 0 to 200 km, respectively.

For the comparisons performed one should consider the various sources of uncertainty involved in the focal depth determinations. Sources of uncertainty are associated with the different methods of location or relocation used in a catalogue as well as with the geotectonic complexity of the Greek region, which produces both shallow and intermediate-depth earthquakes. The uncertainty is particularly high in the pre-1964 time period, i.e. before the operation of the national seismograph network within the frame of the WWSSN. For these reasons the insertion of fixed focal depths is quite often for that period. In the ISC-GEM catalogue three values of fixed focal depth can be found: 10 km, 15 km, 25 km. In the AUTH catalogue a frequent fixed focal depth used to indicate shallow source is the value 0. In the UOA catalogue, however, the 0 value is less frequently inserted.

Comparing $h_{ISC\text{-}GEM}/h_{UOA}$ and $h_{ISC\text{-}GEM}/h_{AUTH}$ all the events listed in ISC-GEM have been considered. In these comparisons, from the UOA and AUTH catalogues all the events that are in common with the ISC-GEM catalogue have been considered, regardless their magnitudes and focal depths. For the M_{UOA}/M_{AUTH} comparison we considered events with $M_{UOA} \geq 5.0$ and all the corresponding events in the AUTH catalogue regardless their magnitudes and focal depths.

4.3.2 $h_{ISC\text{-}GEM}$ / h_{UOA} comparison

The $h_{ISC\text{-}GEM}$/h_{UOA} comparison shows that the earthquakes can be classified in four groups according to the focal depth distribution in the two catalogues (Fig. 4.13). One group includes earthquakes with the same or about the same $h_{ISC\text{-}GEM}$ and h_{UOA} values. The other three groups are the ones comprising events with $h_{ISC\text{-}GEM}$ fixed at 10, 15 km and 25 km. In these groups the h_{UOA} varies in a wide range of values. The most wide range is the one extending from 2 km to 215 km and corresponding to fixed $h_{ISC\text{-}GEM}$=15 km.

The average difference $\delta h=h_{ISC\text{-}GEM}-h_{UOA}$ was found equal to -14.91±28.37, which reflects two main features. The first is that h_{UOA} is systematically larger than $h_{ISC\text{-}GEM}$, which is particularly valid before 1963. To interpret this feature one may consider that in the UOA catalogue 605 earthquakes with available first arrival readings in the time period 1917-1963, were relocated with the Joint Epicenter Determination method (Douglas, 1967) and Herrin68 travel-time tables (Herrin et al., 1968). Focal depths of the remaining events in the catalogue were collected from various sources but after 1985 earlier versions of the ISC-GEM catalogue were adopted. On the other hand, for the pre-1963 period the ISC-GEM catalogue is dominated by fixed shallow focal depths with only a few intermediate-depth cases. The second feature, which is indicated by the high standard deviation involved in the average δh value, is that there are significant focal depth discrepancies for several events.

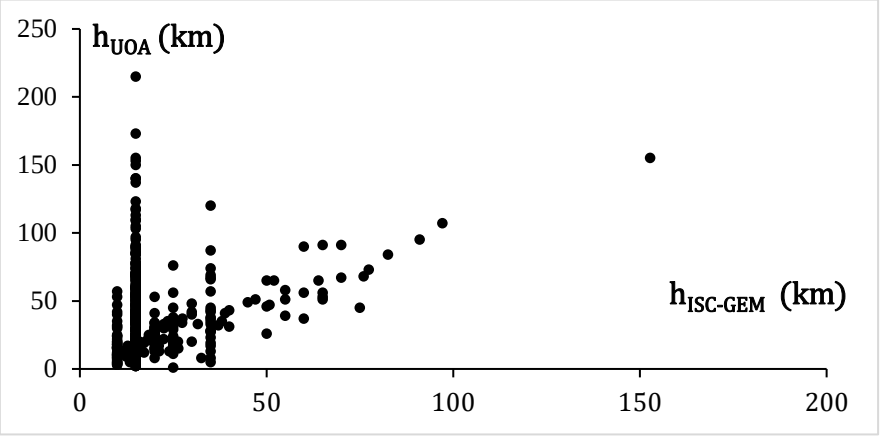

Figure 4.13. Plot of focal depth h_{UOA} against focal depth $h_{ISC\text{-}GEM}$. The issue of the fixed focal depths is noted in the text.

4.3.3 $h_{ISC\text{-}GEM}$ / h_{AUTH} comparison

In the pair $h_{ISC\text{-}GEM}$/h_{AUTH} several groups can be found too (Fig. 4.14). One group includes earthquakes with the same or about the same $h_{ISC\text{-}GEM}$ and h_{AUTH} values. Three groups are the ones comprising events with $h_{ISC\text{-}GEM}$ fixed at 10, 15 and 25 km. In these groups the h_{AUTH} varies in a wide range of values, e.g. from 0 to 180 km for $h_{ISC\text{-}GEM}$ fixed at 15 km, although 0 value in the AUTH catalogue just means shallow event. The average difference $\delta h=h_{ISC\text{-}GEM}-h_{AUTH}$ is 9.53±21.96, which indicates that $h_{ISC\text{-}GEM}$ is systematically larger than h_{AUTH} but there are significant focal depth discrepancies for several events. However, one may consider that in the AUTH catalogue shallow earthquakes, which make the vast majority in the catalogue, are given h=0 until the year 1963. On the contrary, for the same period the ISC-GEM catalogue for shallow earthquakes as a rule provides fixed depths at 10, 15 or 25 km. We recalculated the difference $\delta h=h_{ISC\text{-}GEM}-h_{AUTH}$ for the time period from 1964 onwards and found δh=4.69±4.74. Since the average is nearly equal to the standard deviation we

concluded that $h_{ISC-GEM}$ is slightly larger that h_{AUTH} but with only small discrepancies. In other words, in this case the difference is rather random.

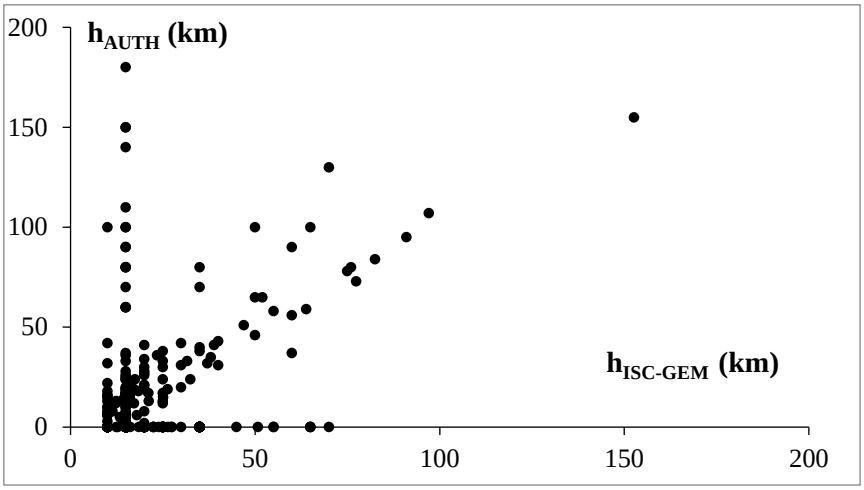

Figure 4.14. Plot of focal depth h_{AUTH} against focal depth $h_{ISC-GEM}$. The issue of the fixed focal depths is noted in the text.

4.3.4 h_{UOA} / h_{AUTH} comparison

We found that the difference $\delta h = h_{UOA} - h_{AUTH}$ is 11.48±6.94. However, in some cases important δh values were found. For example, focal depths h_{UOA}=150 km and h_{AUTH}=0 km have been estimated for the event of 5 April 1925 (M_{UOA}=5.6, M_{AUTH}=5.9); for the event of 9 July 1956 (M_{UOA}=M_{AUTH}=6.9) h_{UOA}=95 km and h_{AUTH}=0 km have been estimated. The plot of h_{AUTH} against h_{UOA} (Fig. 4.15) illustrates that the earthquakes can be distinguished in four main groups with the next features: (1) h_{UOA}=h_{AUTH} in the entire magnitude range; this is due to that focal depths in the UOA catalogue have been adopted from AUTH catalogue at large extend, except for the period 1917-1963; (2) $\delta h = h_{UOA}$ for h_{AUTH}=0, with the majority of events (619) being of $h_{UOA} \geq 10$ km; (3) small δh values in the range 0-30 km; (4) large δh values for h>30 km in both catalogues.

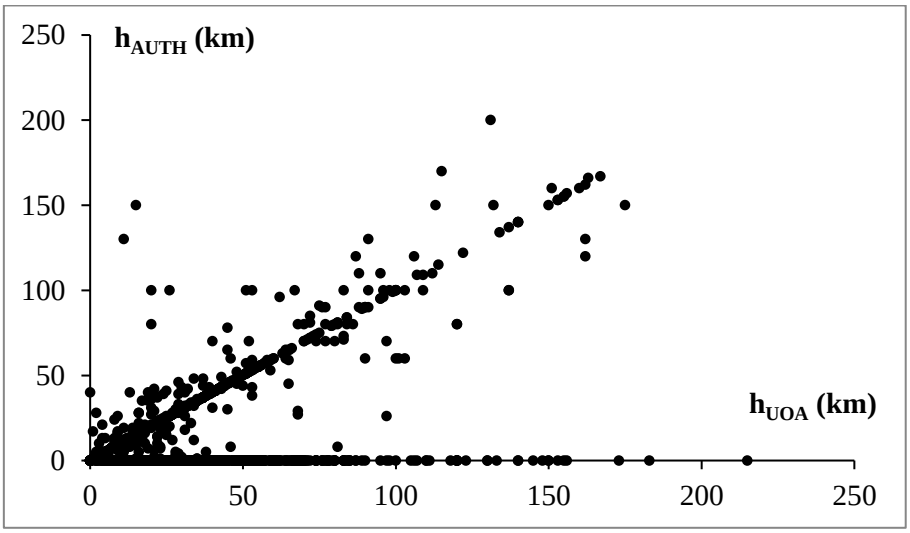

Figure 4.15. Plot of focal depth h_{AUTH} against focal depth h_{UOA}. The issue of the fixed focal depths is noted in the text.

4.4. Summary of Chapter 4

The magnitude $M_{ISC\text{-}GEM}$ is overestimated, as a rule, with respect to the M_{UOA} and the M_{AUTH} for the magnitude range <6.0 particularly before 1964. $M_{ISC\text{-}GEM}$ overestimates also the M_{UOA} in the upper magnitude bound, i.e. for $M_{UOA} \geq 7$. However, for $M_{AUTH}>5.9$ the M_{AUTH} overestimates the $M_{ISC\text{-}GEM}$. M_{UOA} is smaller than M_{AUTH} as an average but for $M_{UOA} \leq 5.5$ it overestimates M_{AUTH} after 1950.

The focal depth h_{UOA} is systematically larger than $h_{ISC\text{-}GEM}$, which is particularly valid before 1964. The h_{AUTH} is systematically larger than $h_{ISC\text{-}GEM}$ but h_{UOA} in general overestimates h_{AUTH} particularly in the range of h>30 km. It should be noted that in the time period 1917-1963 the focal depths in the UOA catalogue have been obtained after a procedure of relocation.

CHAPTER 5. THE GREEK EARTHQUAKE IMPACT DATABASE (GEIDB)

5.1 Introduction

The construction of the Greek Earthquake Impact Database (GEIDB) is one of the main objectives of the present thesis. In this Chapter, after a short review about the efforts made internationally as well as in Greece for the compilation of earthquake impact data sets, we describe the construction of the GEIDB. To this aim we collected and evaluated data from a large number of sources as well as during our post-event field surveys performed after recent strong earthquakes in Greece. After a detailed analysis of the sources used, the structure and the content of the GEIDB is presented. Particular attention has been given to the selection of the seismicity parameters inserted in the GEIDB based on the findings of the Chapters 2, 3 and 4.

Here the term "earthquake impact data" is referred to data regarding the direct effects of earthquakes on the population and on the buildings as a result of the ground shaking. From the environmental earthquake effects, tsunami information is also included in the GEIDB. However, tsunamis cause their own effects on the population and on the built environment. Therefore, in Chapter 8 we organized the Greek Tsunami Impact Database (GTIDB), which is a supplement to the GEIDG.

5.2 Global review

5.2.1 Compilations of earthquake impact data

Earthquake impact data can be found in a long list of seismicity catalogues, reports, books, scientific papers and websites regarding earthquakes occurring in both the historical and the instrumental periods of seismicity. Earthquake impact data were first inserted in descriptive global earthquake catalogues compiled as early as the 19th century, including the catalogues by Perrey (1844-1873) and Mallet (1850-58) and later by Montesus de Balore (1906), Milne (1912), Sieberg (1932), Montandon (1953) and Rothé (1969).

In the 1970s the National Oceanic and Atmospheric Administration (NOAA) of USA started systematic compilation of earthquake impact data and organized a database of significant earthquakes of the world. The Significant Earthquake Database of NOAA contains information on destructive earthquakes occurring from 2150 B.C. up to the present under the condition that meet at least one of the following criteria: moderate damage (approximately $1 million or more), 10 or more deaths, magnitude 7.5 or greater, Modified Mercalli (MM) Intensity X or greater, or generation of tsunami by the earthquake. Data contained in that database appeared from time to time in several internal reports (e.g., Ganse and Nerlson, 1981).

Utsu (1990) made a significant contribution with the organization of a world list of hundreds of earthquakes that caused some kind of impact, i.e. death and/or injured people and/or building damage. The list starts from 3000 BC and terminates in 1989. Apart from the earthquake focal parameters, the list contains the numbers of casualties and injuries as well as a qualitative indication about the level of building damage, e.g. limited, some, moderate or severe damage. In 1992 the Executive Committee

for IDNDR (International Decade for Natural Disaster Reduction) in the International Symposium on Earthquake Disaster Reduction Technology, Japan, published the Earthquake Disaster Reduction Handbook (EDRH, 1992). The handbook included a catalogue of destructive earthquakes in the world in the time period 1500-1992 along with the number of people killed per event. Apart from the death toll there is also an indication about surface faulting and/or tsunami generation that accompanied the earthquakes.

Xinlian (1992) compiled a list of large ($M \geq 7$) earthquakes which caused heavy damage in China from 1900 to 1988. This list includes the number of people killed or injured as well as numbers or percentage of buildings damaged, destroyed or collapsed. A list of deadly earthquakes in the World for the years 1500-2000 was compiled by Utsu (2002). This list contains information for earthquakes that reportedly killed at least 50 people. The data have been collected from various sources, research articles, and reports. However, this list is neither complete nor accurate especially for the old-time events.

Samardjieva and Badal (2002) examined human losses after strong earthquakes that occurred in the world during the 20^{th} century. These authors found that the numbers of deaths in general increase with the earthquake magnitude but, on the other hand, the population density plays also an important role. Similar results were reached in the contribution by Chen et al. (2005) who examined earthquakes that caused deaths and injuries in the Chinese mainland from 1980 up to 2000. It is noteworthy that M_s=5.0 is the minimum magnitude of earthquake inserted in the list compiled by Chen et al. (2005). An updated list of earthquake disaster losses in China mainland from 1992 to 2017, including the number of deaths and injured people as well as of the economic losses, was published by Jia et al. (2019).

In the last decades several efforts have been made to compile global or regional electronic earthquake impact databases. These efforts are reviewed briefly in the next lines (see Table 5.1 for a summary). One of the first efforts is the Significant Earthquake Database of NOAA mentioned previously. The United States Geological Survey (USGS) maintains a database of significant earthquakes around the world. For each earthquake event parametric information is provided. The Cambridge Earthquake Impact Database (CEQID) contains building damage data since 1960 (Spence et al., 2011). This database provides total recorded casualties, deaths and injuries, as well as casualty rates as a proportion of population and information on dominant types of injury, age groups etc. Analytical tools enable relationships between casualty rates, building classes and ground motion parameters to be determined (Spence et al., 2011).

EM-DAT is a database that contains natural and technological disaster data at global level and for the time period from 1900 up to now. The Centre for Research on the Epidemiology of Disasters (CRED) at the School of Public Health of the Université Catholique de Louvain in Brussels, Belgium, maintains the EM-DAT database. The Asian Disaster Reduction Center (ADRC) organized a global disasters database and proposed GLIDE (GLobal IDEntifier Number) as a common Unique ID code for disasters, including earthquakes. Daniell et al. (2011) developed the database CATDAT that contains data from globally damaging earthquakes as well as secondary effects triggered from strong events. The database covers both the historical and instrumental periods of seismology. The database, however, is not freely accessible.

Table 5.1. Information about Global Earthquake Databases (last access, 9 January 2021).

Name	***Organization***	***Website***
EM-DAT	Catholic University of Louvain	http://www.emdat.be
GLIDE	Asian Disaster Reduction Center (ADRC)	https://glidenumber.net/glide/public/search/search.jsp
Significant Earthquake Database	National Oceanic and Atmospheric Administration (NOAA, USA)	https://www.ngdc.noaa.gov/hazard/earthqk.shtml
Significant Earthquake Database	US Geological Survey (USGS)	https://earthquake.usgs.gov/earthquakes/
CEQID	Cambridge University	http://www.ceqid.org/CEQID/Home.aspx
GEMECD	Global Earthquake Model (GEM)	https://platform.openquake.org/ecd/eventsmap/

The Earthquake Consequences Database (GEMECD), organized in the frame of the Global Earthquake Model (GEM), is a GIS relational database integrated into the GEM OpenQuake web portal (So, 2014). For current events, GEMECD will serve as a clearinghouse of information, posted by users based on the standards and protocols set in the GEMECD documentation. In the long term, GEMECD will be a repository of the most relevant and validated data on consequences of the significant events of the last 40 years around the world. The GEMECD project began in November 2010 and was a 3-year initiative aimed at creating a global database of standardized information of consequences due to the most significant events in the recent past. The GEMECD repository would be the first of its kind, where a full spectrum of earthquake consequences captured in a single database.

5.3 The Mediterranean and Balkans region

The historical record of earthquake occurrences and their impacts in the Mediterranean and the Balkans region is particularly rich due to the long history of the countries in this part of the Earth. Relevant data for that region can be found in descriptive earthquake catalogues of global, regional and national scale. Here we shortly review sources for the earthquake impact in the Mediterranean and Balkans region but leaving Greece for a particular review in the next section.

Global descriptive catalogues which include earthquake impact data for the Mediterranean and the Balkans region are those organized during the 19th and the 20th centuries and reviewed in the previous section. At regional level we find several catalogues including those by Kárník (1969), Evagelatou-Notara (1993), Ambraseys et al. (1994), Guidoboni et al. (1994), Ambraseys and Finkel (1995), Guidoboni and Comastri (2005) and Ambraseys (2009).

A critical review was presented by Tiedemann (1992) who underlined that there are several uncertainties involved in the existing data sets on loss of life. This author presented examples of very divergent death tolls reported for specific earthquakes. A characteristic example is the destructive earthquake that hit Messina, South Italy, on 28 December 1908. The loss of life estimates varies from 58,000 to 100,000 people. Tiedemann (1992) noted also that the factors influencing the loss of life reporting include reliability of the source, mobility of population and the number of people present in the event.

An interesting review on the losses due to historical earthquakes in the Balkan region was published by Abolmasov et al. (2011). These authors collected data from various sources but mainly from the EM-DAT/CRED International Disaster Database. The analysis by Abolmasov et al. (2011) included numbers of fatalities, size of the affected population and costs of material damages caused by 62 earthquakes in countries within the region: Slovenia, Croatia, Bosnia and Herzegovina, Montenegro, Albania, Serbia, Romania, Bulgaria, North Macedonia and Greece. The analysis showed that a significant number of people in the Balkan region were killed (4,974) or were affected (2,033,723) by earthquakes and that many countries suffered significant material damages of 10,410.16 million USD during the analyzed period. Those authors, however, noted that the main disadvantage of using publicly available sources is the lack of consistent data on earthquake damages.

At national level several efforts have been made to compile data related to the earthquake impact in the Mediterranean countries. Here we refer briefly to only some recent examples. In Italy, Del Gaudio et al. (2017) collected damage data on RC buildings after the 2009 L'Aquila earthquake and developed empirical fragility curves. Dolce et al. (2019) organized a damage WebGIS database of past Italian earthquakes under the name Da.D.O. (Observed Damage Database). The WebGIS platform is meant to store and to share data from large post-earthquake damage campaigns. This platform at present includes data sets relevant to nine seismic events that occurred from 1976 (Friuli earthquake) to 2012 (Emilia-Romagna earthquake).

5.4 Review for Greece

Historical documentation for earthquakes and their impact in Greece goes back to the 6th century BC. In the next lines we briefly review the main sources of earthquake impact data, which include earthquake catalogues, books, various studies, databases or other data compilations.

5.4.1 Catalogues, books and studies

Data on the historical earthquake occurrences and their impacts in Greece can be found in the various global and regional earthquake catalogues and books already reviewed in the previous sections and, therefore, they are not repeated here. The book by Sieberg (1932) is an exceptional case for the global earthquake record since it is frequently used as a reference work for Greece as well. However, the reliability of the data contained in Sieberg's book has been questioned, e.g. Albini et al. (2018) supported that the work of Sieberg should be handled with great care. In this section we review national and local compilations starting from mid-19th century.

Systematic collection of macroseismic observations for earthquakes occurring in Greece was established in 1859 by Julius Schmidt, who served as the Director of the National Observatory of Athens (NOA) from 1858 until 1884. The observations were collected by a network of local observers who sent their material to NOA regularly. Observations were also collected from press reports and personal field trips performed by J. Schmidt himself. A catalogue listing more than 3,000 earthquakes was organized and published in the famous book by Schmidt (1879). However, this effort interrupted after J. Schmidt passed away in 1884.

The effort restarted in 1892 by Prof. D. Eginitis, the new NOA Director. The macroseismic material collected by the network of observers managed by NOA was archived in the two-volume unpublished manuscript titled "Book of Earthquakes" (Anonymous, 1893-1901 and Anonymous, 1902-1915; see section 3.3.2). Part of this macroseismic material has been published in the NOA Bulletins (e.g. Eginitis, 1905, 1910, 1912). The gap of the interim period of 1879-1892 was filled in by the publication of Galanopoulos (1953) who collected observations about Greek earthquakes and their impact from contemporary press reports. The publication of macroseismic information in the Bulletins of NOA continued until 1935 but interrupted in the period 1936-1949.

The tradition continued after 1949 with the systematic collection of macroseismic data by the Institute of Geodynamics of NOA and their publication in the Bulletin of NOA. In parallel, several catalogues and books containing earthquake impact data in Greece were published by various authors. Galanopoulos (1955, 1960, 1961) offered a synoptic overview of the earthquake impact in Greece since the antiquity. The same author organized a parametric and descriptive catalogue of the significant earthquakes in Greece and their impact in the time period 1950-1980 (Galanopoulos, 1981). The catalogue contains information regarding the numbers of killed and injured people as well as the number of damaged or destroyed buildings, classifying the level of damage/destruction in four classes: total destruction, partial destruction, heavy damage, light damage.

Papazachos and Papazachou (1989, 1997, 2003) continued the effort providing a gradually updated parametric and descriptive catalogue of earthquakes and their impact in Greece and the surrounding areas from the antiquity up to 2001. The descriptive catalogue published by Spyropoulos (1997) for the Greek earthquakes and their impact since the antiquity is relying mainly on the books by Papazachos and Papazachou (1989, 1997).

The publications by Papazachos and Papazachou (2003), PP03 for reasons of brevity, as well as by Ambraseys (2009), are reference books which contain important amount of information about the seismic phenomena in Greece, including earthquake impact data. However, PP03 provides information for only strong earthquakes of estimated magnitude $\geq$6.0. Each earthquake event inserted in that book is described in a synoptic way but citations are given for each one of the events. On the other hand, the book by Ambraseys (2009), hereafter abbreviated as AM09, is a descriptive catalogue covering the Eastern Mediterranean for the historical period extended from the antiquity up to 1899 AD. For strong earthquakes that book includes English translations of original texts that document the events. A variety of earlier publications, e.g. Schmidt (1879), Sieberg (1932) and Galanopoulos (1981), have been taken into account and utilized by both PP03 and AM09. However, AM09 includes more events than PP03. One reason is that PP03 lists only strong earthquakes. Another reason is that AM09 used more historical sources as compared to PP03. On the other hand, PP03 provides focal

parameters (origin time, epicentral coordinates, magnitude) and intensity assignment for all the events listed. On the contrary, AM09 does not provide such parameters for all the earthquakes.

Papadopoulos et al. (2000) compiled a detailed historical parametric earthquake and tsunami catalogue for the area of Corinth rift, Central Greece, including a reliability indicator for each event. Descriptions of the impact for some selected earthquakes are also included in that publication. In a subsequent book, the same author (Papadopoulos, 2011) presented an exhaustive collection of geological, archeological, historical and instrumental observations and impact data regarding earthquakes and tsunamis occurring in the area of the Hellenic Arc, from 2000 BC up to AD 2011. This book provides earthquake descriptions in the original language (e.g. Greek, Italian etc.) followed by a translation in English. A reliability indicator for each event is also included.

5.4.2 Databases and data compilations

Earthquake impact data for Greece can be found in various compilations of data sets as well as in international, national and local databases containing relevant information either about sets of earthquakes occurring the entire Greece or for only individual earthquakes. Such databases include the ones by NOAA, USGS, EM-DAT, GLIDE and CEQID (Table 5.1). The global database organized by Nievas et al. (2020), only for moderate-magnitude earthquakes that accompanied by damage and/or casualties, includes also Greek earthquakes. At national level, the Directorate General for Natural Disasters Rehabilitation (DGNDR), Ministry of Infrastructures and Transportations, Greece, collects data sets for the impact of earthquakes occurring in Greece in the last years.

In his global database, Utsu (1990) included several Greek earthquakes with short description of their impact. In the Earthquake Disaster Reduction Handbook (EDRH, 1992) 45 damaging or destructive earthquakes in Greece are listed. In an updated compilation for the post-1500 period, Samardjieva and Badal (2002) examined human losses after strong earthquakes that occurred in the world during the 20th century. However, these authors compiled a list of human losses which is not complete for Greece. Utsu (2002b) included 49 lethal earthquakes occurring in Greece, the first in 1508 (Crete Isl.) and the last in the metropolitan area of Athens in 1999.

Building damage and/or human losses data for individual earthquakes were collected and analyzed by various authors, including Ambraseys and Jackson (1981) for the 1981 February-March earthquake sequence in the eastern Corinth Gulf, Anagnostopoulos et al. (1987) and Andrikopoulou (1989) for the 1986 Kalamata earthquake, Karantoni and Bouckovalas (1997) for the 1993 Pyrgos earthquake, Fardis et al. (1999) for the 1995 Aegion earthquake, Pomonis (2002), Kappos et al. (2007) and Eleftheriadou and Karabinis (2011) for the 1999 Athens earthquake. Several of these data sets were examined by Pomonis et al. (2009) with the aim to assess the seismic vulnerability and collapse probability of buildings in Greece. Kouskouna and Sakkas (2013) organized a database of macroseismic data points (in EMS-98 scale) for 1,178 Greek earthquakes. This database is freely available on the website of the Geology Department, University of Athens (http://macroseismology.geol.uoa.gr/).

5.5 Collection of Earthquake Impact Data for Greece

5.5.1 Definitions and explanatory remarks

Area and earthquakes of interest

The area covered by Greece has been historically changed. Therefore, the analysis of the earthquake impact has been restricted to the today territory of Greece with the purpose to standardize the area under examination. A first statistics performed in Chapter 1 for the earthquake impact in Greece, in terms of the maximum macroseismic intensity, MMI_o, reported for each event, showed that the reporting rate of destructive earthquakes ($MMI_o \geq VIII$) is nearly complete in the time period from 1800 onwards given that the rate remained constant in that period. Based on this result we decided to organize the GEIDB for the reference time period from 1800 to 2020 inclusive, although we collected data for the pre-1800 period too. However, for the reference period our search for impact data has not been restricted to earthquakes of only $MMI_o \geq VIII$ but has been extended to all events that made impact regardless their MMI_o value. Also, our investigation has not been restricted only to mainshocks but also to dependent events, i.e. foreshocks and aftershocks, although in several cases it is hard to discriminate the damage caused by a mainshock from that caused by its dependent events, e.g. the sequence of strong earthquakes that occurred in the eastern Corinth Gulf during the February-March 1981 (Khoury et al., 1983).

Types of earthquake impact data

The earthquakes cause a variety of direct and indirect effects on the human communities and their properties as well as on the natural environment. The term “direct impact” is meant to describe effects caused by the ground shaking itself. Indirect impact includes economic, social, psychological and other earthquake effects. A particular type of the earthquake impact in Greece is the effect on cultural goods, which may include either outdoor damage or destruction in archaeological sites, monuments and monumental buildings or indoor damage in the various exhibits in museums and in other cultural units.

The direct earthquake effects on human communities are extended to the built environment and to the population. The effects on buildings may vary from slight to heavy damage or destruction, to partial or total collapse. Such types of data have been inserted in the GEIDB. The most common direct earthquake effect on the population is the cause of physical suffering, such as deaths, injuries, homeless and diseases. Data on deaths and injuries are available for a plenty of earthquakes in Greece in the reference period. Data on homeless, however, were found only for a limited number of events. On the other hand, no cases of diseases resulting from the seismic activity were found.

The majority of the earthquakes that made impact on buildings and on the population in the Greek territory had their epicenters in this territory as well. A few exceptions, however, were found, such as the earthquake (M_w=7.4, UOA) of 4 April 1904 in SW Bulgaria that caused casualties in the city of Thessaloniki, and the earthquake (M_w=7.30, ISC-GEM) of 18 March 1953 in Yenise, NW Turkey, that caused casualties in the Greek island of Lesvos.

In the natural environment the earthquakes may cause various changes mainly in the ground as well as in the sea and the lakes. In the ground the most common earthquake effects include surface fault traces, ground displacements (uplift or subsidence) and several types of failures, such as landslides, soil liquefaction and rockfalls as well as hydrological changes. On the other hand, in the sea the earthquakes may cause tsunamis and seiches but the submarine landslides should not be neglected. Similar earthquake-induced phenomena have been occasionally observed in lakes.

Compilation of earthquake impact data

For the reference period (1800-2020) the GEIDB contains data for earthquakes that caused direct impact on the built environment and on the population. A supplementary database has been organized for the tsunami impact data (Chapter 8). In Chapter 1 a first statistics has been performed for the earthquakes that caused various types of ground failures. However, further examination of the ground failures caused by earthquakes in Greece is beyond the scope of this study. The main attributes of the Greek Earthquake Impact Database (GEIDB) are summarized in Table 5.2.

Table 5.2. Main attributes of the Greek Earthquake Impact Database (GEIDB).

Geographic area	**Time period**	**Types of Impact**				
Current territory of Greece	1800-2020	Built environment		Population (casualties)		Natural environment
		Buildings	Infrastructures	Fatalities	Injuries	Tsunamis

The various types of information about the earthquake effects are collected and reported either by the scientific community or by non-scientists. Both scientists and non-scientists may collect primary data referring directly on the earthquake effects. Scientists and engineers provide also sets of metadata in terms of shaking (macroseismic) intensities. In this study we are interested on the compilation of primary earthquake impact data but intensity data are still useful.

The flow chart of the procedure followed for the final earthquake impact data compilation is illustrated in Figure 5.1. Three main steps have been followed. The first included the data compilation from a variety of sources, which are explained in the next subsection. However, before the data adoption they have been filtered through a procedure of reliability control, correction and final adoption or even rejection.

In the remaining part of this Chapter dates of historical events are given in the New Style [N.S., Gregorian] calendar unless otherwise reported, i.e. Old Style [O.S., Julian] calendar. The origin time of earthquakes is in UTC (GMT) unless otherwise reported.

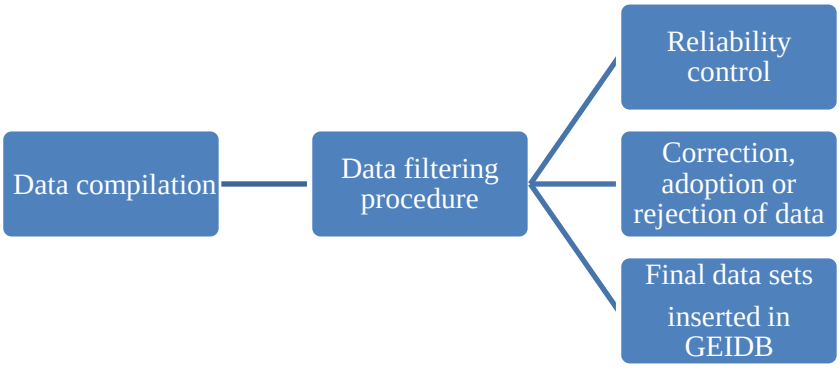

Figure 5.1. Flow chart of the procedure followed for the earthquake impact data compilation.

5.6 Sources of earthquake impact data

A variety of sources have been used to collect data about the earthquake impact in Greece. They include scientific publications, e.g. journal conference papers and books, technical reports, institutional bulletins and archives, electronic databases, other published books and documents, unknown or little known documents as well as press reports. Post-event field surveys conducted after recent earthquake and tsunami events, in the frame of either the present thesis or other research projects, offered impact data sets as well. The candidate participated actively in such post-event field surveys organized in the aftermath of strong earthquakes that occurred from 2014 to 2020.

5.6.1 Scientific publications

Books and theses

Two are the main reference publications which are in extensive use to draw on information about the earthquake phenomena in Greece including earthquake impact data. The books PP03 and AM by Papazachos and Papazachou (2003) and Ambraseys (2009), respectively. These books have examined and took into account a long number of previous publications and other sources. From the PP03 and AM09 reference books we have collected impact data for many earthquake and tsunami events occurring in the Greek area from 1800 to 2001 and from 1800 to 1899, respectively. However, for several earthquakes we re-examined many sources used by PP03 and AM09. Moreover, we collected and examined additional sources not quoted by these two books and referring to several earthquakes, such as the large earthquake of 12 October 1856 in the South Aegean Sea, the large earthquake of 8 November 1905 in Athos, the moderate earthquake of 15 July 1909 in Elis, NW Peloponnese, the moderate earthquake of 8 February 1926 in Kos island and the strong earthquake of 23 April 1933 again in Kos island. More details about some of these events are presented in the section about the case studies.

Lekkas et al. (1997) compiled data regarding earthquakes that occurred in Zakynthos Island from the 15th century up to 1988. This data compilation has been already utilized by PP03 and others. More recently, the book by Papadopoulos (2011) revised extensively the earthquakes and tsunamis occurring in the Hellenic arc and trench from pre-historic times up to 2011 and included impact data for a long number of events. Papadopoulos (2011) took into account the reference books PP03 and AM09 but used also several unknown or little-known sources, such as the unpublished earthquake archive by Vlastos (1850-1926). In a series of books published by Papadopoulos (2012, 2014, 2015)

new and/or revised impact data for Greek earthquakes and tsunamis occurring from the antiquity up to modern times were also collected for the area of Kythira island (e.g. 6 February1866, 17 October 1889, 11 August 1903 and 8 January 2006), for Rhodes island (e.g. 28 February 1851, 12 October 1856, 24 May 1862, 22 April 1863, 27 October 1896, 25 April 1957, 23 May 1961 and 10 June 2012), for Lesvos island (e.g. 11 October 1845, 7 March 1867 and 26 October 1889), as well as for the area of Chios and Psara islands (e.g. 25 November 1856, 12 November 1865, 3 April 1881, 5 June 1886, 26 May 1890, 21 May 1949 (foreshock) and 23 July 1949 (mainshock).

In his doctoral thesis, Taxeidis (2003) studied the historical seismicity of the eastern Aegean islands and presented some new data which have been utilized by Papadopoulos (2015). The book by Papaioannou (2018), referring to the destructive earthquake (M_s=6.3) of 1 March 1941 in Larissa, Thessalia province, provides a comprehensive literature review and earthquake impact data compilation along with pictorial documentation.

Journal and conference papers

There is a long number of published papers which have not been used by PP03 and AM09 for several reasons: (1) papers published after PP03 and AM09; (2) papers referring to events either occurring after 1899, which is the last year of examination by AM09, or of magnitude less than 6.0, which is the lower magnitude threshold for PP03; (3) papers that simply escaped the attention of PP03 or AM09. For the historical period our collection includes, among others, the paper by Kouskouna (2001), who studied the moderate 1892 Larisa earthquake and offered impact data. Papadopoulos and Plessa (2001) revised the historical earthquakes and tsunamis occurring in the South Ionian Sea from 1591 to 1837 and reported on the impact of the events of 1809, 1810, 1820 and 1837 in Zakynthos island.

For the instrumental period of seismicity, a collection of papers examined and utilized include those by Drakopoulos and Srivastava (1970), Bairaktaris and Roussopoulos (1976), Jackson et al. (1982), Koukis and Rozos (1985), Papastamatiou and Mouyiaris (1986), Papazachos et al. (1988), Mariolakos et al. (1989), Papadopoulos and Profis (1990), Papadopoulos (1993), Papadopoulos et al. (1994), Pavlides et al. (1995) Stiros (1995), Stiros and Vougioukalakis (1996), Lekkas et al. (1998), Koukouvelas (1998), Koukouvelas and Doutsos (1996), Papadopoulos et al. (2002), Pavlides et al. (2002), Papadopoulos et al. (2003), Papathanasiou et al. (2005), Papathanasiou and Pavlides (2007), Ganas et al. (2009), Koukouvelas et al. (2010), Papadopoulos et al. (2010) and Papathanasiou et al. (2017). Very recently, Bocchini et al. (2020) and Papadopoulos et al. (2020) documented macroscopic and instrumental details about the local tsunamis observed in the coastal area of Ierapetra, SE Crete, in association with the earthquakes of 1 July 2009 (M_w=6.4) and of 2 May 2020 (M_w=6.6), respectively. Dogan et al. (2019), conducted post-event field surveys and presented detailed documentation of the tsunami that followed the 20 July 2017 strong earthquake (M_w=6.6) in the coastal zones of Bodrum and Kos.

Post-event field surveys-Papers published in the frame of the present thesis

In the frame of the present thesis some case studies were performed regarding the impact of selected earthquakes in Greece. These case studies included two sets of earthquakes: (i) recent events, i.e. the Samos earthquake (M_w=7.0) and tsunami of 30 October 2020, the 20 July 2017 Bodrum-Kos

earthquake (M_w=6.6) and tsunami, and the Cephalonia earthquakes of 26 January 2014 (M_w=6.0) and 3 February 2014 (M_w=5.9); (ii) earlier events which remained little known so far and include the Mt Athos large (M_w=7.24, ISC-GEM 2018) earthquake and tsunami of 8 November 1905, as well as the earthquakes that hit the island of Kos on 8 February 1926 (M_s=5.5) and on 23 April 1933 (M_w=6.5). For the Samos 2020, Kos 2017 and Cephalonia 2014 earthquakes impact data were collected during post-event field-surveys with the participation of the candidate. For the earlier events of 1905, 1926 and 1933 impact data have been collected from documentary sources, which remained unknown to the seismological tradition so far.

Results about the above case studies have been already published in various papers and technical reports (Lekkas et al., 2020, Triantafyllou et al., 2020a,b, 2021, Papadopoulos et al., 2014c). Therefore, only the main results about these cases are presented in the section 5.12 referring to the case studies. On the other hand, more details about the impact of tsunamis that associated the earthquakes of Mt Athos 1905, Kos 2017 and Samos 2020 are analyzed in Chapter 8.

Figure 5.2 Damage in a two storey building in Ayios Dimitrios, Cephalonia Island, after the 26 January 2014 (M_w=6.0) earthquake (left) and after the 3 February 2014 (M_w=5.9) earthquake (right) (photos credit, I. Triantafyllou).

Technical reports

Earthquake and tsunami impact data can be found in many technical reports produced by the scientific staff of universities and research centers as well as of public services. For example, a rich collection of such reports has been produced by geologists of the Hellenic Survey of Geology and Mineral Exploration, former Institute of Geology and Mineral Exploration (IGME), after post-event field surveys. These reports contain data on the impact of many Greek earthquakes occurring from 1953 up to recently (e.g. Paschos et al., 1996). Similarly, several technical reports containing impact data for Greek earthquakes have been also produced in the frame of post-event field surveys or other projects performed by the Institute of Engineering Seismology and Earthquake Engineering (ITSAK) for the post-1985 period, by the Earthquake Planning and Protection Organization (EPPO) for the post-1986 period, as well as by the Post-Graduate Program on Environmental, Disaster and Crisis

Management Strategies, University of Athens. The last documented the impact of various earthquakes in the Newsletter of Environmental, Disasters and Crises Management Strategies since 2017, e.g. Lekkas et al. (2017, 2020). In the frame of a project organized by the Joint Research Center, EC, Annunziato et al. (2017) collected macroscopic observations about the local tsunami event generated by the 12 June 2017 Lesvos island earthquake (M_w=6.3).

5.6.2 Institutional bulletins and archives

The two-volume unpublished manuscript titled *Book of Earthquakes* (Anonymous, 1893-1901 and Anonymous, 1902-1915) has been utilized to retrieve impact data for several earthquakes. The impact data published in the Bulletins of NOA have been re-collected and utilized extensively by previous authors, such as Galanopoulos (1981) and Papazachos and Papazachou (2003). However, these Bulletins have been reexamined by us for several earthquakes.

5.6.3 Electronic databases

The various international databases reviewed in section 5.2.1 are incomplete as regards impact data of Greek earthquakes. On the other hand, these databases list data already known from several publications. At national level, the Directorate General for Natural Disasters Rehabilitation (DGNDR), Ministry of Infrastructures and Transportations, Greece, maintains a database for the impact of recent Greek earthquakes. For the time period of 2009-2019 data on building damage were provided by the DGNDR for several earthquakes: 7 August 2013 (M_w=5.4) in Fthiotis (Central Greece), 24 May 2014 (M_w=6.9) in Samothraki island, 17 November 2015 (M_w=6.5) in Lefkada island, 12 June 2017 (M_w=6.3) in Lesvos island, 20 July 2017 (M_w=6.6) in Kos island, 2018 (M_w=5.1) in Trikala (Central Greece), 25 October 2018 (M_w=6.8) in Zakynthos island and 19 July 2019 (M_w=5.1) in the Attika region (Central Greece).

5.6.4 Press articles and reports

Articles in local journals and press have been systematically published by Papaioannou (e.g. 1999, 2002, 2018), a civil engineer, who collected data for several historical and instrumental earthquakes occurred in the Thessalia province, Central Greece. A long number of press reports and correspondences have been published in Greek and foreign newspapers since the 19th century up to modern times. We have examined a set of many such reports for several earthquakes, including those of 9 February 1893 in Samothraki island, 8 November 1905 in Mt Athos, 23 April 1933 in Kos island, 19 April 1955 in Magnesia (Central Greece) and of 6 January 2008 in Leonidio area, eastern Peloponnese. Press reports were also advised for some selected events occurring during the early instrumental period of 1900-1910 (Chapter 3).

5.7 Data filtering procedure

Although the observational material published about the impact of earthquakes in Greece in the reference period (1800-2020) is quite extensive, the completeness and reliability of the relevant information available is not satisfied for the purposes of our study due to several reasons. The first is that this material is not concentrated in a unified data compilation, e.g. publication, database or report, which implies that it remains without standardization while a unified style of organization is lacking.

On the other hand, from a preliminary investigation we found that in some instances erroneous information has been uncritically used and propagated from one compilation to others. Another issue is that inconsistent information can be found in different sources referring to an individual earthquake. In addition, our investigation revealed several little-known or even unknown sources, which have not been utilized so far by the seismological community.

Before we insert impact data in the GEIDB, a procedure of final data selection was followed consisting of two main stages (Figure 5.1). The first stage has been the collection of earthquake impact data from a variety of sources as analyzed earlier. In the second stage we followed a procedure for data filtering separately for each one of the earthquakes. The filtering procedure started with a data reliability control through cross-correlation and critical evaluation of the sources collected. This procedure, which concerns the historical earthquakes of the period 1800-1899, followed the practice introduced in some of the previous historical seismicity catalogues (Papadopoulos et al., 2000, Papadopoulos, 2011). Namely, for every single earthquake event of that period a reliability score, Rel, has been given in a scale ranging from 1 (improbable event), 2 (probable event), 3 (very probable event) to 4 (definite event). In the GEIDB no events of Rel=1 have been inserted. One event is given Rel=2. For 16 events Rel=3 has been assigned. All the rest events that occurred during the 19th century and all the events instrumentally recorded during the period 1900-2020 have assigned reliability score Rel=4.

After the data filtering procedure every piece of earthquake impact information was finally corrected, adopted or even rejected. This chain of analysis is typical for earthquakes that occurred during the 19th century and the first decades of the 20th century. For the rest part of the period examined the data reliability increases and the application of the filtering procedure frequently is not needed. The list with corrected impact data through cross-correlation and evaluation of sources includes several events. Typical examples include the large earthquake of 8 November 1905 in Mt Athos, the moderate earthquake of 8 February 1926 and the strong earthquake of 23 April 1933 both in Kos island. Results on these cases have already been published (Triantafyllou et al., 2020a,b).

A characteristic example of erroneous impact data, which propagated from one author to others, is related to the earthquake that hit the island of Chalki, Dodecanese island complex, on 18 October 1843 after a series of smaller earthquakes felt in the island the previous days. Although there is a dispute in the various sources regarding the date of the earthquake occurrence, here we focus on the earthquake impact data. Perrey (1848) reported that the earthquake killed 600 people in the island of Chalki. This information propagated to other authors and databases, which reproduced this information until recently (Figure 5.3), and has been also copied by a large number of popular science and press websites.

Ambraseys (2009), however, questioned if the earthquake caused human victims. We cross-correlated the information with additional sources not examined so far by others. Namely, the eminent archaeologist Ross (1852), who visited that island, mentioned the 1843 earthquakes but nothing about human victims. This is consistent with two contemporary press reports, namely *Αθήνα (Athina)* 19 October 1843 and *Προινός Κήρυξ (Proinos Kirix*) 20 October 1843. According to these reports the earthquakes caused landslides that destroyed 600 houses. However, no victims were noted in the island. Eventually, after this analysis we rejected the piece of information that "600 persons were

killed by the earthquake" and adopted a correction which reads as follows: "600 houses destroyed by landslides triggered by the earthquakes but no human victims were caused".

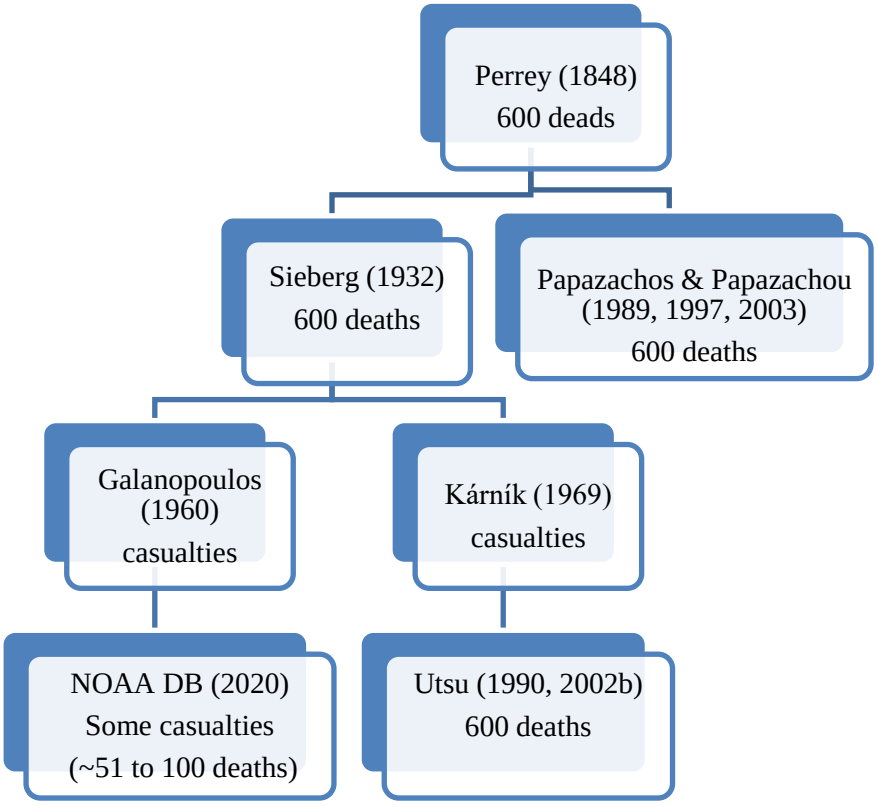

Figure 5.3. Information flow regarding casualties reportedly caused in Chalki Island due to the 18 October 1843 earthquake.

5.8 Format, structure and content of the GEIDB

The Greek Earthquake Impact Database (GEIDB) has been organized in Access format and consists of 248 entries, each entry corresponding to every single earthquake inserted in the database. The time period covered is extended from 1800 to 2020.

The GEIDB is structured in the next four main sections (Fig. 5.4), each one devoted to a different kind of information:
(1) The *Quick-Look Seismicity Section (QLSS);*
(2) The *Quick-Look Impact Section (QLIS)*;
(3) The *Impact Metadata Section (IMS)*;
(4) The *References File (RF)*.
Extracts from the Quick-Look parts 1, 2 and 3 of the GEIDB are illustrated in Figure 5.5. In the next lines the four sections of the GEIDB are introduced.

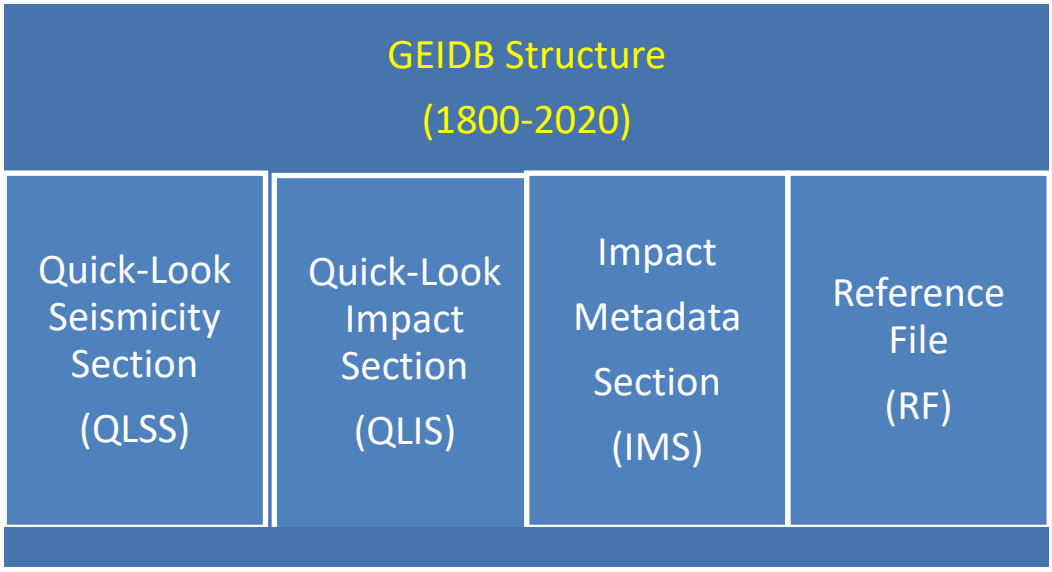

Figure 5.4. Basic structure of the GEIDB.

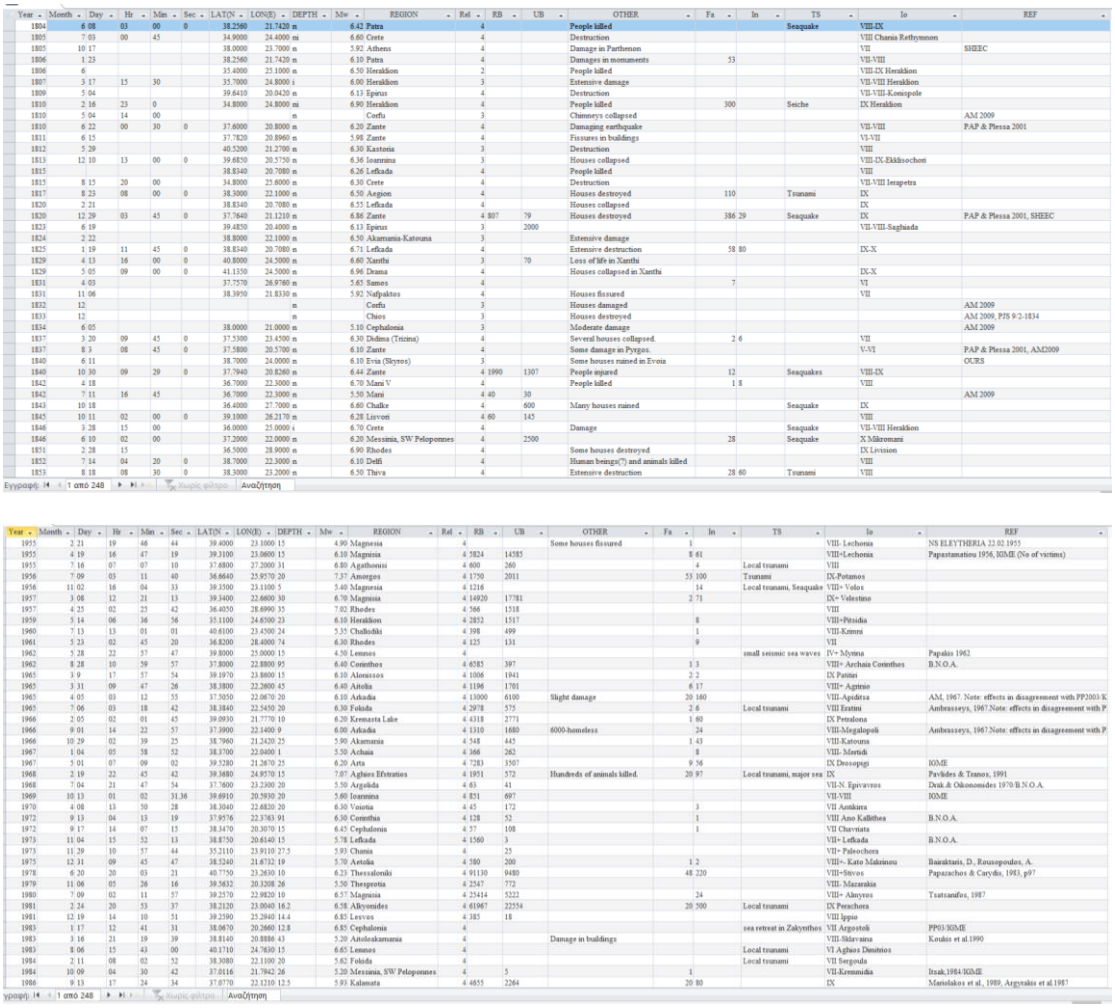

Year	Month	Day	Hr	Min	Sec	LAT(N)	LON(E)	DEPTH	Mw	REGION	Ref	RB	UB	OTHER	Fa	In	TS	Io	REF
1804	6	08	03	00	0	38.2560	21.7420	m	6.42	Patra	4			People killed			Seaquake	VIII-IX	
1805	7	03	00	45		34.9000	24.4000	mi	6.60	Crete	4			Destruction				VIII Chania Rethymnon	
1805	10	17				38.0000	23.7000	m	5.92	Athens	4			Damage in Parthenon				VII	SHEEC
1806	1	23				38.2560	21.7420	m	6.10	Patra	4			Damages in monuments	53			VII-VIII	
1806	6					35.4000	25.1000	m	6.50	Heraklion	2			People killed				VIII-IX Heraklion	
1807	3	17	15	30		35.7000	24.8000	i	6.00	Heraklion	3			Extensive damage				VII-VIII Heraklion	
1809	5	04				39.6410	20.0420	m	6.13	Epirus	4			Destruction				VII-VIII-Konispole	
1810	2	16	23	0		34.8000	24.8000	mi	6.90	Heraklion	4			People killed	300		Seiche	IX Heraklion	
1810	5	04	14	00				m		Corfu	3			Chimneys collapsed					AM 2009
1810	6	22	00	30	0	37.6000	20.8000	m	6.20	Zante	4			Damaging earthquake				VII-VIII	PAP & Plessa 2001
1811	6	15				37.7820	20.8960	m	5.98	Zante	4			Fissures in buildings				VI-VII	
1812	5	29				40.5200	21.2700	m	6.30	Kastoria	3			Destruction				VIII	
1813	12	10	13	00	0	39.6850	20.5750	m	6.36	Ioannina	3			Houses collapsed				VIII-IX-Ekklisochori	
1815						38.8340	20.7080	m	6.26	Lefkada	4			People killed				VIII	
1815	8	15	20	00		34.8000	25.6000	m	6.30	Crete	4			Destruction				VII-VIII Ierapetra	
1817	8	23	08	00	0	38.3000	22.1000	m	6.50	Aegion	4			Houses destroyed	110		Tsunami	IX	
1820	2	21				38.8340	20.7080	m	6.55	Lefkada	4			Houses collapsed				IX	
1820	12	29	03	45	0	37.7640	21.1210	m	6.86	Zante	4	807	79	Houses destroyed	386	29	Seaquake	IX	PAP & Plessa 2001, SHEEC
1823	6	19				39.4850	20.4000	m	6.13	Epirus	3		2000					VII-VIII-Saghiada	
1824	2	22				38.8000	22.1000	m	6.50	Akarnania-Katouna	3			Extensive damage					
1825	1	19	11	45	0	38.8340	20.7080	m	6.71	Lefkada	4			Extensive destruction	58	80		IX-X	
1829	4	13	16	00	0	40.8000	24.5000	m	6.60	Xanthi	3		70	Loss of life in Xanthi					
1829	5	05	09	00	0	41.1350	24.5000	m	6.96	Drama	4			Houses collapsed in Xanthi				IX-X	
1831	4	03				37.7570	26.9760	m	5.65	Samos	4				7			VI	
1831	11	06				38.3950	21.8330	m	5.92	Nafpaktos	4			Houses fissured				VII	
1832	12							m		Corfu	3			Houses damaged					AM 2009
1833	12							m		Chios	3			Houses destroyed					AM 2009, PJS 9/2-1834
1834	6	05				38.0000	21.0000	m	5.10	Cephalonia	3			Moderate damage					AM 2009
1837	3	20	09	45	0	37.5300	23.4500	m	6.30	Didima (Trizina)	4			Several houses collapsed.	2	6		VII	
1837	8	3	08	45	0	37.5800	20.5700	m	6.10	Zante	4			Some damage in Pyrgos.				V-VI	PAP & Plessa 2001, AM2009
1840	6	11				38.7000	24.0000	m	6.10	Evia (Skyros)	3			Some houses ruined in Evoia					OURS
1840	10	30	09	29	0	37.7940	20.8260	m	6.44	Zante	4	1990	1307	People injured	12		Seaquakes	VIII-IX	
1842	4	18				36.7000	22.3000	m	6.70	Mani V	4			People killed	1	8		VIII	
1842	7	11	16	45		36.7000	22.3000	m	5.50	Mani	4	40	30						AM 2009
1843	10	18				36.4000	27.7000	m	6.60	Chalke	4		600	Many houses ruined			Seaquake	IX	
1845	10	11	02	00	0	39.1000	26.2170	m	6.28	Lisvori	4	60	145					VIII	
1846	3	28	15	00		36.0000	25.0000	i	6.70	Crete	4			Damage			Seaquake	VII-VIII Heraklion	
1846	6	10	02	00		37.2000	22.0000	m	6.20	Messinia, SW Peloponnes	4		2500		28		Seaquake	X Mikromani	
1851	2	28	15			36.5000	28.9000	m	6.90	Rhodes	4			Some houses destroyed				IX Livision	
1852	7	14	04	20	0	38.7000	22.3000	m	6.10	Delfi	4			Human beings(?) and animals killed				VIII	
1853	8	18	08	30	0	38.3000	23.2000	m	6.50	Thiva	4			Extensive destruction	28	60	Tsunami	VIII	

Year	Month	Day	Hr	Min	Sec	LAT(N	LON(E)	DEPTH	Mw	REGION	Ref	RB	UB	OTHER	Fa	In	TS	Io	REF
1955	2	21	19	46	44	39.4000	23.1000	15	4.90	Magnesia	4			Some houses fissured	1			VIII- Lechonia	NS ELEYTHERIA 22.02.1955
1955	4	19	16	47	19	39.3100	23.0600	15	6.10	Magnisia	4	5824	14585		8	61		VIII+Lechonia	Papastamatiou 1956, IGME (No of victims)
1955	7	16	07	07	10	37.6800	27.2000	31	6.80	Agathonisi	4	600	260		4		Local tsunami	VIII	
1956	7	09	03	11	40	36.6640	25.9570	20	7.37	Amorgos	4	1750	2011		53	100	Tsunami	IX-Potamos	
1956	11	02	16	04	33	39.3300	23.1100	5	5.40	Magnesia	4	1216			14		Local tsunami, Seaquake	VIII+ Volos	
1957	3	08	12	21	13	39.3400	22.6600	30	6.70	Magnesia	4	14920	17781		2	71		IX+ Velestino	
1957	4	25	02	25	42	36.4050	28.6990	35	7.02	Rhodes	4	566	1518					VIII	
1959	5	14	06	36	56	35.1100	24.6500	23	6.10	Heraklion	4	2852	1517		8			VIII+Pitsidia	
1960	7	13	01	01	01	40.6100	23.4300	24	5.35	Chalkidiki	4	398	499		1			VIII-Krinni	
1961	5	23	02	45	20	36.8200	28.4000	74	6.30	Rhodes	4	125	131		9			VII	
1962	5	28	22	57	47	39.8000	25.0000	15	4.50	Lemnos	4						small seismic sea waves	IV+ Mytilini	Papakis 1962
1962	8	28	10	39	57	37.8000	22.8800	95	6.40	Corinthos	4	6585	397		1	3		VIII+ Archaia Corinthos	B.N.O.A.
1965	3	9	17	57	54	39.1970	23.8600	15	6.10	Alouissos	4	1006	1941		2	2		IX Patitiri	
1965	3	31	09	47	26	38.3800	22.2600	45	6.40	Aitolia	4	1196	1701		6	17		VIII+ Agrinio	
1965	4	05	03	12	55	37.5050	22.0670	20	6.10	Arkadia	4	13000	6100	Slight damage	20	160		VIII-Agiditsa	AM, 1967. Note: effects in disagreement with PP2003-K
1965	7	06	03	18	42	38.3840	22.5450	20	6.30	Fokida	4	2978	575		2	6	Local tsunami	VIII Eratini	Ambraseys, 1967.Note: effects in disagreement with P
1966	2	05	02	01	45	39.0930	21.7770	10	6.20	Kremasta Lake	4	4318	2771		1	60		IX Petralona	
1966	9	01	14	22	57	37.3900	22.1400	9	6.00	Arkadia	4	1310	1680	6000-homeless	24			VIII-Megalopoli	Ambraseys, 1967.Note: effects in disagreement with P
1966	10	29	02	39	25	38.7960	21.2420	25	5.90	Akarnania	4	548	445		1	43		VIII-Katouna	
1967	1	04	05	58	52	38.1700	22.0400	1	5.50	Achaia	4	366	262		8			VIII- Meriadi	
1967	5	01	07	09	02	39.5280	21.2670	25	6.20	Arta	4	7283	3507		9	56		IX Drosopigi	IGME
1968	2	19	22	45	42	39.3680	24.9570	15	7.07	Aghios Efstratios	4	1951	572	Hundreds of animals killed.	20	97	Local tsunami, major sea	IX	Pavlides & Tranos, 1991
1968	7	04	21	47	54	37.7600	23.2300	20	5.50	Argolida	4	63	41					VII-N. Epivavtos	Drak.& Oikonomides 1970/B.N.O.A.
1969	10	13	01	02	31.36	39.6910	20.5930	20	5.60	Ioannina	4	851	697					VII-VIII	IGME
1970	4	08	13	30	28	38.1040	22.6820	20	6.30	Voutsa	4	45	172		3			VII Aetokira	
1972	9	13	04	13	19	37.9576	22.3763	91	6.30	Corinthia	4	128	52		1			VIII Ano Kallithea	B.N.O.A.
1972	9	17	14	07	15	38.3470	20.3070	15	6.45	Cephalonia	4	57	108		1			VII Chavriata	
1973	11	04	15	52	13	38.8750	20.6140	15	5.78	Lefkada	4	1560	3					VII+ Lefkada	B.N.O.A.
1973	11	29	10	57	44	35.2110	23.9110	27.5	5.80	Chania	4		25					VII+ Paleochora	
1975	12	31	09	45	47	38.5240	21.6732	19	5.70	Aetolia	4	580	200		1	2		VIII+- Kato Makrinou	Ilainiktanis, D., Rousopoulos, A.
1978	6	20	20	03	21	40.7750	23.2630	10	6.23	Thessaloniki	4	91130	9480		48	220		VIII+Stivos	Papazachos & Carydis, 1983, p97
1979	11	06	05	26	16	39.5632	20.3208	26	5.50	Thesprotia	4	2547	772					VIII- Mazarakia	
1980	7	09	02	11	57	39.2570	23.9820	10	6.57	Magnesia	4	25414	5222		24			VIII+ Almyros	Tsatsanifos, 1987
1981	2	24	20	53	37	38.2120	23.0040	16.2	6.58	Alkyonides	4	61967	22554		20	500	Local tsunami	IX Perachora	
1981	12	19	14	10	51	39.2590	25.2840	14.4	6.85	Lesvos	4	385	18					VII Ippio	
1983	1	17	12	41	31	38.0670	20.2660	12.8	6.85	Cephalonia	4						sea retreat in Zakynthos	VII Argostoli	PP03/IGME
1983	3	16	21	19	39	38.8140	20.8886	43	5.20	Attoloakarnania	4			Damage in buildings				VIII-Sklavaina	Koukis et al.1990
1983	8	06	15	43	00	40.1710	24.7650	15	6.65	Lemnos	4						Local tsunami	VI Aghios Dimitrios	
1984	2	11	08	02	52	38.3080	22.1100	20	5.62	Fokida	4						Local tsunami	VII Stergoula	
1984	10	09	04	30	42	37.0116	21.7942	26	5.20	Messinia, SW Peloponnes	4	5			1			VII-Kremmidia	Itsak.1984/IGME
1986	9	13	17	24	34	37.0770	22.1210	12.5	5.93	Kalamata	4	4655	2264		20	80		IX	Mariolakos et al., 1989, Argyrakis et al.1987

Figure 5.5. Extracts from the Quick-Look parts 1, 2 and 3 of the GEIDB.

5.9 The Quick-Look Seismicity Section (QLSS)

5.9.1 Format

For every single earthquake inserted in the database this section includes the focal parameters, i.e. date, origin time, epicentral coordinates, focal depth and magnitude. The focal parameters are arranged according to the following format:
Date: year, month, day (in N.S.),

Origin time: hr, min, sec (in GMT),

Epicentral coordinates: geographic latitude and longitude (in degrees),

Focal depth, h: this is given in km. If no numerical value is available then we used the notation *n* for surface earthquake (h<60 km) and *i* for intermediate-depth earthquake (h≥60 km).

Magnitude: moment magnitude M_w.

In addition, for every single earthquake of the pre-instrumental period (1800-1899) a reliability score, Rel, has been given as analyzed in section 5.7.

5.9.2 Seismicity parameters

The selection of seismicity parameters is not an easy task due to the various earthquake catalogues existing for both the instrumental and historical seismicity periods. For this reason the catalogues of the historical and instrumental periods have been examined and compared in Chapters 2, 3 and 4. Based on the results found in those Chapters we developed a set of rules for the selection of earthquake focal parameters.

Historical period (1800-1899)

For the earthquakes that occurred in the time interval from AD 1800 to 1899 seismicity parameters have been taken from the catalogue of SHEEC. For events not included in the SHEEC catalogue seismicity parameters have been taken from the catalogues of Papazachos and Papazachou (2003) and Papazachos et al. (2000), otherwise from Papadopoulos et al. (2000), Papadopoulos and Plessa (2001) and Papadopoulos (2011), for the areas of Corinth Gulf, Ionian Sea, and the Hellenic arc, respectively.

For some earthquakes no magnitude determinations are available in the existing catalogues. In these cases we estimated magnitude from empirical relationships developed between magnitude and macroseismic intensity for earthquakes of the instrumental period (see Fokaefs et al., 2004, Papadopoulos, 2011 and an application by Triantafyllou et al., 2020a). However, for a set of four damaging earthquakes, that occurred during the 19th century and are reported by Ambraseys (2009), the dates are known but no epicentral coordinates and no magnitude are available. These earthquakes are the next: 22 June 1810 and December 1833 both in Corfu island; December 1833 in Chios island; 8 July 1882 in Ioannina.

Early instrumental period (1900-1910)

For this time period, the magnitude of each event has been taken as the average of the M_w magnitudes listed in the catalogues of AUTH (Papazachos and Papazachou, 2010), UOA (Makropoulos et al., 2012), ISC-GEM (2018), AMR (Ambraseys, 2001; M_w calculated by us from M_s as explained in Chapter 3) and AG (Agamennone magnitude, calculated in Chapter 3, Table 3.2). Hypocentral parameters have been taken from the catalogue of AUTH except for five events the epicenters of which have been revised in Chapter 3, Table 3.2.

Instrumental period (1911-2020)

Magnitudes determined from the GCMT project have been preferred for the post- 1975 time interval. For the time period from 1911 to 1975, ISC-GEM magnitudes have been preferred, if available, otherwise they have been taken as the average magnitude from the AUTH and UOA catalogues. However, for some strong earthquakes significant magnitude differences exist in the various catalogues. These cases include the earthquakes of 6 October 1947 in Messinia, 2 February 1948 in Karpathos island, 9 July 1956 in the South Aegean Sea, 25 April 1957 in Rhodes island and 19 February 1968 in the North Aegean Sea. In these cases the average magnitude from the AUTH, ISC-GEM, UOA and AMR catalogues was adopted.

Hypocenters for the time interval from 1911 to 1916 are from AUTH but for the interval 1917-1963 the UOA solutions have been adopted. The reason is that the period 1917-1963 hypocenters have been relocated in the UOA catalogue. Hypocenters for the earthquakes that occurred in the period 1964-2010 were adopted from ISC-GEM. Since 2011 hypocenters were taken from NOA.

5.10. The Quick-Look Impact Section (QLIS)

This section includes information about the various direct earthquake effects on the built environment and on the population. The impact on buildings is categorized in two classes, i.e. repairable and unrepairable buildings, for reasons explained below. The impact on the population is referring to the casualties caused and is categorized as fatalities and injuries. This section includes also short information about the occurrence of tsunamis.

The QLIS includes the following entries:

Repairable Buildings, RB. This category includes the sum of slight or more heavily damaged but repairable buildings.

Unrepairable Buildings, UB. This includes the sum of partially or totally collapsed buildings as well as heavily damaged not repairable buildings.

Fatalities, Fa. This is the number of deaths.

Injuries, In. This is the number of injuries, regardless the type of injury, e.g. heavy, no important, etc.

Tsunamis. In this section only synoptic tsunami information is given. The reason is that for the impact of tsunamis observed in the Greek region the GTIDB has been organized (Chapter 8), which is a supplement to the GEIDB

As regards the earthquake impact on buildings and on the population numerical data are preferably inserted, if available; otherwise only descriptive information is provided. In some of the data sources used, which contain abundant data, such as the Bulletins of NOA and relevant publications (e.g., Galanopoulos, 1981, Papazachos and Papazachou, 2003), the earthquake impact on buildings is categorized in four categories: collapses, unrepairable damages, serious but repairable damages, light damages. However, the first two categories as well as the last two categories are not clearly discriminated. The inability to compile detailed data classified according to the four degrees of damage or destruction for most of the Greek earthquakes has been already noted by Papazachos and Papazachou (2003). On the other hand, only for a few disastrous earthquakes that occurred in the last decades detailed data sets are available, such as the number of buildings suffering different degrees of damage or destruction, or other building features like the number of building floors and the building types. For these reasons, a realistic solution has been to calculate numbers of repairable buildings (RB) and unrepairable buildings (UR), a practice preferred by Papazachos and Papazachou (2003) too. In this classification RB includes buildings that suffered light damages and serious but repairable damages. On the other hand, UB includes buildings that suffered unrepairable damage, like partial or total collapse.

5.11. The Impact Metadata Section (IMS) and the References File (RF)

5.11.1 The Impact Metadata Section (IMS)

In this section the epicentral intensity, I_o, of the earthquake event is included. I_o is listed separately from the QLIS for the reason that although it is a description of the earthquake impact it is not a direct impact datum but only a metadata attribute.

Macroseismic Intensity, I_o. This is the maximum (epicentral) intensity assigned to each event in 12-grade scales, MM or EMS-98, unless otherwise indicated. This has been taken from the reference sources corresponding to each individual earthquake event. In some occasions, however, I_o has been assigned by us. For a few events described in the NOA Book of Earthquakes (Anonymous, 1893-1901 and 1902-1915), macroseismic intensity is given in the Rossi-Forel (RF) 10-grade scale. For the conversion of RF to MM we applied the correspondence between the two scales published by Richter (1958).

5.11.2 The References File (RF)

References File, RF. The various sources used to collect information about the previous three sections of the GEIDB are organized as a reference list in word format.

5.12 Case studies

5.12.1 The 30 October 2020 earthquake in Samos Island

The large M_w=7.0 earthquake of 30 October 2020**,** which ruptured offshore Samos Island, caused heavy destruction in the Izmir area, western Turkey, but the earthquake impact in the Greek area has

been relatively limited. Damage in hundreds of houses was reported from the islands of Samos and Chios as well as in port facilities in Samos (Lekkas et al., 2020). However, until writing these lines the official inspection of building damage was still ongoing. The earthquake caused in Samos two fatalities and 19 injuries. From our field inspection we assigned maximum intensity of VII-VIII in EMS98 scale in Vathy town of Samos. Damage was caused also by the tsunami that was generated by the earthquake. Results on this tsunami and its impact already published by Triantafyllou et al. (2021a) and are analyzed in Chapter 8. Several ground failures caused by the earthquake in Samos are very important (Lekkas et al., 2020, Evelpidou et al., 2021, Triantafyllou et al., 2021) but they are beyond the scope of this study.

Figure 5.6. External and internal damage at the Church of Christ in Ano Vathy, Samos, after the earthquake (M_w=7.0) of 30 October 2020 (photos credit, I. Triantafyllou).

5.12.2 The 25 February 1933 and 20 July 2017 earthquakes in Kos Island: a comparative study

A comparative study has been performed between the 20 July 2017 (M_w=6.6) and the 23 April 1933 (M_w=6.5) destructive earthquakes in the island of Kos (Fig. 5.7). The impact of these earthquakes has been compared in details and the results already published by Triantafyllou et al. (2020b). Therefore, here only a summary of this study is presented. The full paper, however, is included as Appendix to this thesis.

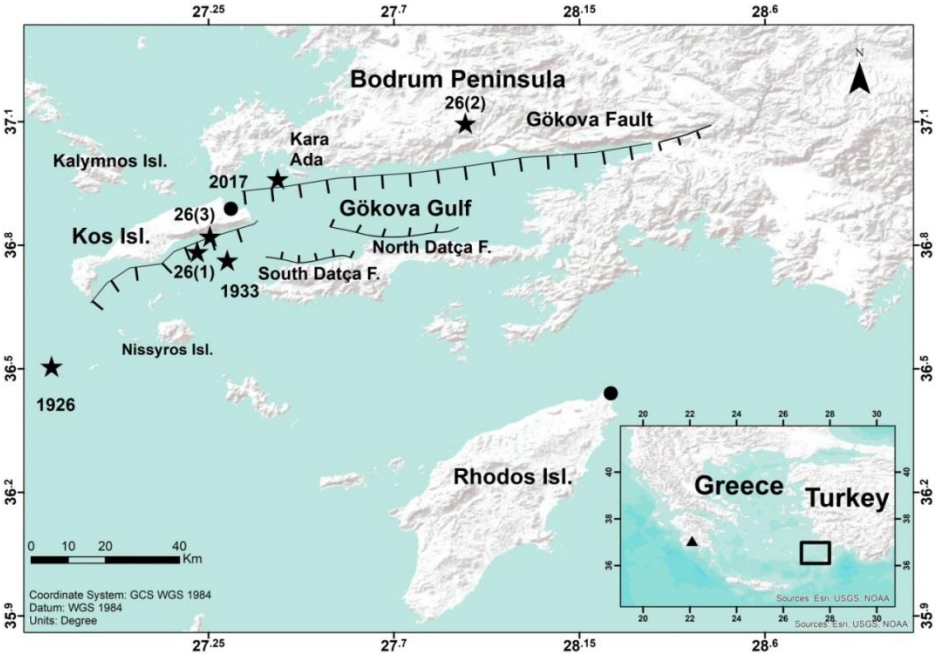

Figure 5.7. The study area. Key: star=earthquake epicenter; solid circles= Kos and Rhodes cities; stars= epicenters of earthquakes mentioned in the text: 1926, 1933 and 2017 stand for the earthquakes of 26 June 1926, 23 April 1933 and 20 July 2017, respectively; 26(1), 26(2) and 26(3) represent the 8 February 1926 earthquake epicenter estimated by Comninakis and Papazachos (1982), Kárnik (1969), Galanopoulos (1981), Ambraseys and Adams (1998), respectively. 26(1) is the preferred solution as dISC-GEMussed in the text. The area of Gökova Gulf is a graben dominated by two main faults, the south-dipping Gökova fault at the north and the north-dipping Datça fault at the south (e.g. Kurt et al., 1999; Altunel et al., 2003; Karasözen et al., 2018; Ocakoğlu et al., 2018). Hatched lines show tectonic faults. Solid triangle in inset shows the location of Baliaga village mentioned in the text.

The impact of the 1933 event was examined from a collection of documentary sources not utilized so far in the seismological literature, while the impact of the 2017 earthquakes was studied from observations collected during post-event field surveys in the island of Kos. The main observations are summarized in Table 5.3. From this Table it comes out that the seismic intensities observed in various towns and villages across Kos Isl. after the 2017 earthquake are systematically lower than the ones caused by the 1933 event. This is attributed to that engineered structures resisted the earthquake better in 2017 than in 1933. One may not ignore, however, that the two earthquakes very likely had different sources which contributed to cause different damage patterns. The 2017 source has been in the area of Karaada islet between Kos Isl. (Greece) and Bodrum peninsula (Turkey) (Fig. 5.7). Although the 1933 epicenter is poorly constrained so far, we suggested that a source placed away from, and to the south of, that of the 2017 earthquake is consistent with the 1933 damage pattern.

Table 5.3. Summary of the 1933 and 2017 damage seismic intensities (DSIs) and environmental seismic intensities ESI-07s assigned. Key: Fa=fatalities, In=injuries, GF=ground failures, SL=soil liquefaction, LD/RF= landslides/rock falls, HC=hydrological changes, TS=tsunami wave.

Event	Island/ Locality	Fa	In	Damage level	GF	SL	LD/ RF	HC	TS	DSI (MM & EMS-98)	ESI-07
1933	*Kos Isl.*										
	Kos city	178	600	destruction	yes					VIII-X	VII-IX
	Pyli	3		serious damage						VIII-IX	
	Vorinas							yes			V-VII
	Antimachia			destruction						IX-X	
	Kardamena			destruction						IX-X	
	Asfendiou			moderate damage						VI-VII	
	Kefalos			little damage						VI-VII	
1933	*Nissyros Isl.*										
	Emporios			little damage			yes			VI-VII	VI-VII
	Pali			little damage						VI-VII	
	Mandraki			little damage						VI-VII	
	Nikia			little damage						VI-VII	
2017	*Kos Isl.*										
	Kos city	2	6	extensive damage	yes	yes			yes	VII-VIII	VII-X
	Kos Marina			strongly felt	yes				yes	V-VI	VII-IX
	Cape Louros			strongly felt		yes			yes	V-VI	VIII-IX
	Therma			strongly felt			yes	yes		V-VI	V-VI

In the two cases examined we found a moderate correlation between the traditional and the environmental seismic intensities. This is due to the different nature of the scales used in assigning traditional and environmental intensities. Important ESI-07 differences were also obtained in the same observation sites from different types of environmental effects caused by the same earthquake. This happened with the 2017 event along the coastal zone of eastern Kos Isl. and particularly in the area of Kos Port where the ESI-07 due to tsunami reached at the level of X. However, adopting the TEE-16 12-grade scale (Lario et al. 2016) the ESI-07 intensity due to tsunami in Kos city is reduced to VI, which is more compatible not only with the ESI-07 estimates in other sites of the city on the basis of different environmental effects but also with the intensity assigned by the Papadopoulos and Imamura (2001) 12-grade generic tsunami intensity scale.

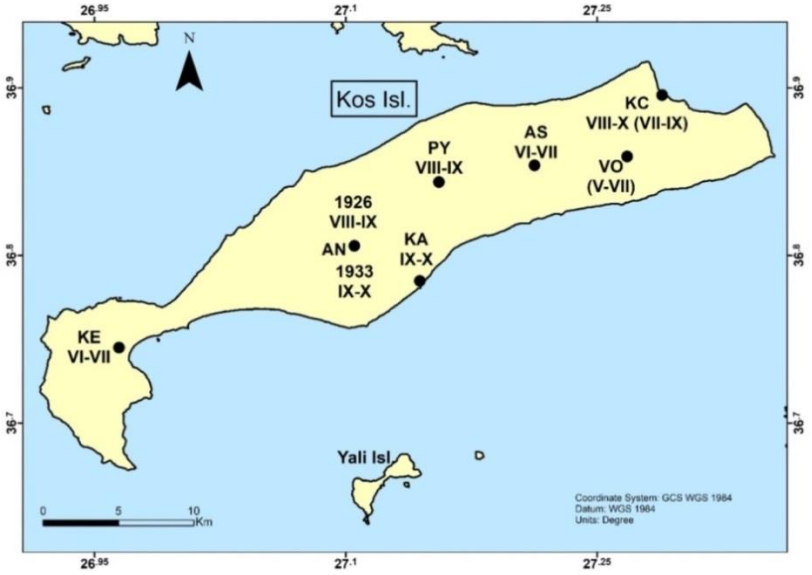

Figure 5.8. Macroseismic and environmental (in parenthesis) intensities assigned at various localities of Kos Isl. in relation to the 1933 earthquake. Macroseismic intensities are according to the MM and EMS-98 scales while environmental intensities were estimated from the ESI-07 scale. Key: KE=Kefalos, KA=Kardamena, PY=Pyli, AS=Asfendiou, VO=Vorinas, KC=Kos City, TH=Therma, CL=Cape Louros. In Antimachia (AN) MM/EMS-98 intensity was estimated in relation due to the 8 February 1926 earthquake too.

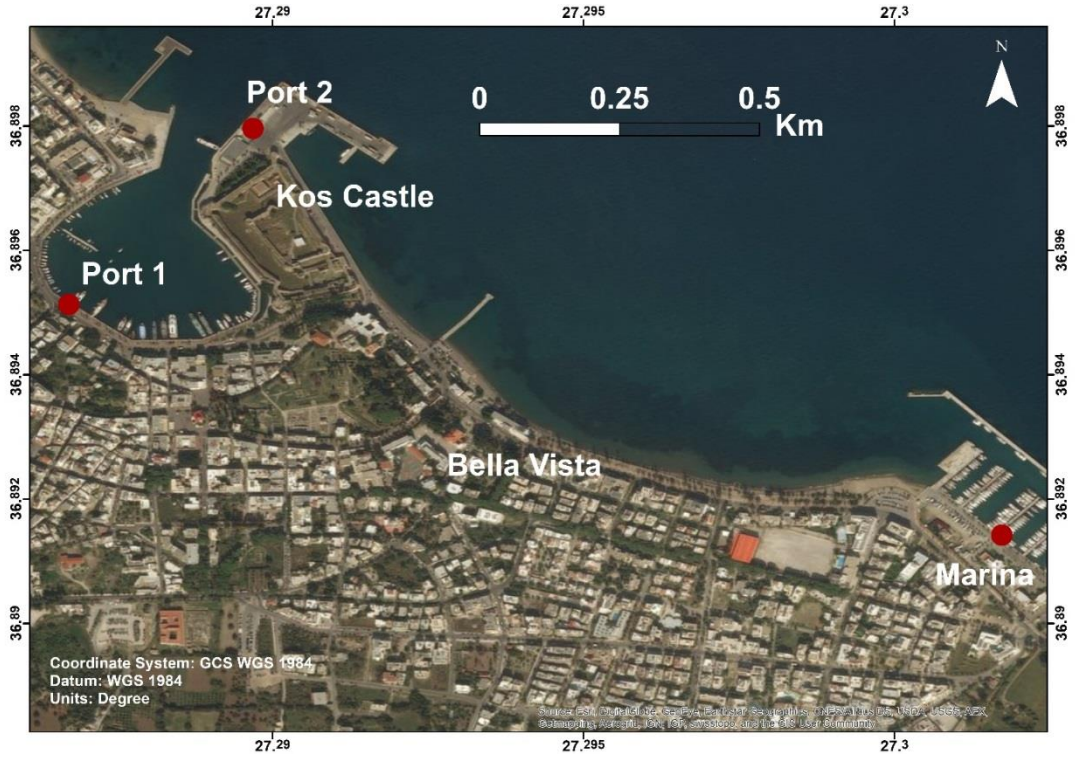

Figure 5.9. Localities in Kos city where ground failures were observed in relation to the 1933 earthquake (Port 1 and Bella Vista) and the 2017 earthquake (Port 1, Port 2, Kos Castle and Marina).

Figure 5.10. A masonry building that survived the 1933 earthquake in the historical center of Kos city. The partial collapse of the upper floor with the 2017 earthquake killed two persons.

Figure 5.11. Eastern Kos: Tsunami inundation zone after the 2017 earthquake. Run-up of maximum 0.8 m, 1.0 m and 1.5 m is illustrated by green, yellow and red, respectively. Seismic intensities assigned at various localities of eastern Kos Isl. in relation to the 2017 earthquake are also illustrated. Intensity estimates in MM and ESI-07 scales are shown.

5.12.3 Earthquake of 8 February 1926, Kos Island

In the seismic intensities assigned in relation to the 1933 earthquake we took into account that in Kos area two destructive earthquakes occurred a few years earlier, namely on February 8th 1926 and on June 26th, 1926 (Fig. 5.7). Therefore, it is of interest to examine if the impact assessment for the 1933

event was biased due to that no full restoration of the 1926 damage was achieved until the 1933 earthquake occurrence. The second 1926 event did cause only negligible damage in Kos Isl. Therefore, a more detailed examination was performed only for the February 8th, 1926 event.

The February 8th, 1926 earthquake is a little known event while its focal parameters are puzzling. Ambraseys (1988, 2001), Makropoulos et al. (2012) as well as the ISC-GEM-GEM Catalogue (2018) do not list the 1926 earthquake. Magnitude of M_s5.4 or 5.5 was calculated by Kárník (1969), Galanopoulos (1981), Comninakis and Papazachos (1982) but Ambraseys and Adams (1998) estimated magnitude as low as M_s5.0. Comninakis and Papazachos (1982) and Ambraseys and Adams (1998) provided nearly identical epicentral location, yet it is only a macroseismic estimation. However, the epicentral location provided by Kárník (1969) and Galanopoulos (1981) falls too far from the previous one (Fig. 5.7). Critikos (1926) listed earthquake origin time 19:49:25 (GMT) while Comninakis and Papazachos (1982) and Ambraseys and Adams (1998) considered 19:48:32 (GMT). However, this is the origin time of another earthquake, which according to Galanopoulos (1960) and Kárnik (1969) occurred at the same date near Zakynthos Isl. in the Ionian Sea.

Critikos (1926, 1928), Cavasino (1927), Sieberg (1932) and Galanopoulos (1955) reported that the February 8th, 1926 earthquake caused damage at the town of Antimachia, western Kos Isl. (Fig. 5.8), but only very little information was provided. To better assess the earthquake impact we collected and evaluated contemporary press reports and a set of documentary sources based on local archives not used so far in the seismological literature (Karpathios 1962, 1968; Chatzivasiliou 1989, 1990; Kinna et al. 2002).

From the above archival documents it results that the earthquake actually occurred at 20:15 local time (GMT+2 hours). According to a newspaper correspondence (*Estia*, 1926) the earthquake destroyed the town of Antimachia situated at the western side of the island of Kos (Fig. 5.8). Only 5 out of 600 houses and only 1 out of 3 churches remained standing, while the school building resisted the earthquake. It was also reported that two people were killed and about 60 injured. However, a more complete and accurate picture of the disaster comes out from a historical review regarding the Church of Kos by Karpathios (1962, 1968). The former author collected details about the 1926 earthquake impact based on local archives. Similar is the information published later by other authors, including Chatzivasiliou (1989, 1990) and Kinna et al. (2002), which likely copied Karpathios (1962, 1968) at some extent. From these publications we learn that in Antimachia many houses collapsed or were damaged killing two persons. It was reported that 200 persons were injured, a figure significantly larger and more reliable than the one reported in an early press report (*Estia*, 1926). Several people were rescued from the ruins by military forces. In addition, all the churches and chapels in the area suffered serious damage. The St. Apostole church rendered useless. Rebuilding started soon with the help of the island's Administration. However, no damage was reported from other areas of the island. That the disaster was important, although only very local, becomes evident from that the local Administration constructed hangars in Antimachia to shelter homeless people. At the same time, help was sent from the capital city of Kos as well as from the nearby island of Kalymnos. In addition, the Church of Kos asked financial help from various organizations established in Athens (Greece) as well as in the USA.

From the building damage caused we concluded that in Antimachia the epicentral intensity may have reached at I_0=VIII-IX in MM and EMS-98 scales. However, the earthquake of February 8th, 1926 had only local impact which very likely was due to its moderate size. On the other hand, from the local archives it results that the building restoration in Antimachia very likely completed before 1933. We

concluded, therefore, that the seismic intensity assignment due to the 1933 earthquake is not biased due to the damage caused by the February 8th, 1926.

5.12.4 Earthquake (M_w=7.24) and tsunami of 8 November 1905, Athos peninsula

This important event has been studied within the frame of this thesis but the results already published in the paper by Triantafyllou et al. (2020a). Therefore, here only a summary of the findings is presented. The full paper, however, is included as Appendix to this thesis.

The large earthquake that occured on 8 November 1905 offshore to the south of Mt Athos, North Aegean Sea, Greece, has been an event that shook large part of the Balkan peninsula. Although the event has been included in several earthquake catalogues (Table 5.4) it remains little known. From the collection of a variety of documentary sources, several of them being unknown so far to the seismological community, we were able to organize a data base of the earthquake impact and reconstruct the earthquake macroseismic field (Figs. 5.12-5.14).

From the new documentary sources collected we concluded that important cascade effects were caused by the 1905 earthquake. Namely, the earthquake produced landslides and rock falls that moved massively from an altitude of at least 300 m downhill to the sea covering a distance of nearly 1 km along the coast. This turned to the generation of a local but powerful tsunami of ~3 m in height in Arsanas (small port) of the locality Perdiki at the Kafsokalivion monastery, southern side of Mt Athos. Other co-seismic effects caused by the 1905 event included local subsidence, the appearance of new water springs and a fiery phenomenon.

At all evidence human victims did not happened due to building collapse but only due to the massive landslides, the rock falls and the local tsunami. Four documents provided relevant information with the total number of victims estimated as equal to 9, 10 (in two documents) and 11. We have concluded that the total number of victims was very likely 11, and that 6 of them killed by the landslide, while the rest 5 were killed by the tsunami.

Table 5.4. Focal parameters of the Mt Athos 8 November 1905 earthquake listed in various earthquake catalogues. Key: y=year, m=month, d=day, φ_N^0 and λ_E^0 are geographic latitude north and longitude east, respectively; l.t.=local time, *h*=focal depth, *n*=shallow earthquake, I_o=epicentral intensity in Modified-Mercalli scale, M_s=surface-wave magnitude, M_w=moment magnitude; * indicates magnitude obtained from modeling. Parameter marked by an asterisk has been derived by modeling of macroseismic data. For the earthquake origin time see explanations in the text.

y	*m*	*d*	φ_N^0	λ_E^0	*Time (GMT)*	*h (km)*	I_o *(MM)*	M_S	*Reference*
1905	11	8	240 km NE from Athens		21:41:54				Eginitis (1910)
1905	11	9	40.00	24.00	22:06:12	*n*		7.8	Richter (1958), Duda (1965)
1905	11	8	40.25	24.25	21:41	*n*	X	~7	Galanopoulos (1960)
1905	11	8	40.25	24.25	21:41	*n*	X	~7	Kárnik (1969)
1905	11	8	40.00	24.00	22.06	*n*	IX-X	7.5	Kárnik (1969)
1905	11	8	40.30	24.40	22:06:00	17		7.4	Shebalin et al. (1974), Makropoulos et al. (2012)
1905	11	8	40.25	24.25			IX-X	7.5	Galanopoulos (1981)

1905	11	8	40.30	24.30	22:06:30	*n*	X	7.5	Comninakis and Papazachos (1982)
1905	11	8	40.00	24.00	22:06	*n*		6.8	Abe and Nogushi (1983)
1905	11	8	40.30	24.40	22:30:30	*n*	X	7.5	Papazachos and Papazachou (1989)
1905	11	8	40.26	24.33	22:30:30	22.4	10.21	8.3*	Papazachos and Papaioannou (1997)
1905	11	8	40.00	24.50	22:07			7.24	Ambraseys (2001)
1905	11	8	40.00	24.50	22:30:30	*n*	X	7.5	Papazachos and Papazachou (1997, 2003)
1905	11	8	40.09	24.63	22:06:11	15		7.24 (M_w)	ISC-GEM (2018)

It is possible that the 1905 earthquake was associated with the dextral strike-slip fault system of the NE-SW trending North Aegean Trough. An alternative, however, is that the event was generated along the nearly ENE-WSW trending dextral strike-slip Athos Fault Zone, which is situated closer, and in parallel, to the southern edge of the Mt Athos peninsula. Regardless the seismotectonic interpretation, the 1905 earthquake remains a key event for better understanding the hazards associated with earthquakes and related phenomena, such as landslides, rock falls and tsunamis, in an important worldwide cultural heritage site like Mt Athos.

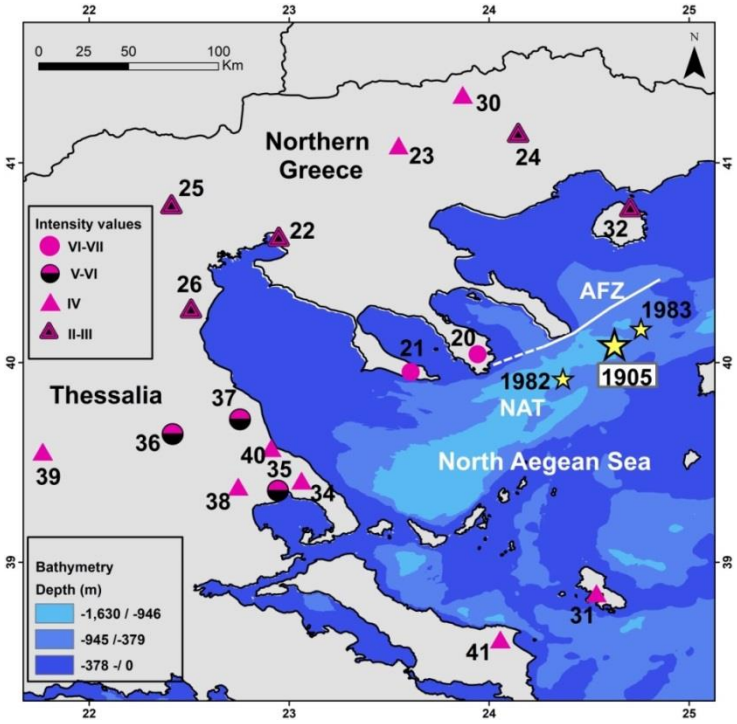

Figure 5.12. Macroseismic intensities in 12-grade MM scale felt at sites in mid epicentral distances due to the Mt Athos earthquake (large star) of 8 November 1905. For intensity documentation and numbering of sites see Table A1. Symbol key: AFZ=Athos Fault Zone (white line, redrafted from Roussos and Lyssimachou, 1991), NAT=North Aegean Trough. Small stars show the epicenters of the 18 Jan.1982 (M_w6.56) and 6 Aug. 1983 (M_w6.65) earthquakes mentioned in the section of Discussion; earthquake focal parameters are from the ISC-GEM (2018) catalogue.

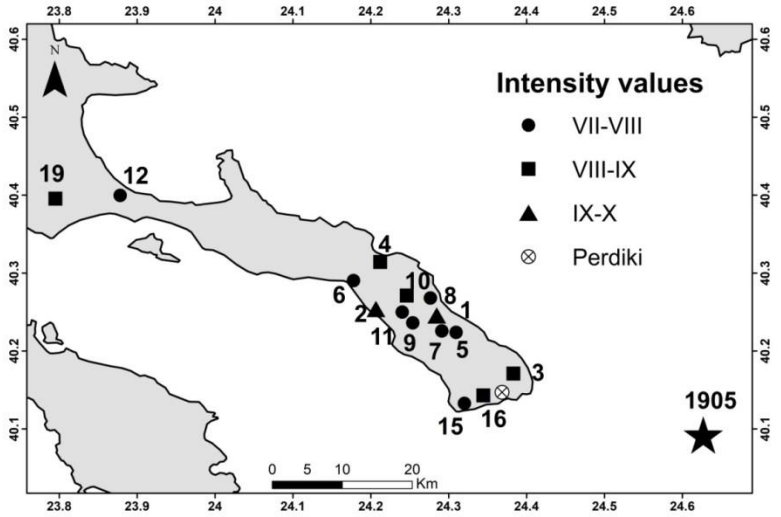

Figure 5.13. Macroseismic intensities in the 12-grade MM scale felt at sites of Mt Athos peninsula due to the 8 Nov. 1905 earthquake. For intensity documentation and numbering of sites see Table A1; star=earthquake epicenter. Earthquake parameters are from the ISC-GEM (2018) catalogue.

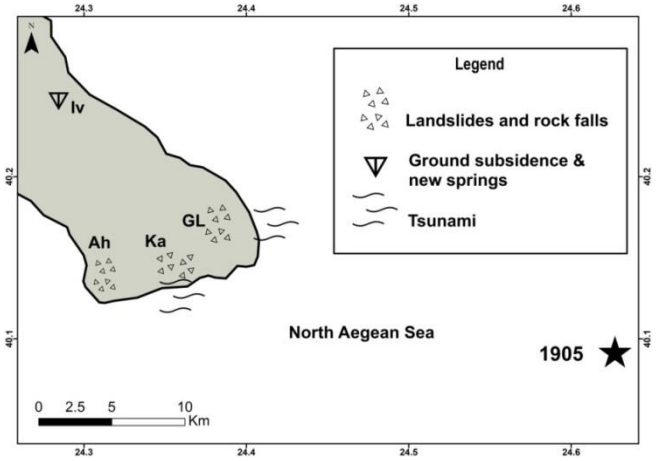

Figure 5.14. Main co-seismic ground failures reported in association to the 1905 Athos earthquake (star). Key for localities: Iv=Iviron Monastery, GL= Great Lavra Monastery, Ka=Kafsokalivion Monastery, Ah=Ayia Anna hermitage. The tsunamis reported offshore Ka and GL were in association to the 1905 and 1585 earthquakes, respectively.

5.13. A short statistics of the GEIDB

From the total number of 248 earthquakes inserted in the GEIDB, the numbers of entries for shallow (focal depth h<60 km) and intermediate-depth (h≥60 km) earthquakes are 229 and 18, respectively. In the 19th century the shallow and intermediate-depth events are 108 and 8, respectively. The respective numbers for the time period from 1900 to 2020 are 121 and 10 and for the time period from 1950 to 2020 are 71 and 5, respectively. The constancy of the event ratios in the entire time period (~1.1 event per year: see Chapter 1) indicates completeness in the reporting of the impactful earthquakes from 1800 to 2020. The frequency of the three main attributes inserted in the GEIDB is illustrated in Figure 5.15.

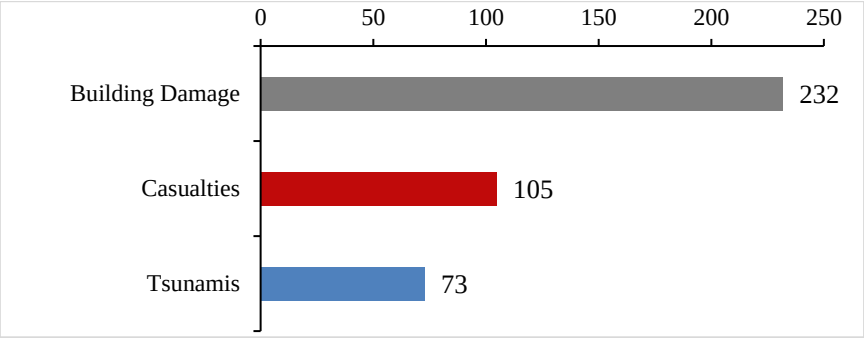

Figure 5.15. Frequency of the three main attributes inserted in the GEIDB.

The magnitude of the events included in the database ranges from M_w=4.8 (Katakolo, 15 April, 1899) to M_w=7.6 (Crete, 12 October 1856) during the 19th century and from M_w=4.9 (11 September 1918, Milos Island; 21 February 1955, Volos) to M_w= 7.37 (ISC-GEM; 9 July 1956, Cyclades) during the time interval 1900-2020. It should be noted, however, that the error involved in the 19th century magnitudes is about 0.3.

5.14 Summary of Chapter 5

After reviewing several international and national sources containing earthquake impact data, the construction of the Greek Earthquake Impact Database (GEIDB) is described. It is organized in Access Format and is structured in four main sections for the seismicity parameters, the earthquake impact data, the impact metadata (macroseismic intensity) and for the references file. The GEIDB covers the time period 1800-2020 and contains 248 earthquake entries. The impact data attributes inserted in the GEIDB are casualties (fatalities and injuries), repairable and unrepairable building damage and tsunamis. However, details on the tsunamis impact have been inserted in the Greek Tsunami Impact Database (GTIDB) organized and explained in Chapter 8. Case studies on the impact of some selected recent and earlier earthquakes have been also performed. For the next recent earthquakes post-event field surveys were organized with the participation of the candidate.

CHAPTER 6. EARTHQUAKE IMPACT METRICS

6.1 Introduction

Apart from organizing the Greek Earthquake Impact Database (GEIDB), one of the main objectives of the research performed in this thesis is the investigation of the factors that the earthquake impact in Greece depends on, e.g. the earthquake focal parameters, the seismicity distribution in space and time as well as the intensity of the earthquakes. Of interest is also to compare the results reached in the Greek region with findings in other seismogenic parts of the world. To this aim there is need to adopt appropriate *Earthquake Impact Metrics (EIMs)* by taking into account the international literature on the topic. For this reason the section 6.2 is devoted to a short literature review, while in section 6.3 the selection of suitable EIMs for Greece has been decided on the basis of the international experience but also by considering the various types of quantitative data which are available and inserted in the GEIDB. However, the variation patterns of the several EIMs selected are examined in depth in Chapter 7.

6.2 Earthquake impact metrics and their variation patterns

6.2.1 A global overview

Several authors investigated correlations between EIMs and various geophysical parameters. Lomnitz (1970) supported that a positive correlation is established between the time of day and the number of victims in Chilean earthquakes. This correlation is attributed to a 24-hr cycle of dwelling occupancy. Of particular interest is the suggestion by Lomnitz (1970) that the incidence of foreshocks lowers the number of human losses. Such results are of value to earthquake engineering design and to emergency measures for the protection of human populations in earthquakes. Lechat (1979) and de Ville de Goyet (1976) suggested, and Alexander (1985) adopted, that the ratio of *mortality* (deaths or fatalities, Fa) to *morbidity* (injuries, In) could be expressed by the integrated index

$$R_i = 100 \times (Fa / In), \qquad (6.1)$$

From data of various earthquakes it was found that $R_i \sim 33$, i.e. as an average one death corresponds to three injured people. When it occurs, a 1:3 ratio is most likely to coincide with an earthquake magnitude in the range 6.5-7.4, but many other ratios of death to injuries may instead be probable. Gueri and Alzate (1984) supported that the 5-9 years and over-60 years age groups are the most vulnerable to death and injury in earthquake disaster.

Ohta et al. (1986) collected fatality and monetary loss data from the NOAA database and correlated them with the earthquake magnitude. This global statistical analysis referred to the time period 1900-1979. As regards the annual variation of damage, in terms of victim and monetary loss, these authors found that for the number of victims there seems no systematic change, but the monetary losses increase gradually (Fig. 6.1). On the other hand, they found that there is a positive correlation between the number of people killed and the earthquake magnitude. On the contrary, a weak correlation between the damage level and the earthquake magnitude was found. Oike (1991) compiled earthquake impact data from several databases in the world covering the time interval from 1890 to

1989 and found that the number of people killed in general increases with the earthquake magnitude. This author found also that in Japan inland earthquakes cause about ten times more dead people than the offshore earthquakes. Oike (1991) studied also the variation of annual numbers of death tolls caused by earthquakes in several countries. This author concluded that in Japan and Taiwan these numbers recently decreased. This result was attributed not to disaster mitigation actions but to the fact that recently no severe events occurred near to populated regions.

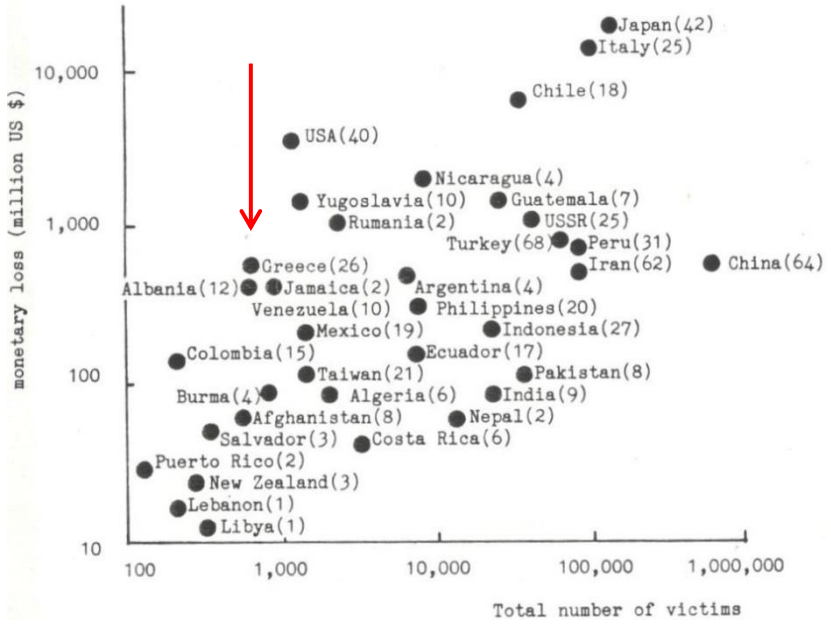

Figure 6.1. Relation between the total number of victims and the total amount of monetary losses according to Ohta et al. (1986). Greece possesses a relatively low position in this relationship.

Coburn and Spence (1992) showed that the number of people killed increases with the number of buildings heavily damaged (Fig. 6.2) and proposed that a general casualty equation for the total deaths, *K*, resulting from an earthquake can be expressed as:

$$K = Ks + K' + K2, \qquad (6.2)$$

where *Ks* is fatalities due to structural damage, *K´* is fatalities from non-structural damage and *K2* is arising from follow-on hazards. They supported that variable *K2* is rare, but where it occurs this is likely to dominate the total. Several years later this was verified with the destructive tsunamis that followed the giant earthquakes of 26 December 2004 (M_w=9.3) in Indian Ocean and of 11 March 2011 (M_w=9.0) in Japan. These two events claimed more than 220,000 and 18,000 human lives, respectively, the great majority due to tsunamis.

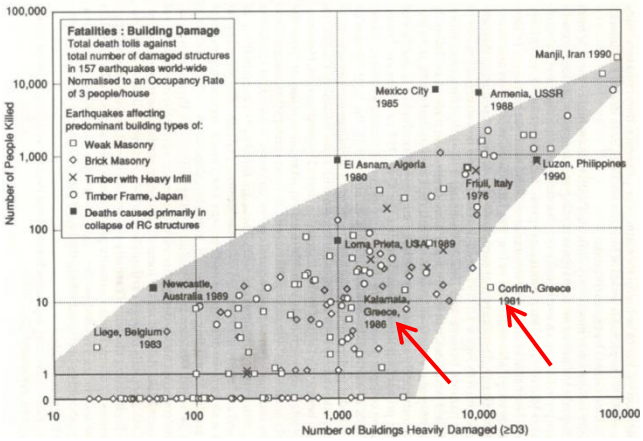

Figure 6.2. Relation of the number of fatalities to the number of buildings damaged in earthquakes (Coburn and Spence, 1992). The position of the Corinth 1981 and Kalamata 1986 earthquakes is relatively low in this relationship.

Hengjian et al. (2003) investigated the relationship between building damage patterns and human casualties in Nishinomiya City – one of the most heavily damaged cities in the 1995 Hanshin-Awaji Earthquake Disaster – using photographs of damaged buildings. First, the photographs of buildings in which casualties occurred were identified, and the building damage patterns were judged based on the photographs considering the existence of survival space. Then the relationship between the building damage pattern and casualty occurrence, and the characteristics of casualty distribution, were investigated. The main findings were as follows: Most casualties occurred in relatively old two-story wooden buildings in which the ground floor completely collapsed without survival space; casualties occurred at all building damage levels including «no damage», and it can be seen that building damage is the major, but not the sole cause, of casualties in an earthquake; in Nishinomiya City, the regional distributions of casualties due to the collapse of buildings that left no survival space is similar to that of casualties due to other types of building damage.

An important contribution came with the report by Jaiswal et al. (2009) who developed an empirical approach for estimating human losses for large earthquakes worldwide aiming to support the U.S. Geological Survey's Prompt Assessment of Global Earthquakes for Response (PAGER) system. These authors defined the earthquake fatality rate as the ratio of the total number of shaking-related fatalities to the total population exposed at a given shaking intensity (in terms of Modified-Mercalli (MM) shaking intensity scale). They examined global earthquake fatality data since 1900, not including other non-shaking related deaths—for example, deaths due to fire, land or mudslide, or ground failure and concluded that clearly, countries like China, Pakistan, Iran, and Turkey dominate the list. Chaoxu et al. (2020), following Jaiswal et al. (2009), listed numbers of human losses and casualty rate for each intensity level for 61 earthquakes that occurred in China from 1966 up to 2014. It is of interest that although the majority of the earthquakes have been of magnitude over 5 there are listed three events of magnitude 4.7 that caused one casualty each. These authors adopted the term *mortality rate* to express the ratio of deaths to total.

A modification of the expression (6.1) was considered by Wyss and Trendafiloski (2009) who examined the ratio of injured, In, to fatalities, Fa, in earthquakes,

$$R = In / Fa, \qquad (6.3)$$

and found that this earthquake impact indicator has increased over time in the post-1950 period. This shows that it is more likely by approximately a factor of 2 that a person survives an earthquake today than 50 years ago. However, those authors noted that the analysis of *R* requires (as a minimum) separation by type of country and by location of epicenters (land or offshore). *R* in earthquakes beneath land is typically half of that for events offshore. *R* in the industrialized world is about two to three times larger than in the developing world. According to those authors, the countries that have made the greatest progress in protecting their population are Japan and China. They also suggested that the ratio *R* can be used as an indicator of building quality. This is because the worldwide statistics have shown that about 75% of the fatalities attributed to earthquakes were caused by the collapse of buildings that were not adequately designed for earthquake resistance, but were built with inadequate materials or were poorly constructed.

The temporal patterns of fatalities caused by 20th century earthquakes have been examined by Scawthorn (2011) who found a significant diurnal variation. Namely, earthquakes that occur at night have relatively more fatalities than they would if they occurred in daylight. Without accounting for diurnal variation, mortality and morbidity estimates can be off by a factor of as much as ± 34%. On the other hand, Wang et al. (2011) developed a model for predicting fatality rates due to earthquakes. To calibrate the prediction model, these authors used fatality data from 61 earthquakes affecting Taiwan from 1999 to 2016, as well as information on the socioeconomic and environmental characteristics of the affected communities.
Various databases have been utilized by some authors for data elaboration and the evaluation of seismic future of cities. For example, to test a theoretical model for the interaction between nature and political economy and earthquake fatalities, Anbarci et al. (2005) collected and evaluated data from various sources regarding 269 large earthquakes occurring worldwide between 1960 and 2002. In their analysis these authors took into account several factors that control the destructiveness of an earthquake, such as magnitude, focal depth and proximity to population centers.

Bilham (2009) examined the future of cities in the light of a deadly earthquake. The author used data collected from Milne (1912), NOAA (Dunbar et al., 1992) and Utsu (2002b) and compared the earthquake fatalities with the estimated global population since 500 BC. Among other issues, Bilham (2009) analyzed the global distribution of deadly earthquakes and presented two main diagrams showing (i) the earthquakes since 1500 with more than 3000 deaths per event, and (ii) all the fatal earthquakes in the time period 1900-2008. An interesting result found by Bilham (2009) is that 12% of all fatal earthquakes are found along the margins of the eastern Pacific, and fully 85% of the world's fatalities have occurred in the Alpine/Himalayan collision belt between western Europe and eastern Asia. A handful of nations, namely Japan, Indonesia, Italy, Iran and Turkey have hosted both the world's most fatal earthquakes, and greatest numbers of them.

6.2.2 Earthquake impact variation in Greece

In this section we focus on the previous studies on the patterns of earthquake impact variation in Greece, while in the later section we extend the examination of this issue in the light of the data inserted in GEIDB. However, it is useful to first discuss the case three earthquakes that can be considered as extreme ones. These extremes share the common feature that in each case more than a

strong single earthquake occurred during a seismic sequence but in short time apart each other. As a consequence, the discrimination of the impact of one single earthquake from the impact of another single earthquake belonging to the same sequence is not always possible. This discussion is useful for the reason that the impact caused by these extreme events often influence the results obtained and, therefore, are frequently quoted in our subsequent analysis.

A few extreme cases

The first noticeable extreme case is the Chios Island 23 April 1881 (M_w=6.47, SHEEC 2017) earthquake that caused 3,550 fatalities and 7,000 injuries (Papadopoulos, 2015). These figures represent the earthquake impact in the Greek territory, i.e. in Chios Island, and do not include the casualties caused in western Turkey. There is evidence that two strong earthquakes occurred with a time difference of only 4 minutes, i.e. on 13.35 the first and on 13.39 the second (see reviews in Papazachos and Papazachou, 2003, Ambraseys, 2009, Papadopoulos, 2015). The high number of casualties has been attributed to several combined factors including houses of relatively heavy construction, particularly in the capital city of the island, and soft soil conditions in a large part of the affected area. Immediately after the first earthquake, which very likely was a strong foreshock, the people run outdoors. A few minutes later the second strong earthquake found the people gathered in the narrow streets of the city and of several villages, thus causing high numbers of fatalities and injuries. Although are unable to determine the casualties numbers from the first shock, if any, we believe that the above figures should be attributed to the second event.

The second case is a series of very strong earthquakes that isolated the central Ionian Islands of Cephalonia, Ithaki and Zakynthos in 9, 11 and 12 August of 1953 measuring magnitudes M_w=6.15, M_w=6.7 and M_w=7.1, respectively (ISC-GEM 2018). Galanopoulos (1981) and Papazachos and Papazachou (2003) reported that in total the seismic sequence caused 455 fatalities, 2412 injuries and 21 missing people. However, they didn't specify the numbers of casualties for each one of the three events. We have considered that the missing people died and, therefore, the total number of fatalities has been as high as 476. From the examination of several sources, e.g. reports, newspapers, we found that the earthquake caused 3 fatalities and 50 injuries in the island of Ithaki. The second earthquake event caused 112 fatalities and 250 injuries, mainly in the island of Cephalonia. The rest numbers of fatalities (=358) and injuries (=2112) have been attributed to the third and largest event of 12 August 1953.

A third case consists by the sequence of very strong earthquakes occurring at the eastern Corinth Gulf during February-March 1981. The strongest event (M_w=6.58, ISC-GEM 2018) happened on 24 February 1981. A few hours later the second earthquake occurred (M_w=6.4). The third event (M_w=6.3) happened on 4 March 1981. The total numbers of casualties reported in the epicentral area are 20 fatalities and 500 injuries (e.g. Papazachos and Papazachou, 2003). Very likely, the number of fatalities represents human losses counted as a result of the first and strongest event. The majority of injuries were also caused by the first event although we should not rule out that some injuries were also caused by the second and third earthquakes of the sequence.

The seismic building code in Greece: a brief overview

The time interval 1800-1910 is the less complete in injuries data. In the post-1910 time interval the data are more complete. The first national seismic building code was officially introduced in Greece in the year 1959. Consequently, since 1960 earthquake-resistant buildings were systematically

constructed in the country. On 20 June 1978 the city of Thessaloniki, North Greece, was struck by a strong earthquake (M_w=6.23, ISC-GEM 2018), which caused 48 fatalities and 220 injuries. That was the first time in modern history of Greece that a large city, populated by ~800.000 in its metropolitan area, was threatened by a strong earthquake. The follow-up came with the sequence of very strong earthquakes occurring at epicentral distance of ~70 km from the capital city of Athens during February-March 1981 already mentioned earlier. The strongest event (M_w=6.58, ISC-GEM 2018), happened on 24 February 1981, caused 20 fatalities and 500 injuries in the epicentral area. This seismic sequence affected the metropolitan area of Athens (e.g. building damage, social consequences) but no human losses were noted there. The series of fatal earthquakes continued with the strong event (M_w=5.93, ISC-GEM 2018) of 13 September 1986 that hit the city of Kalamata in southern Greece. This earthquake caused 20 fatalities and 80 injuries. After these experiences gained within a short time of only 8 years, the Greek state took measures for the improvement of the building code in 1984 as well as for the establishment of organized and well-trained rescue corps of the fire brigade in 1986. Drastic improvement of the building code was established by the beginning of the 1990s, while a further improvement was noted in 2000 after the earthquake (M_w=5.98, ISC-GEM 2018) of 7 September 1999 that caused 143 fatalities and 1600 injuries in the metropolitan area of Athens.

Previous studies

Ambraseys and Jackson (1981) studied the earthquake hazard and vulnerability in the northeastern Mediterranean emphasizing on the earthquake sequence of February-March 1981 in the eastern Corinth Gulf, Greece. They found that the main factors on which the total building damage following an earthquake depends on the population density, the building type and the earthquake magnitude. These authors examined relationships between (1) total damage and epicentral intensity, (2) total damage and surface-wave magnitude, and (3) different building types and earthquake magnitude. The authors developed regression relationships and found that the epicentral intensity alone is not a good predictor of total damage. The same authors concluded that the total damage produced by earthquakes with epicenters offshore or close to coastline is about half as large as that caused by events with epicentral areas on land.

According to Ohta et al. (1986), Greece is ranked as eighth in a list of 19 earthquake prone countries all over the world. In addition, they correlated the total number of victims with the total amount of monetary losses and found that Greece is 26th out of 64 countries. Coburn and Spence (1992) showed in a diagram the relationship of the number of fatalities to the number of buildings heavily damaged in earthquakes (Fig. 6.2). They found that the Corinth 1981 and Kalamata 1986 earthquakes claimed relatively low fatality numbers as compared to other earthquakes in other parts of the world. Lekkas and Kranis (1997) examined the distribution of the mortality related to earthquake faulting. The case studies analyzed included the main shocks occurring during 1995 in Kobe, Japan (M=7.2), in Egion, Greece (M=6.1) and in Dinar, Turkey (M=6.1). They found that the majority of victims was observed at a distance of no more than 4-5 km from the fault line.

From data of the period 1950-1986, Papazachos and Papazachou (2003) showed that in Greece both the average annual numbers of seismic destructions (buildings collapsed and heavily damaged) and seismic damages (repairable buildings and light damaged buildings) increase with the maximum macroseismic intensity MMI_o. The same authors found that the average annual numbers of deaths

(fatalities), *FA*, and injuries, *IN*, increase also with the maximum macroseismic intensity following the next empirical relationships:

$$\log Fa = -8.07 + I_o \,, \qquad (6.4)$$

and

$$\log In = -7.33 + I_o \,, \qquad (6.5)$$

The relationships (6.4) and (6.5) indicate that the number of injuries is about five times the number of deaths.

In their worldwide analysis, Jaiswal et al. (2009) found for Greece that in the time period 1900-1999 the *Maximum shaking deaths (10 or more) due to any single earthquake since 1900* is 800. This figure was attributed to the large earthquake of 12 August 1953 in the Ionian Sea with M_w=6.81 according to ISC-GEM or M=7.2 according to Jaiswal et al. (2009). They also found that the *Total shaking deaths by all earthquakes since 1900* is 1,313, the *Total fatal (one or more deaths) earthquakes since 1900* is 25 and the *Average shaking deaths per earthquake since 1900* is 53. The fatality rate estimated by Jaiswal et al. (2009) for Greek earthquakes is one death per 1270 people exposed to shaking intensity IX. This figure reduces to one per 43,300 people at shaking intensity VII. However, these estimations need reconsideration for the reason that the database used by Jaiswal et al. (2009) is not updated and contains erroneous data. For example, they adopted that the 1953 earthquake caused 800 human losses but this figure is overestimated and nearly doubles the number of human victims caused by the Ionian Sea 1953 earthquake.

In his extensive global earthquake fatality statistics, Bilham (2009) found that in Greece the cumulative number of fatalities since 1500 is very low as compared to other nations. This result indicates the low mortality of Greek earthquakes in general and per event, although Greece stands at a higher position as regards the fatal earthquakes in the time period 1900-2008. Wyss and Trendafiloski (2009), in their study of the worldwide ratio of injured to fatalities in earthquakes, $R = In / Fa$, showed that it has increased over time in the post-1950 period. Countries where the ratio R has not increased with time include Iran, Turkey, and Greece. However, the data set used for Greece is limited.

Pomonis et al. (2009) estimated that in Greece, around 90% of the 1,419 deaths reported in 50 fatal earthquakes that took place between 1900 and 2008 were due to building collapse. In the last 40 years (1969-2008) almost 85% of the earthquake-related life losses have been associated with the collapse of reinforced concrete (RC) buildings (out of 271 deaths in 1969-2008, 230 occurred due to the collapse of 35-40 RC buildings).
In the last few decades several studies and books were published regarding the economic, social and psychological consequences of the earthquakes in Greece as well as relevant urban planning issues. However, such types of earthquake effects are not of interest in the present study.

6.3 Selection of Earthquake Impact Metrics (EIMs)

Various authors have found that inland earthquakes are more destructive as compared to offshore earthquakes (e.g. Ambraseys and Jackson, 1981, Oike, 1991, Wyss and Trendafiloski, 2009). This has been taken into account in our examination of the spatial distribution of the earthquake impact on buildings, i.e. of the numbers of Repairable Buildings (RB) and Unrepairable Buildings (UB). As regards the earthquake focal depth, h, we considered two classes, shallow (h<60 km) and intermediate-depth earthquakes (h≥60 km). On the other hand, it has been found that building damage is dependent on earthquake magnitude and population density (e.g. Ambraseys and Jackson, 1981, Oike, 1991) while the number of fatalities is correlated to the number of buildings heavily damaged (e.g. Coburn and Spence, 1992). Such correlations were also investigated in our study (Chapter 7).

Similar correlations were investigated for the numbers of fatalities, Fa, and injuries, In. Another metric relevant to the earthquake impact on the population was introduced by Alexander (1985), which is the ratio Fa/In integrated over 100 and is expressed by the formula (6.1). However, one may consider a non-integrated mode termed *survival ratio* and is defined simply as *In*/*Fa* (e.g. Wyss and Trendafiloski, 2009). Badal et al. (2005) defined the *casualty rate* as the ratio between the number of killed people and the number of inhabitants of the affected region. Such a metric requires definition of the affected region and good population data in the region. However, in Greece data regarding the population in the region affected are available only for the last decades. Eventually, we adopted the concept of survival ratio R (6.6) and its integrated version 100 x R:

$$R = \text{morbidity / mortality} = In / Fa, \qquad (6.6)$$

In their worldwide analysis, Jaiswal et al. (2009) estimated for several countries, including Greece, the *Maximum shaking deaths (10 or more) due to any single earthquake since 1900 (MSD)*, the *Total shaking deaths by all earthquakes since 1900* (TDE), the *Total fatal (one or more deaths) earthquakes* since 1900 (TFE) and the *Average shaking deaths per earthquake since 1900 (ADE)*. Aiming to update the results obtained by Jaiswal et al. (2009) we re-estimated these parameters on the basis of the data inserted in GEIDB. In addition, we introduced respective metrics for earthquakes causing injuries.

The epicenters of the 248 impactful earthquakes listed in GEIDB, regardless the kind of impact, are mapped in Figure 6.3. This map illustrates that practically the epicenters distribution covers nearly the entire country. However, the central Aegean Sea and the northeastern side of the country are exceptions, which are due to that the seismicity in that area is very low anyway, at least in the reference period examined (1800-2020). As one may expect the epicenters of the intermediate-depth earthquakes are restricted to the South Aegean Sea area since the active lithospheric subduction in the area takes place underneath this area.

Table 6.1 summarizes the various Earthquake Impact Metrics (EIMs) which have been selected in this study. This selection balances the availability of relevant quantitative impact data sets for statistical elaboration and mapping, with the need to compare our results with the findings of other authors not only in Greece but also in other parts of the world.

Table 6.1. Summary of the Earthquake Impact Metrics (EIMs) used.

Attribute	Impact Metrics			
Human Losses				
Fatalities (Mortality)	Mortality per earthquake (Fa)	Number of fatal earthquakes (FaE)	Average mortality per earthquake (AFa)	Maximum mortality due to any single earthquake (MFa)
Injuries (Morbidity)	Morbidity per earthquake (In)	Number of earthquakes causing injuries (InE)	Average morbidity per earthquake (AIn)	Maximum morbidity due to any single earthquake (MIn)
Fatalities/ Injuries	Survival Ratio (R=Fa/In)		Survival Ratio integrated (R_i=100 x R)	
Buildings				
Repairable Buildings	Number of Repairable Buildings per earthquake (RB)	Average number of Repairable Buildings per earthquake (ARB)		Maximum RB due to any single earthquake (MRB)
Unrepairable Buildings	Number of Unrepairable Buildings per earthquake (UB)	Average number of Unrepairable Buildings per earthquake (AUB)	Average Damage Ratio per earthquake (ADR=RB/UB)	Maximum UB due to any single earthquake (MUB)

Epicenters maps of the earthquakes that caused impact on the population and on the buildings are presented in Chapter 7. Some of the shallow earthquakes caused tsunamis too. The epicenters map of these earthquakes is presented in Chapter 8.

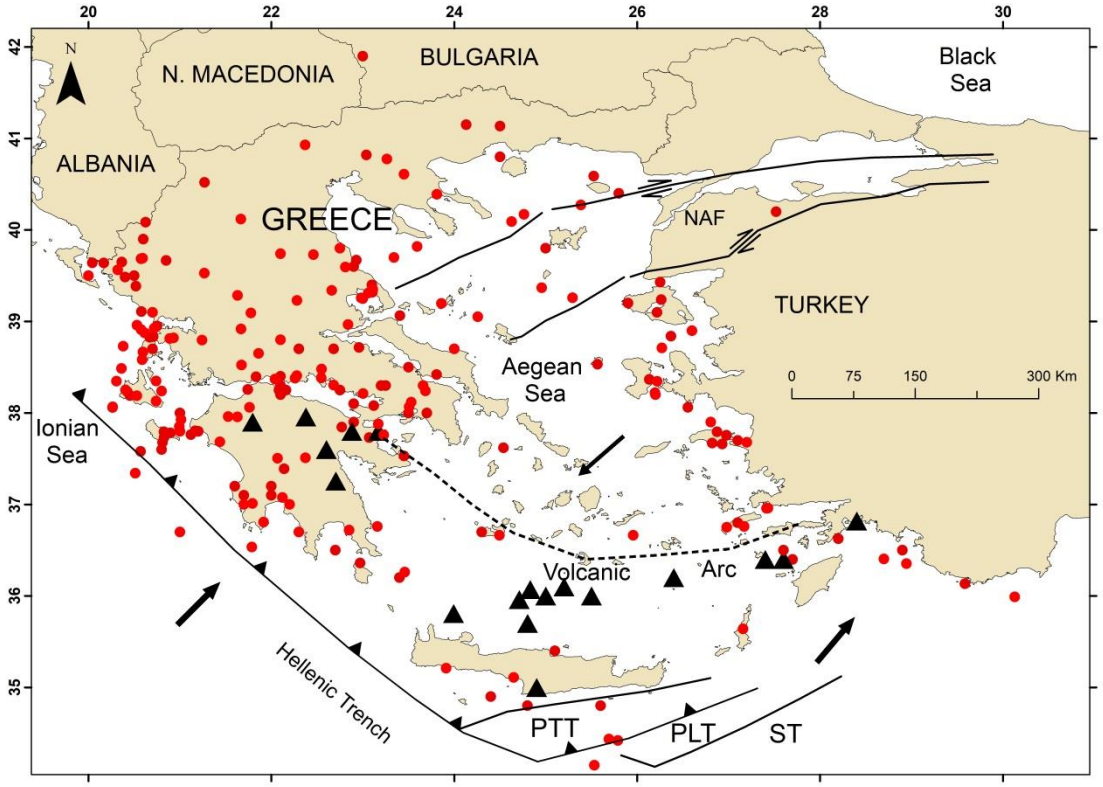

Figure 6.3. Epicenters of all the earthquakes that during the period AD 1800-2020 caused impact of any kind considered in GEIDB, i.e. building damage or destruction, and/or human losses (fatalities and/or injuries)

and/or tsunami. Symbol key: red dot=shallow earthquake, black triangle=intermediate-depth earthquake, arrow shows plate or fault motion, NAF=North Anatolian Fault.

6.4 Summary of Chapter 6

A review of the international literature indicates that several Earthquake Impact Metrics (EIMs) are in place but their use depends on the types of impact data that are available. In Greece only limited effort has been made so far to select appropriate EIMs. Taking into account both the international experience and the types of data which are available and have been included in the GEIDB a set of EMIs were selected regarding the next attributes: fatalities, injuries, repairable buildings, unrepairable buildings.

CHAPTER 7. VARIATION PATTERNS OF EARTHQUAKE IMPACT METRICS IN GREECE

7.1 Introduction

From an international review (Chapter 6) it results that the impact of earthquakes on the population and on the built environment depends on several factors that include the earthquake focal parameters (epicentral location, focal depth, magnitude), the population density as well as the type and quality of buildings and, therefore, on the macroseismic intensity. In addition, seasonal and diurnal patterns may drive the impact on the population.

In this Chapter we investigate variation patterns of the Earthquake Impact Metrics (EIMs) used for the casualties caused in Greece in the reference period (1800-2020). The examination focused on the EIMs dependence on seismicity parameters, i.e. on the earthquakes epicenter location, magnitude, and focal depth. Of interest is also the examination of possible seasonality and diurnal variation of the casualties EIMs. In addition, correlations between EIMs and metadata attributes, such as the macroseismic intensity, have been investigated. For the performance of such types of investigations quantitative impact data are needed. In the Greek Earthquake Impact Database (GEIDB) quantitative data are available for the casualties, i.e. fatalities and injuries, the repairable buildings and the unrepairable buildings. In addition, the number of tsunamigenic earthquakes is also known for the reference period.

7.2 Variation patterns of EIMs for casualties

From the 248 earthquakes listed in the GEIDB the number of those that caused casualties, i.e. fatalities and/or injuries, during the reference period of 1800-2020 is 105. For the casualties caused in Greece in the reference period 1800-2020, several EIMs have been used and include the number of fatalities per event, Fa, the number of injuries per event, In, the number of fatal earthquakes that caused at least one fatality, FaE, the number of earthquakes that caused at least one injury, InE, the average Fa (AFa), the average In (AIn), the survival Ratio, R=In/Fa, the integrated survival Ratio, Ri=100 x In/Fa, the maximum Fa caused by a single event, MFa, and the maximum In caused by a single event, MIn.

After some general considerations the EIMs Fa, In and R are examined in details as regards their variation in space and time and their possible dependence on seismicity parameters and on the macroseismic intensity. These examinations have been performed separately for shallow and intermediate-depth earthquakes.

7.2.1 A first statistics

A summary of the values found for Fa, In, R and Ri are shown in Table 7.1. From the data included in GEIDB it results that a total number of 8,796 fatalities and 19,164 injuries were caused from 86 and 81 earthquakes, respectively. The mean, μ, of the mortality and of the morbidity, i.e. the average numbers of fatalities and injuries, were calculated as equal to 102 Fa/yr (σ=400) and 237 In/yr (σ=831), respectively. The relatively high values of the coefficient of variation, i.e. $c_v=\sigma/\mu$, which is c_v=3.92 and c_v=3.51 for the mortality and the morbidity, respectively, implies that the mortality and

morbidity both vary greatly from one earthquake to the other. The Chios Island earthquake (M_w=6.47, SHEEC) of 3 April 1881 constitutes the most extreme case that caused anomalously high numbers of casualties in the Greek territory as compared to the numbers of casualties that other events caused in Greece: MFa=3550, MIn=7000. If we remove the mortality caused by the Chios 1881 earthquake the mean μ reduces by a factor of ~2 (μ=62±131) but the coefficient c_v still remains relatively high: c_v=2.11. A similar behavior was found with the morbidity statistics after the exclusion of the 1881 Chios event, μ=152±335, c_v=2.20.

Table 7.1. EIMs for casualties. Symbol key: Fa=number of fatalities per event, In=number of injuries per event, FaE=number of earthquakes that caused at least one fatality, InE=number of earthquakes that caused at least one injury, AFa=average Fa, AIn=average In, R=In/Fa, R_i= 100 x R, MFa=maximum Fa caused by a single event, MIn=maximum In caused by a single event.

Attribute	**Earthquake Impact Metrics**			
Mortality (Fatalities)	Fa=8,796	FaE=86	AFa=102±400 (62±131)	MFa=3,550
Morbidity (Injuries)	In=19,164	InE=81	AIn=237±831 (152±335)	MIn=7,000
Injuries/ Fatalities	R=2.18 (2.32)	R_i=218 (232)	_	_

The average survival Ratio (R=In/Fa) was found equal to 2.18. Then, the integrated R_i becomes 218, which is lower as compared to ~300 found by Alexander (1985) from various fatal earthquakes occurring around the globe in the 1969-1984 time interval. Removing the mortality and morbidity data corresponding to the Chios extreme event of 1881, which returns R=1.97 and Ri=197 for this event, we found average Ri=256. Alexander (1985) noted that when the 3:1 ratio occurs is most likely to coincide with an earthquake magnitude in the range 6.5-7.4, but many other ratios of death to injuries may instead be probable. From our data it comes out that this ratio coincides mainly with magnitude in the range 6.2-6.8.

The relatively lower value of R found here is attributable to that in the GEIDB we have inserted data from earthquakes occurring not only in the last decades but also in the historical period. One may expect that the more recent earthquakes would be characterized by higher R values with respect to older ones. This issue is examined in details later.

7.2.2 Casualties from shallow earthquakes

Correlation of casualties with the spatial distribution of shallow earthquakes

In Figure 7.1 the epicenters of the shallow, fatal earthquakes, regardless the number of injuries caused, if any, are plotted according to the fatality and magnitude classes. A feature of the geographical distribution of epicenters is that all fatal earthquakes had their epicenters on land, near the coast or at distance less than 30 km from the closest coast. The majority of the epicenters is concentrated in the central and southern Greek mainland as well as in the Ionian islands. Large geographical parts of the country do not host epicenters of fatal earthquakes, such as the northwestern and northeastern parts as well as large part of the Aegean sea area. Figure 7.1 shows also that low mortality (Fa number 1-10 per event) is associated with the entire magnitude spectrum. However, higher mortality of over 10 fatalities per event has been caused by only strong and large earthquakes with magnitudes ranging from 5.4 to 7.4.

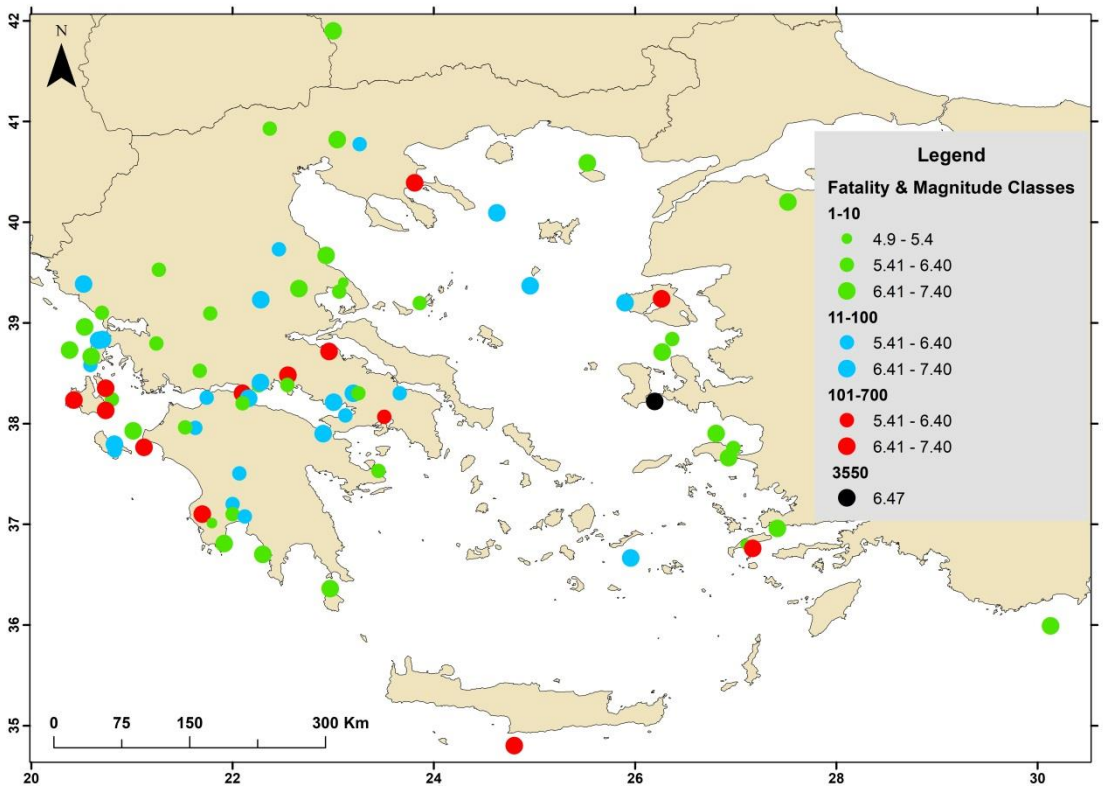

Figure 7.1. Spatial distribution of the epicenters of shallow, fatal earthquakes occurring in Greece from 1800 up to 2020.

The epicenters of shallow earthquakes that caused at least one injury in Greece from 1800 up to 2020 are plotted in Figure 7.2. The overall picture is in general similar to the one obtained for the shallow, fatal earthquakes (Fig. 7.1).

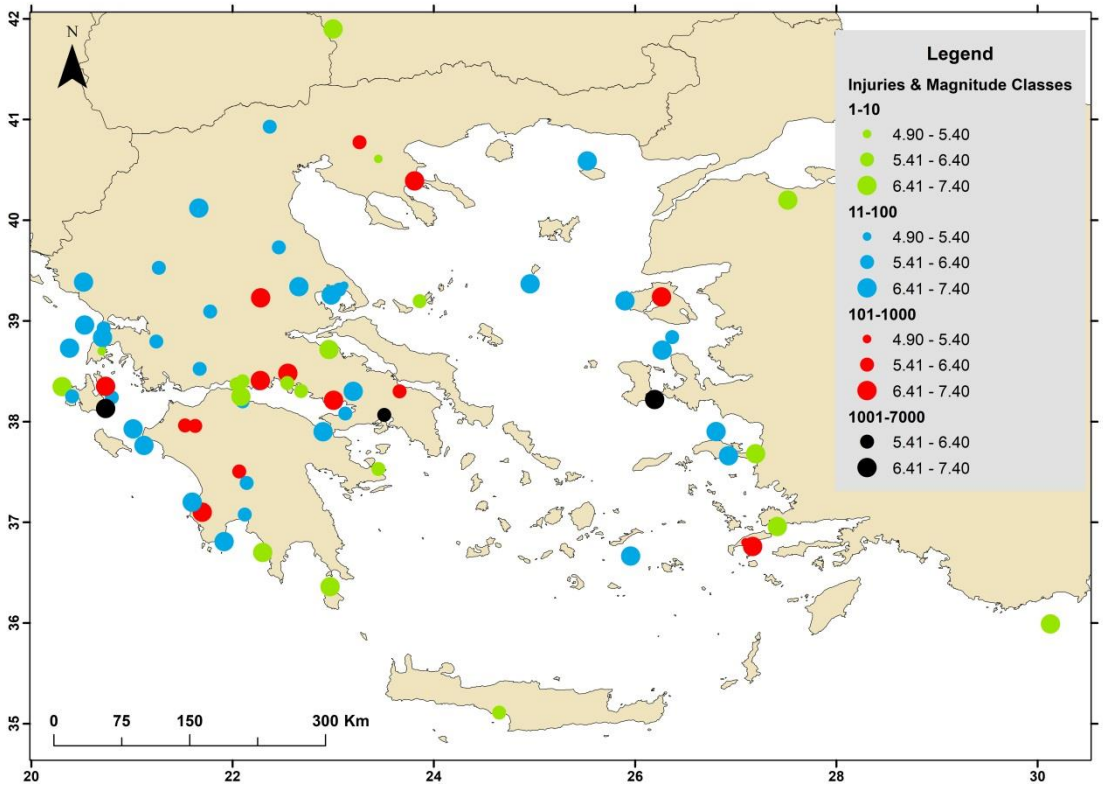

Figure 7.2. Epicenters of shallow earthquakes that caused injuries in Greece from 1800 up to 2020.

Two large earthquakes occurring outside the Greek territory caused a limited number of casualties in Greece. The first is the earthquake (M_w=7.34, UOA) of 4 April 1904 in SW Bulgaria that caused 3 fatalities and 5 injuries in the city of Thessaloniki. The second event has been the earthquake (M_w=7.20, ISC-GEM 2018) of 18 March 1953 in Yenise, NW Turkey, that caused 1 fatality and 7 injuries in the Greek island of Lesvos.

Correlation of casualties with the time distribution of shallow earthquakes

The time distribution of the casualties caused by shallow earthquakes in the period 1800-2020 is shown in Figure 7.3. The mortality distribution is dominated by the casualties reported in relation to five events. Two events happened during the 20th century. The first occurred in the Ionian Islands on 12 August 1953 (M_w=7.1, 361 fatalities, 2112 injuries), while the second hit the metropolitan area of the capital city of Athens, Central Greece, on 7 September 1999 (M_w=5.98, ISC-GEM 2018; 143 fatalities, 1600 injuries,). The other three events occurred during the 19th century in Lesvos Island on 7 March 1867 (M_w=6.85, ISC-GEM 2018; 700 fatalities, 816 injuries), in Chios Island on 3 April 1881 (M_w=6.47, SHEEC; 3550 fatalities, 7000 injuries) and in SW Peloponnese on 27 August 1886 (M_w=6.80, SHEEC; 326 fatalities, 796 injuries).

The mortality in general decreases with time, particularly after the 1950's. A relative decrease of the morbidity is also observed after the 1950's, although the high number of injuries due to the 7 September 1999 earthquake makes an exception in the general trend.

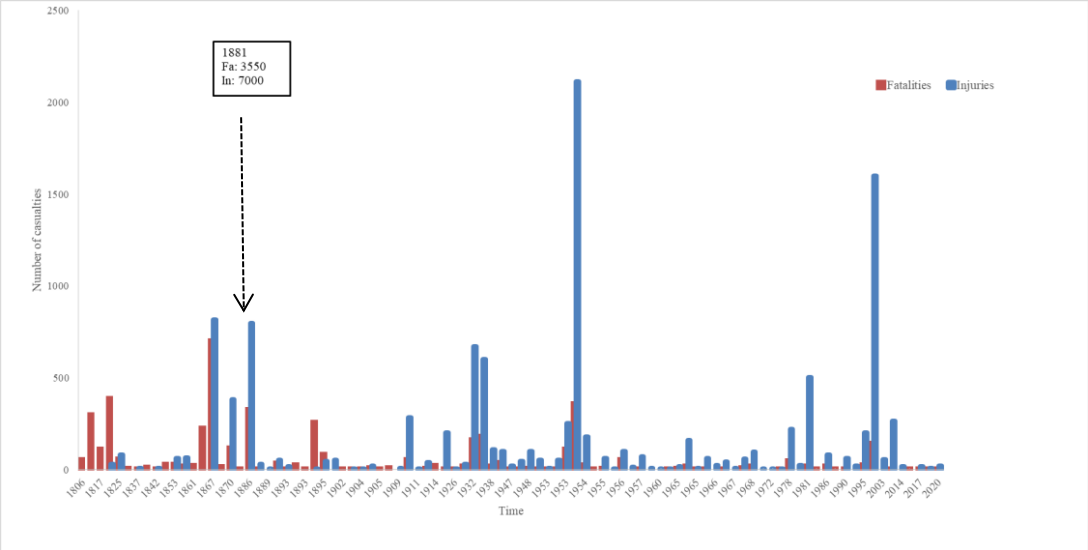

Figure 7.3. Casualties caused in Greece by single, shallow earthquakes occurring from 1800 up to 2020. The extremely high numbers corresponding to the Chios island earthquake of 3 April 1881 are out of scale.

In the examination of the time variation of the survival ratio, R, we faced several difficulties that have arisen due to the data incompleteness particularly in the 19th century. In that period 29 earthquakes caused either fatalities, Fa, or injuries, In or both. The fatal earthquakes are 28, with 8 out of 28 having caused more than 100 fatalities. However, the events that caused injuries are only 16 out of 29, the rest 13 events remaining without reporting injuries (In=0). Therefore, it is reasonable to suggest that counting the numbers of injuries very likely escaped historical record for several events occurring in that period.

The log R is plotted against time in Figure 7.4. The 13 events, as well as a few others without injuries in the post-1899 time period, have been excluded since log (0/Fa) is not identified. A gradual but slight increase of log R with time is evident. However, this result suffers important uncertainty due to the lack of injuries data in several events. To check further the time variation of the mortality, of the morbidity and of the survival ratio, we recalculated the mean value, m, and the respective standard deviation, σ, of each one of these attributes in four separate time segments: 1800-1899, 1900-1959, 1960-1979, 1980-2020. The selection of these time segments is based on the impact data completeness (Chapter 1) as well as on the gradual progress noted in the construction of earthquake-resistant buildings and in the organization of rescue corps in the country. A short overview of these developments was introduced earlier in subsection (6.2).

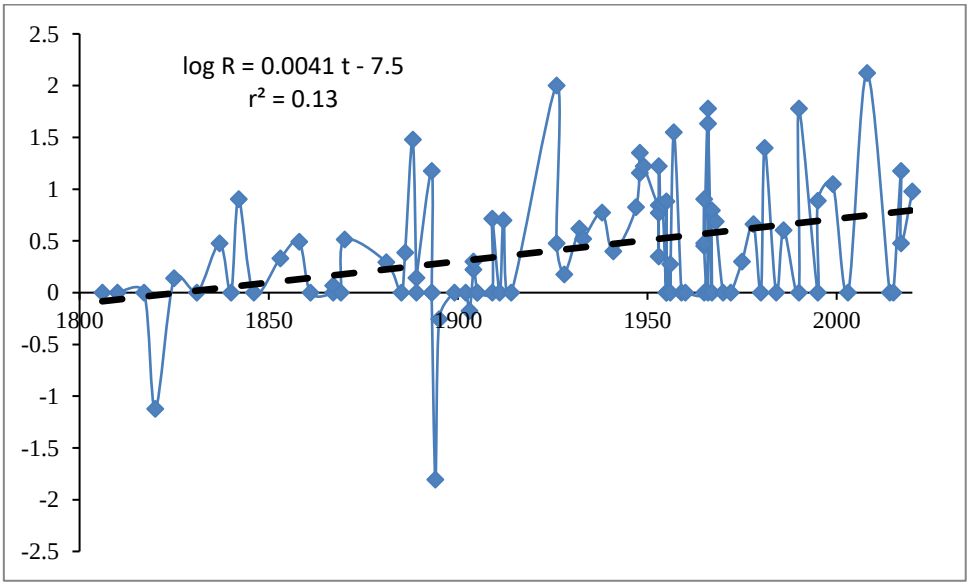

Figure 7.4. Time variation of the survival ratio, R, in the time period 1800-2020; r=correlation coefficient.

Our recalculation showed a gradual decrease of m during the first three time segments for both the mortality and the morbidity (Table 7.2). However, in the time segment 1980-2020 the value of m is slightly increased for the mortality but significantly increased for the morbidity. This is due mainly to a single earthquake event, that of 7 September 1999 (M_w=5.98). This earthquake caused 143 fatalities and 1600 injuries, with these figures being exceptionally high as compared to the impact of larger earthquakes occurring in that time segment. Removing this extreme event the mortality drops further but the morbidity remains relatively high.

Table 7.2. Time variation of the numbers of fatalities (mortality) and injuries (morbidity) and of the survival Ratio as well as of their coefficient of variation. In the time segment marked with * the 7 September 1999 extreme event is not included.

Time segment	Mortality m±σ; c_v	Morbidity m±σ; c_v	Mean survival Ratio m±σ; c_v
1800-1899	104±164; 1.58	537±1588; 2.96	2.7±6.3; 2.33
1900-1959	34±73; 2.15	172±394; 2.29	9.6±19.1; 1.99
1960-1979	7.3±13.2; 1.81	40±62; 1.55	9.6±20.5; 2.14
1980-2020	13.8±4.1; 0.30	220±438; 1.99	22±39; 1.77
1980-2020*	5.2±8.8; 1.69	189±413; 2.19	23±40; 1.74

Calculation of R for each one of the four time segments showed a gradual increase with time (Table 7.2). During the 19th century the morbidity over mortality was about 3, while it increased to about 10 in the time segments 1900-1959 and 1960-1979. The ratio increased further to 22 in the most recent time segment of 1980-2020. These results leave no doubt that the relative number of fatalities, as compared to the number of injuries, decreased drastically with time.

7.2.3 Casualties from intermediate-depth earthquakes

Correlation of casualties with the space-time distribution of intermediate-depth earthquakes

The number of intermediate-depth earthquakes that caused at least one fatality and/or at least one injury from 1800 up to 2020 has been only 10. As expected the epicenters of these earthquakes are concentrated only in the South Aegean Sea area (Fig. 7.5). The small number of intermediate-depth earthquakes that caused casualties makes the statistics of time distribution unstable. However, there is a general trend for the number of casualties, particularly of the fatalities, to decrease with time (Fig. 7.6).

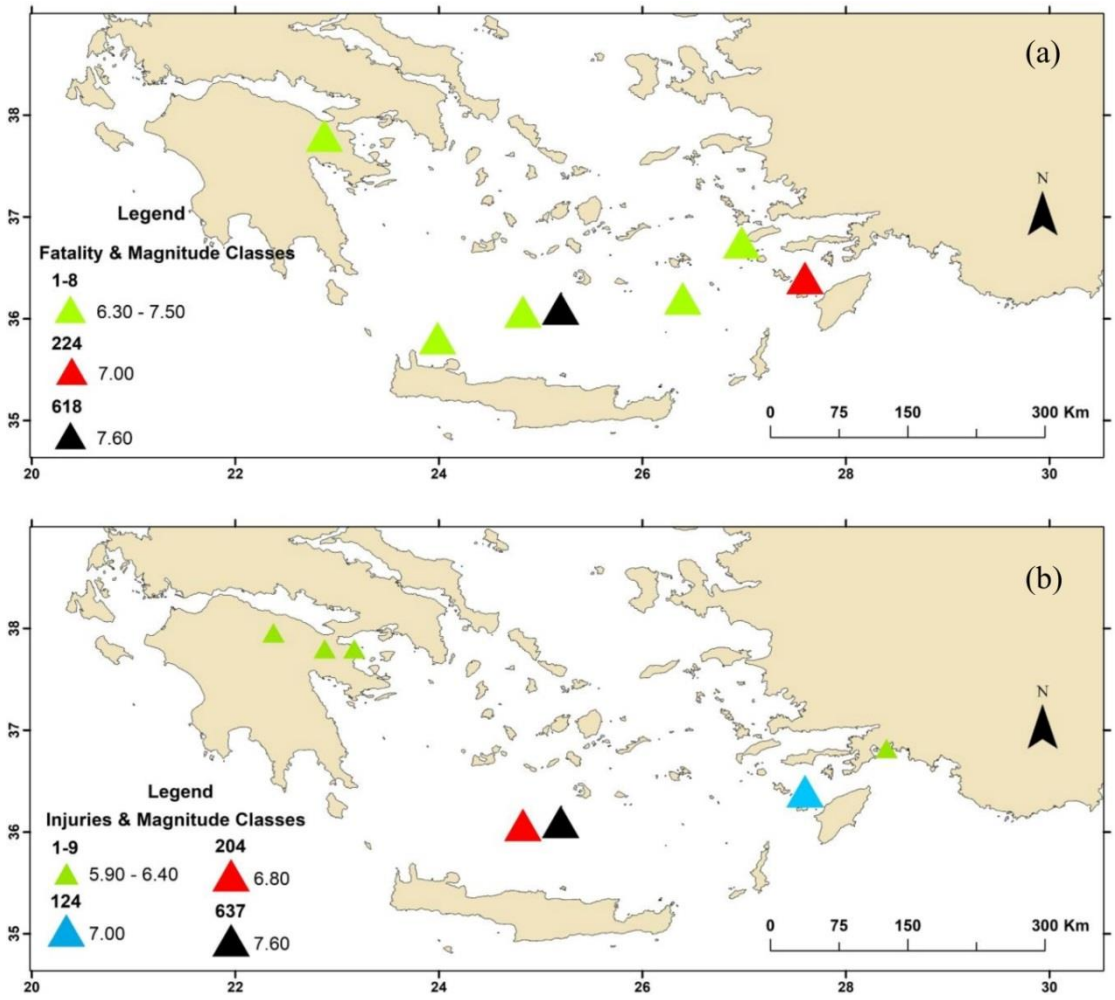

Figure 7.5. Epicenters of intermediate-depth earthquakes that caused at least one fatality (a) and at least one injury (b) from 1800 up to 2020.

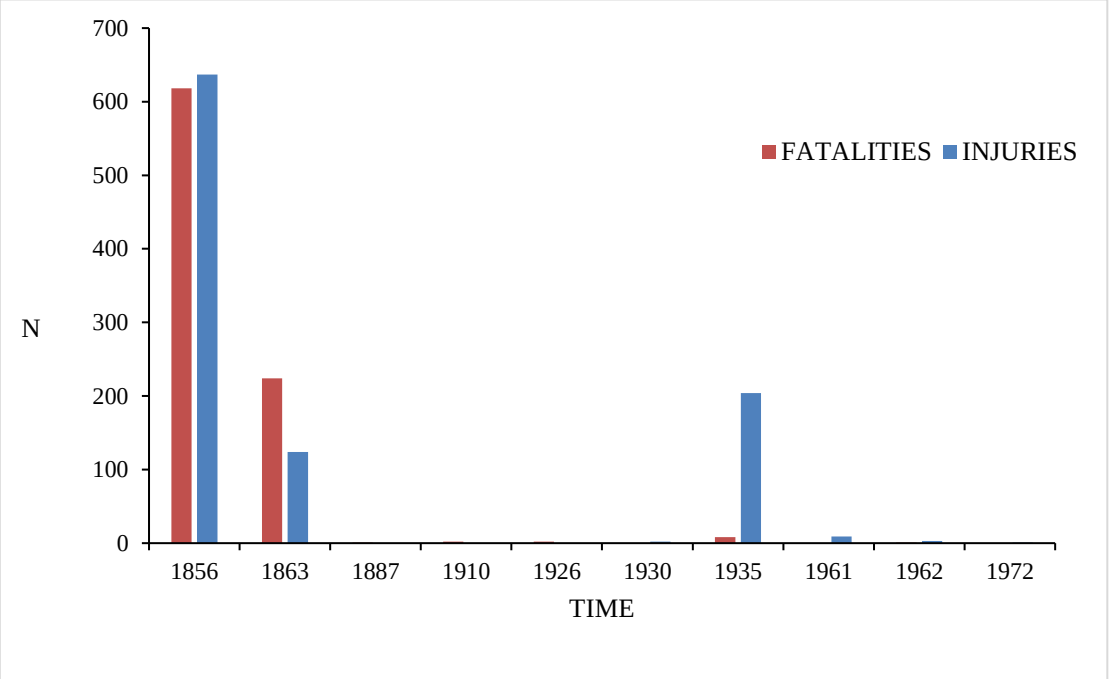

Figure 7.6. Number of casualties, N, caused in Greece by single, intermediate-depth earthquakes from 1800 up to 2020.

7.2.4 Dependence of casualties on earthquake magnitude

Although the fatalities number, Fa, in general increases with the earthquake magnitude, M, it is varying greatly in each magnitude bin (Fig. 7.7). For shallow earthquakes the correlation Fa/M is very weak. However, for intermediate-depth earthquakes the correlation appears better and is expressed by the relation

$$\log Fa = 1.26\ M - 7.79, \qquad r^2=0.43 \quad (7.1)$$

A similar pattern is valid for the variation of the injuries number, In, but the correlation In/M is poor for intermediate-depth earthquakes too (Fig. 7.8):

$$\log In = 0.95\ M - 5.46, \qquad r^2=0.22 \quad (7.2)$$

The minimum and maximum magnitudes, M_{min} and M_{max}, of fatal earthquakes and the ones that caused injuries are summarized in Table 7.3. M_{min} for shallow earthquakes is 4.9, which is one order of magnitude lower than the respective M_{min}=5.95 for intermediate-depth earthquakes. However, the M_{max} for the two classes of earthquakes are close each other, 7.37 and 7.60 for shallow and intermediate-depth earthquakes, respectively. Noticeable mortality and morbidity, with numbers of fatalities and injuries over 10, are caused from shallow earthquakes of M_{min}~5.9 and M_{min}~5.5, respectively. For intermediate-depth earthquakes the respective magnitudes are M_{min} ~6.9 and M_{min} ~6.3. The difference is again equal to about one order of magnitude.

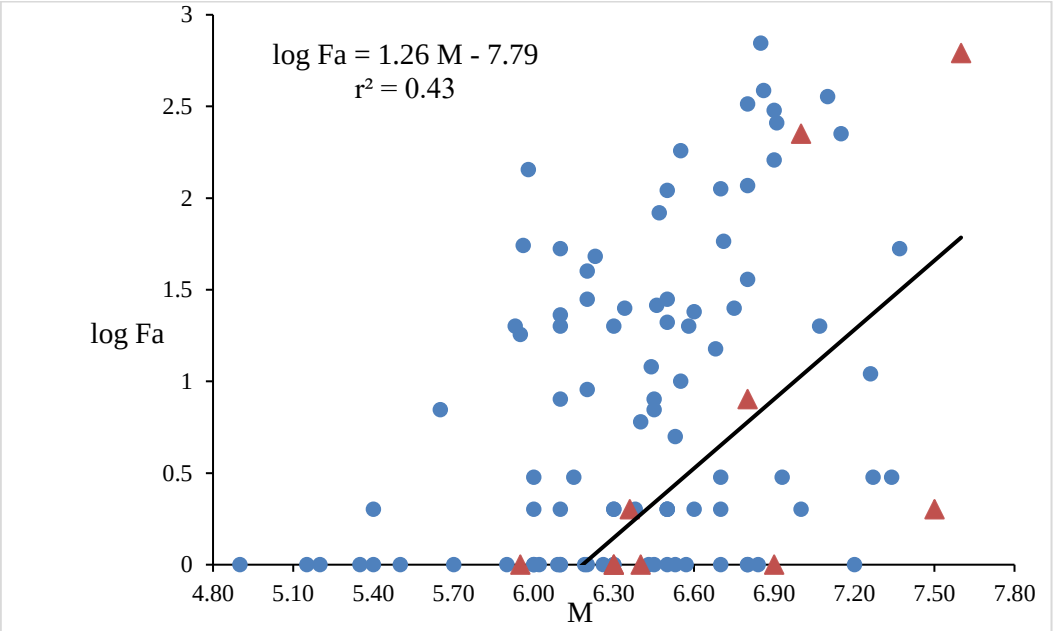

Figure 7.7. Variation of the fatalities number, Fa, with the earthquake magnitude, M, for the time period 1800-2020. Key: circle=shallow earthquake, triangle=intermediate-depth earthquake. Best-fit regression line is for intermediate-depth earthquakes; r=correlation coefficient. M/Fa correlation for shallow earthquakes is very weak.

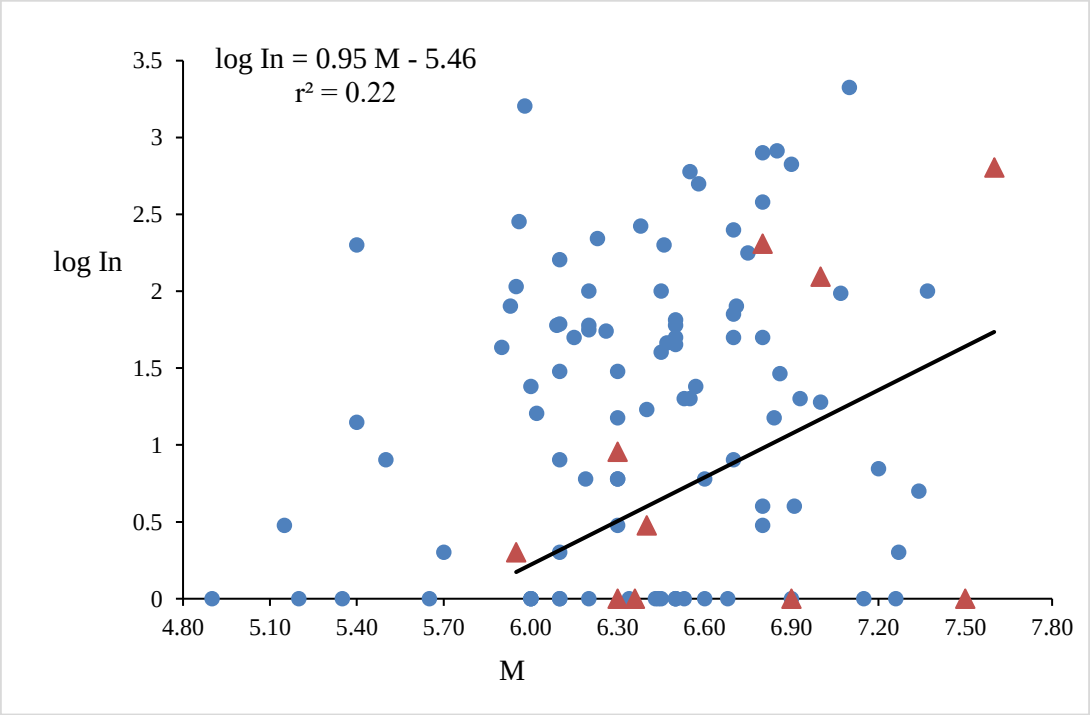

Figure 7.8. Variation of the injuries number, In, with the earthquake magnitude, M, for the time period 1800-2020. Key: circle=shallow earthquake, triangle=intermediate-depth earthquake. Best-fit regression line is for intermediate-depth earthquakes; r=correlation coefficient. M/In correlation for shallow earthquakes is very weak.

Table 7.3. Minimum (M_{min}) and maximum (M_{max}) magnitudes of earthquakes that caused casualties in the time period 1800-2020. Key: Fa=number of fatalities, In=number of injuries.

	Casualties					
	Fa	In	Fa>10	In>10	Fa	In
	Magnitude					
Focal depth class	M_{min}				M_{max}	
Shallow (h<60 km)	4.90	4.90	5.9	5.5	7.37	7.37
Intermediate-depth (h≥60 km)	5.95	5.95	6.9	6.3	7.60	7.60

7.2.5 Dependence of casualties on macroseismic intensity

The correlation of both the mortality and morbidity with the maximum macroseismic intensity, I_o, in MM scale has been examined for the shallow and intermediate-depth earthquakes.

Mortality dependence on macroseismic intensity

The fatalities number, Fa, caused by both the shallow and intermediate-depth earthquakes in the time interval 1800-2020 in general increases with the increase of the maximum intensity MMI_o (Fig. 7.9). The minimum value of I_o, associated with at least one fatality, is 5 and 7 for the shallow and intermediate-depth earthquakes, respectively (Fig. 7.9). However, I_o of 8 and 9 degree is required for Fa>10 to be caused by the shallow and intermediate-depth earthquakes, respectively. The results found indicate that the seismic intensity controls the lower limits of mortality.

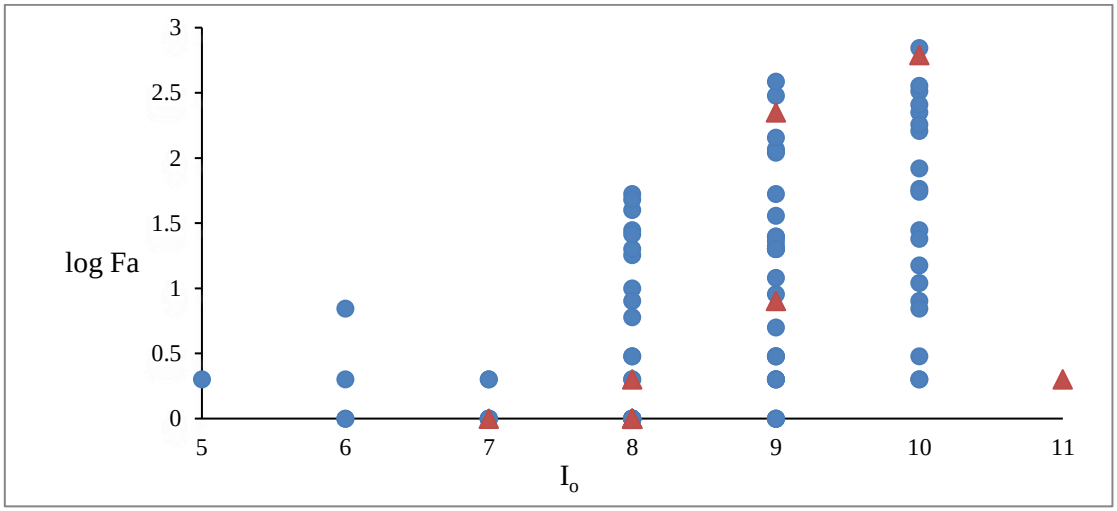

Figure 7.9. Variation of the fatalities number, Fa, with the maximum intensity, I_o, in the time period 1800-2020. Key: solid circle=shallow earthquake, red triangle=intermediate-depth earthquake.

A characteristic feature of the Fa distribution is that it varies greatly in each intensity degree in the higher-degree classes, i.e. from 8 to 10 (Fig. 7.9). Therefore, a weak dependence of the average Fa on I_o is expected. On the other hand, the upper bound of Fa is clearly controlled by I_o. The Fa upper bound, however, is lower for intermediate-depth events as compared to that for shallow events. These issues are examined further in the next lines.

Empirical relations between the number of casualties and I_o for Greek earthquakes are the (6.4) and (6.5) ones developed by Papazachos and Papazachou (2003). However, these relations are based on casualty data of the time period 1950-1985, which is relatively short as compared to the period 1800-

2020 covered by our data set. Our examination has been performed separately for shallow and intermediate-depth earthquakes.

The correlation between Fa and I_o for shallow earthquakes occurring in the period 1800-2020 is illustrated in Figure 7.10. The best-fit regression line is expressed by the formula

$$\log Fa = - 2.75 + 0.42\ I_o, \quad r^2 = 0.31 \qquad (7.3)$$

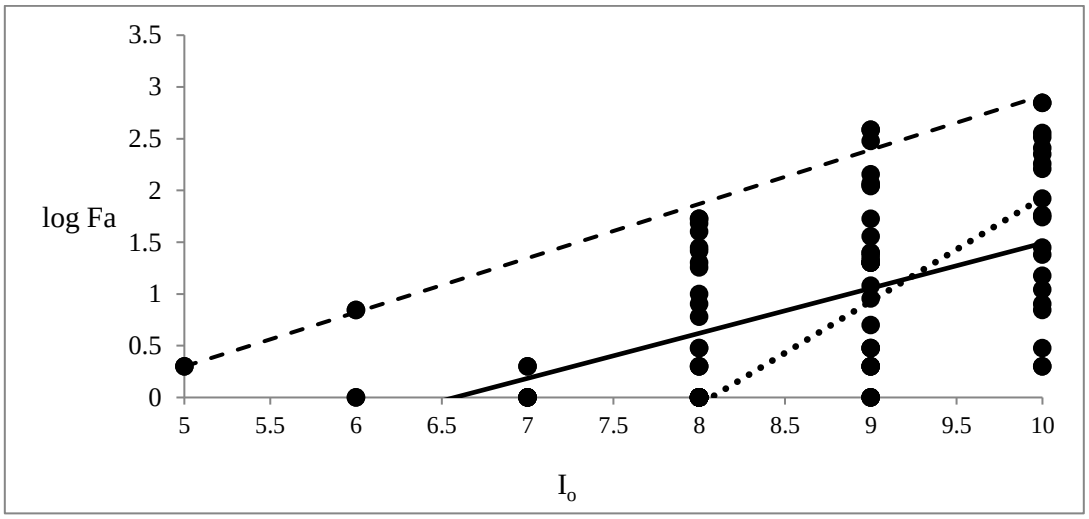

Figure 7.10. Correlation between the number of fatalities, Fa, and the intensity, I_o, for shallow earthquakes that occurred in the time interval 1800-2020. Key: solid and dashed lines represent the best-fits to all data (relation 7.3) and to the upper bound Fa values (relation 7.6), respectively; round dot line is the relation (6.4) found by Papazachos and Papazachou (2003).

Comparing (7.3) with (6.4) we see that the last overestimates Fa for $I_o>9$ but underestimates it for $I_o\leq 9$. We repeated the calculations for the time periods 1900-2020 (Fig. 7.11) and 1960-2020 (Fig. 7.12) and found

$$\log Fa = - 2.46 + 0.38\ I_o, \quad r^2 = 0.30 \qquad (7.4)$$

and

$$\log Fa = - 1.56 + 0.26\ I_o, \quad r^2 = 0.17 \qquad (7.5)$$

respectively. Contrary to the weak I_o/Fa correlation found for all data (relations 7.3-7.5), which is due to the great variability of the Fa values corresponding to each intensity degree, excellent correlation has been found between the upper bound of Fa in each intensity degree, Fa(max), and the I_o value. The respective upper bound best-fit regression lines found for the time periods 1800-2020 (Fig. 7.10), 1900-2020 (Fig. 7.11) and 1960-2020 (Fig. 7.12) are:

$$\log Fa(max) = - 2.32 + 0.52\ I_o, \ r^2 = 0.99 \qquad (7.6)$$

$$\log Fa(max) = - 2.09 + 0.47\ I_o, \quad r^2 = 0.99 \qquad (7.7)$$

$$\log Fa(max) = - 2.01 + 0.46\ I_o, \quad r^2 = 1.0 \qquad (7.8)$$

These relations predict the upper limit of the fatalities number expected for a given maximum intensity value.

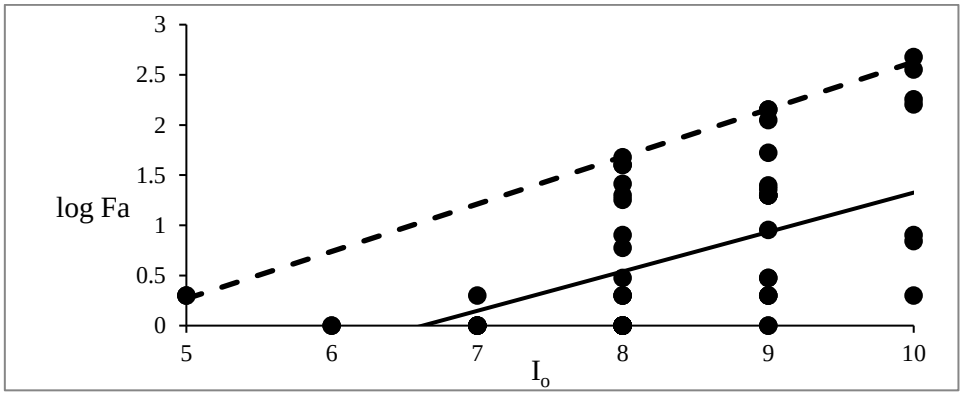

Figure 7.11. Correlation between the number of fatalities, Fa, and the maximum intensity, I_o, for shallow earthquakes that occurred in the time interval 1900-2020. Key: solid and dashed lines represent the best-fits to all data (relation 7.4) and to the upper bound Fa values (relation 7.7), respectively.

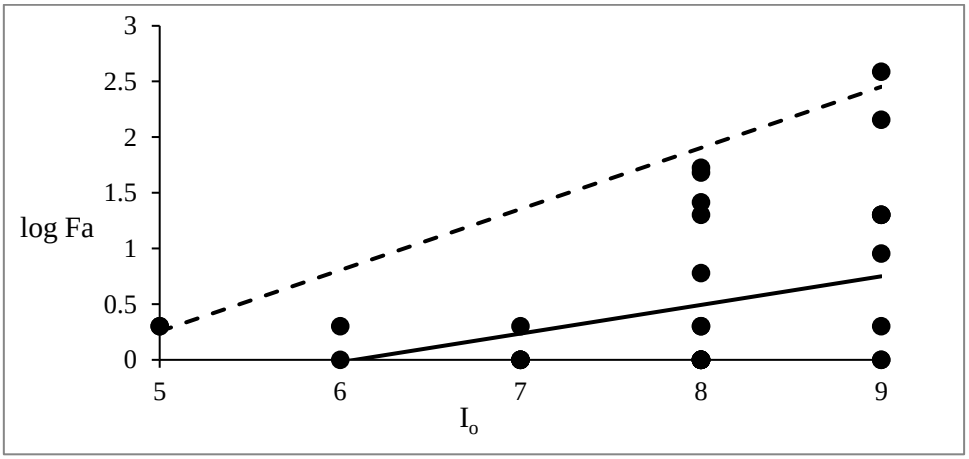

Figure 7.12. Correlation between the number of fatalities, Fa, and the maximum intensity, I_o, for shallow earthquakes that occurred in the time interval 1960-2020. Key: solid and dashed lines represent the best-fits to all data (relation 7.5) and the upper bound best fit to I_o values of 5, 8, and 9 (relation 7.8), respectively.

Morbidity dependence on macroseismic intensity

The results obtained for the dependence of the morbidity on the intensity, I_o (Fig. 7.13), are similar to those reached for the dependence of the mortality on I_o. The number of injuries, In, in general increases with the intensity, I_o. However, the parameter In is varying greatly in each intensity degree for $I_o \geq 7$ (Fig. 7.13). The minimum value of I_o, associated with at least one fatality, is 5 and 7 for the shallow and intermediate-depth earthquakes, respectively (Table 7.4). However, I_o of 8 and 9 degree is required for In>10 to be caused by shallow and intermediate-depth earthquakes, respectively. The correlation between In and I_o is further examined for shallow earthquakes in the next lines. However, the examination of the intermediate-depth events is meaningless due to the very low number of events.

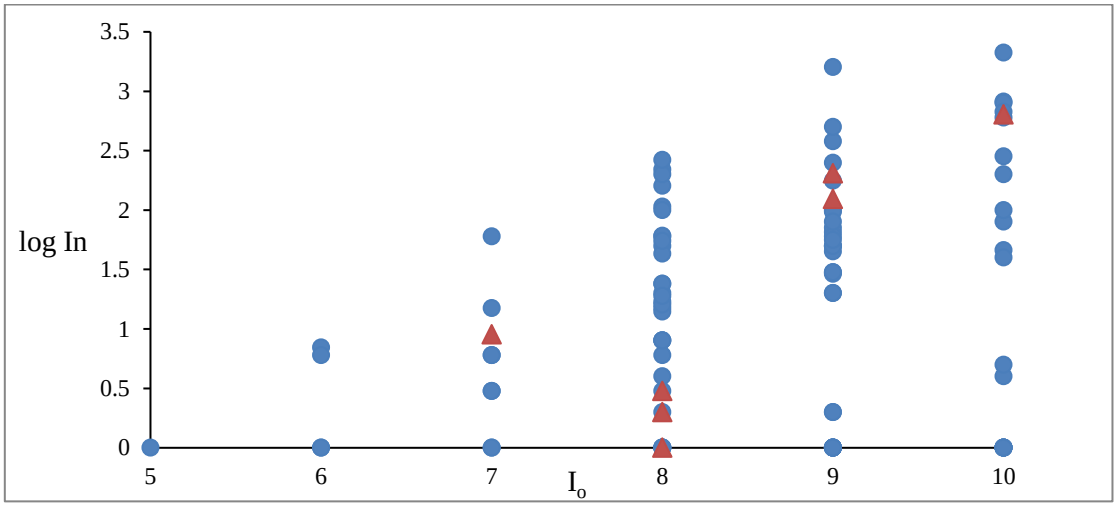

Figure 7.13. Correlation of the injuries number, In, with the intensity, I_o, in the time period 1800-2020. Key: solid circle=shallow earthquake, red triangle=intermediate-depth earthquake.

Table 7.4. Minimum (I_{omin}) and maximum (I_{omax}) intensities of earthquakes that caused casualties in the time period from 1800 to 2020. Key: Fa=number of fatalities, In=number of injuries.

	Casualties			
	Fa	In	Fa>10	In>10
Focal depth class	**Intensity, I_{omin}**			
Shallow (h<60 km)	5	5	8	8
Intermediate-depth (h≥60 km)	7	7	9	9

For shallow earthquakes and for the reference period 1800-2020 the correlation I_o/In is very weak for the entire data set (formula 7.9, Fig. 7.14):

$$\log In = - 0.88 + 0.24\ I_o, \quad r^2 = 0.08 \qquad (7.9)$$

The empirical I_o/In formula (6.5) suggested by Papazachos and Papazachou (2003) (Fig. 7.14) overestimates the In for I_o>8 as compared to (7.9) However, better correlation was found for data of the time periods 1900-2020 (formula 7.10, Fig. 7.15) and 1960-2020 (formula 7.11, Fig. 7.16):

$$\log In = - 2.46 + 0.47\ I_o, \quad r^2 = 0.33 \qquad (7.10)$$

$$\log In = - 2.76 + 0.52\ I_o, \quad r^2 = 0.35 \qquad (7.11)$$

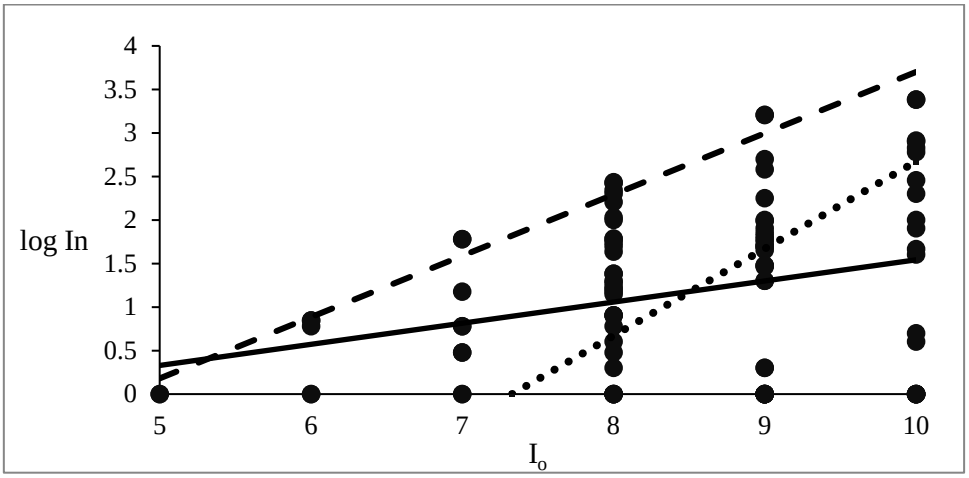

Figure 7.14. Correlation of the injuries number, In, with the intensity, I_o, for shallow earthquakes in the time interval 1800-2020. Key: solid and dashed lines represent the best-fits to all data (relation 7.9) and to upper bound In values (relation 7.12), respectively; rounded dot line is the relation (6.5) found by Papazachos and Papazachou (2003).

The correlation between the upper bound of In in each intensity degree, denoted as In(max), and the I_o value is excellent for all the data sets, i.e. for 1800-2020 (formula 7.12, Fig. 7.14), 1900-2020 (formula 7.13, Fig. 7.15) and 1960-2020 (formula 7.14, Fig. 7.16) and for the entire intensity spectrum from 5 to 10:

$$\log In(max) = - 3.34 + 0.70\ I_o, \quad r^2 = 0.99 \qquad (7.12)$$

$$\log In(max) = - 3.34 + 0.70\ I_o, \quad r^2 = 0.97 \qquad (7.13)$$

$$\log In(max) = - 4.00 + 0.81\ I_o, \quad r^2 = 0.99 \qquad (7.14)$$

These relations predict the upper limit of the injuries number expected for a given maximum intensity value.

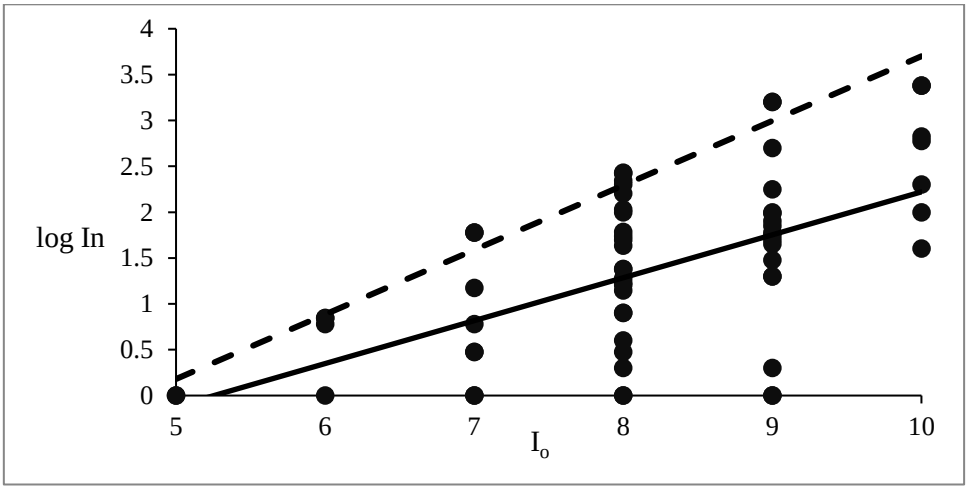

Figure 7.15. Correlation of the injuries number, In, with the intensity, I_o, for shallow earthquakes in the time interval 1900-2020. Key: solid and dashed lines represent the best-fits to all data (relation 7.10) and to upper bound In values (relation 7.13), respectively.

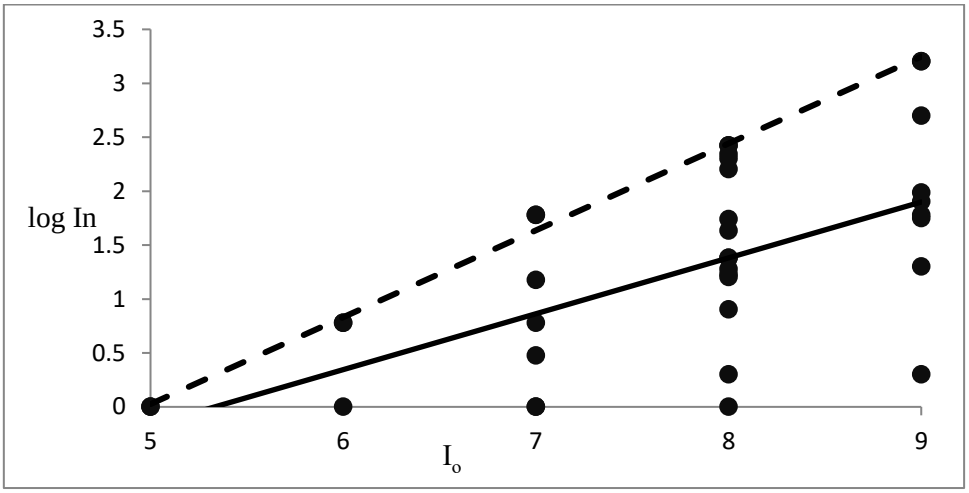

Figure 7.16. Correlation of the injuries number, In, with the intensity, I_o, for shallow earthquakes in the time interval 1960-2020. Key: solid and dashed lines represent the best-fits to all data (relation 7.11) and to upper bound In values (relation 7.14), respectively.

7.2.6 Seasonal and diurnal variation of the mortality and morbidity

A possible seasonal variation of the seismicity has been described in several seismogenic areas of the world (e.g. Matsumura, 1986). In Greece, Galanopoulos (1985) found that the monthly number of earthquakes tends to be relatively higher in the spring season, while the amount of the seismic energy release per month seems to be relatively higher in the summer months. However, a statistically significant seasonal trend was found for intermediate-depth earthquakes (M≥6.0) occurring in the Hellenic Arc but not for shallow earthquakes (M≥5.2) (Polymenakos, 1993). On the other hand social conditions may control the diurnal variation of mortality and morbidity (e.g. Lomnitz, 1970). Such results motivated the investigation of possible seasonal and diurnal variations of the earthquake mortality and morbidity in Greece.

Seasonal variation of the mortality and morbidity

The seasonal distribution of the fatalities and injuries caused by the earthquakes in Greece in the time interval 1800-2020 is illustrated in Figure 7.16. This distribution clearly reflects a significant excess of both the mortality and morbidity in the 6-month spring-summer season as compared to those in the 6-month autumn-winder season. However, this non-uniform distribution might be driven by the extreme mortality and morbidity caused by two distinct earthquakes that occurred in spring-summer season. The first is the Chios Island 3 April 1881 earthquake (M_w=6.47, SHEEC) that caused 3,550 fatalities and 7,000 injuries. The second event is the sequence of very strong earthquakes that isolated the Ionian islands from 9 to 12 August 1953 (maximum M_w=7.10) causing in total 476 fatalities and 2412 injuries. Removing these two events we observe that the excess in the number of injuries remains but for the number of fatalities does not (Fig. 6.21).

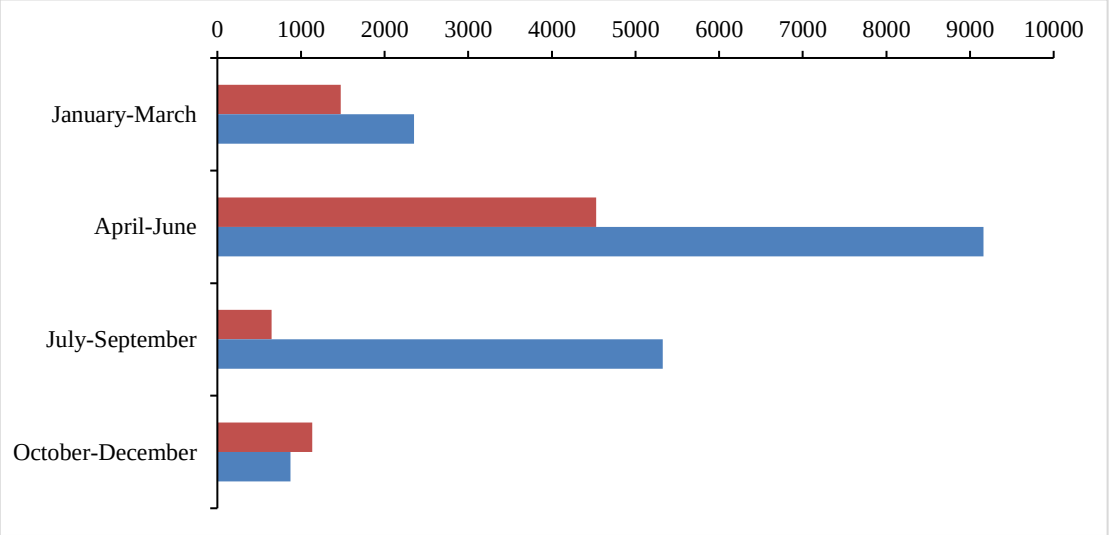

Figure 7.17. Seasonal distribution of the numbers of fatalities (red) and injuries (blue) in the time period 1800-2020.

To check further the seasonal distribution of both the mortality and morbidity we repeated the calculations only for the time period from 1900 to 2020 for the reason that the 19th century data are less complete and accurate. The data sets including the 1953 extreme event (Fig. 7.19) and excluding this event (Fig. 7.20) both show the clear excess of the numbers of fatalities and injuries in the spring-summer season as compared to the numbers in the autumn-winder season.

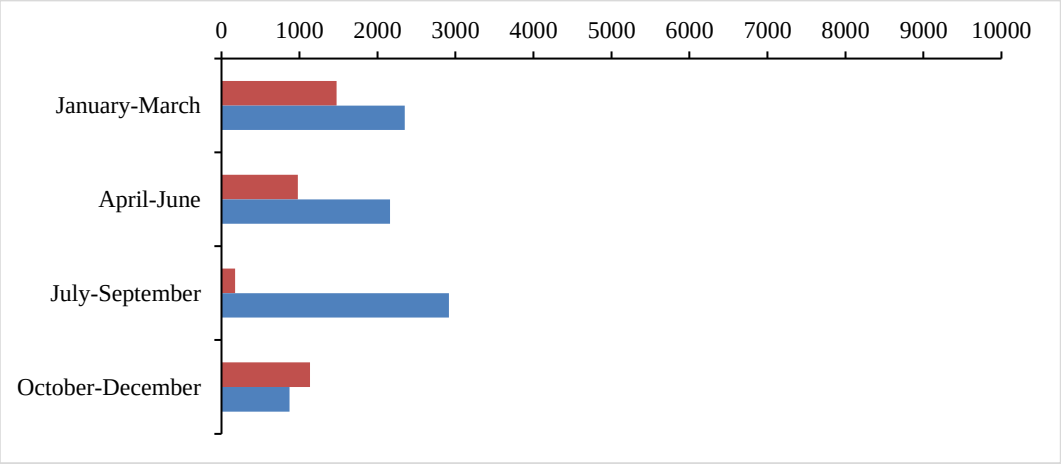

Figure 7.18. Seasonal distribution of the numbers of fatalities (red) and injuries (blue) in the time period 1800-2020 excluding data from the 1881 and 1953 extreme events.

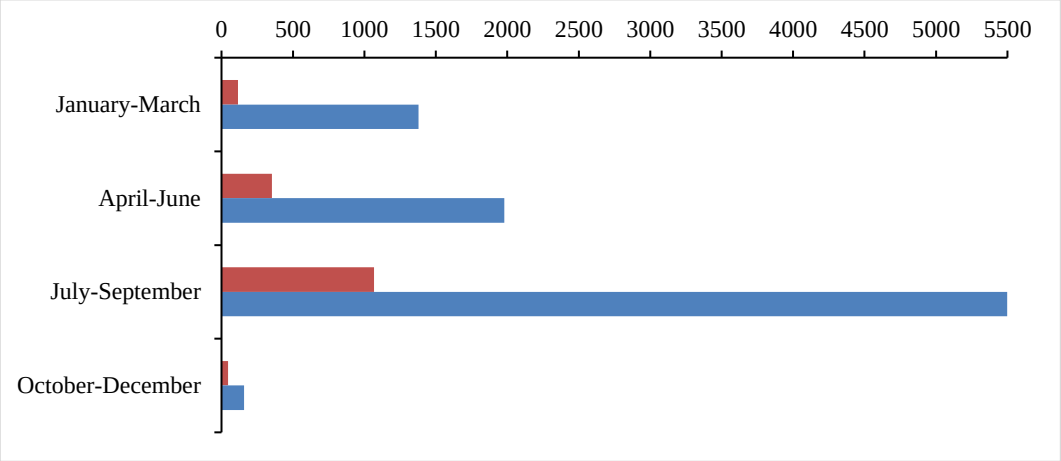

Figure 7.19. Seasonal distribution of the numbers of fatalities (red) and injuries (blue) in the time period 1900-2020.

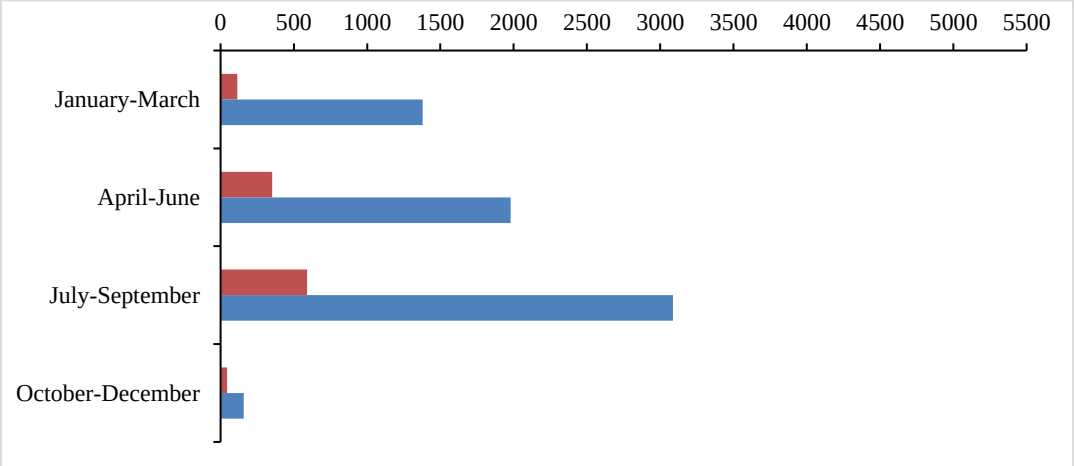

Figure 7.20. Seasonal distribution of the numbers of fatalities (red) and injuries (blue) in the time period 1900-2020 excluding the 1953 extreme event.

Diurnal variation of the mortality and morbidity

In this examination it has been found that it is slippery to include data from the 19th century since there are several reasons for not trusting most of the earthquake origin times. In several cases different information sources reported different origin times for the same event. On the other hand, the reported times are not precise anyway. In addition, origin times are lacking for a few seismic events.

To secure the results reliability we have considered data for the time period 1900-2020. We divided the seismic events in two groups based on their origin time and by taking into account that Greece is characterized by typical Mediterranean climate (CSa type). This climate type favors staying outdoors for several hours of the 24-hour cycle and for about 7 months of the year, i.e. from April to October. Based on these criteria the two groups include “day earthquakes” and “night earthquakes”, i.e. events occurring from 09:00 to 20:59 and from 21:00 to 08:59, respectively. In this classification Greek local time (+2 hours GMT) has been considered without taking into account the Daylight Saving Time (DST), which has been applied in Greece since 1975.

In the time period under examination (1900-2020) the total number of fatalities caused by 26 “evening earthquakes” has been as high as n=816, which provides an average of μ=31.4 fatalities per event (Fig. 7.21). On the other hand, 25 “day earthquakes” occurring in the same time period caused n=763 fatalities with μ=30.5 fatalities per event. These last figures, however, are dominated by the single seismic event of 12 August 1953 in the Ionian Islands, which caused 361 fatalities. Removing the 1953 event we get only μ=15 fatalities per event. These results indicate an excess in the fatalities number caused in night hours as compared to that in day hours.

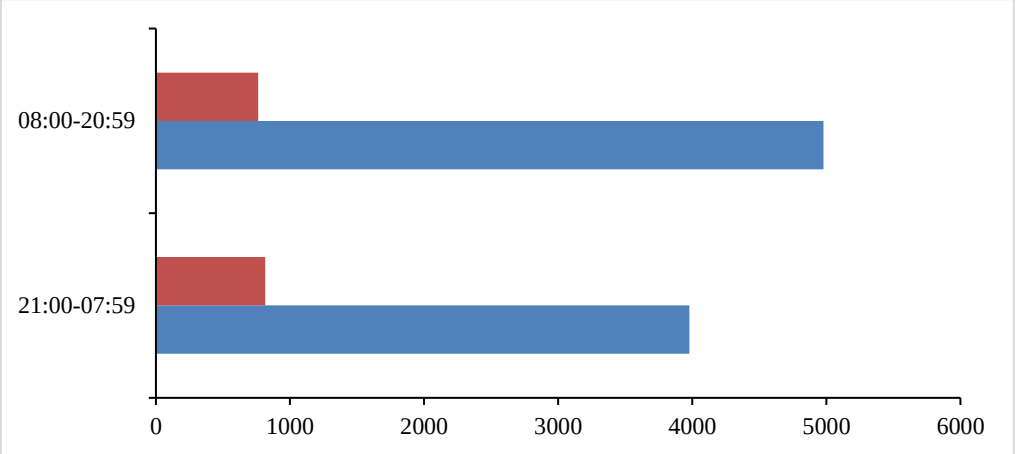

Figure 7.21. 24-hr distribution of the numbers of fatalities (red) and injuries (blue) in the time period 1900-2020. Local Greek time has been considered.

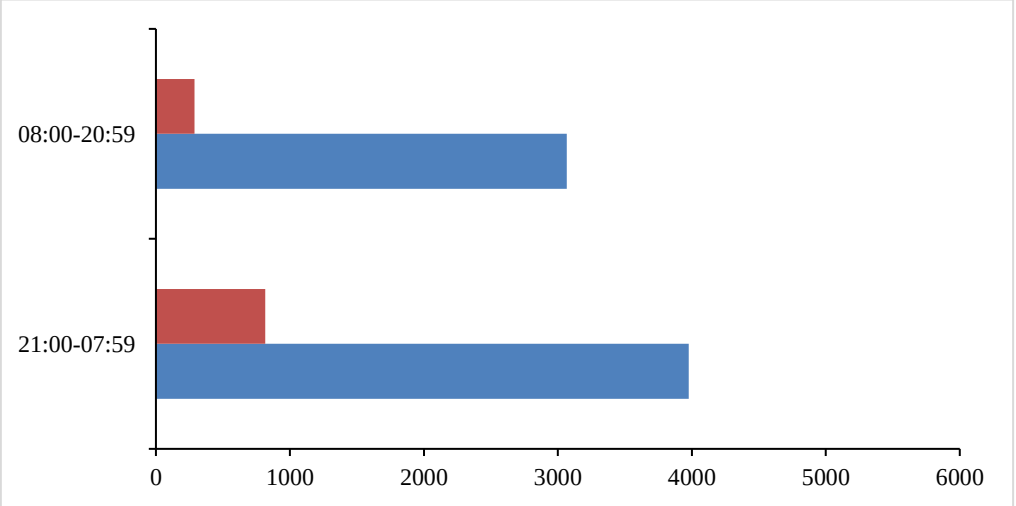

Figure 7.22. 24-h distribution of the numbers of fatalities (red) and injuries (blue) in the time period 1900-2020 after removing the earthquake event of 12 August 1953. Local Greek time has been considered.

As regards the number of injuries, in the time period 1900-2020 the number of injured people from 28 earthquakes is 3726 (average μ=133 injuries/event) during night hours. A number of 5229 injured people have been caused by 31 earthquakes (μ=169 injuries/event) during day hours. Removing the event of 12 August 1953 that caused 2112 injuries, then the number reduces to μ=104 injuries/event in day hours. This is an evidence for increased number of injuries in night hours.

7.3 Variation patterns of EIMs for buildings damage

7.3.1 A first statistics

Out of 248 earthquakes listed in the GEIDB the total number of those that caused damage to buildings during the reference period of 1800-2020 is 232. However, for several earthquakes only descriptive information of the building damage is given. Numerical data on the building damage has been found for 194 out of 232 events. Table 7.4 shows a summary statistic on the building damage caused in Greece in the period 1800-2020. The numbers of damaging earthquakes, that caused repairable buildings (RB), and of destructive earthquakes, that caused unrepairable buildings (UB), have been found equal to 80 and 114, respectively. This difference may indicate that the reporting of RB is very likely incomplete particularly in the 19th century data set. However, the total number of RB reported exceeds that of UB so that the average RB is larger than the average UB by a factor of ~2.3, while the average damage ratio, DR=RB/UB, is 1.6.

The maximum RB due to a single earthquake event is the one caused by the strong (M_w=6.23, ISC-GEM 2018) earthquake of 20 June 1978 with epicenter at a distance of ~20 km to the east Thessaloniki, the second largest city in Greece. The maximum UB due to a single earthquake event is the one caused by the large (M_w=7.1) earthquake of 12 August 1953 that hit the Central Ionian Sea islands. It is noteworthy that this event was the largest of a series of strong shocks that occurred a few days ago, the strongest being those of 9 and 11 August 1953 with M_w=6.4 and M_w=6.8, respectively. The damage caused by the first earthquakes very likely contributed to the extensive destruction that followed with the largest event.

Table 7.5. EIMs for buildings damaged or destroyed. Symbol key: RB=total number of repairable buildings, UB=total number of unrepairable buildings, RBE=number of earthquakes that caused repairable buildings, UBE=number of earthquakes that caused unrepairable buildings, ARB=average number of repairable buildings per earthquake event, AUB=average number of unrepairable buildings per earthquake event, MRB=maximum RB caused by a single event, URB=maximum UB caused by a single event, ADR=average damage ratio.

Attribute	**Earthquake Impact Metrics**				
Repairable Buildings (RB)	RB=369,582	RBE=80	ARB=4,620		MRB=91,130
Unrepairable Buildings (UB)	UB=231,608	UBE=114	AUB=2,032	ADR=1.6	MUB=30,964

7.3.2 Spatial distribution of the damaging and destructive earthquakes

The spatial distributions of the damaging and destructive earthquakes, that caused repairable and unrepairable building damage, respectively, are characterized by similar patterns (Fig. 7.23, 7.24, 7.25 and 7.26). The epicenters of the majority of earthquakes that caused either repairable or unrepairable building damages are mainly concentrated in the central and southern parts of the continental country as well as in the Ionian Sea islands. Such a spatial pattern is anticipated since in that parts of the country the seismicity is high and, at the same time, the largest proportion of the population is concentrated there with many cities, towns and other settlements being situated close to

the various seismic sources. In the NW and NE sides of the continental country, which are of relatively low seismicity, only a few epicenters of destructive earthquakes can be found, for example the Kozani-Grevena earthquake (M_w=6.53, ISC-GEM 2018) of 13 May 1995. This event, however, is not represented in Figure 7.24 since we were unable to find out accurate data for the RB number. In the central part of northern Greece, along the Serbo-Macedonian massif, several earthquakes happened during the reference time period, some of them being damaging or destructive.

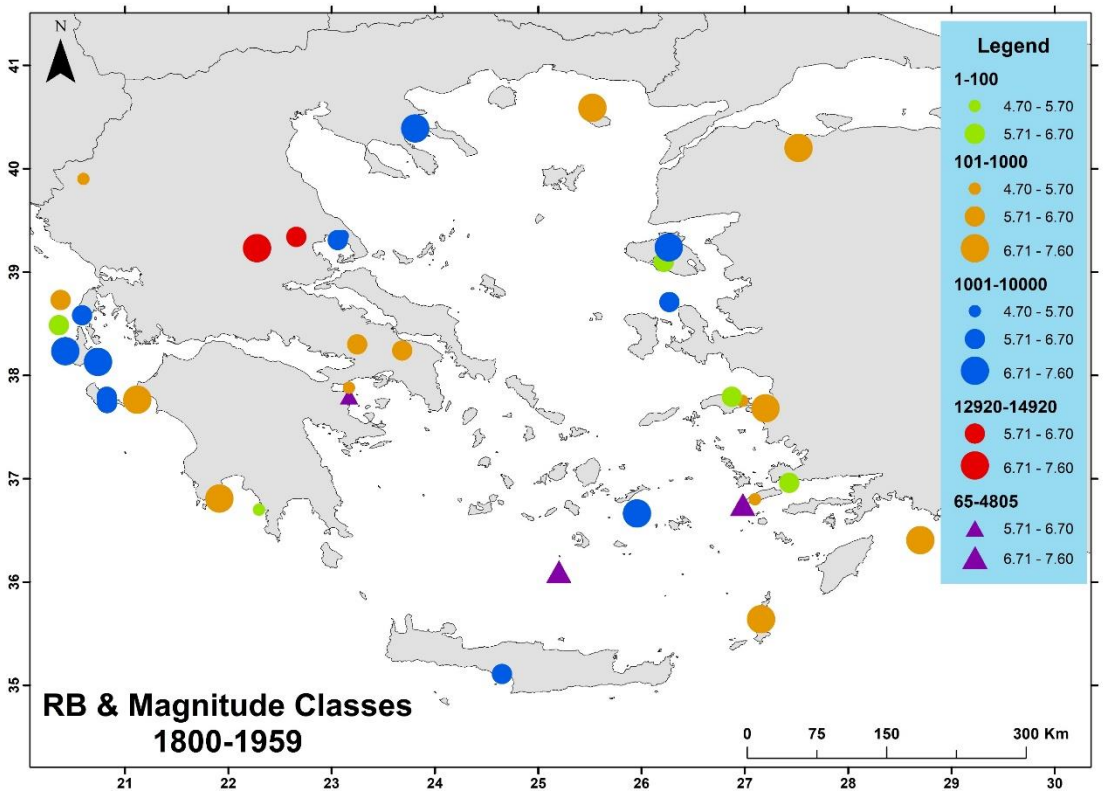

Figure 7.23. Spatial distribution of the shallow (circle) and intermediate-depth (triangle) earthquakes that caused repairable building (RB) damages in Greece in the time interval 1800-1959. Numbers of RB are represented with different colors in the Legend. Symbol size increases with the increase of magnitude class.

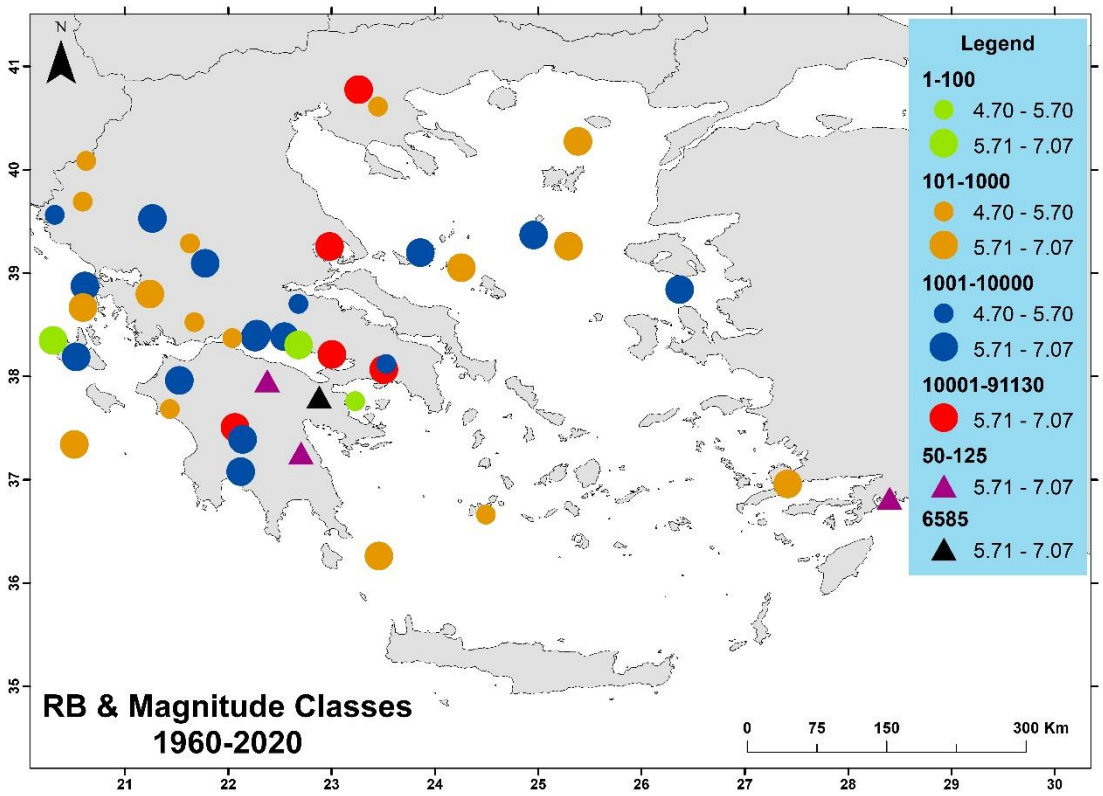

Figure 7.24. Spatial distribution of the shallow (circle) and intermediate-depth (triangle) earthquakes that caused repairable building (RB) damages in Greece in the time interval 1960-2020. Numbers of RB are represented with different colors in the Legend. Symbol size increases with the increase of magnitude class.

Both the North and South Aegean Sea areas host epicenters of earthquakes that caused unrepairable and/or repairable building damage but the density of epicenters is smaller than that in continental Greece since in these two areas most of the earthquake activity occurs offshore. In the area of the Central Aegean Sea, which is of low seismicity, no epicenters of damaging or destructive earthquakes exist. The spatial distribution of the damage ratio, DR, is illustrated in Figure 7.27. A special distribution pattern is not observed. The extremely high value of DR=180 is associated with the moderate earthquake (M_w=5.1) that occurred in the western suburban of Athens on 19 July 2019.

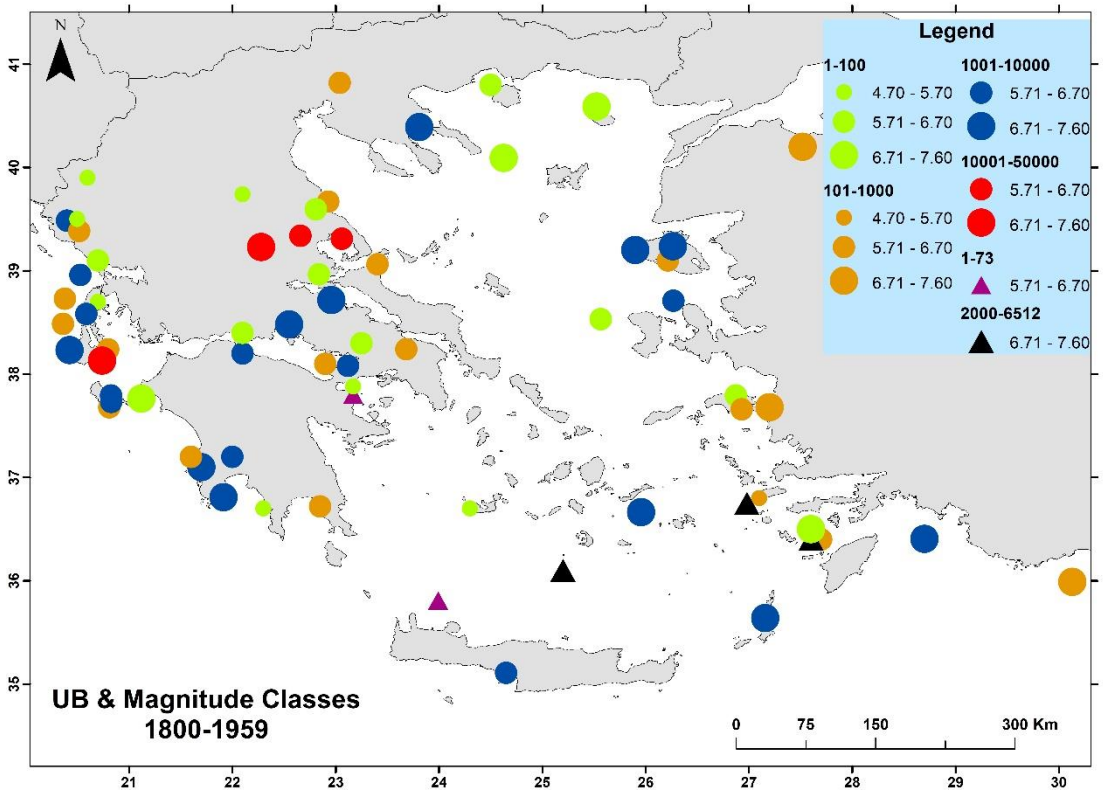

Figure 7.25. Spatial distribution of the shallow (circle) and intermediate-depth (triangle) earthquakes that caused unrepairable building (UB) damages in Greece in the time interval 1800-1959. Numbers of UB are represented with different colors in the Legend. Symbol size increases with the increase of magnitude class.

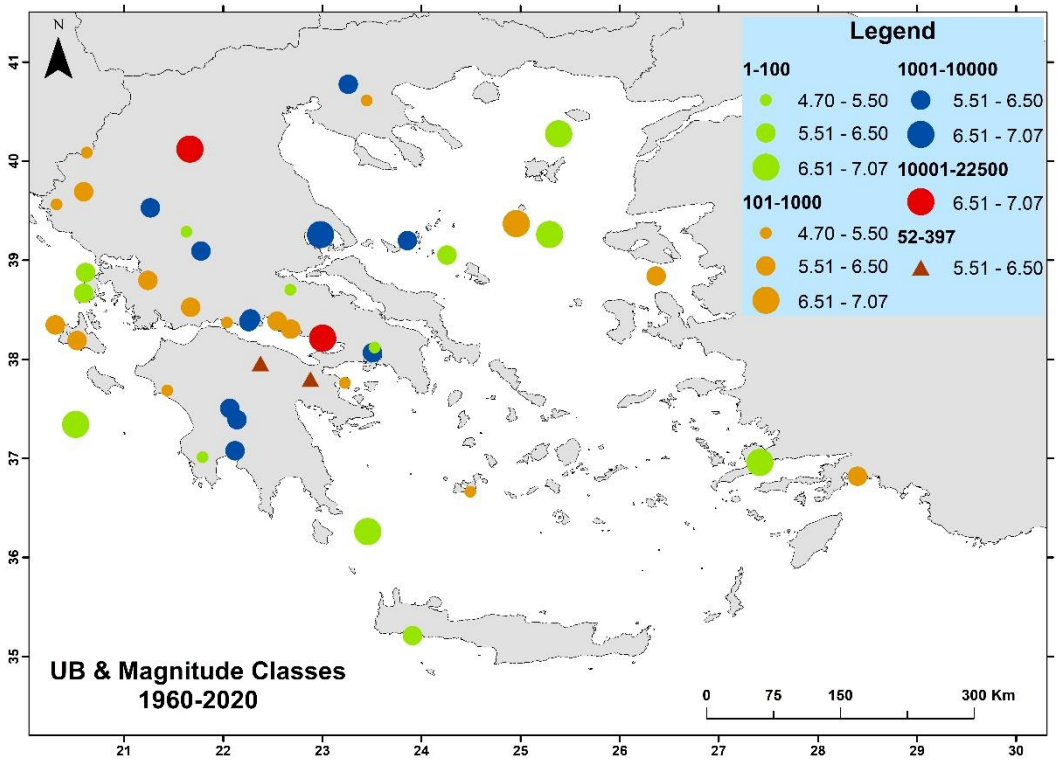

Figure 7.26. Spatial distribution of the shallow (circle) and intermediate-depth (triangle) earthquakes that caused unrepairable building (UB) damages in Greece in the time interval 1960-2020. Numbers of UB are represented with different colors in the Legend. Symbol size increases with the increase of magnitude class.

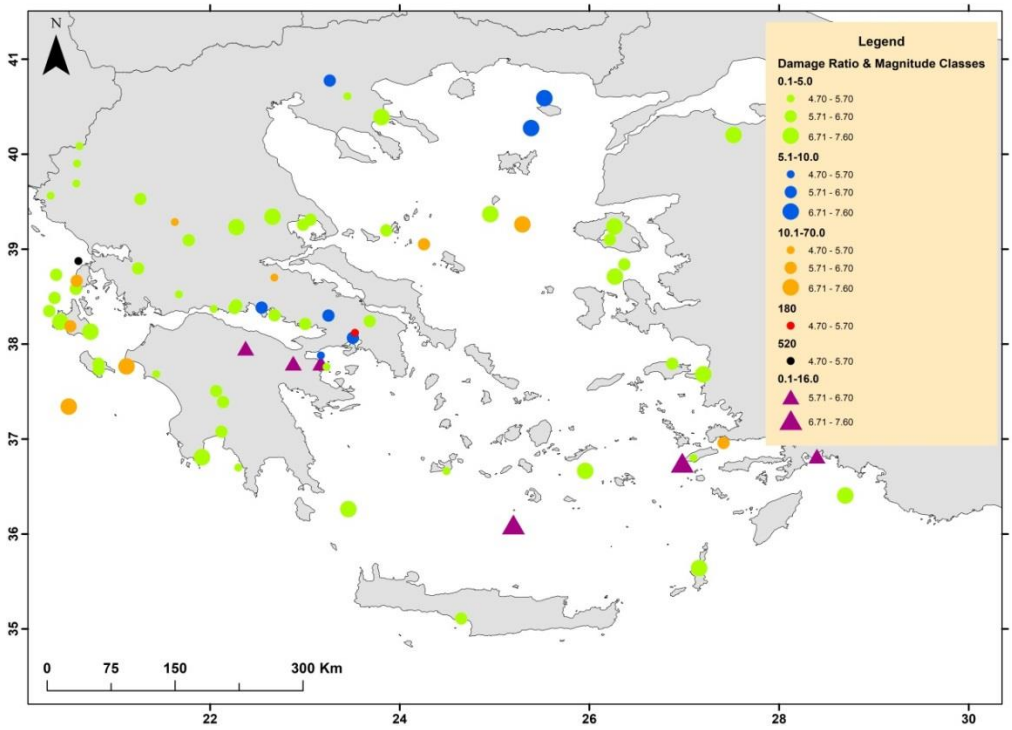

Figure 7.27. Spatial distribution of the damage ratio, DR, for shallow (circle) and for intermediate-depth (triangle) earthquakes in Greece in the time interval 1800-2020. Values of DR are represented with different colors in the Legend. Symbol size increases with the increase of magnitude class.

7.3.3 Dependence of building damage on earthquake magnitude and intensity

The dependence of the numbers of RB and UB per event on the earthquake magnitude, M, and on the maximum intensity, Io, has been examined for the shallow and the intermediate-depth earthquakes. The examinations were performed for the entire period 1800-2020 as well as for the period 1960-2020. Similar examinations have been made for the dependence of the damage ratio, R.

Both the numbers of RB and UB per event in general increase with the increase of M and Io but the RB and UB variabilities in each magnitude and intensity bin is great. For shallow events no correlation has been found between the RB number per event and M (Fig. 7.28). Although weak correlation was found for the intermediate-depth earthquakes it is quite unstable due to the very low number of events. However, the upper bound of RB is very well controlled by the earthquake magnitude. The best-fit regression line calculated (Fig. 7.28) is an approach of the maximum number of RB expected in each magnitude bin. On the other hand, the UB number per event is weakly correlated with M, while the M/UB correlation is better for the intermediate-depth events (Fig. 7.29). The upper bound of UB is very well controlled by the earthquake magnitude, with the best-fit regression line calculated (Fig. 7.29) being an approach of the maximum number of UB expected in each magnitude bin.

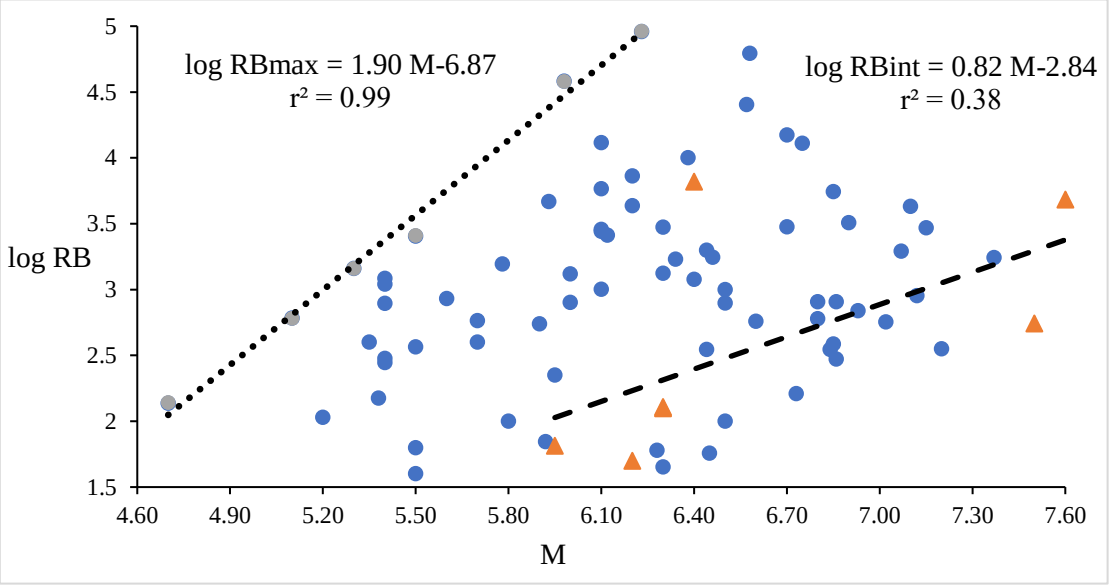

Figure 7.28. Correlation between the number of RB per event and the earthquake magnitude, M, for the period 1800-2020. RB for shallow shocks is not correlated with M. A weak M/RBint correlation was found for intermediate-depth events (dashed line). The RBmax upper bound (gray circles) is well controlled by M (round dot line). Key: circle=shallow event, triangle=intermediate-depth event; gray circle=upper bound RB points for shallow events. RBint=RB for intermediate-depth events; RBmax=RB for upper bound points; r=correlation coefficient.

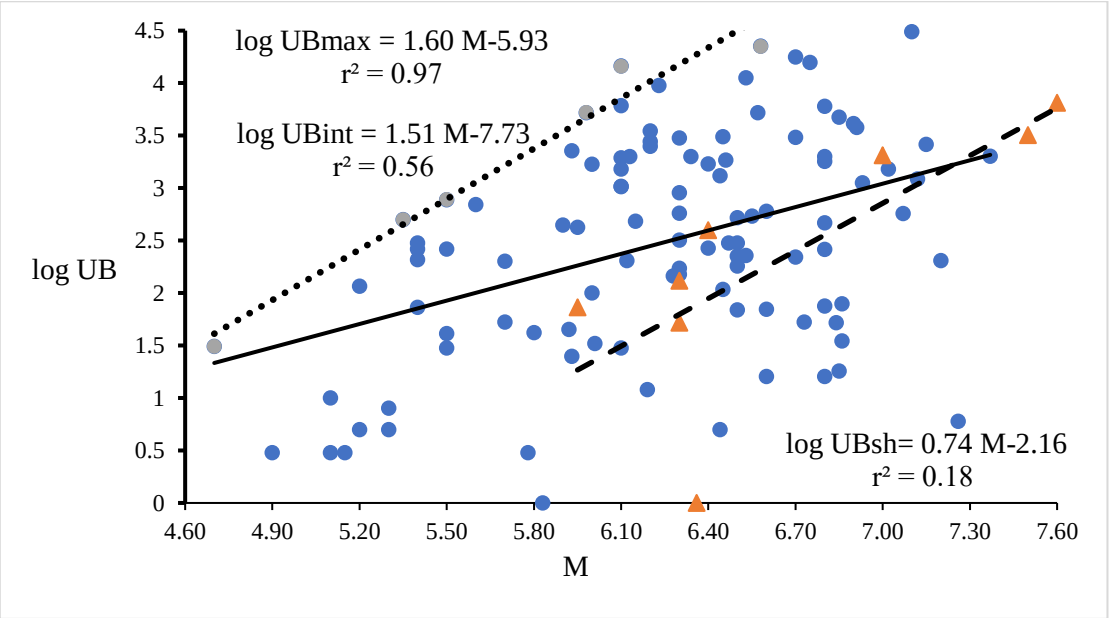

Figure 7.29. Correlation between the number of UB per event and the earthquake magnitude, M, for the period 1800-2020. UBsh for shallow shocks is weakly correlated with M (solid line). A good M/UB correlation was found for intermediate-depth events (dashed line). The UBmax upper bound (gray circles) is well controlled by M (round dot line). Key: circle=shallow event, triangle=intermediate-depth event; gray circle=upper bound UB points for shallow events. RBint=RB for intermediate-depth events; RBmax=RB for upper bound points; r=correlation coefficient.

The I_o/RB correlation is very weak for shallow events but better for intermediate-depth events (Fig. 7.30). Both the upper and lower RB bounds are very well controlled by the intensity, thus providing estimations of the maximum and minimum RB expected for each intensity bin (see regression lines in Fig. 7.30).

The I_o/UB correlation is weak for shallow events but good for intermediate-depth events (Fig. 7.31). The upper RB bound is well enough controlled by the intensity, thus providing estimations of the maximum UB expected for each intensity bin (see regression line in Fig. 7.31). However, the lower UB bound is not well enough controlled by the intensity.

In the time interval 1960-2020 weak I_o/RB correlation has been found (Fig. 7.32). However, both the upper and lower RB bounds are very well controlled by the intensity, thus providing estimations of the maximum and minimum RB expected for each intensity bin (see regression lines in Fig. 7.32).

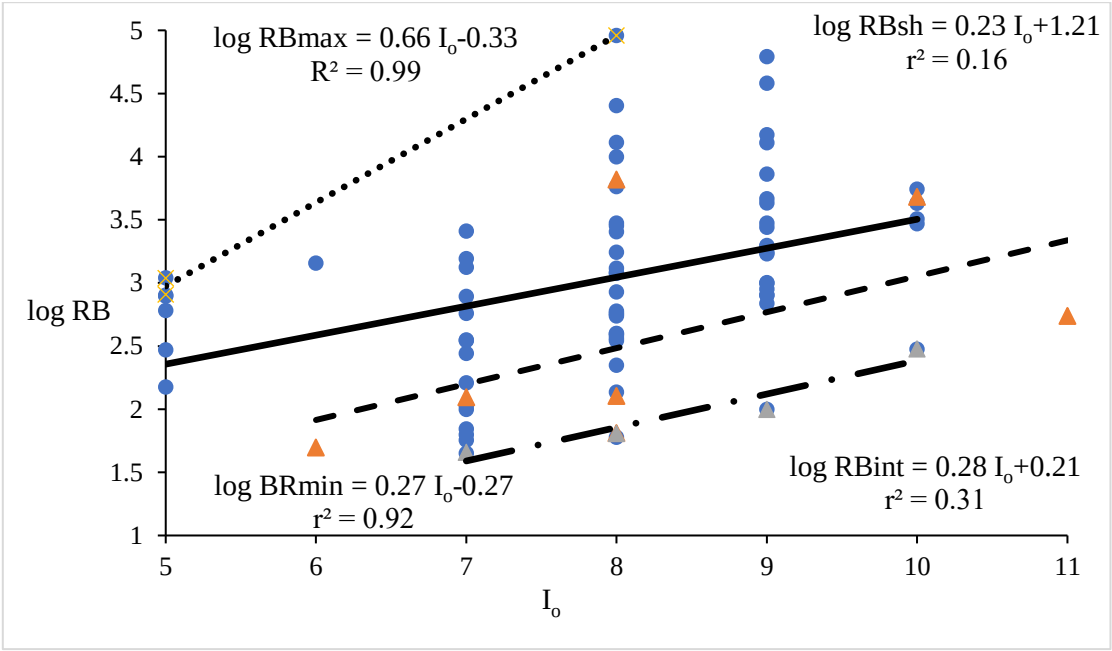

Figure 7.30. Correlation between the number of RB per event and the intensity, I_o, for the period 1800-2020. RBsh for shallow shocks is very weakly correlated with I_o (solid line). A weak M/RBint correlation was found for intermediate-depth events (dashed line). The RBmax upper bound (round dot line) and the RBmin lower bound (long dash dot line) (gray circles) are both very well controlled by I_o. Key: circle=shallow event, triangle=intermediate-depth event; RBsh=RB for shallow events; RBint=RB for intermediate-depth events; RBmax=RB for upper bound points; RBmin=RB for lower bound points; r=correlation coefficient.

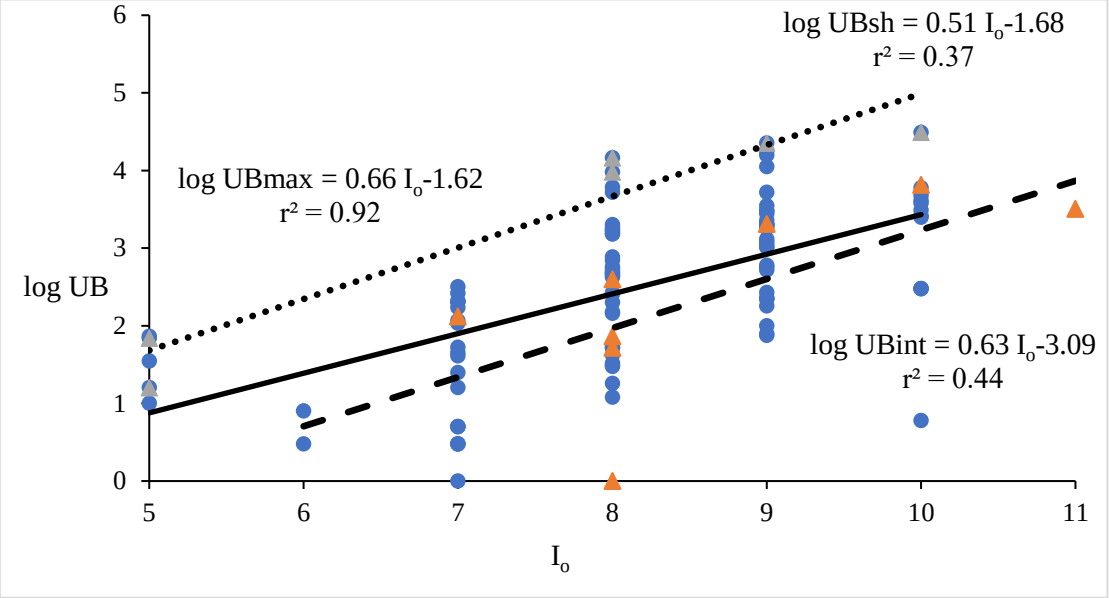

Figure 7.31. Correlation between the number of UB per event and the intensity, I_o, for the period 1800-2020. UBsh for shallow shocks is weakly correlated with I_o (solid line). A better I_o/RBint correlation was found for intermediate-depth events (dashed line). The RBmax upper bound (round dot line) (gray circles) is well enough controlled by I_o. Key: circle=shallow event, triangle=intermediate-depth event; RBsh=RB for shallow events; RBint=RB for intermediate-depth events; RBmax=RB for upper bound points; r=correlation coefficient.

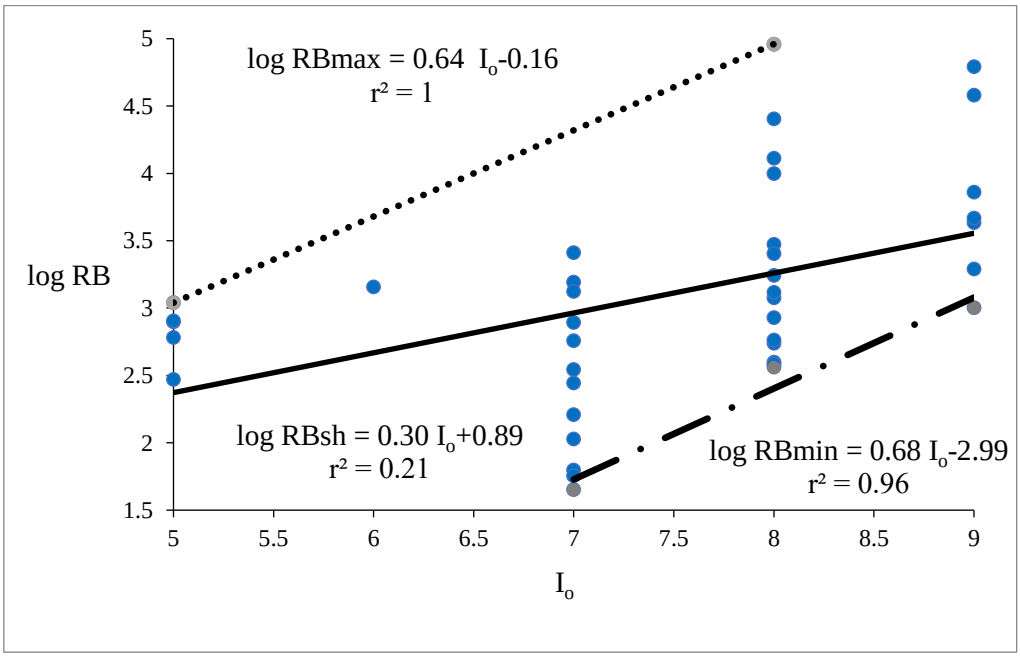

Figure 7.32. Correlation between the number of RB per event and the intensity, I_o, for the period 1960-2020. RBsh for shallow shocks is weakly correlated with Io (solid line). The RBmax upper bound (round dot line) and the RBmin lower bound (long dash dot line) (gray circles) are both very well controlled by I_o. Key: circle=shallow event, RBsh=RB for shallow events; RBmax=RB for upper bound points; RBmin=RB for lower bound points; r=correlation coefficient.

Good I_o/UB correlation has been found for the time interval 1960-2020 (Fig. 7.33). The upper and lower UB bounds are very well controlled by the intensity, thus providing estimations of the maximum and minimum UB expected for each intensity bin (see regression lines in Fig. 7.33).

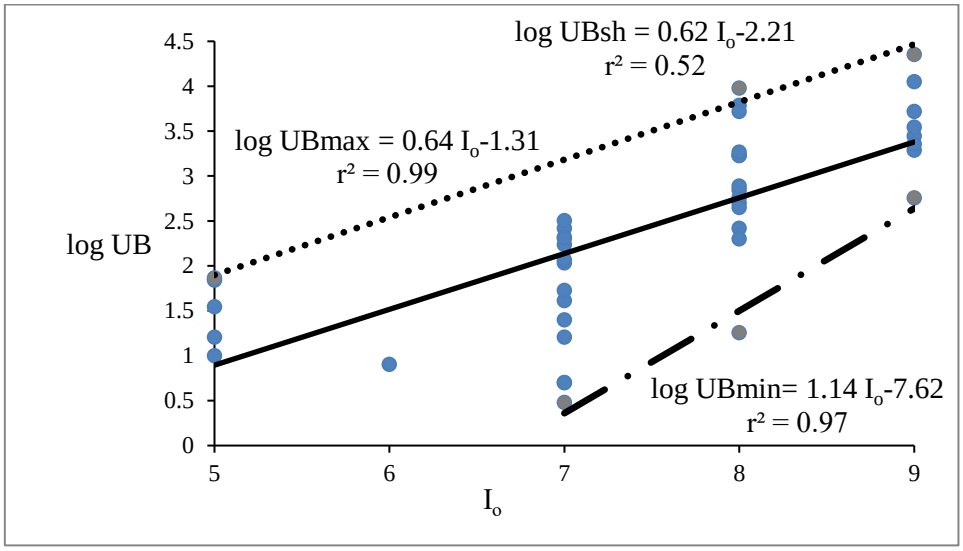

Figure 7.33. Correlation between the number of UB per event and the intensity, I_o, for the period 1960-2020. RBsh for shallow shocks is well correlated with I_o (solid line). The UBmax upper bound (round dot line) and the UBmin lower bound (long dash dot line) (gray circles) are both very well controlled by I_o. Key: circle=shallow event, UBsh=UB for shallow events; UBmax=UB for upper bound points; UBmin=UB for lower bound points; r=correlation coefficient.

7.3.4 Variations of the damage ratio DR

The log DR (DR=damage ratio) does not correlate with the magnitude, M, neither in the 1800-2020 nor in the 1960-2020 time intervals. However, there is a trend of DR to decrease with the increase of I_o in the 1800-2020 time interval (Fig. 7.34). This is does not change in the 1960-2020 interval. This implies that in higher degree intensities (I_o>7) the number of UB is relatively increased with respect to RB as compared to the number in lower degree intensities (I_o<7). This trend is valid for both the shallow and intermediate-depth earthquakes. At the same time, the intensity controls the upper bound of DR. The upper bound limiting line shown in Figure 7.34 predicts the expected maximum DR for each intensity bin.

Of interest is also the gradual increase of DR with time. This is valid for the entire reference period 1800-2020 but is better expressed in the time interval 1960-2020 (Fig. 7.35). This result practically indicates that the relative number of repairable buildings gradually increases with respect to the number on unrepairable buildings. A reasonable explanation could be that the buildings become more and more earthquake-resistant through time and particularly after 1960 when the first national seismic building code was applied in the country.

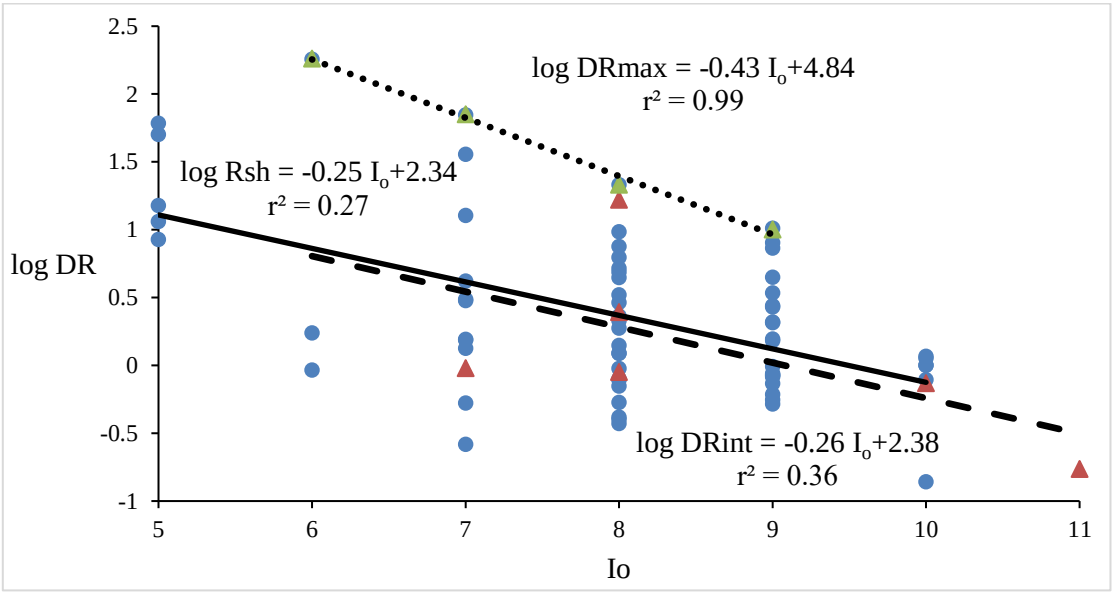

Figure 7.34. Correlation between the damage ratio, DR, per event and the intensity, I_o, for the period 1960-2020. DRsh for shallow shocks (circles) is weakly correlated with I_o (solid line) but the correlation is better for intermediate-depth earthquakes (DRint) (triangles). The DRmax upper bound (round dot line) is very well controlled by Io; r=correlation coefficient.

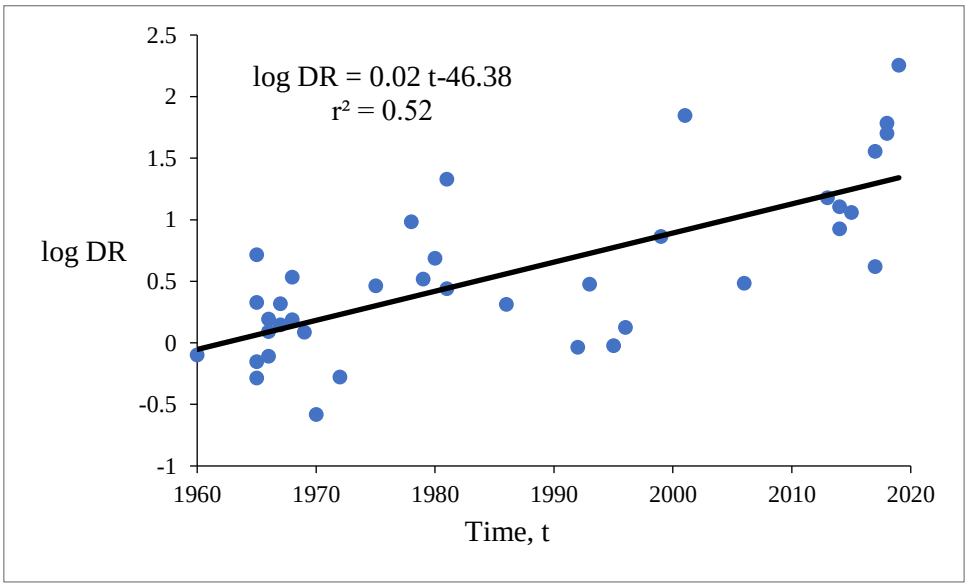

Figure 7.35. Gradual increase of DR for shallow shocks in the time period 1960-2020; r=correlation coefficient. The correlation is not very good.

7.4 Summary of Chapter 7

Based on the international experience, as well as on the types of data available in the Greek Earthquake Impact Database (GEIDB), several Earthquake Impact Metrics (EIMs) were selected for the casualties and the building damages caused by earthquakes in Greece. The most important EIMs selected are the numbers of fatalities, Fa, and injuries, In, the survival ratio, R=In/Fa, the numbers of repairable and unrepairable buildings, RB and UB, and the damage ratio, DR=RB/UB. The variation patterns of these metrics have been investigated. The average Fa and In in a given time segment gradually decrease with time, while the survival ratio increases with time. There is evidence that increased numbers of Fa and In possibly follow a seasonal pattern, which perhaps follow seismicity

seasonal variation (e.g. Galanopoulos 1985), while their diurnal variation is also possible. The metric R is roughly 3:1 for M ranging from 6.2 to 6.8 but other ratios were also found. Fa and In vary greatly in a given bin of magnitude, M, or intensity, I_o, and, therefore, we found that they only roughly increase with the increase of M and of I_o. However, the upper bound values of both the Fa and In are very well controlled by the intensity. This result is useful for the estimation of the maximum values of Fa and In expected for certain values of I_o.

The metrics RB and UB do not correlate with M but their upper bound values are controlled by the Io. The UB is well correlated with the I_o but Rb is not well correlated. The damage ratio increases gradually with time, particularly after 1960, which indicates that the relative number of In increases with respect to the Fa number. The majority of the impactful earthquakes that caused Fa, In, RB and UB have their epicenters in the central and southern parts of the continental country as well as in the islands of the Central Ionian Sea.

CHAPTER 8. THE GREEK TSUNAMI IMPACT DATABASE (GTIDB) AND TSUNAMI RISK ASSESSMENT

8.1 Introduction

The tsunamis are considered as low-frequency but of high impact natural events. Around the globe, including the Greek area, tsunamis do not occur as frequently as the earthquakes do for the obvious reason that not all the earthquakes produce tsunamis. However, the experience from the devastating mega tsunamis of 26 December 2004 in the Indian Ocean and of 11 March 2011 in Japan, generated by earthquakes of M_w=9.3 and M_w=9.0, respectively, clearly shows the catastrophic potential of large tsunamis. A tsunami may have impact either in the human communities and their properties or in the natural environment or in both. In the human communities and their properties the tsunami impact may include fatalities and injuries, damage or even destruction in buildings, infrastructures and life lines, in small or big vessels, in animals, in coastal cultivated zones as well as material damage of several types. In the natural environment there are several effects caused by the tsunamis, including destruction of flora and fauna, ground erosion, deposition of tsunami sediments, removal of boulders and others. Negative effects, such as social disruption or losses in financial terms are beyond the scope of this thesis and, therefore, are not included in our analysis.

In Greece and in the Mediterranean non-parametric or semi-parametric tsunami catalogues were published since the 1960's (e.g. Galanopoulos, 1960, Ambraseys, 1962). Although the efforts continued in the 1980's with the introduction of parametric catalogues (e.g. Papadopoulos and Chalkis, 1984, Papazachos et al., 1986) the cataloguing of tsunamis became quite systematic and followed a standard format thanks to a series of EC-supported research projects, which resulted in the establishment of the New European Tsunami Catalogue since the early of 1990s (e.g. Tinti and Maramai, 1996, Papadopoulos, 2001, 2003, Papadopoulos et al, 2007, Maramai et al., 2014). A zonation of tsunamigenic sources in the Mediterranean and the associated seas in illustrated in Figure 8.1.

In spite of the progress made in organizing tsunami catalogues, the organization of a tsunami impact data base is still lacking in the entire European-Mediterranean region including Greece. The Greek Earthquake Impact Database (GEIDB, Chapter 5) provides only synoptic information about the tsunamis caused by earthquakes inserted in the GEIDB, without providing details about the tsunami events and their impact. Besides, the GEIBD does not provide information for tsunamis caused by non-seismic sources, e.g. volcanic eruptions and landslides. For these reasons, we organized the Greek Tsunami Impact Database (GTIDB) as a supplement of the GEIDB. The very recent tsunami

caused by the large (M_w=7.0) Samos earthquake in the East Aegean Sea area on 30 October 2020 has been already studied (Triantafyllou et al., 2021) and inserted in the GTIDB. Also, we studied in details the local but fatal tsunami caused from landslides triggered in Mt Athos by the large (M_w=7.24, ISC-GEM 2018) North Aegean Sea earthquake of 8 November 1905 (Triantafyllou et al., 2020a). This is a new event to be listed in the Greek tsunami catalogue and inserted in the GTIDB. These two tsunami episodes are analyzed later.

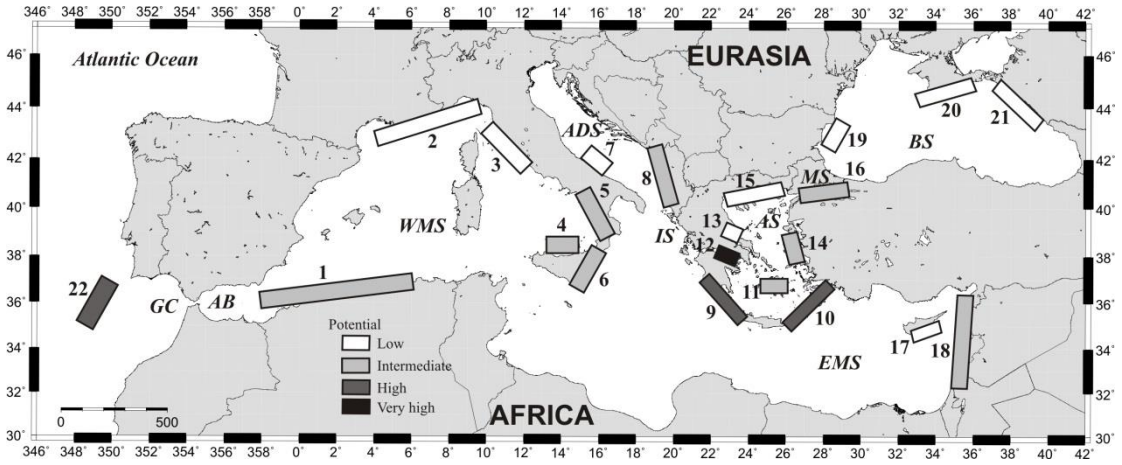

Figure 8.1. Tsunamigenic zones, defined from documentary sources, and their relative tsunami potential classification. WMS, western Mediterranean Sea; GC, Gulf of Cádiz; AB, Alboran Basin; EMS, Eastern Mediterranean Sea; AS, Aegean Sea; ADS, Adriatic Sea; MS, Marmara Sea; BS, Black Sea. Zonation key: 1, East Alboran Sea/North Algerian Margin Sea; 2, Liguria and Côte d'Azur; 3, Tuscany; 4, Aeolian islands; 5, Tyrrhenian/Calabria; 6, Eastern Sicily and Messina Straits; 7, Gargano Promontory; 8, East Adriatic Sea; 9, West Hellenic Arc; 10, East Hellenic Arc; 11, Cyclades; 12, Corinth Gulf; 13, Maliakos Bay; 14, East Aegean Sea; 15, North Aegean Sea; 16, Marmara Sea; 17, Cyprus; 18, Levantine Sea; 19, Bulgaria; 20, Crimea; 21, East Black Sea; 22, South West Iberia (after Papadopoulos et al., 2014a).

The tsunami data collected are useful for better understanding the various types of impact caused by tsunamis in Greece, their space-time distribution as well as the occurrence frequency of the potentially damaging or destructive tsunamis. In the next lines we describe the structure and the content of the GTIDB and present details on the tsunami events of 8 November 1905 and of 30 October 2020. Tsunami risk assessment is performed based on the extreme scenario method and its application in the test-site of Heraklion, the capital city of Crete Island.

Approaches for the probabilistic tsunami hazard assessment (PTHA) are already in place and are shortly reviewed later. The tsunami catalogue data combined with the impact data set allow us to introduce and test a new approach for the probabilistic tsunami risk assessment (PTRA) for the first time in Greece and in the entire European-Mediterranean region. The approach has been inspired by

the PTHA method introduced by Kijko and Smith (2017) and Smit et al. (2017, 2019), which is based on the utilization of historical (incomplete) and instrumental (complete) files of tsunami wave heights. The method has been extended to utilize incomplete and complete files of tsunami impact data.

8.2 Content and structure of the GTIDB

Usually tsunamis are generated by submarine or coastal earthquakes. However, tsunamis are also generated from other types of sources including volcanic eruptions, landslides and meteorological changes (meteotsunamis). This is also valid for the Greek area. In some historical occasions, however, the causative event remains unknown. Since a tsunami is a secondary effect of a primary causative event, e.g. earthquake, a tsunami database should contain information about the causative event, the tsunami as a physical event, the tsunami impact and the tsunami intensity as a tsunami impact metadata. In view of these peculiarities the GTIDB is structured in four main sections: (1) Parameters of the Tsunami Sources, (2) Tsunami Data, (3) Tsunami Impact Data and (4) Tsunami Impact Metadata. Data for the sections (1)-(3) have been taken from several catalogues, papers, books, technical reports and other publications, which have been already reviewed in Chapter 5. The section on Tsunami Impact Metadata includes estimation of the maximum tsunami intensity and the coastal place it has been observed.

The GTIDB is organized in Access Format and covers the time period from the antiquity up to the present time. However, the part from AD 1800 to 2020 is presented here for reasons of consistency with the GEIDB (Fig. 8.2). Tsunamis travel away from their sources with low rate of energy dissipation. Therefore, they have the potential to cause damage or even destruction in large distances from the source. As a consequence, tsunami impact data have been inserted in the GTIDB only for the Greek area leaving aside the impact caused further away in other areas of the Mediterranean basin. This practically implies that the GTIDB does not contain information about tsunamis that are known and included in several catalogues but didn't cause impact in the Greek area. Eventually, 16 tsunami events have been inserted in the GTIDB for the reference period. Fourteen out of 16 tsunamis were caused by earthquakes and only two have been triggered by gravitational earth slides. The earlier event is the destructive tsunami associated with an equally destructive earthquake (M_w=6.5) that ruptured the western Corinth Gulf on 23 August 1817, while the last event inserted in the GTIDB is the very recent damaging tsunami caused in the East Aegean Sea area by the Samos M_w=7.0 earthquake of 30 October 2020. However, the most destructive one has been the large tsunami generated by the large (M_w=7.24, ISC-GEM 2018) earthquake of 9 July 1956 in the South Aegean Sea.

Year	Month	Day	Hr	Min	Sec	LAT(N)	LON(E)	Depth	Mw	Region	Io	Source type	Source subregion	Short description	Rel	Fa	In
1817	8	23	8	00	00	38.3000	22.1000	n	6.50	West Corinth Gulf	9	ER	Aegion	Destructive waves in Aegion	4	Fatalities	
1856	11	25	11	40	00	38.3670	26.1330	n	6.13	East Aegean Sea	7-8	ER	Chios	Damaging tsnami at Chios	3	people lost	
1861	12	26	6	28	00	38.2500	22.1600	n	6.60	West Corinth Gulf	10	EL	Aegion	Damaging waves in Aegion	4		
1867	9	20	3	44	00	36.5000	22.7000	n	6.50	Gythion Gulf	11	ER	Gythion	Damaging waves in Gythion	4		
1883	6	27	00	00	00	39.5000	20.0000	n	5.50	North Ionian Sea		ER	Corfu	Sudden withdrawal at St. Georges	3		
1893	2	9	18	02	00	40.5890	25.5260	n	6.84	North Aegean Sea	8	ER	Samothraki	Damaging wave at Agistron	4		
1905	11	8	22	30	30	40.0920	24.6270	15	7.26	North Aegean Sea	10	ER	Athos	Fatal tsunami at Athos	4	5	
1948	2	9	12	58	13	35.6400	27.1580	15	7.12	South Aegean Sea	9	ER	Karpathos	Damaging wave at Karpathos	4		
1956	7	9	03	11	40	36.6640	25.9570	20	7.37	South Aegean Sea	9	ER	Amorgos	Destructive tsunami in Cyclades	4	1	2
1963	2	7	7	28	00	38.2000	22.2000			West Corinth Gulf	0	GS	Aegion	Destructive wave in Aegion	4	2	12
1965	7	6	3	18	42	38.3840	22.5450	20	6.30	West Corinth Gulf	8	EL	Eratini	Strong wave in Eratini	4	1	
1996	1	1	1			38.2500	22.1170			West Corinth Gulf	0	GS	Aegion	Sea wave in Aegion	4		
2000	4	5	4	36	59	34.4210	25.7900	33	5.50	Crete	3	ES	Heraklion	Sea oscilation in Heraklion	4		
2002	4	3	12	00	00	36.4500	28.2000			Dodecanese Islands	0	GS	Rhodes	3-4m high waves in Rhodes	4		
2017	7	20	22	31	11	36.9590	27.4150	6	6.60	Dodecanese Islands	7	ER	Kos Island and Bodrum Peninsula	Strong tsunami with small damage	4		
2020	10	30	11	51	27	37.9000	26.8060	6	7.00	East Aegean Sea	7-8	ER	Samos Island and Smyrne region	Strong tsunami with small damage	4		

VESSELS SERIOUSLY DAMAGED	VESSELS DAMAGED	OTHER DAMAGE	K
several		caltivated lands, ware houses	8
			8
	merchant ships, raw boats	port facilities, caltivated land	5
		caltivated land in Zante	7
	3		4
		animals killed, 2 houses collapsed	4
			8
vessels destroyed		houses damaged	7
73	20	Buildings, caltivated lands, port infrastractures, ware houses, animals, property	8
	some fishing boats	houses, caltivated land, property	7
		damage	5
		houses, caltivated land	5
		boats damaged	5
		property damage	5
	few small boats	damage in shops	5
a few boats lost	a few boats damaged	damage in shops, cars, property	5

Figure 8.2. Excerpt of the GTIDB for the time period 1800-2020.

8.2.1 Parameters of Tsunami Sources

This section provides parametric information about the earthquakes or other types of sources that generated tsunamis. In case of seismic tsunamis the seismicity parameters inserted in the GTIDB are the respective ones contained in the GEIDB. The seismicity parameters included are the next:

Date: Year, month, day (in N.S.),

Origin time: in hr, min, s (in UTC),

Epicentral coordinates: geographic latitude and longitude in degrees and minutes,

Focal depth, h (in km): if no numerical value is available then we used the notation: *n*, surface earthquake (h≤60 km); *i*, intermediate depth earthquake (h>60 km),

Magnitude: M_s, surface-wave magnitude or M_w, moment magnitude.

For tsunamis produced by other causes, e.g. landslide, the place as well as date and origin time are also provided. The earthquake and other sources that produced impactful tsunamis in Greece in the time period 1800-2020 are illustrated in Figure 8.3.

8.2.2 Tsunami Data

This section concerns the tsunami event *per se*, regardless the extent and the type(s) of impact caused. A short description of the event is provided. Also, a reliability score, Rel, of the tsunami causative event is also given.

8.2.3 Tsunami impact data and metadata

The impact of each event inserted in the GTIDB is presented in this section. An effort has been made to introduce quantitative data at the extent it is possible (e.g., numbers of fatalities and injuries, numbers of buildings or vessels damaged, etc.). However, it is dependent on the data availability. From the impact of an event the maximum tsunami intensity, *K*, has been estimated according to the 12-grade scale of Papadopoulos and Imamura (2001). The intensity scale proposed by Lekkas et al. (2013) provides the same estimations.

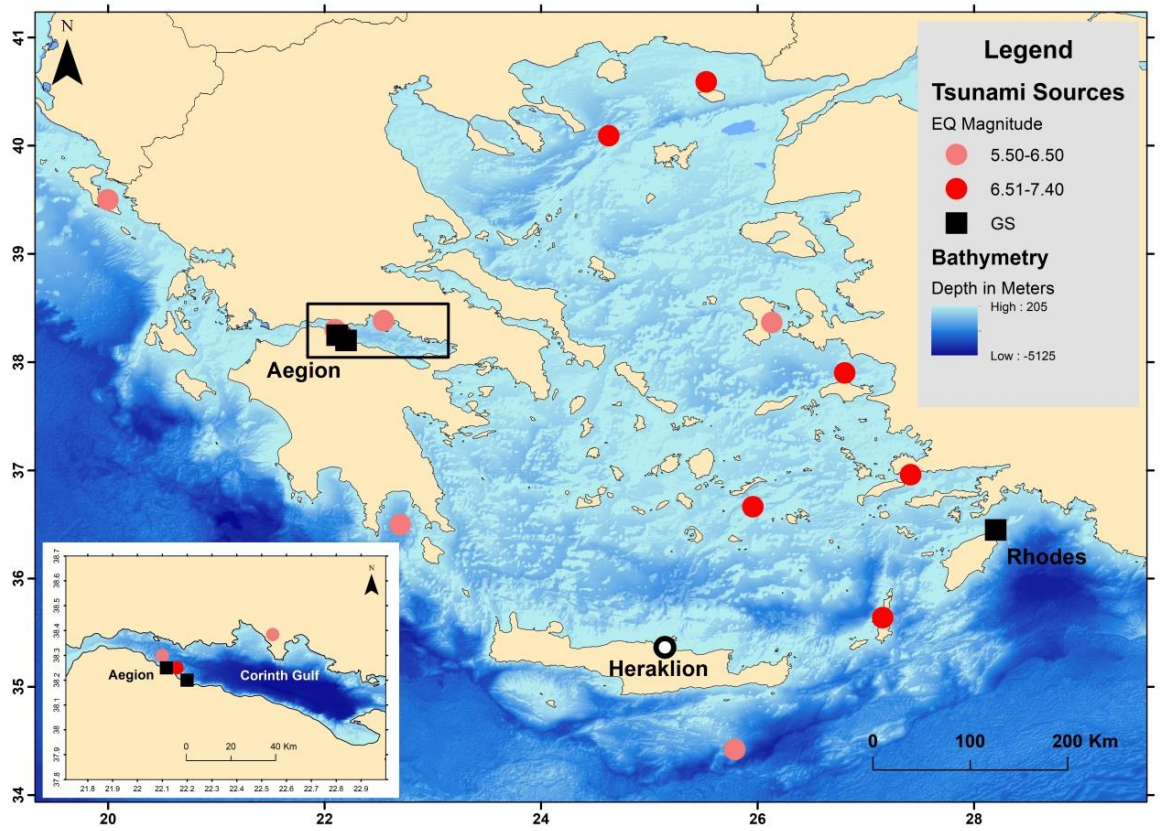

Figure 8.3. Earthquake and other sources that produced impactful tsunamis in Greece in the time period 1800-2020: Bathymetry data are from EMODNET. GS means gravity slide.

8.2.4 Tsunami impact statistics

From the tsunami impact data collected it results that in the reference period 1800-2020 only a very limited number of casualties occurred due to tsunamis in Greece. The total numbers are 9 fatalities and 15 injuries. However, in some cases, an identified number of fatalities happened. The tsunami caused in Aegion, Corinth Gulf, killed people but the historical sources do not provide number. With the Chios Island tsunami people was reportedly lost but again no number has been given. Therefore, the above human losses due to tsunamis in Greece should be considered as the minimum ones. On the other hand, no serious building damage has been reported due to tsunamis. On the contrary, noticeable damage or destruction was caused in vessels, port infrastructures, coastal cultivated lands and in property.

8.3 Tsunami case studies

In this section we study two tsunami events and their impact. The first is the tsunami caused by the large earthquake (M_w=7.24, ISC-GEM) of 8 November 1905 in Mt. Athos and the second is the tsunami caused very recently by the large earthquake (M_w=7.0) of 30 October 2020 in Samos Island.

8.3.1 The tsunami caused by the earthquake (M_w=7.24) of 8 November 1905, Mt Athos

The large earthquake (M_w=7.24) that ruptured the North Aegean Sea to the south of Athos peninsula has been studied in Chapter 5, while the study and the results obtained have been already published in the paper by Triantafyllou et al. (2020a) (see and Appendix to this thesis). One of the findings of that study is that the earthquake caused massive landslides (Fig. 8.4), which run downslope in the sea and triggered a local but powerful tsunami. It was reported that the tsunami killed 5 persons.

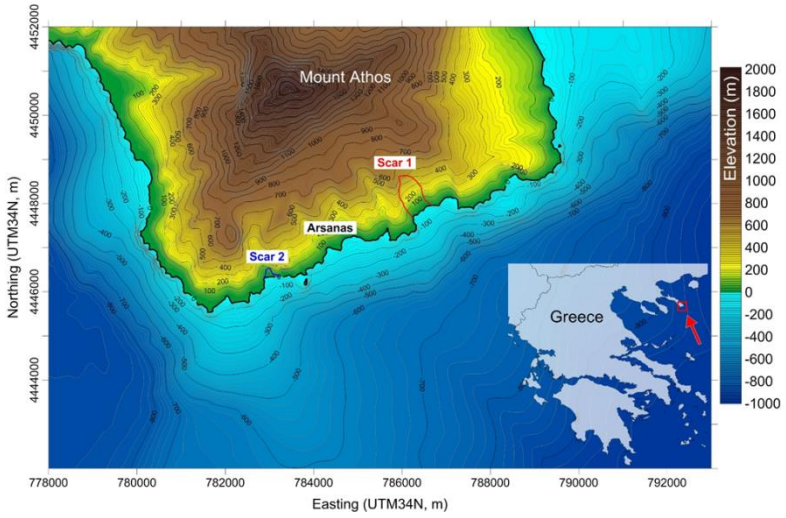

Figure 8.4. The tsunami was reported from the southern end of the Mt Athos peninsula and the surrounding. The two possible landslide source areas are marked in red (Scar 1) and in blue (Scar 2) (in collaboration with the UNIBO tsunami team, Triantafyllou et al. 2020a).

Numerical simulation of the landslide and ensuing tsunami has been performed in close collaboration with the tsunami research team of the University of Bologna, Italy. The numerical scheme adopted consists of two basic steps: simulation of the falling mass and simulation of the ensuing tsunami. The first simulation is performed by means of the code UBO-BLOCK1, developed by the University of Bologna tsunami team. It assumes a Lagrangian approach, dividing the mass into deformable portions and allowing one to compute the time-changing thickness of the mass during the motion. The code needs as input the undisturbed sliding surface, the initial top surface of the sliding body, the path followed by the blocks' center of mass (CoM hereafter), and the lateral boundaries accounting for the slide lateral spreading (Fig. 8.5). A full description of the model can be found in Tinti et al. (1997).

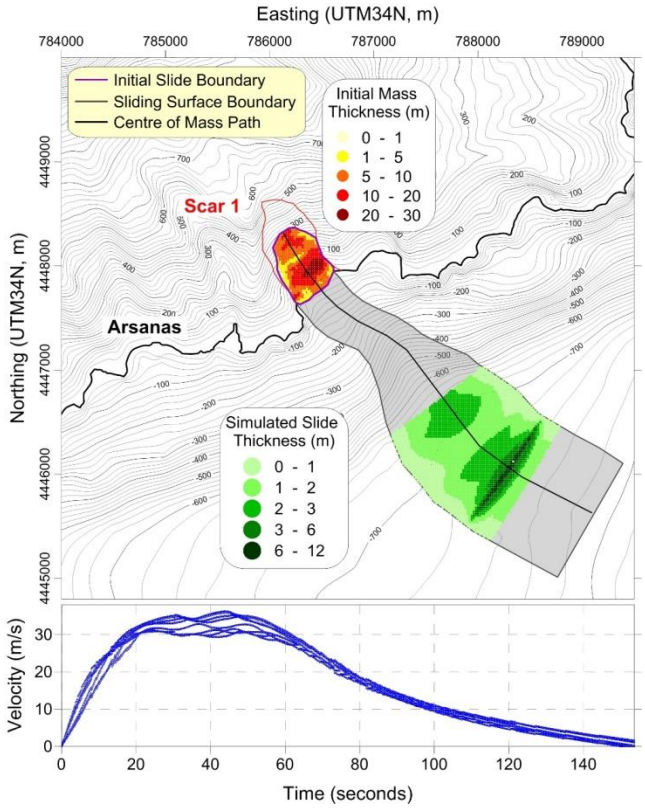

Figure 8.5. Upper panel: Initial sliding mass assumed for case S1 (area within the purple boundary inside the scar area delimited by the red line, and slide thickness given in the yellow-red scale). Predefined Center of Mass (CoM) trajectory and lateral boundaries are drawn as black and grey curves, respectively. The final deposit thickness is represented by the different scales of green, from light to dark. Lower panel: blocks' CoM velocity vs. Time (in collaboration with the UNIBO tsunami team, Triantafyllou et al. 2020a).

The tsunamigenic impulse, i.e. the vertical water displacement induced by the landslide at the sea surface, is evaluated by an intermediate code, UBO-TSUIMP (Fig. 8.6). In practice, the sea bottom vertical change due to slide motion is transferred to the sea surface by a filtering function that depends on the local water depth and cuts the higher frequencies. Further, a space time-interpolator maps the sliding dynamics on the nodes of the tsunami computational grid.

The propagation of the tsunami, which is the second step of the numerical scheme, is simulated by solving the shallow-water equations, through a finite-difference technique that implements the leap-frog scheme with the staggered-grids approach. The impulse given by the slide enters as a perturbation term in the continuity equation. On the grid boundaries full transparency condition is implemented in the open sea, while the interaction with the coastal boundary can be tuned. If the user aims at assessing land inundation, as is the case for the simulations run in this work, a moving boundary condition is adopted. Instead, if the no-inundation option is selected, a total reflection condition is imposed. All these tasks are implemented in the code UBO-TSUFD, described in details by Tinti et al. (2013). The above numerical procedure has been tested and validated in numerous

cases of landslide-induced tsunamis. For some examples, one can refer to Tinti et al. (2011), Zaniboni et al. (2014a, 2014b, 2016, 2019) and further references therein.

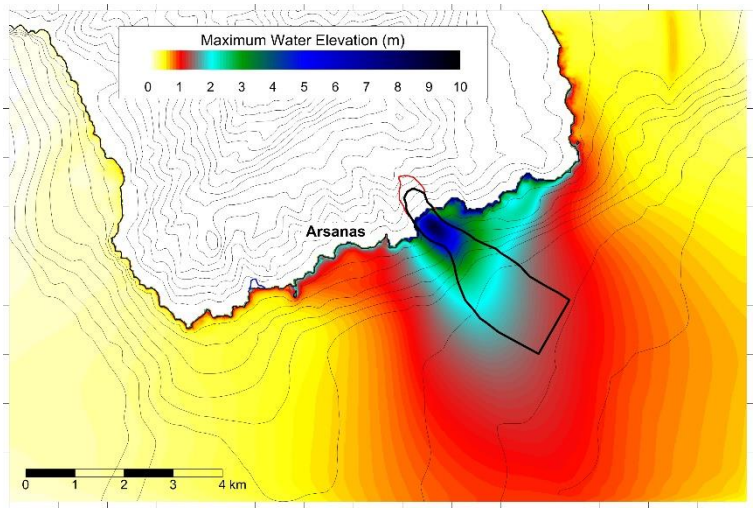

Figure 8.6. Maximum water elevation for scenario S1. The red line marks the Scar 1 boundary. The black boundary evidences the sliding surface (in collaboration with the UNIBO tsunami team, Triantafyllou et al. 2020a).

The simulation was based on two landslide scenarios by following the historical accounts collected by us and the current geomorphology of the area. Two alternatives were considered, the first involving a scar situated east of Arsanas locality with a landslide volume of ~2.7 million m^3 and the second being of only 160 x 10^3 m^3 to the west of Arsanas.

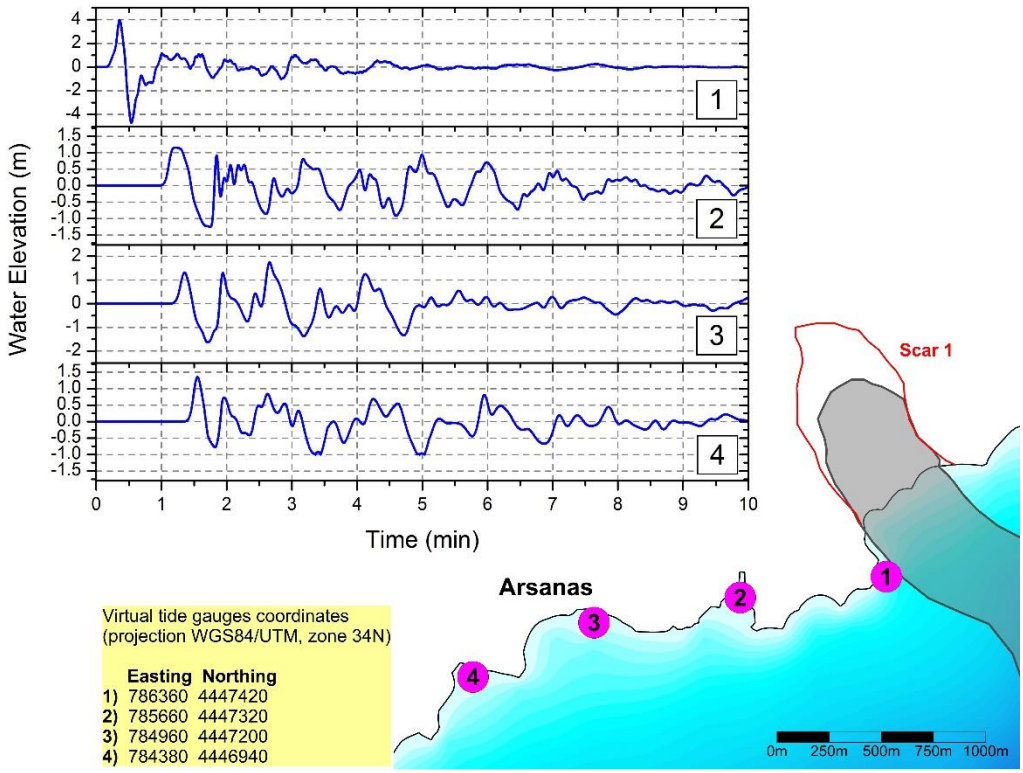

Figure 8.7. Virtual tide gauges at the points 1, 2, 3 and 4 to the west of Scar 1, and synthetic tide gauge records obtained for the tsunami generated by landslide scenario S1. Grey area represents the sliding surface (in collaboration with the UNIBO tsunami team, Triantafyllou et al. 2020a).

The simulated tsunami waves with the first scenario (S1) provided results consistent with the existing historical descriptions (Fig. 8.7). Therefore, it is a very good candidate source for the tsunami generation. On the contrary, the second scenario (S2) underestimated drastically the tsunami height historically reported.

8.3.2 The tsunami caused by the Samos earthquake (M_w=7.0) of 30 October 2020

The study of the 2020 Samos tsunami was based on post-event field surveys, video records, eyewitness accounts and records in far-field tide-gauges (Figs. 8.8, 8.9). The post-event field survey in Samos was organized by the Department of Geology & Geoenvironment, National & Kapodistrian University of Athens under the leadership of Prof. E. Lekkas and was performed from 31st October to 2nd November 2020. Observations were also collected from the islands of Chios, Ikaria and Andros. A relevant paper has been already published (Triantafyllou et al., 2021) (see and Appendix to this thesis). Therefore, here only the main points of this study are presented.

The 2020 Samos tsunami has been an important event from several perspectives. First, it has been the largest tsunami in the eastern Mediterranean, if not in the entire Mediterranean basin, since the occurrence of the large tsunami observed after the M_w=7.7 earthquake of 9 July 1956 in the south Aegean Sea. In addition, it has been a characteristic near-field event with the maximum sea level rise

arriving at the shortest epicentral distance (Δ~12 km) in Ayios Nikolaos settlement, north coast of Samos, within only ~4 min. Considering average sea depth of ~200 m between the epicenter and Ayios Nikolaos the theoretical arrival time was found equal to 4.5 min.

In most observation sites around the source, including Samos north coast, Ikaria Island and western Turkey localities, the leading wave has been a sea recession implying tsunami generation mechanism due to seismic dislocation. The wave heights measured have been ~1 m, which is consistent with the estimated displacement amplitude at the tsunami source. The wave height reached up or close to 2 m only in bays and ports, such as in Vathy and Karlovasi, north Samos, and in a couple of western Turkey localities. In the bay of Vathy town an initial sea recession has not been reported. Two inundation phases, with arrival times of 13 min and 19 min after the earthquake, have been documented from field observations, video records and eyewitness accounts. The second inundation was the strongest with measured run-up 2.0 m asl at inundation distance d~100 m (Fig. 8.10). However, a sea recession as first wave motion cannot be excluded but not observed in the bay for various reasons. In several localities of the south coast of Samos wave height of ~0.5 m or less was observed.

In Ayios Nikolaos a measured extreme wave height of 3.35 m asl, or more conservatively of 2.80 m asl, needs explanation. A key element is that the powerful wave motion was oblique along the beach as is clearly seen in an accurate video record. This reminds the 2018 Palu-Indonesia tsunami produced by a coupling of seismic and landslide tsunamis. In Samos, the seismic tsunami coupled with a tsunami produced by small scale submarine landslide may explain the extreme tsunami height measured in Ayios Nikolaos.

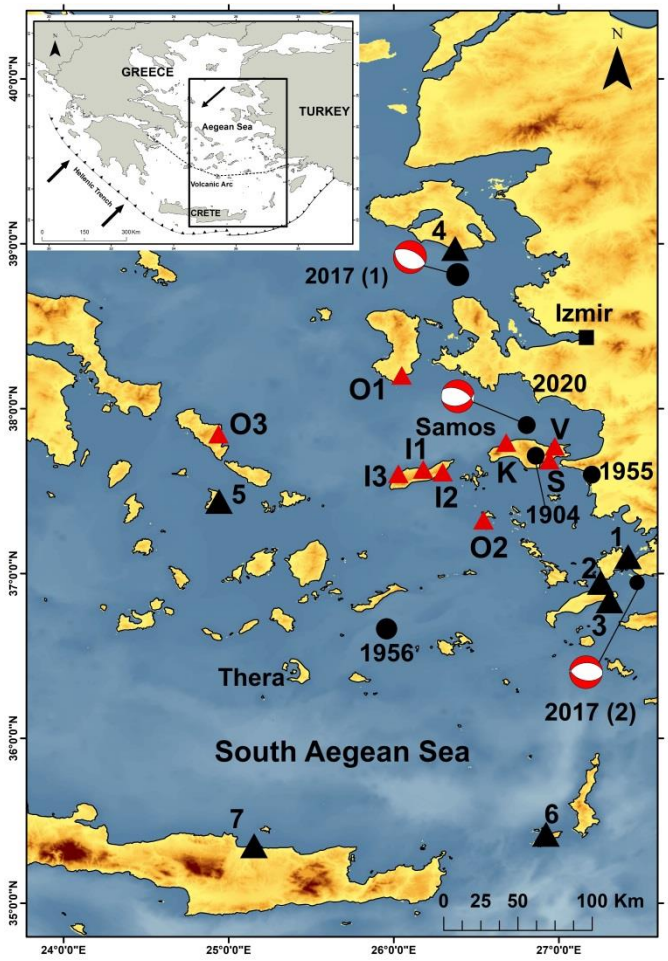

Figure 8.8. Map showing the record of the tsunami generated by the Samos 30 October 2020: solid triangle shows tide-gauge station, 1=Bodrum, 2=Kos, 3=Kos-Marina, 4=Plomari, 5=Syros, 6=Kasos, 7=Heraklion; red triangle shows main sites of tsunami observation: Samos Isl., V=Vathy, K=Karlovasi, S=south Samos; Ikaria Isl.: I1=Evdilos, I2=Ayios Kirykos, I3=Gialiskari; O1=Komi (Chios Isl.), O2=Scala (Patmos Isl.), O3=Nimporio (Andros Isl.) (for more details see in text); black circles show epicenters of earthquakes mentioned in the text, 2017 (1) and 2017 (2) stand for the 12 June and 20 July earthquakes, respectively; beach-ball shows earthquake focal mechanism, from moment tensor solution, indicating about WNW- ESE normal faulting (after National Observatory of Athens, https://bbnet.gein.noa. gr/HL/seismicity/mts/revised-moment-tensors). Arrow in inset shows direction of lithospheric plate motion.

From several video records we estimated wave velocity gradually decreasing from offshore north Samos (23 m/s), along the north Samos beach (7.8 m/s) and in the Vathy bay (3.3 m/s). Even smaller velocity was estimated on land during the upstream water motion. In Vathy it was found ~0.8 m/s for the first inundation and from 0.92 m/s to 1.4 m/s for the second inundation. From the run-up values obtained little doubt remains that the tsunami amplified in ports and narrow bays. However, we found a power-law decay of the wave height away from the source. Empirical formula (1) is very likely the

most reliable proposed so far in the Mediterranean basin for the wave height decay of seismic tsunamis.

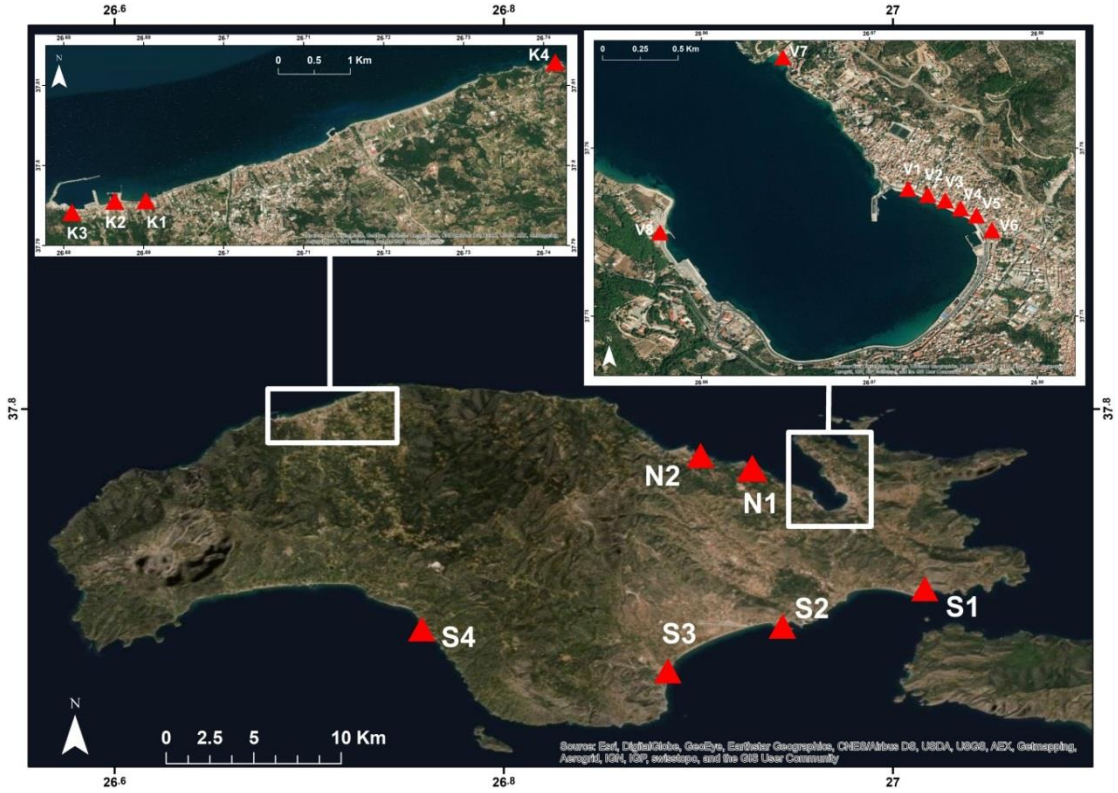

Figure 8.9. Sites of tsunami field-survey in Samos: V1-V6=Vathy town, V7=Gagou beach, V8=Malagari, N1=Kedros, N2=Kokkari, K1-K3=observation sites in Karlovasi town, K4=Ayios Nikolaos; S stands for south Samos coasts, S1=Psili Ammos, S2=Pythagorion Port, S3=Heraion, S4=Kampos. For more details see the text.

Wave heights measured at seven far-field mareograms returned tsunami magnitude M_t=M_w=6.8, which is a good approximation of the earthquake magnitude calculated independently from seismic records. Even better results were obtained by considering wave height from field data only (M_t=7.1) and wave height from field data and mareograms taken altogether (M_t=7.0). The successful Mt estimation not only of the Samos 2020 tsunami, but also of other recent events, indicates that the development of a tsunami magnitude scale in the Mediterranean basin is a realistic goal. The tsunami source area was found equal to about 1960 km^2, which doubles the aftershock area. This result is consistent with results based on global data sets.

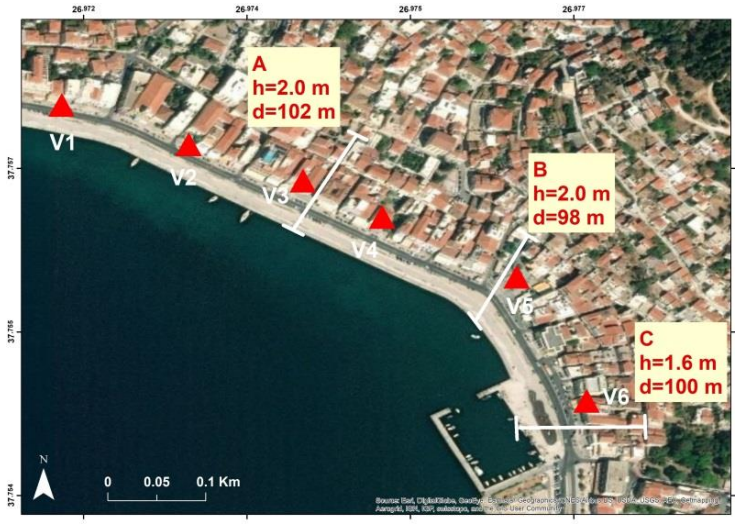

Figure 8.10. Observation sites V1 to V6 (red triangles) along the Vathy bay east coast and three characteristic tsunami transects A,B,C (white lines) measuring maximum run-up, h, at respective run-in distance, d (for details see in text).

The tsunami caused material damage in cars, in small vessels and in various coastal stores, offices, hotel lobbies, restaurants and other tourist and commercial shops particularly in Vathy (Fig. 8.11) and Karlovasi in Samos Isl. as well as in western Turkey localities. However, no structural damage to buildings was observed because of the tsunami. A few small boats were damaged or lost in the sea. In several observation sites fishes, sand, pebbles, salt and extensive littering was left behind by the wave. In at least one coastal spot the tsunami withdrawal caused local ground erosion. In south Chios Island small vessels damaged. It is noteworthy that damage was observed in sites with wave run-up of ~1 m asl or more. No damage caused with run–up values less than 1 m. Tsunami damage was extended in an area of ~4000 km^2 around the seismic source which is about twice the tsunami source area.

The mortality caused by the tsunami has been nearly zero since only one fatality was reported in western Turkey. This is due to that the wave height and run-up have not been large enough to cause massive casualties. According to coastal field observations the island of Samos very likely uplifted co-seismically with amplitude varying from ~0.15 m to ~0.25 m. Coastal uplift may have contributed to reduce the run-up and, consequently, the impact of the tsunami wave. Further research regarding this point is a challenge. There is evidence that in both Samos and western Turkey people at large extent evacuated inland immediately after the earthquake. The warning message disseminated to the general public of the eastern Aegean Sea Greek islands may have also contributed to protect people from the second inundation in Vathy town. An investigation on this issue is ongoing by our research team.

Figure 8.11. Site V2. Indoor material damage caused by the tsunami attack in the fish restaurant (a). Water mark at h~1.09 m was measured at run-in distance of ~45 m (b) (photos credit, I. Triantafyllou).

Low tsunami hazard has been considered so far in the eastern Aegean Sea area. However, the Samos 2020 tsunami is the third occurring in the area in the last years after the tsunamis caused by strong earthquakes occurring on 12 June 2017 (M_w=6.3) and 20 July 2017 (M_w=6.6) to the north and south of Samos, respectively. These tsunami waves, although have been of only local impact, call for a reevaluation of the tsunami hazard level and the preparedness for tsunami risk mitigation in the area.

8.4 Tsunami hazard and risk assessment: a short review

8.4.1 Discrimination of hazard and risk

An early definition of the term *risk* related to earthquakes were given in the frame of UNESCO in 1978 (Algermissen et al. 1979; Fournier d' Albe 1982). In that definition, the concept of risk is considered as a multidisciplinary attribute mathematically expressed by the convolution of three attributes: *hazard*, *vulnerability*, and *value* exposed to hazard:

$$Risk = hazard * vulnerability * value \quad (8.1)$$

This definition was generalized and applied to other kinds of risks (e.g. Smith 1992) and adopted also for the tsunami risk (e.g. Papadopoulos and Dermentzopoulos 1998; Curtis and Pelinovsky 1999), which is consistent with definitions of relevant terms and glossaries (UNISDR 2009; EC-Working Paper 2010; IOC 2013). In this context hazard is a potentially damaging or destructive natural process or phenomenon, and risk is an expression of the expected natural event's impact. A direct consequence of formula (8.1) is that the hazard assessment is a prerequisite of the risk assessment.

8.4.2. Tsunami magnitude and intensity

In this point there is need to clarify the use of terms such as "tsunami magnitude" and "tsunami intensity". Sieberg (1923, 1927) was the first to introduce a 6-degree tsunami intensity scale which is analogous to the 12-degree seismic intensity scales, e.g. the Mercalli-Sieberg scale (see also in Ambraseys, 1962). In the seismological tradition the term "intensity" is not a physical feature of the earthquake event but an expression of the earthquake impact level. In this sense the Sieberg's scale followed the seismological tradition.

Imamura (1942, 1949), Iida (1956, 1970) and Iida et al. (1967) introduced the concept of tsunami magnitude and adopted that the tsunami maximum height, H_{max} (in m), observed in the coast or measured in tide-gauge records, can be considered as a metric of tsunami magnitude, m:

$$m = \log_2 H_{max} \qquad (8.2)$$

The Imamura-Iida magnitude scale was arranged to consist of 6 points with range from –1 to 4. Soloviev (1970) and Soloviev and Go (1974) proposed an improvement of the Imamura-Iida's scale and introduced the concept of tsunami intensity, S, expressed by:

$$S = \log_2 \sqrt{2}(H) \qquad (8.3)$$

where H (in m) is the mean tsunami height measured in the coast closest to the source. However, as Papadopoulos and Imamura (2001) noted, H is still a physical quantity and, therefore, it is rather an expression of tsunami magnitude than of tsunami intensity. A scale measuring tsunami size was proposed by Shuto (1993)

$$i = \log_2 H \qquad (8.4)$$

where H is the local tsunami height (in m). Shuto's (1993) intension was to use formula (8.4) for the establishment of an intensity scale for the description of tsunami damage. Therefore, he proposed to define H according to its possible impact; in this sense H is taken as the tsunami crest height above the ground level at the shoreline. Eventually, a 6-grade classification of tsunami impact index, i, was organized for the description of the expected tsunami impact as a function of H, with i ranging from 0 to 5.

The distinction between tsunami intensity and tsunami magnitude became more clear after the introduction of several approaches for the establishment of tsunami magnitude scales by several authors including Hatori (1979), Abe (1979, 1985, 1989), Murty and Loomis (1980), Okal and Titov (2007). All the relevant efforts followed the seismological tradition in establishing earthquake magnitude scales. Papadopoulos and Imamura (2001) introduced for the first time a 12-grade tsunami intensity scale which is analogues to the 12-grade macroseismic scales. The reviews by Papadopoulos

and Imamura (2001) and Papadopoulos et al. (2020) have contributed substantially to discriminate between tsunami magnitude and tsunami intensity in the frame of the long-lasting seismological tradition.

8.4.3 Methods for the tsunami hazard and risk assessment

The various methodologies proposed for the tsunami hazard assessment can be grouped in the scenario-based and the probability-based approaches. Several authors were based on a variety of deterministic or probabilistic models to assess tsunami hazard (e.g. Rikitake and Aida 1988; Hebert et al. 2005; Tinti et al. 2005; Geist and Parsons 2006; Burbidge et al. 2008; Lorito et al. 2007; Power et al., 2012; Sørensen et al. 2012; Løvholt et al. 2015; Li et al. 2016; Davies et al. 2017, Basili et al., 2021; see also review in Behrens et al. 2021). The deterministic approach is usually based on the largest sources (*extreme tsunami scenario*) for the study area or on the so-called *worst-case credible tsunami scenario*. On the other hand, various models or approaches have been tested to assess vulnerability, exposure and risk (e.g. Pararas-Carayannis 1988; Qinghai and Adams 1988; Karim and Yamazaki 2003; Papathoma and Dominey-Howes 2003; Papathoma et al. 2003; Sato et al. 2003; Kulikov et al. 2005; Dias et al. 2009; Omira et al. 2010; Dall' Osso et al. 2010; 2016; Gardi et al. 2011; Strunz et al. 2011; Tonini et al. 2011; Valencia et al. 2011; Wegscheider et al. 2011; Jelínek et al. 2012; Benchekroun et al. 2013; Suppasri et al. 2013a,b; Yeh et al. 2013; Charvet et al. 2014; González-Riancho et al. 2014; Leelawat et al. 2014; Tarbotton et al. 2015; Pagnoni et al. 2015, Pagnoni and Tinti 2016).

Each one of the several components involved in the tsunami risk assessment is susceptible to a variety of epistemic and aleatory uncertainties. Therefore, risk assessment is a highly complex procedure which also suffers from uncertainties of various origins. As a consequence, the several qualitative, semi-quantitative or fully quantitative approaches, which have been tested so far, are quite variable and closely dependent on the data availability as well as on the reliability and quality of the data. For this reason, no standard methodologies have been concluded so far, although some general recommendations for tsunami risk assessment have been organized (e.g. Jelínek and Krausmann 2008; IOC 2009, 2013; Hettiarachchi et al. 2011). In this context, no abundant studies are available on the quantitative risk assessment in terms of expected economic losses due to tsunami building replacement, which includes both repairable damage and building reconstruction if unrepairable destruction occurs. Such losses have been expressed using as metrics either the probable maximum loss for a given return period of the extreme tsunami event (e.g. Dominey-Howes et al. 2010) or the probabilistic average annual loss and the loss exceedance curve (e.g. Jaimes et al. 2016; Goda and Song 2019).

8.5. The extreme scenario approach – Heraklion (Crete) test-site

8.5.1 Introductory remarks

A scenario-based tsunami risk assessment approach is suitable where the available historical tsunami data are not sufficient to organize reliable tsunami statistics, e.g. magnitude-frequency relationships (e.g. Nadim and Glade 2006; Pagnoni and Tinti 2016; Rehman and Cho 2016). Although this approach does not provide probabilistic information it has the advantage that historical data combined with results of wave numerical simulation yield the tsunami physical features needed for the determination of the hazard (inundation) zone expected from the selected extreme event. Several assets of the anthropogenic system, such as buildings, infrastructures and life lines, vessels and other property, cultivated land, population, insured and non-insured values, are exposed to tsunami hazard. In this report we selected to focus on the quantitative risk assessment in terms of economic losses due to the need for building replacement.

In the Mediterranean and the adjacent seas only a few relevant studies were performed so far. In Istanbul, Marmara Sea, in a study performed by Hancilar (2012) only the exposure of buildings to tsunami inundation was approached but no estimation of physical tsunami damages to buildings was estimated. Therefore, the total monetary value of the exposed buildings was calculated only as an indicative figure. Pagnoni et al. (2015) performed scenario-based assessment of building damage and population exposure due to earthquake-induced tsunamis for the town of Alexandria, Egypt, and estimated the amount of buildings that may suffer damage of various levels. Tsunami vulnerability and damage models for the town of Syracuse, Sicily (Italy), were tested by Pagnoni and Tinti (2016).

8.5.2 The test site

In our research (Triantafyllou et al., 2018) we selected to apply the extreme scenario method and to calculate the expected economic losses at the moment of the study performance in terms of absolute monetary cost for building replacement due to disaster after an extreme tsunami attack. The coastal segment to the west of Heraklion, the capital city of Crete Isl., Greece (Fig. 8.12), was selected as one of the test-sites for the European tsunami research project ASTARTE (EU-FP7, 2013-2017) for the reason that the coastal zone of Heraklion and its surroundings is highly exposed to tsunamis. Studies towards assessing tsunami risk and vulnerability in Heraklion were performed several years ago (e.g. Papadopoulos and Dermentzopoulos 1998; Papathoma et al. 2003). However, neither building vulnerability nor risk assessments were quantitatively included in those early studies. In our study we developed a methodology for the *ex-ante* tsunami risk estimation in terms of absolute monetary values. The new contribution relies on that we propose to translate to building replacement cost the direct building physical damage due to tsunami attack. Building replacement includes either

repair or reconstruction. The method was tested in Heraklion based on the extreme tsunami scenario concept, on the determination of the inundation zone through tsunami numerical modelling and on the use of GIS tools for mapping and estimation of building damage levels and the resulting replacement costs.

Figure 8.12. The study area of the western segment of Heraklion city (Gazi), Crete Isl., in Google Earth map. The area is characterized by the Yofiros river and the nearby stadium in the eastern side, by the Xeropotamos river and a free of buildings area in the central side and by the motorway running from east to west at the south side (see details in Triantafyllou et al., 2018).

8.5.3 Work Flow

The methodology proposed for the building risk assessment follows a work flow (Fig. 8.13) which is adjusted to the adopted concept, i.e. risk is a convolution of three main factors according to the equation (1). To this aim we estimated quantitatively each one of the three main parameters involved in the adopted risk concept: tsunami hazard, building vulnerability, building values exposed to tsunami hazard. Finally, the risk was assessed in terms of expected absolute economic cost for building replacement.

The steps followed according to this flow chart are the next: (a) selection of a testing coastal segment (Heraklion) and of the worst case scenario (the Minoan volcanic tsunami was selected); (b) tsunami numerical simulation; (c) determination and GIS mapping of the inundation (hazard) zone through tsunami numerical simulation; (d) assessment and GIS mapping of the building exposure based on types of building material and use; (e) calculation with the use of GIS tools of the expected damage level as a function of the building type and the water depth, i.e. the depth of the sea water column in the inundation zone; (f) calculation of absolute monetary cost from the number of buildings that would need replacement, i.e. either only reparation or complete reconstruction due to damage beyond repair. Steps (a)-(c) represent the tsunami hazard determination, while building vulnerability

assessment is represented by steps (d) and (e). The final step (f) represents the building value exposed to hazard. Then, it is possible to perform an *ex-ante* calculation of the expected economic losses in terms of absolute monetary cost for building replacement.

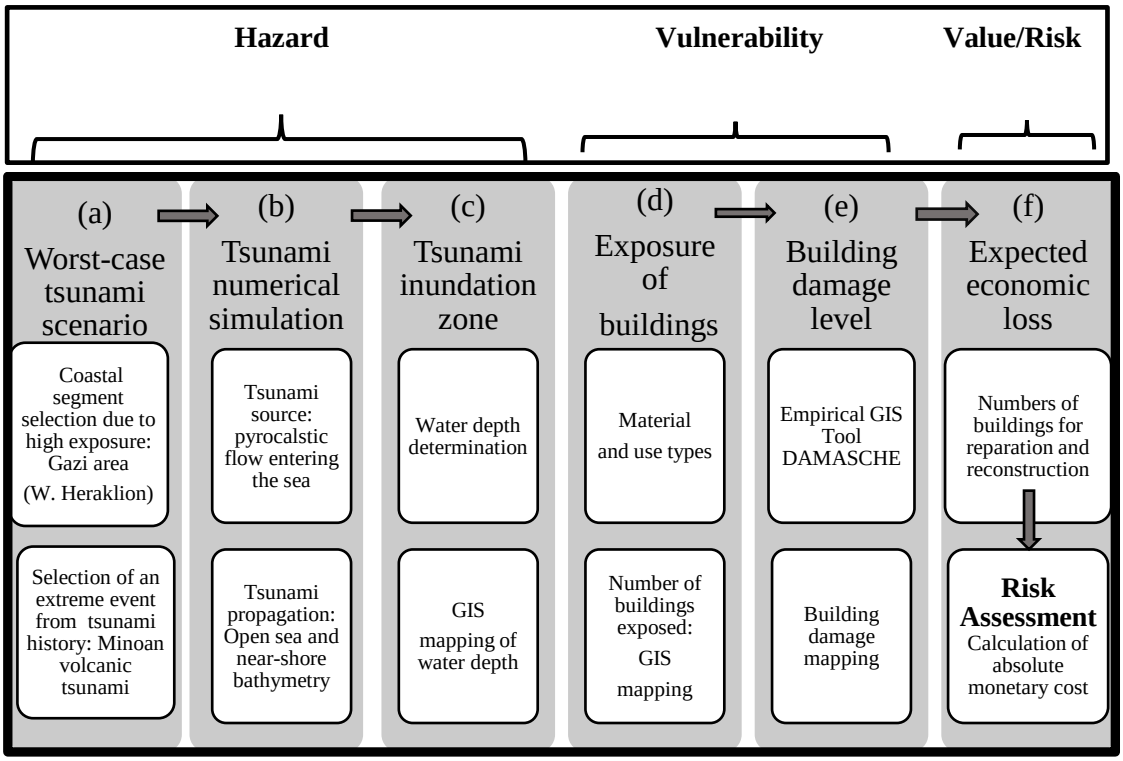

Figure 8.13. Flow chart of the procedures followed to calculate expected losses due to tsunami building damage in terms of absolute monetary cost (Triantafyllou et al., 2018).

The numerical simulation results showed that the maximum water depth obtained is about 14 m (Fig. 8.14). Water depth of 0.5 m has been considered as the lowest value for the determination of the inundation zone. This consideration is based on that the 0.5 m value is the lowest limit for a tsunami to become damaging according to the decision matrix decided to be used for tsunami warning purposes in the frame of the North-Eastern and Mediterranean Tsunami Warning System/UNESCO (e.g. Tinti et al., 2012). In the coastal zone examined the width of the inundation zone with water depth of more than ~ 0.5 m ranges from ~350 m to ~1000 m with the exception of the eastern side of the area where the inundation zone width reached ~1.2 km due to the existence of a local river mouth.

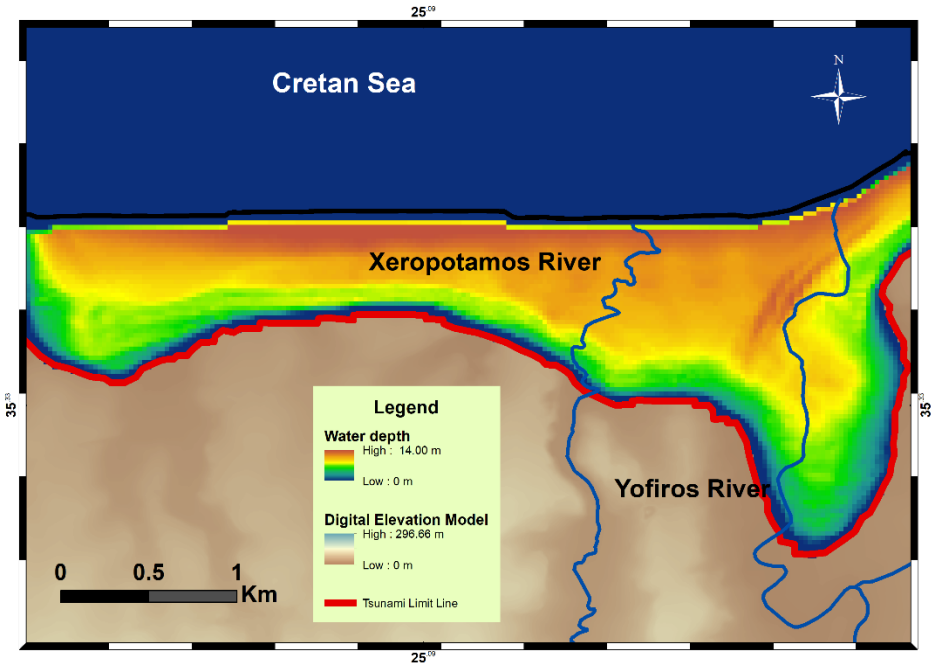

Figure 8.14. Tsunami inundation zone and the DEM beyond this zone in the study area (Triantafyllou et al., 2018).

8.5.4 Vulnerability assessment with the DAMASCHE GIS tool

The building vulnerability assessment has been performed with the application of a relevant GIS tool, called DAMASCHE, developed in the frame of the EU-FP6 project SCHEMA and tested in various test sites of the European and the Mediterranean region (Gardi et al. 2009, Valencia et al. 2011). The tool is based on data collected in the aftermath of the Indian Ocean 26 December 2004 tsunami and relates the damage level with the building structural material and the water depth (Table 8.1). The results obtained are illustrated in Figure 8.15.

Table 8.1. Building damage level as a function of the water depth (in m) in the inundation zone (Gardi et al. 2009; Valencia et al., 2011). The building classification is according to the construction material types listed in Table 8.2.

Damage level		Class A	Class B	Class C	Class D	Class E
No damage	D_0	0 m	0 m	0 m	0 m	0 m
Light damage	D_1	0 – 1.8 m	0 – 2 m	0 – 2.5 m	0 – 2 m	0 – 3 m
Important damage	D_2	1.8– 2.2 m	2 – 3 m	2.5 – 4 m	2 – 4.5 m	3 – 6 m
Heavy damage	D_3	2.2– 2.6 m	3 – 4 m	4 – 6 m	4.5 –6.5 m	6 – 9.5 m
Partial collapse	D_4	2.6– 3.8 m	4 – 5 m	6 – 8 m	6.5 – 9 m	9.5–12.5m
Total collapse	D_5	> 3.8 m	> 5 m	> 8 m	> 9 m	> 12.5 m

Table 8.2. Building vulnerability classification (Leone et al. 2011).

Building Class	Type of buildings
A	Light constructions on wood or timber without any design
B	Brick not reinforced masonry
C	Brick with reinforced column and masonry filling
D	Collective buildings, no concrete reinforced
E	Well-designed buildings, made of reinforced concrete with columns and infill walls.

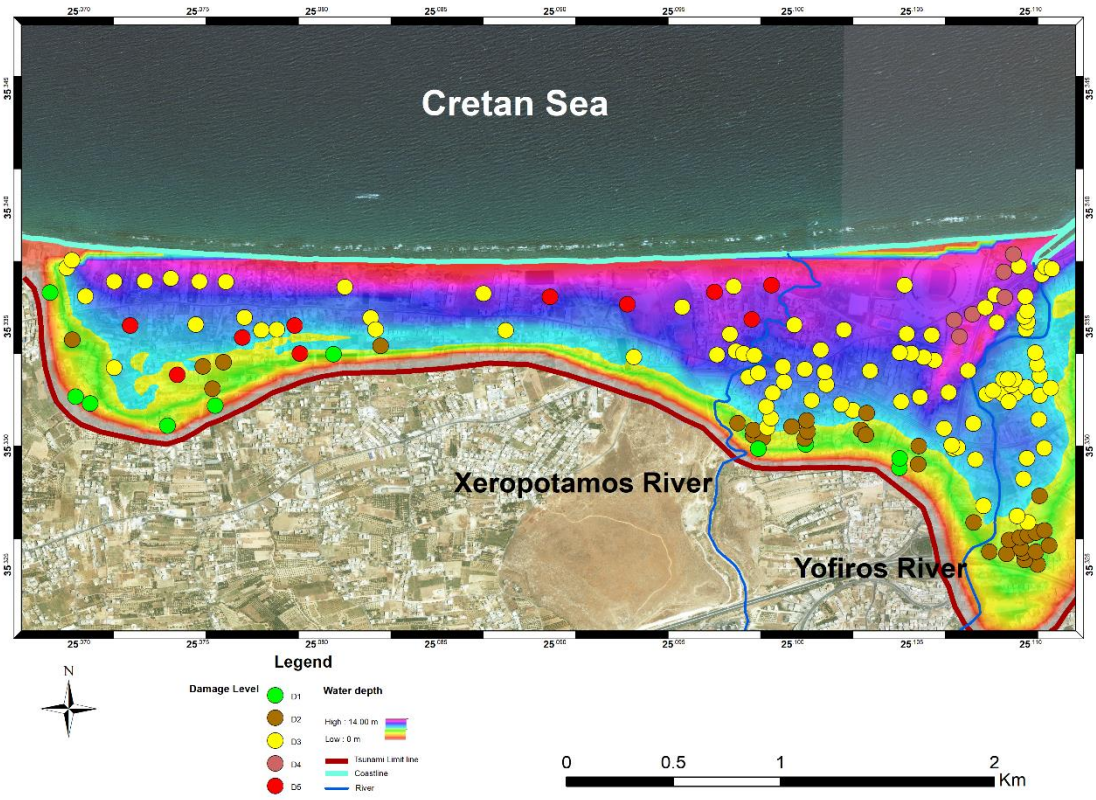

Figure 8.15. Mapping of the tsunami inundation zone with water depth (in m) and building damage level per building block as determined from the application of the DAMASCHE GIS tool (Triantafyllou et al., 2018).

8.5.5 Estimation of the cost expected from the tsunami impact to buildings

In order to calculate the cost expected from the tsunami impact to buildings we took into account that no strong, damaging tsunamis have affected the Mediterranean region in the last 62 years or so and consequently no building damage data are available. Consequently, for the cost implied by building replacement due to tsunami damage we considered as a proxy the cost implied by earthquake building damage. To this aim, we adopted the official cost rates declared by the Greek government for the State Housing Aid program put in force after the strong damaging earthquakes that hit Cephalonia Isl., Ionian Sea, on 24th January and 3rd February 2014 with magnitudes M_w=6.0 and M_w=5.9, respectively.

The results obtained for building reparation cost are summarized in Table 8.3, which shows that for the suggested extreme tsunami scenario the estimated cost to the state is in the order of 52 million Euros. For the calculation of the cost for building reconstruction we considered damage levels of D4 (partial collapse) and D5 (total collapse). In this case the calculated cost for reconstruction (Table 8.4) is about 5.5 times less than the one for reparation. The total cost for building replacement, both reparation and reconstruction, is in the order of 61 million Euros.

Table 8.3. Calculated cost for reparation of buildings suffering damage level D2 and D3 due to strong tsunami attack in the inundation area of Gazi, west of Heraklion, Crete Isl. We adopted that the ratio of residential/commercial buildings equals 4 and that the average surface of residential and commercial buildings is 100 m^2 and 80 m^2, respectively. Then, the average building surface is 96 m^2.

Damage level according to Table 1	Number of buildings	Average building surface (m^2)	Cost/m^2 (€)	Cumulative cost (€)
D2	281	96	250	6,744,000
D3	1,037	96	450	44,798,400
Total	1,318			51,542,400

Table 8.4. Calculated cost for reconstruction of buildings suffering partial or total collapse (damage levels D4 and D5 combined together) due to strong tsunami attack in the inundation area of Gazi, west of Heraklion, Crete Isl.

Building use	Number of buildings	Average building surface (m^2)	Cost/m^2 (€)	Cumulative cost (€)
Residential	37	100	1,000	3,700,000
Commercial	146	80	500	5,840,000
Total	183			9,540,000

8.6 Probabilistic Tsunami Risk Assessment (PTRA) from incomplete data files

8.6.1 Maximum likelihood Probabilistic Tsunami Risk Assessment (PTRA)

The probabilistic tsunami hazard assessment (PTHA) follows in many ways the experience gained from the probabilistic seismic hazard assessment (PSHA). Details on the numerous PTHA methodologies developed so far have been reviewed in several papers including those by Geist and Parsons (2006), Orfanogiannaki and Papadopoulos (2007), Koravos et al. (2015), Smit et al. (2017, 2019), Sabah and Sil (2020), Basili et al. (2021) and Behrens et al. (2021). However, of particular interest here is the "method of incomplete files", which utilizes extreme (incomplete) and complete catalogs with different threshold magnitudes (Kijko and SelIevoll, 1989), incorporates in the calculations magnitude heterogeneity (Kijko and SelIevoll, 1992) and, in addition, incorporates the uncertainty of the earthquake-occurrence model (Kijko et al. 2016). One of the advantages of the method is that it applies even with catalogues of small number of events. The method has been tested successfully in several earthquake-prone areas of the world including Greece (e.g. Papadopoulos and Kijko, 1991).

The method of incomplete files is quite promising for the PTHA. The reason is that the tsunami catalogues are highly incomplete and uncertain and characterized by relatively small numbers of events and of size heterogeneity. The approach is focused on the empirical assessment of the tsunami recurrence parameters, i.e. the mean tsunami activity rate λ_T, the frequency-magnitude power law b_T-value, and the coastline-characteristic, maximum possible tsunami size using only tsunami event catalogues (Kijko and Smith 2017, Smit et al., 2017, 2019). The mean (annual) tsunami activity (occurrence) rate λ_T describes the number of tsunamis expected to occur within specified stretch of coastline with size equal to or larger than $s_{\min}$ within a unit of time, e.g. 1 year. In PTHA the parameter b_T plays the same role as the parameter b_{GR} in the frequency-magnitude Gutenberg-Richter relationship for earthquakes. Empirical studies show that the tsunami size follows the same power-law distribution as the earthquake magnitude, M, when the applied scale of tsunami size is one of the scales introduced by Sieberg (1927), Soloviev (1970), Ambraseys (1962) or Papadopoulos and Imamura (2001). Perhaps the most difficult parameter to assess is the coastline characteristic maximum possible tsunami size $s_{\max}$. In this method the assessment of this parameter is done in a similar way as the assessment of the regional characteristic maximum possible earthquake magnitude $M_{\max}$.

The three characteristic recurrence parameters are estimated by maximum likelihood techniques, while the errors involved in the tsunami size are modeled by Gaussian distribution. The uncertainties involved in the recurrence parameters are estimated through the formalism called "Weighted

Maximum Likelihood-WML" (Schoenberg, 1997). Regardless the quality of the data, prehistoric and historic information can be combined with instrumental records (Figure 8.16) using Bayesian statistics (see details in Smit et al., 2017, 2019).

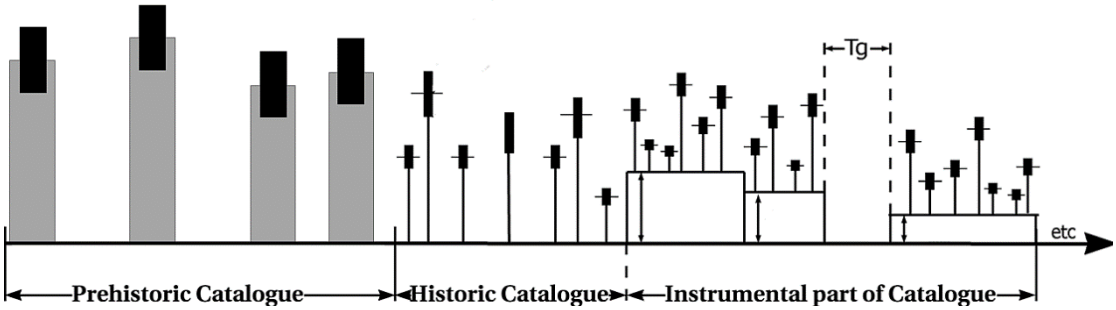

Figure 8.16. Typical illustration of data used for assessment of model recurrence parameters based on prehistoric, historic, and instrumental datasets; vertical dimension expresses event size (e.g. magnitude or intensity). Prehistoric data are subject to uncertainty relevant to the time of occurrence, the exact size of the event, and incompleteness in terms of the probability of detecting an event. Historic data, consisting of the largest observed events, and instrumental datasets are subject to incompleteness and uncertainty relevant to the observed event size, varying levels of certainty regarding the exact location of an event, and varying probabilities of all events above a certain minimum size being observed. Time gaps T_g represent missing event records (figure adapted from Smit et al., 2019).

The method provides for incompleteness of the tsunami catalogue, uncertainty in the tsunami intensity determination, and uncertainty associated with the parameters in the applied tsunami occurrence models. Aleatory and epistemic uncertainty is introduced in the tsunami models by means of the use of mixture distributions. Both the mean tsunami activity rate λ_T of the Poisson occurrence model, and the b_T-value of the frequency-size power law relationship, are random variables. The outputs include estimates of the probabilities of exceedance and return periods of given tsunami size levels. The work flow of the method is illustrated in Figure 8.17.

The several approaches used for the PTHA in general follow the tradition for the probabilistic seismic hazard assessment (PSHA).

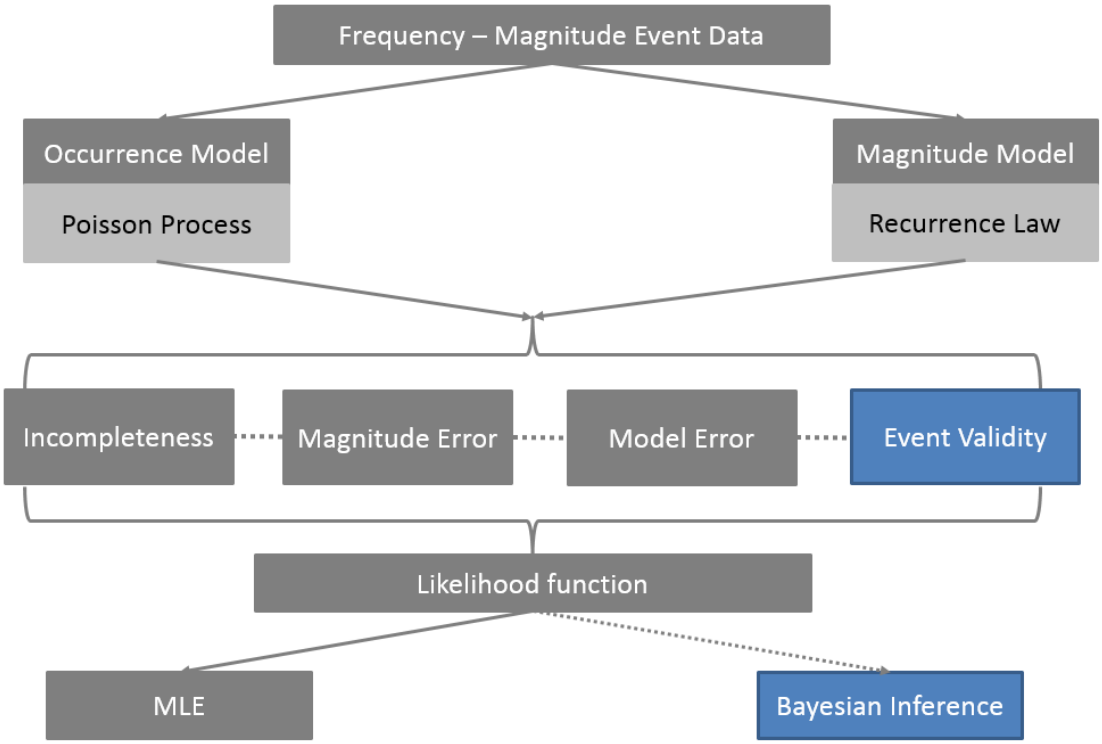

Figure 8.17. Flow diagram of the methodological steps followed for the probabilistic tsunami hazard assessment (PTHA) with maximum likelihood estimate (MLE) with the use of incomplete and uncertain tsunami catalogue data sets (figure adapted from Smit et al., 2019).

In spite of the progress noted in PTHA, very little progress has been made as regards the probabilistic tsunami risk assessment (PTRA)(Attary et al. 2019, Song and Goda 2019, Jaimes et al. 2016, Løvholt et al. 2015, Behrens et al. 2021 presented an exhaustive review on research gaps in PTHA and PTRA). This is due to that for the hazard assessment data only on the physical parameters of the events are needed while for the risk assessment vulnerability and value data are also required. Tsunami vulnerability data, however, are limited worldwide and lacking in the Mediterranean Sea. In addition, the existing tsunami catalogues are complete only in the last few decades. In view of these limitations the PTRA could be approached with methodologies that consider tsunami intensity as a metric of risk and, on the other hand, utilize incomplete and uncertain data files.

As noted earlier, however, the concept of tsunami intensity, according to the Soloviev's (1970) definition, in reality is a concept of tsunami magnitude. For this reason, Smit et al. (2017, 2019), although used the term tsunami intensity as a metric of tsunami size, they correctly are referring to PTHA than to PTRA. In order to advance the method and obtain a "real" PTRA approach there is need to use "real" tsunami intensity as a metric of risk. In this prospect we applied the methodology developed by Smit et al. (2017, 2019) with Greek tsunami event catalogues incorporating tsunami intensity data. The maximum likelihood estimates have been made by following the procedure by Kijko and Sellevoll (1989).

8.6.2 Maximum likelihood PTRA in Greek test-sites: tsunami data

The methodology described in the section 8.6.1 has been applied with three tsunami data sets for three selected coastal cities which suffered from destructive tsunamis in the past: (1) Rhodes city (Rhodes island), (2) Heraklion city (Crete island), (3) Aegion city (western Corinth Gulf, central Greece) (Fig. 8.3). The three data sets include events of both the historic and instrumental periods but for Heraklion and Aegion palaeotsunami data are also available. The data used are listed in Table 8.6 and explained in the next lines. The tsunami size is expressed in terms of tsunami intensity in the 12-grade scale (Papadopoulos and Imamura, 2001). The reliability of an event, R, scales from 0 to 1; R=0 means no tsunami event, R=0.5 means 50% confidence, R=1 means 100% confidence.

The tsunami data (Table 8.5) have been collected from the data compilations by Papadopoulos et al. (2014a) and Papadopoulos (2011, 2014, 2015). In Rhodes, the event 2017 has been the tsunami generated by the Bodrum-Kos strong earthquake (M_w=6.6) of 20 July 2020 and was recorded with small amplitude by the tide-gauge station in Kalathos. In Heraklion, the 2020 event is the tsunami generated by the Samos large earthquake (M_w=7.0) of 30 October 2020 and was recorded with small amplitude by the tide-gauge station in Heraklion. In the same area, the event -1613 is the Minoan tsunami generated by the Late Bronge Age Thera (Santorini) eruption. The Minoan tsunami was a large event leaving behind sediment deposits in several coastal sites in the east Mediterranean. Therefore, intensity K=10 has been adopted.

Table 8.5. Tsunami data used for the PTIA in the cities of Rhodes, Heraklion and Aegion. Symbol key: K=tsunami intensity in the 12-grade scale by Papadopoulos and Imamura (2001), SD(K)=standard deviation of K, R=reliability, symbol – means BC.

Year	month	day	K	SD(K)	R
Test site: *Rhodes*					
148	**7**	**1**	7	1.0	0.5
1303	8	8	7	0.5	1.0
1481	3	5	7	0.5	1.0
1609	4	**15**	8	1.0	0.75
1741	1	31	8	0.5	1.0
1956	7	9	1	1.0	1.0
2002	3	24	5	1.0	1.0
2012	6	10	2	0.5	0.75
2017	7	20	1	0.5	1.0
Test site: *Heraklion*					
-1613	**7**	**1**	**10**	1.0	1.0
1303	8	8	10	1.0	1.0

1494	7	1	4	1.0	0.75
1612	11	8	4	1.0	0.75
1650	10	10	6	1.0	1.0
1741	2	15	4	1.0	0.75
1956	7	9	5	0.5	1.0
2000	4	5	4	0.5	1.0
2020	10	30	1	0	1.0
Test site: *Aegion*					
-2750	**7**	**1**	**7**	1.0	0.75
-1050	**7**	**1**	**7**	1.0	0.5
-550	**7**	**1**	**7**	1.0	0.5
-373	**12**	**15**	9	1.0	1.0
1742	2	21	5	1.0	0.75
1748	5	25	9	0.5	1.0
1817	8	23	8	0.5	1.0
1861	12	26	3.5	0.5	1.0
1963	2	7	7	0.5	1.0
1995	6	15	3	0.5	1.0
1996	1	1	5	0.5	1.0

Paleotsunami data of 2750, 1050 and 550 BC in Aegion test site have been taken from Kontopoulos and Avramidis (2003) and Kortekaas et al. (2011). Since no dates are known for the paleotsunami events, the date 1st July has been conventionally given. In addition, for paleotsunami events no intensities are known. However, these tsunamis should have been strong enough to leave behind tsunami sediment deposits. Consequently intensity K=7 has been adopted. However, due to the geological uncertainties involved in the recognition of the deposits as such, reliability R=0.5 has been decided with the exception of the event -2750 to which R=0.75 was given for the reason that it was recognized in the Aliki site, near Aegion, by Kontopoulos and Avramidis (2003), as well as in Kirra, north coast of Corinth Gulf, by Kortekaas et al. (2011).

The paleotsunami data are more uncertain as compared to the data of the historical and instrumental periods. To test how the results are influenced by the inclusion or exclusion of paleotsunami events in the data sets, the calculations for Heraklion and Aegion were performed with two data sets, one with the inclusion of paleotsunamis and another without paleotsunamis.

8.6.3. Maximum likelihood PTRA in Greek test-sites: results and sensitivity analysis

The results obtained for each one of the three test-sites provide the return period, RP in years, of tsunami intensity, K, and the probability of exceedance, P, of a certain intensity value in time intervals

of 1, 10, 50 and 100 years. RP has been calculated for K values of 4, 6 and 8. Intensity K=4 means that the tsunami is largely observed by the people but is not damaging. For K=6 the tsunami is slightly damaging but for K=8 the tsunami is heavily damaging. The results obtained are summarized in Table 8.6 and illustrated in Figures 8.18-8.20 for Rhodes, in Figures 8.21-8.23 for Heraklion, and in Figures 8.24-8.26 for Aegion. To compare the results among the three test-sites we use the values of λ, RP and P each one notated with the subscripts R for Rhodes, H for Heraklion and A for Aegion. RP's are in years while λ is in events/year.

From the Table 8.6 it comes out that for intensity K=4 we get $\lambda_R > \lambda_H > \lambda_A$. In other words the low intensity, non-damaging tsunamis are more frequent in Rhodes, less frequent in Heraklion and even less frequent in Aegion. This is also shown by that RP_R=57.6, RP_H=67.8 and RP_A=93.4. We also observe that RP_H=78.7 and RP_A=92.4 if no paleotsunamis are considered for Heraklion and Aegion. This implies the RP in Heraklion increases significantly if the one paleotsunami event is omitted. On the contrary, the RP in Aegion does not change significantly if the three paleotsunamis are considered.

Table 8.6. Results of the probabilistic tsunami risk assessment in three test sites. Key: K=tsunami intensity (scale by Papadopoulos and Imamura, 2001), λ=tsunami activity rate (events/yr), RP=Return Period (yrs), P=probability of exceedance in T years.

No.	K	λ	RP	P (T=1)	P (T=10)	P (T=50)	P (T=100)
Test site: *Rhodes*							
	4	1.7348e-02	5.76e+01	0.0172	0.1585	0.5703	0.8074
	6	5.7699e-03	1.73e+02	0.0058	0.0560	0.2487	0.4327
	8	4.9890e-04	2.00e+03	0.0005	0.0050	0.0246	0.0486
Test site: *Heraklion* *(including paleotsunamis)*							
	4	1.4746e-02	6.78e+01	0.0146	0.1365	0.5136	0.7560
	6	6.5659e-03	1.52e+02	0.0065	0.0634	0.2775	0.4745
	8	2.3835e-03	4.20e+02	0.0024	0.0235	0.1120	0.2107
Test site: *Heraklion* *(excluding paleotsunamis)*							
	4	1.2714e-02	7.87e+01	0.0126	0.1189	0.4639	0.7058
	6	5.2033e-03	1.92e+02	0.0052	0.0506	0.2275	0.4007
	8	1.7635e-03	5.67e+02	0.0018	0.0175	0.0842	0.1609
Test site: Aegion *(including paleotsunamis)*							
	4	1.0707e-02	9.34e+01	0.0106	0.1012	0.4094	0.6453
	6	2.8384e-03	3.52e+02	0.0028	0.0280	0.1318	0.2452
	8	5.3196e-04	1.88e+03	0.0005	0.0053	0.0262	0.0517
Test site: *Aegion* *(excluding paleotsunamis)*							
	4	1.0819e-02	9.24e+01	0.0108	0.1022	0.4126	0.6490
	6	3.4115e-03	2.93e+02	0.0034	0.0335	0.1561	0.2865
	8	7.2727e-04	1.38e+03	0.0007	0.0072	0.0357	0.0700

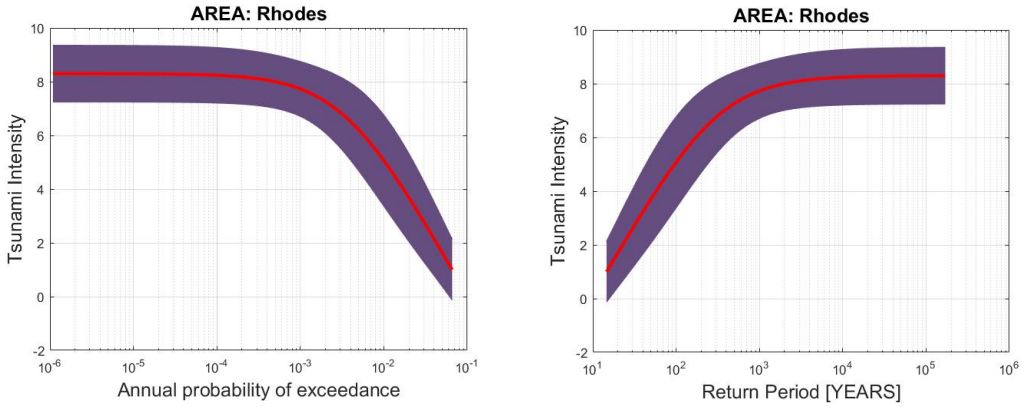

Figure 8.18. Annual probability of exceedance (left) and return period (right) of tsunami intensity values for the city of Rhodes; tsunami intensity in 12-grade scale.

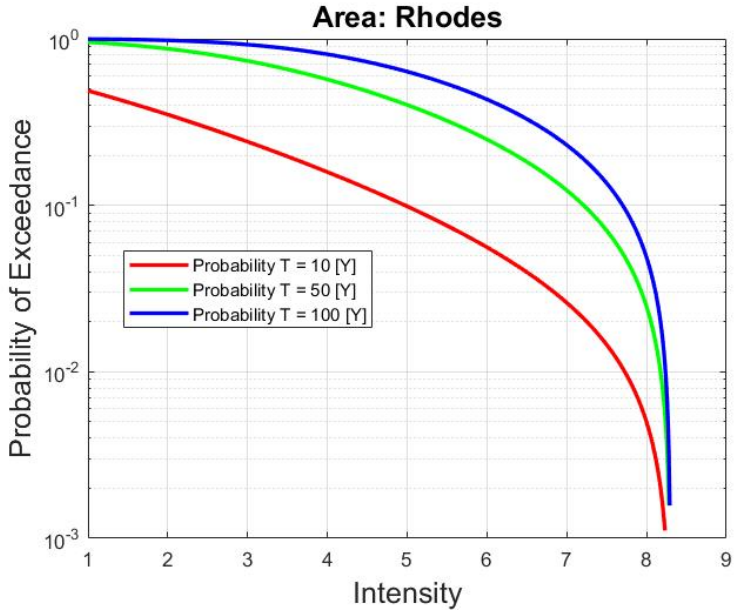

Figure 8.19. Probability of exceedance of tsunami intensity values for the city of Rhodes for return periods of 10, 50 and 100 years; tsunami intensity in 12-grade scale.

For intensity K=6 we get $\lambda_H > \lambda_A > \lambda_R$, which indicates that slightly damaging tsunamis are more frequent in Heraklion and then in Aegion and in Rhodes. This result is reflected in the repeat times obtained: RP_H=152, RP_R=173 and RP_A=352. However, if we do not take into account the paleotsunami events in the Heraklion and Aegion data sets, then we have $\lambda_R > \lambda_H > \lambda_A$ and RP_H=192, RP_A=173 and RP_A=293. These results underlines again the importance of including or excluding paleotsunami events in the data sets.

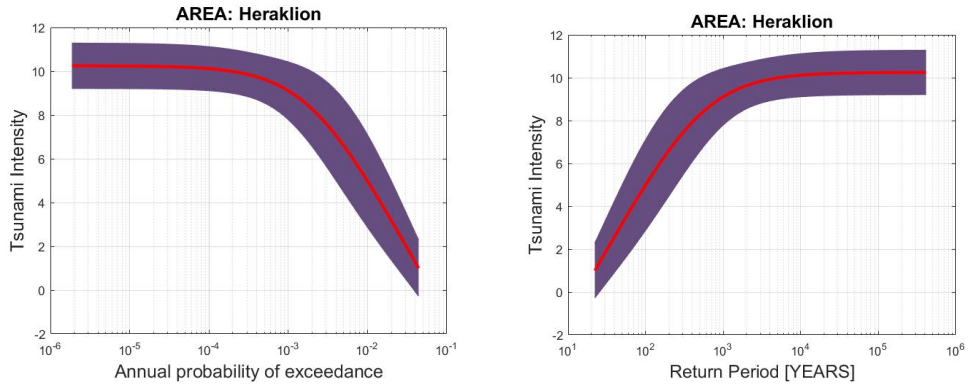

Figure 8.20. Annual probability of exceedance (left) and return period (right) of tsunami intensity values for the city of Heraklion; tsunami intensity in 12-grade scale.

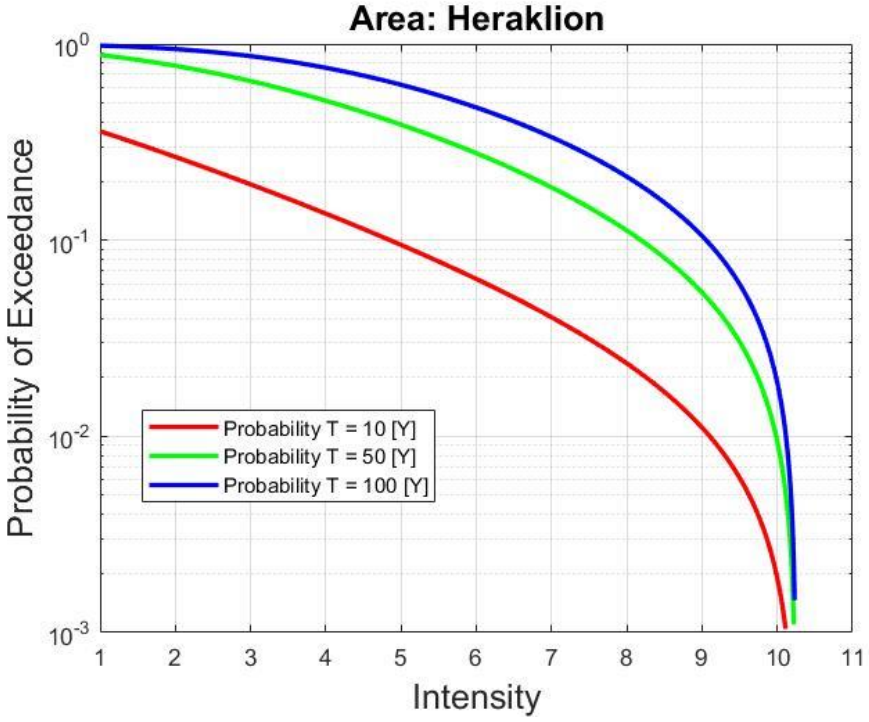

Figure 8.21. Probability of exceedance of tsunami intensity values for the city of Heraklion, including paleotsunami data, for return periods of 10, 50 and 100 years; tsunami intensity in 12-grade scale.

For intensity K=8 we get $\lambda_H>\lambda_R>\lambda_A$, which indicates that heavily damaging tsunamis are more frequent in Heraklion and then in Rhodes and in Aegion. This result is also reflected in the repeat times obtained: RP_H=2000, RP_H=420 and RP_A=1880. However, if we do not take into account the paleotsunami events in the Heraklion and Aegion data sets, then we have again $\lambda_H>\lambda_R>\lambda_A$ and RP_R=2000, RP_H=567 and RP_A=1380. We observe that the repeat time in Heraklion increases significantly while in Aegion decreases significantly. These results underline again the importance of including or excluding paleotsunami events in the data sets. The probability of exceedance of K=8 in 100 years in Rhodes, Heraklion and Aegion is P_R=0.0486, P_H=0.2107 and P_A=0.0517, respectively. However, the exclusion of paleotsunami events returns P_H=0.1609 and P_A=0.0700.

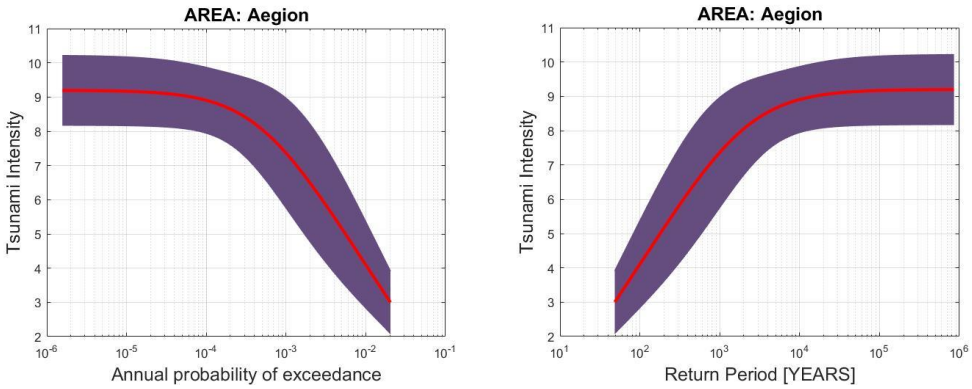

Figure 8.22. Annual probability of exceedance (left) and return period (right) of tsunami intensity values for the city of Aegion; tsunami intensity in 12-grade scale.

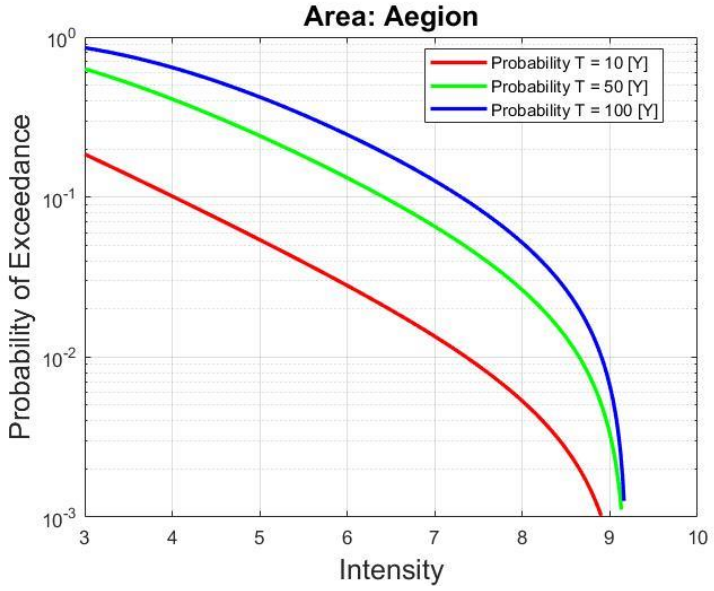

Figure 8.23. Probability of exceedance of tsunami intensity values for the city of Aegion, including paleotsunami data, for return periods of 10, 50 and 100 years; tsunami intensity in 12-grade scale.

8.7 Summary of Chapter 8

The Greek Tsunami Impact Database (GTIDB) has been organized for the first time as a supplement of the Greek Earthquake Impact Database (GEIDB). A number of 16 damaging or destructive tsunami events have been inserted in the GTIDB for the reference period 1800-2020. The large tsunami of 9 July 1956 has been the most destructive in that period. In general, however, the overall tsunami impact is extremely low as compared to the earthquake impact. Two case studies were performed: one for the 8 November 1905 tsunami in Mt Athos, North Aegean Sea area, which revealed only very recently from documentary sources (Triantafyllou et al., 2020a), and another for the very recent event of 30 October 2020 Samos tsunami (Triantafyllou et al., 2021). The tsunami risk assessment has been approached with the extreme scenario method, selecting the Heraklion city in Crete as a test-site (Triantafyllou et al., 2018) as well as with a maximum likelihood Probabilistic Tsunami Risk Assessment method with the use of incomplete and complete data files.

9. CONCLUSIONS AND DISCUSSION

The compilation of earthquake impact data is multifold useful since it helps to better understand the seismic past of an area and to better prepare for the seismic future of the area. The Greek region is characterized by very high seismicity and earthquake phenomena are documented since the 6th century BC. Although earthquake impact data can be found in a countless number of books, scientific publications, technical reports, press reports, historical documents and various archives, so far they have not been compiled in a unified way and in a digital form. This is the first time that such an effort was undertaken and this has been the first main objective of the present thesis, i.e. the organization of the Greek Earthquake Impact Database (GEIDB). Another major objective of our study has been the investigation of the patterns of variations of the earthquake impact in time and space as well as their dependence on various physical factors, such as the seismicity parameters and the intensity of the earthquakes. The achievement of these two main objectives required for an extensive effort in three directions: (i) compilation of earthquake impact data, (ii) selection of the "best" seismicity parameters, and (iii) the selection of appropriate Earthquake Impact Metrics (EIMs).

A first statistics showed that earthquake impact data in Greece are mainly available since AD 1800. Therefore the reference period for this study has been from 1800 to 2020 inclusive. Earthquake impact data were collected for that period and for the current Greek territory. However, it is still of interest to collect data for the pre-1800 time period for the reason that the results expected could help to reconsider historical seismology issues and, on the other hand, to better understand the long-term impact of the earthquakes in a highly seismogenic region.

The data collected and inserted in the GEIDB concern the impact of earthquakes on the population and on the built environment. From the examination of a very long number of written sources, and from the observations performed during our post-event field surveys in the last years, it has been possible to collect parametric or descriptive data on the fatalities and injuries caused as well as on the buildings that suffered repairable or unrepairable damage from 248 earthquakes occurring in the reference period. There is no doubt that the impact data collected are neither complete nor accurate, and that their completeness and accuracy change with time. Yet, they allowed us to investigate some general patterns of the earthquake impact in Greece at least in the reference period.

The selection of the "best" seismicity parameters has not been an easy task for the reason that several earthquake catalogues are available for both the historical (19th century) and the instrumental periods and each catalogue is characterized by different features of completeness, accuracy and homogeneity. Therefore, a research strategy was decided to deal with this complicated issue. First, for the post-1975 time period earthquake magnitudes were adopted mainly from the GCMT project catalogue, while hypocentral parameters have been mainly taken from the determinations of NOA. For the entire period 1800-1975 we used modern parametric and non-parametric techniques to determine the level of the completeness magnitude in the various catalogues. In addition, we performed a comparative statistical study on the differences in magnitudes and in focal depths in the various catalogues. Based on the results obtained certain criteria were developed for the selection of the "best" seismicity parameters for the several time segments of the period of study. The results are more widely useful, e.g. for seismicity analysis and seismic hazard assessment studies, since they provide on a comparative basis a clear picture about the features that characterize the several catalogues.

For the early instrumental period of 1901-1910, however, it has been possible to re-determine magnitudes of 52 earthquakes of magnitude ~5 and over both shallow and of intermediate-depth. To this aim we utilized for the first time amplitude records of five Agamennone-type seismographs of intermediate natural period, that operated in the country in that period. The "Agamennone magnitudes" obtained have been calibrated over surface-wave magnitudes calculated since the 1960s and 1970s for earthquakes of the post-1911 time period. The missfit of the magnitudes obtained from magnitudes listed in other catalogues are small, which indicates that the method works. For earthquakes inserted in the GEIDB we adopted the average of the magnitudes from the various catalogues and the new "Agamennone magnitude". The amplitude data used are listed in the Bulletins of NOA. Since these Bulletins list amplitude data for many smaller earthquakes, this method opens the way to determine magnitudes for several events for which the epicentral locations are known from macroseismic observations listed in the Bulletins too.

The GEIDB covers the time period 1800-2020, contains 248 earthquake entries and has been organized in Access Format. Its internal structure include four main sections: the selected "best" seismicity parameters, the collected earthquake impact data, the impact metadata (macroseismic intensity) and the references file. The impact data inserted in the GEIDB are about casualties, i.e. fatalities and injuries, repairable and unrepairable building damages. Information about tsunamis is also included for the reason that tsunamis cause their own impact. Case studies on the impact of some selected earthquakes both recent (Cephalonia, 2014, Kos 2017 and Samos 2020 after post-event field surveys in the three areas) and earlier ones (Mt Athos, 1905, Kos 1926 and 1933), which remained little known, have also been performed.

Since the GEIDB is the first of this kind for Greece, possible suggestions from the community would be helpful for improvements in the future. Another prospect is the future development of GEIDB as a web database with the additional specifications needed for such a purpose. Of interest is also the extension of the GEIDB in the pre-1800 time in spite of the increased data incompleteness.

After reviewing the international literature and taking into account the types of impact data available, several EIMs were selected and their variation patterns have been investigated. A generic pattern concerns the spatial distributions of the impactful earthquakes. It has been found that most of them have their epicenters in the central and southern parts of the continental country as well as in the islands of the Central Ionian Sea. The less affected areas are the NW and NE sides of continental Greece and the "aseismic" plateau of the Central Aegean Sea. The incompleteness of the impact data does not affect this geographical pattern, which is controlled by the seismicity distribution but also of the population distribution. Although there is evidence for a seasonal pattern and diurnal variation of the numbers of fatalities, Fa, and injuries, In, the main trend is a gradual decrease with time of both metrics. At the same time, the survival ratio, In/Fa, gradually increases with time. Taking into account an approximately four-fold population increase in Greece since mid-19th century one may assume that a reasonable explanation for the survival ratio increase is the gradual construction of earthquake resistant structures, particularly after 1959 when the first the national building code was applied. This is consistent with the gradual increase of the damage ratio RB (repairable)/UB (unrepairable) buildings. On the other hand, the various metrics vary greatly in each bin of the earthquake magnitude and of the macroseismic intensity. However, the upper bound of the metrics values is well controlled by the intensity, which allows to estimate the expected maximum Fa, In, RB and UB in each

magnitude and intensity bin. These results are promising for operational utilization for the seismic risk mitigation.

To understand the tsunami impact in Greece, the Greek Tsunami Impact Database (GTIDB) has been organized as a supplement to the GEIDB. The number of impactful tsunami events that have been inserted in the GTIDB for the reference period 1800-2020 amounts to 16. Two case studies were performed for the 8 November 1905 Mt Athos tsunami, which remained unknown so far, and for the very recent event of 30 October 2020 Samos tsunami. The overall tsunami impact is extremely low as compared to the earthquake impact. The low tsunami risk has been shown with the application in three test-sites (Aegion, Heraklion, Rhodes) of a maximum likelihood Probabilistic Tsunami Risk Assessment method with the use of incomplete and complete data files. However, it is well-known that in the pre-1800 historical and prehistorical periods large tsunamis caused extensive destruction in Greece, thus verifying that tsunamis are low-frequency but high-impact natural events. In view of this an extreme scenario method was applied in Heraklion city, Crete, which was selected as a test-site for the impact assessment of a Minoan type tsunami attacking the north coast of Crete Island.

The overall concept in this thesis has been selected to support rather risk-oriented than hazard-oriented approaches. We do hope that this selection contributes to close the gap in this kind of studies in Greece and beyond.

REFERENCES

Abe, K., 1979. Size of great earthquakes of 1837-1974 inferred from tsunami data. J. Geophys. Res. 84, 1561- 1568.

Abe, K., 1985. Quantification of major earthquake tsunamis of the Japan Sea. Phys. Earth Planet. Inter. 38, 214 – 223.

Abe, K., 1989. Quantification of tsunamigenic earthquakes by the Mt scale Tectonophysics 166, 27 – 34.

Abe, K., Nogushi, S., 1983. Revision of magnitudes of large shallow earthquakes, 1897-1912. Phys. Earth Plan. Inter., 33, 1-11.

Abolmasov, B., Jovanovski, M., Feri, P., Mihali, S., 2011. Losses due to historical earthquakes in the Balkan region: Overview of publicly available data. Geofizika, 28, 161-181.

Albini, P., Antonucci, A., Locati, M., Rovida, A., 2018. Should Users Trust or Not Trust Sieberg's Erdbebengeographie (1932)?. Seismological Research Letters. 90. 10.1785/0220180187.

Alexander, D., 1985. Death and injury in earthquakes Disasters, 9, 57-60.

Algermissen, S.T., Perkins, D.M., Isherwood, W., Gordon, D., Reagor, G., Howard, C., 1979. Seismic risk evaluation of the Balkan region. Proc. Sem. Seismic Zoning Maps, UNESCO, Skopje 1976, 2, 172-240.

Altunel, E., Stewart, I., Barka, A., Piccardi, L., 2003. Earthquake Faulting at Ancient Cnidus, SW Turkey. Turkish J. Earth Sci., 12(1), 137-151

Ambraseys, N.N., 1962. Data for the investigation of seismic sea waves in the Eastern Mediterranean Bull. Seism. Soc. Am. 52, 895-913.

Ambraseys, N.N., 2001. Assessment of surface-wave magnitudes of earthquakes in Greece. J. Seismol., 5, 103-116.

Ambraseys, N.N., 2009. Earthquakes in the Mediterranean and Middle East, A Multidisciplinary Study of Seismicity up to 1900. Cambridge Univ. Press, Cambridge, UK, pp. 947.

Ambraseys, N.N., Adams, R.D., 1998. The Rhodes earthquake of 26 June 1926. - J. Seismology 2: 267-292.

Ambraseys, N.N., Finkel, C., 1995. The Seismicity of Turkey and adjacent areas. A Historical Review, 1500-1800. Eren, Istanbul, 240 pp.

Ambraseys, N.N, Jackson, J.A., 1981 Earthquake hazard and vulnerability in the northeastern Mediterranean: the Corinth earthquake sequence of February-March 1981. Disasters. Dec;5(4):355-68. doi: 10.1111/j.1467-7717.1981.tb01108.x. PMID: 20958498.

Ambraseys, N. N., Melville, C. P., Adams, R. D., 1994. The Seismicity of Egypt, Arabia and the Red Sea: a historical review. Cambridge Univ. Press, UK, 181 pp.

Anagnostopoulos, S. A., Rinaldi, D., Lekidis, V.A., Margaris, V.N., Theodulidis, N.P., 1987. The Kalamata, Greece, earthquake of September 13, 1986. Earthquake Spectra, V. 3, No. 2, pp. 365-402.

Anbarci, N., Escaleras, M., Register, Ch.-A., 2005. Earthquake fatalities: the interaction of nature and political economy. Journal of Public Economics, 89 (9-10), 1907-1933, https://doi.org/10.1016/j.jpubeco.2004.08.002.

Andrikopoulou, K. P., 1989. Damage assessment from the earthquakes of Kalamata on 1986 – Correlation of damage distribution with soil conditions in Kalamata: national report. Bulletin of the International Institute of Seismology and Earthquake Engineering, Japan, V. 23, 169-188.

Annunziato, A., Papadopoulos, G. A., Yalciner, A., et al., 2017. Analysis of the Tsunami Event caused by the Mw 6.3 Lesvos Island (East Aegean Sea) Earthquake of 12th June 2017. Joint Research Center Report, 73 pp.

Anonymous, 1893-1901. Book of the Earthquakes observed in Greece in the time interval 1893-1901. Institute of Geodynamics, National Observatory of Athens, 181 pp. (manuscript in Greek).

Anonymous, 1902-1915. Book of the Earthquakes observed in Greece in the time interval 1902-1915. Institute of Geodynamics, National Observatory of Athens, 399 pp. (manuscript in Greek).

Armijo, R., Flerit, F., King, G., Meyer, B., 2004. Linear elastic fracture mechanics explains the past and present evolution of the Aegean: Earth & Planetary Sciences Letters 1-2 (217), 85-95, doi: 10.1016/S0012-821X(03)00590-9.

Attary, N., Van De Lindt, J.W., Barbosa, A.R., Cox, D.T., Unnikrishnan, V.U., 2019. Performance-based tsunami engineering for 1100 risk assessment of structures subjected to multi-hazards: tsunami following earthquake. Journal of Earthquake Engineering, 1- 1101 20. doi:10.1080/13632469.2019.1616335.

Badal, J., Vázquez-prada, M., González, Á., 2005. Preliminary Quantitative Assessment of Earthquake Casualties and Damages. Nat Hazards 34, 353–374, https://doi.org/10.1007/s11069-004-3656-6

Bairaktaris, D., Roussopoulos, A., 1976. The Earthquake of Trihonis of. December 31, 1975 Technika Chronika-. April, May, June 1976.

Basili, R.,.., Triantafyllou, I.,…, Zaytsev, A. (33 Authors), 2021. The making of the NEAM Tsunami Hazard Model 2018 (NEAMTHM18), Front. Earth Sci., 2021, 8:616594. doi: 10.3389/feart.2020.616594

Båth, M., 1983. The Seismology of Greece. Tectonophysics, 98, 165-208.

Becker, D., Meier, Th., 2010. Seismic slip deficit in the Southwestern forearc of the Hellenic subduction zone. Bull. Seism. Soc. Am., 100, 325-342.

Behrens, J.,..., Triantafyllou, I.,…, Vyhmeister, E. (39 authors), 2021. Probabilistic Tsunami Hazard and Risk Analysis-A Review of Research Gaps. Front. Earth Sci., 2021, doi: 10.3389/ feart.2021.628772

Benchekroun, S., Omira R., Baptista, M. A., El Mouraouah, A., Iben Brahim, A., Toto, E. A., 2013. Tsunami impact and vulnerability in the harbor area of Tangier, Morocco. Geomatics, Natural Hazards and Risk, doi: 10.1080/19475705.2013.858373.

Bilham, R., 2009. The seismic future of cities. Bull Earthquake Eng 7, 839 https://doi.org/10.1007/s10518-009-9147-0.
Boccaletti, M., Manetti, P., Peccerillo, A., 1974. The Balkanids as an instance of back-arc thrust belt: possible relation with the Hellenids, Geol. Soc. Am. Bull., 85, 1077-1084.

Bocchini, G.M., 2018. Big and small earthquakes along the subduction interface: impact on natural hazards. PhD Thesis, National and Kapodistrian University of Athens, 234pp.

Bocchini, G. M., Brüstle, A., Becker, D., Meier, T., van Keken, P. E., Ruscic, M., Papadopoulos, G.A., Rische, M., Friederich, W., 2018. Tearing, segmentation, and backstepping of subduction in the Aegean: New insights from seismicity. Tectonophysics, 734-735, 96-118.

Bocchini, G.M., Novikova, T., Papadopoulos, G.A. et al., 2020. Tsunami Potential of Moderate Earthquakes: The July 1, 2009 Earthquake (M_w6.45) and its Associated Local Tsunami in the Hellenic Arc. Pure Appl. Geophys., 177, 1315–1333, https://doi.org/10.1007/s00024-019-02246-9.

Bohnhoff, M., Harjes, H.P., Meier, T., 2005. Deformation and stress regimes in the Hellenic subduction zone from focal Mechanisms. J. Seismol., 9, 341–366 https://doi.org/ 10.1007/s10950-005-8720-5.

Bondár, I., Engdahl, E.R., Villaseñor, A., Harris, J., Storchak, D.A., 2015. ISC-GEM: Global Instrumental Earthquake Catalogue (1900-2009): II. Location and seismicity patterns, Phys. Earth Planet. Int., 239, 2-13, doi: 10.1016/j.pepi.2014.06.002.

Bondár, I., Storchak, D., 2011. Improved location procedures at the International Seismological Centre. Geophysical Journal International, Vol. 186, Iss. 3, 1220–1244, https://doi.org/ 10.1111/ j.1365-246X.2011.05107.x

Burbidge, D., Cummins, P. R., Mleczko, R., Thio, H. A., 2008. Probabilistic tsunami hazard assessment for Western Australia, Pure Appl. Geophys., 165, 2059–2088.
Burton, P.W., Xua, Y., Qina, Ch., Tselentis, G.-A., Sokos, E., 2004. A catalogue of seismicity in Greece and the adjacent areas for the twentieth century, Tectonophysics, 390, 117–127.

Cavasino, A., 1927. Macrosismi avvertiti in Italia e Colonie nell' ano 1926. Boll. Soc. Sism. Ital. 27, 25-40

Chaoxu, X., Gaozhong, N., Xiwei, F., Junxue, Z., Huayue, L., Xiaoke, P., 2020. Research on the rapid assessment of earthquake casualties based on the anti-lethal levels of buildings. Geomatics, Natural Hazards and Risk, 11:1, 377-398, DOI: 10.1080/19475705.2019.1710581.

Charvet, I., Ioannou, I., Rossetto, T., Suppasri, A., Imamuara, F., 2014. Empirical fragility assessment of buildings affected by the 2011 Great East Japan tsunami using improved statistical models. Nat. Hazards, 73, 951-973.
Chatzivasiliou, V., 1989. Oi katastreptikoi seismoi tis Ko apo tin archaiotita mechri simera (The destructive earthquakes of Kos from the antiquity up to day). Dodecanisiaka Chronika, 8, 265-270 (in Greek)

Chatzivasiliou, V., 1990. Istoria tis nisou Ko (A history of Kos island). Edition by Kos Municipality, Kos, pp. 771 (in Greek)

Chen, Q.-F., Mi, H., Huang, J., 2005. A simplified approach to earthquake risk in mainland China, Pure and Applied Geophysics 162, 1255–1269.
Coburn, A., Spence, R., 1992. Earthquake protection. John Wiley & Sons Ltd, Chichester, 355 pp.

Comninakis, P. E., Papazachos, B. C., 1986. A catalogue of earthquakes in Greece and the surrounding area for the period 1901-1985. Univ. Thessaloniki Geophys. Lab., Publ.1, 167 pp.

Comninakis, P., Drakopoulos, J., Papazachos, B.C., 1987. Historical seismograms in Greece. Gerl. Beitr. Geophysik, 96 (5), 416-422.

Comninakis, P.E., Papazachos, B.C., 1982. A catalogue of earthquakes in Greece and the surrounding area for the period 1901-1980. Publ. of the Univ. of Thessaloniki, Geophys. Lab., 5, 146 pp.

Critikos, N.A., 1926. Sur la sismicité des Cyclades et de la Crete. Annales Observ. Ntl. Athènes, Athens, 9, 92.

Critikos, N.A., 1928. Le tremblement de terre de la mer de Crete du 26 juin 1926; étude macroséismique. Annales Observ. Natl. Athènes, Athens, 10, 39-46.

Curtis, G.D., Pelinovski, E.N., 1999. Evaluation of tsunami risk for mitigation and warning. Science of Tsunami Hazards, 17/3, 187-192.
D'Alessandro, A., Papanastassiou, D., Baskoutas, I., 2011. Hellenic Unified Seismological Network: An evaluation of its performance through SNES method, Geophys. J. Int., 185, 1417–1430.
Dall' Osso, F., Dominey-Howes, D., Tarbotton, C. et al., 2016. Revision and improvement of the PTVA-3 model for assessing tsunami building vulnerability using "international expert judgment": introducing the PTVA-4 model. Nat Hazards, 83: 1229.

Dall'Osso, F., Maramai, A., Graziani, L., Brizuela, B., Cavalletti, A., Gonella, M., Tinti, S., 2010. Applying and validating the PTVA-3 Model at the Aeolian Islands, Italy: assessment of the vulnerability of buildings to tsunamis, Nat. Hazards Earth Syst. Sci., 10, 1547-1562.

Daniell, J. E., Khazai, B., Wenzel, F., Vervaeck, A., 2011: The CATDAT damaging earthquakes database, Nat. Hazards Earth Syst. Sci., 11, 2235–2251, https://doi.org/ 10.5194/ nhess-11-2235-2011.

Davies, G., Griffin, J., Løvholt, F., Glimsdal, S., Harbitz, C., Thio, H.K., Lorito, S., Basili, R., Selva, J., Geist, E., Baptista, M.A., 2017. A global probabilistic tsunami hazard assessment from earthquake sources. From: Scourse, E. M., Chapman, N. A., Tappin, D. R., Wallis, S. R. (eds) Tsunamis: Geology, Hazards and Risks. Geol. Soc. London, Spec. Publ., 456, doi.org/10.1144/SP456.5.

de Ville de Goyet C., 1976. Earthquake in Guatemala: Epidemiological evaluation of the relief effort, Pan American Health Organization Bull., 10(2), 95-109.

Del Gaudio, C., De Martino, G., Di Ludovico, M. et al., 2017. Empirical fragility curves from damage data on RC buildings after the 2009 L'Aquila earthquake. Bull Earthquake Eng. 15, 1425–1450, https://doi.org/10.1007/s10518-016-0026-1

Deshcherevskii, A. V., Sidorin, A. Y., 2012. Changes in representativity of the earthquake catalogue for Greece in time and space, Seism. Instrum. 48, 292–302.

Di Giacomo, D., Bondar, I., Storchak, D.A, E., Engdahl, R., Bormann, P., Harris, J., 2015. ISC-GEM: Global Instrumental Earthquake Catalogue (1900–2009), III. Re-computed MS and mb, proxy MW, final magnitude composition and completeness assessment, Phys. Earth Planet. Inter., 239, 33–47.

Di Giacomo, D., Engdahl, E.R., Storchak, D.A., 2018. The ISC-GEM Earthquake Catalogue (1904-2014): status after the Extension Project, Earth Syst. Sci. Data, 10, 1877-1899, doi: 10.5194/essd-10-1877-2018.

Dias, W. P. S., Yapa, H. D., Peiris, L. M. N., 2009. Tsunami vulnerability functions from field surveys and Monte Carlo simulation. Civ. Eng. Environ. Syst., 26, 181–194.

Dogan, G.G., Annunziato, A., Papadopoulos, G.A. et al., 2019. The 20th July 2017 Bodrum–Kos Tsunami Field Survey. Pure Appl. Geophys., 176, 2925–2949, https:// doi.org/10.1007/ s00024-019-02151-1.

Dolce, M., Speranza, E., GiorDano, F., Borzi, B., Bocchi, F., Conte, C., Di Meo, A., Faravelli, M., Pascale, V., 2019. Observed damage database of past Italian earthquakes: the Da.D.O. WebGIS. Boll. Geof. Teor. Appl., 60 (2), 141-164, DOI 10.4430/bgta0254.

Dominey-Howes D., Dunbar P., Varner J., Papathoma-Kohle M., 2010. Estimating a probable maximum loss from a Cascadia tsunami. Nat. Hazards, 53(1), 43-61.

Douglas, A., 1967. Joint Epicenter Determination. Nature, 215, 47-48.

Drakopoulos, J.C., Srivastava, H.N., 1970. Investigation of the aftershocks of July 4, 1968 earthquake in Epidavros. Ann. Geofis., 23, 1-20.

Duda, S.J., 1965. Secular seismic energy release in the circum-Pacific belt. Tectonophysics, 2, 409-452, doi:10.1016/0040-1951(65)90035-1.

Dunbar, P.K., Lockridge, P.A., Whiteside, L.A., 1992. Catalogue of significant earthquakes (2150 BC-1991 AD), Rep. SE-49, Natl. Ocean. and Atmosph. Administration.

Dziewonski, A. M., Chou, T.-A., Woodhouse, J. H., 1981. Determination of earthquake source parameters from waveform data for studies of global and regional seismicity. J. Geophys. Res., 86, 2825-2852, 1981. doi:10.1029/JB086iB04p02825.

Earthquake Disaster Reduction Handbook, 1992. Executive Committee for IDNDR International Symposium on Earthquake Disaster Reduction Technology, Building Research Institute, Ministry of Construction Government of Japan, 304 pp.

EC-Working Paper 2010. Commission Staff Working Paper-Risk Assessment and Mapping, Guidelines for Disaster Management. SEC (2010), 1626 final, Brussels, 42 pp.

Eginitis, D., 1905. Etude des seismes survenus en Grèce pendant les années 1900-1903. Annales de l' Observatoire National d' Athènes, IV, p.135 and p. 488.

Eginitis, D., 1910. Etude des seismes survenus en Grèce pendant les années 1904-1908. Annales de l' Observatoire National d' Athènes, V, p.66 and 586-587.

Eginitis, D., 1912. Etude des seismes survenus en Grèce pendant les années 1909-1912. Annales de l' Observatoire National d' Athènes, VI, p.36 and 318-320.

Ekström, G., Nettles, M., Dziewonski, A. M., 2012. The global CMT project 2004-2010: Centroid-moment tensors for 13,017 earthquakes. Phys. Earth Planet. Inter., 200-201, 1-9, doi: 10.1016/j.pepi.2012.04.002.

Eleftheriadou, A.K., Karabinis, A.I., 2011. Development of damage probability matrices based on Greek earthquake damage data. Earthquake Engineering and Engineering Vibration, 10 (1), 1-13.

Engdahl, E.R., van der Hilst, R., Buland, R., 1998. Global teleseismic earthquake relocation with improved travel times and procedures for depth determination. Bull. Seismol. Soc. Am., 88 (3),722–743.

Evagelatou-Notara, F., 1993. Sismoi sto Vyzantio apo ton 13o mexri ton 15o aiona – Istoriki exetasi. Parousia, 24, 1-179 (in Greek with Engl. Summary).

Evangelidis, C.P., 2017. Seismic anisotropy in the Hellenic subduction zone: Effects of slab segmentation and subslab mantle flow, Earth Planet. Sci. Lett., doi: 10.1016/j.epsl.2017.10.003.

Evelpidou, N., Karkani, A., Kampolis, I., 2021. Relative Sea Level Changes and Morphotectonic Implications Triggered by the Samos Earthquake of 30th October 2020. J. Mar. Sci. Eng., 9, 40. http://doi.org/10.3390/jmse9010040.

Fardis, M.N., Karantoni, F.B., Kosmopoulos, A., 1999. Study and statistical processing of the damages from the 15-6-95 Aigio earthquake. Final report to OASP.

Floyd, M. A., Billiris, H., Paradissis, D., Veis, G., Avallone, A., Briole, P., McClusky, S., Nocquet, J.-M., Palamartchouk, K., Parsons, B., England, P. C., 2010. A new velocity field for Greece: implications for the kinematics and dynamics of the Aegean. J. Geophys. Res., 115, Article: B10403.

Fokaefs, A., Roussopoulou, C., Papadopoulos, G.A., 2004. Magnitudes of historical Greek earthquakes estimated by magnitude/intensity relationships. Proc. 5th International Symposium on Eastern Mediterranean Geology, Thessaloniki, 14–20 Apr. 2004, 2, 568-571.

Fournier d' Albe, E.M., 1982. An approach to earthquake risk management. Engineering Structures, 4, 147-152.

Galanopoulos, A. G., 1953. Katalog der Erdbeben in Griechenland für die zeit von 1879 bis 1892. Ann. Geol. Pays Hellen., 5, 144-229.

Galanopoulos, A.G., 1955. The seismic geography of Greece. Ann. Geol. Pays Hellen., 6, 83–121.

Galanopoulos, A.G., 1960. A catalogue of shocks with I0 ≥ VI or M ≥ 5 for the years 1801–1958. Seismol. Lab. Univ. Athens, Athens, 119 pp.

Galanopoulos, A. G., 1960. Tsunamis observed on the coasts of Greece from Antiquity to present

time. Ann. di Geof., 13, 369-386.

Galanopoulos, A. G., 1961. Greece–A catalogue of shocks with $I_o \geq$ VII for the years prior to 1800. Natl. Obs. Athens, Seismol. Inst., Rep., 19 pp.

Galanopoulos, A., 1966. Seismological Institute Bulletin 1962, no. 13, p. 5, Natl. Obs. Athens.

Galanopoulos, A. G., 1981. The damaging shocks and the earthquake potential in Greece. Ann.

Géol. Pays Hellen., 30, 648-724 (in Greek with Engl. abstr.).

Galanopoulos, A. G., 1985. On the earthquake activity occurring per month in Greece. Praktika Academy of Athens, 60, 152-180.

Ganas, A., Parsons, T., 2009. Three-dimensional model of Hellenic Arc deformation and origin of the Cretan uplift. J. Geophys. Res., 114, B06404, doi:10.1029/ 2008JB005599.

Ganas, A., Serpelloni, E., Drakatos, G., Kolligri, M., Adamis, I., Tsimi, Ch., Batsi, E., 2009. The Mw 6.4 SW-Achaia (Western Greece) Earthquake of 8 June 2008: Seismological, Field, GPS Observations, and Stress Modeling. J. Earthq. Engin., 13:8, 1101-1124, DOI: 10.1080/ 13632460902933899.

Ganse, R.A, Nelson, J.B., 1981. Catalog of significant earthquakes 2000 B.C. to 1979, including quantitative casualties and damage. Bull. Seismol. Soc. Am., 72 (3): 873–877.

Gardi, A., Valencia, N., Guillande, R., André C., 2011. Inventory of uncertainties associated with the process of tsunami damage assessment on buildings (SCHEMA FP6 EC co-funded project). Nat. Hazards Earth Syst. Sci., 11, 883-893.

GCMT, 2021. Global Centroid Moment Tensors, GCMT [WWW Document]. URL http://www.globalcmt.org/CMTsearch.html (last access 22.02.21).

Geist, E. L., Parsons, T., 2006. Probabilistic analysis of tsunami hazards, Nat. Hazards, 37, 277–314.

Goda, K., Song, J. 2019. Influence of Elevation Data Resolution on Tsunami Loss Estimation and Insurance Rate-Making. Frontiers in Earth Science, 7, 246.

González-Riancho, P., Aguirre-Ayerbe, I., García-Aguilar, O., Medina, R., González, M., Aniel-Quiroga, I., Gutiérrez, O.Q., Álvarez-Gómez, J., Larreynaga, A J., Gavidia, F., 2014. Integrated tsunami vulnerability and risk assessment: application to the coastal area of El Salvador. Nat. Hazards Earth Syst. Sci., 14, 1223–1244, doi:10.5194/nhess-14-1223-2014.

Grünthal, G., Wahlström, R., Stromeyer, D., 2013. The SHARE European Earthquake Catalogue (SHEEC) for the time period 1900-2006 and its comparison to EMEC. J. of Seismology, 17, 4, 1339-1344, doi: 10.1007/s10950-013-9379-y.

Grünthal, G., Wahlström, R., 2012. The European-Mediterranean Earthquake Catalogue (EMEC) for the last millennium. J. of Seismology, 16, 3, 535-570.

Gueri, M., Alzate, H., 1984. The Popayan earthquake: A preliminary report on its effects on health. Disasters 8(1), 18-20.

Guidoboni, E., Comastri, A., 2005. Catalogue of Earthquakes and Tsunamis in the Mediterranean Area from the 11th to the 15th century, Istituto Nazionale di Geofisica e Vulcanologia, Rome, 1037pp.

Guidoboni, E., Comastri, A., Traina, G., 1994. Catalogue of ancient earthquakes in the Mediterranean area up to the 10th Century. ING-SGA, Rome-Bologna, Italy, 504 pp.

Guidoboni, E., Ferrari, G., Mariotti, D., Comastri, A., Tarabusi, G., Sgattoni, G., Valensise, G., 2018. Historical earthquake data from the CFTI5Med catalogue. PANGAEA, https://doi.org/ 10.1594/ PANGAEA.896754.

Guidoboni, E., Ferrari, G., Tarabusi, G., Sgattoni, G., Comastri, A., Mariotti, D., Ciuccarelli, C., Bianchi, M. G., Valensise, G., 2019. CFTI5Med, the new release of the catalogue of strong earthquakes in Italy and in the Mediterranean area. Scientific Data, 6(1), https://doi.org/10.1038/s41597-019-0091-9.

Gutenberg, B., 1945. Amplitudes of surface waves and magnitudes of shallow earthquakes. Bull. Seismol. Soc. Am., 35, 3–12.

Gutenberg, B., Richter, C. F., 1944. Frequency of earthquakes in California. Bull. Seismol. Soc. Am., 34, 184–188.

Gutenberg, B., Richter, C. F., 1954. Seismicity of the Earth and associated phenomena. Princeton Univ. Press, Princeton, N.J., 310 pp.

Halpaap, F., Rondenay, S., Ottemöller, L. 2018. Seismicity, deformation, and metamorphism in the Western Hellenic Subduction Zone: New constraints from tomography. Journal of Geophysical Research: Solid Earth, 123, 3000– 3026. https://doi.org/10.1002/2017JB015154.

Hancilar, U.,2012. Identification of elements at risk for a credible tsunami event for Istanbul, Nat. Hazards Earth Syst. Sci., 12, 107-119, doi:10.5194/nhess-12-107-2012.

Hansen, S. E., Evangelidis, C. P., Papadopoulos, G. A., 2019. Imaging slab detachment within the Western Hellenic Subduction Zone. Geochemistry-Geophysics-Geosystems, 20. https://doi. org/10.1029/ 2018GC007810.

Hatori, T., 1979. Relation between tsunami magnitude and wave energy. Bull. Earthq. Res. Inst. (University of Tokyo), 54, 531-541.

Hébert, H., Schindele, F., Altinok, Y., Alpar, B. & Gazioglu, C., 2005. Tsunami hazard in the Marmara Sea (Turkey): A numerical approach to discuss active faulting and impact on the Istanbul coastal areas. Mar. Geol., 215, 23–43.

Hengjian, L., Kohiyama, M., Horie, K. et al.,2003. Building Damage and Casualties after an Earthquake. Natural Hazards 29, 387–403, https://doi.org/10.1023/A: 1024724524972.

Herrin, E., Tucker, W., Taggart, D., Gordon, W, Lobbell, J.L., 1968. Estimation of source focus P travel times. Bull. Seism. Soc. Am., 58, 1273-1291.

Hettiarachchi, S.S.L., Samarawickrama, S.P.,Wijeratne, N., 2011. Risk Assessment and Management for Tsunami Hazard-Case Study of the Port City of Galle. UNDP, 30 pp.

Hollenstein, Ch., Muller, M.D., Geiger, A., Kahle, H.-G., 2008. Crustal motion and deformation in Greece from a decade of GPS measurements, 1993–2003. Tectonophysics, 449, 17–40, doi: 10.1111/j.1365-246X.2005.02804.x.

Iida, K., 1956. Earthquakes accompanied by tsunamis occurring under the sea off the islands of Japan J. Earth Sciences Nagoya Univ. 4, 1 – 43.

Iida, K., 1970. The generation of tsunamis and the focal mechanism of earthquakes. In :Adams, W.M., ed. Tsunamis in the Pacific Ocean, Honolulu: East-West Center Press, 3-18.

Iida, K., Cox, D.C., Pararas-Carayannis, G., 1967. Preliminary Catalog of Tsunamis Occurring in the Pacific Ocean, Data Rep. 5, HIG-67-10, Hawaii Inst. of Geophys., Univ. of Hawaii.

Imamura, A., 1942. History of Japanese tsunamis Kayo-No-Kagaku (Oceanography) 2, 74-80 (in Japanese).

Imamura, A., 1949. List of tsunamis in Japan J. Seismol. Soc. Japan 2, 23-28.

IOC-Intergovernmental Oceanographic Commission, 2009. Tsunami risk assessment and mitigation in the Indian Ocean; Knowing your tsunami risk – and what do about it. IOC Manuals and Guides, 52, UNESCO, Paris.

IOC-Intergovernmental Oceanographic Commission, 2013. Tsunami Glossary, Technical Series 85, UNESCO, 1-42.

ISC-GEM, 2018. The ISC-GEM Global Instrumental Earthquake Catalogue, Version 5.1 (http:// www.isc.ac.uk/iscgem/download.php).

Jackson, J.A., Gagnepain, J., Houseman, G., King, G.C.P., Papadimitriou, P., Soufleris, C., Virieux, J., 1982. Seismicity, normal faulting and the geomorphical development of the Gulf of Corinth: the Corinth earthquakes of February and March 1981, Earth Planet. Sci. Lett., 57, 377-397.

Jaimes, M.A., Reinoso, E., Ordaz, M., Huerta, B., Silva, R., Mendoza, E., Rodríguez, J.C., 2016. A new approach to probabilistic earthquake-induced tsunami risk assessment. Ocean & Coastal Management 119, 68-75.

Jaiswal, K.S., Wald, D.J., Hearne, M., 2009. Estimating casualties for large earthquakes worldwide using an empirical approach: U.S. Geological Survey Open-File Report OF 2009–1136, 78 p.

Jelínek, R., Krausmann, E., 2008. Approaches to tsunami risk assessment. European Commission Joint Research Centre, Scientific and Technical Reports, EUR 23573 EN, Ispra, Italy.

Jelínek, R., Krausmann, González, E. M., Álvarez-Gómez, J. A., Birkmann, J., Welle, T., 2012. Approaches for tsunami risk assessment and application to the city of Cádiz, Spain. Nat. Hazards, 60, 273-293, DOI 10.1007/s11069-011-0009-0.

Jia, H., Lin, J., Liu, J., 2019. An Earthquake Fatalities Assessment Method Based on Feature Importance with Deep Learning and Random Forest Models. Sustainability, 11, 2727, https:// doi.org/10.3390/su11102727.

Jolivet, L., Faccenna, C., Huet, B., Labrousse, L., Le Pourhiet, L., Lacombe, O., Lecomte, E., Burov, E., Denèle, Y., Brun, J.P., Philippon, M., Paul, A., Salaün, G., Karabulut, H., Piromallo, C., Monié, P., Gueydan, F., Okay, A.I., Oberhänsli, R., Pourteau, A., Augier, R., Gadenne, L., Driussi, O., 2013. Aegean tectonics: progressive strain localization, slab tearing and trench retreat. Tectonophysics, 597-598, 1-33, 10.1016/j.tecto.2012.06.011.

Kahle, H.-G., Cocard, M., Peter, Y., Geiger, A., Reilinger, R., Barka, A., Veis, G., 2000. GPS-derived strain rate field within the boundary zones of the Eurasian, African, and Arabian Plates. J. Geophys. Res., 105 (B10), 23353– 23370, doi:10.1029/2000JB900238.

Kahle, H.-G., Mtiller, M. V., Geiger. A., Danuser, G., Mueller, St. Veis, G. Billiris, H., Paradissis, D., 1995. The strain field in NW Greece and the Ionian Islands: results inferred from GPS measurements. Tectonophysics 249 (1-2), 41-52.

Kalafat, D., Güneş, Y., Kara, M., Deniz, P., Kekovali, K., H., Kuleli, S., Gülen, L., Yilmazer, M., Özel, N. M., 2007. A revised and extented earthquake catalogue for Turkey since 1900 (M≥4.0). Boğaziçi Üniversitesi.

Kappos, A.J., Lekidis, V., Panagopoulos, G., et al. 2007. Estimation of economic loss for buildings in the area struck by the 1999 Athens earthquake and comparison with actual repair costs. Earthquake Spectra, 23(2), 333-355.

Karantoni T., Bouckovalas G., 1997. Description and Statistical Analysis of Damage from Pyrgos 1993 (Greece) Earthquake. Soil Dynamics & Earthquake Engineering, 16, 141-150.

Karasözen, E., Nissen, E., Büyükakpınar, P., Cambaz, M.D., Kahraman, M., Ertan, E.K., Abgarmi, B., Bergman, E., et al. 2018. The 2017 July 20 Mw 6.6 Bodrum–Kos earthquake illuminates active faulting in the Gulf of Gökova, SW Turkey. Geophys. J. Int., 214, 185–199, doi:10.1093/gji/ggy114

Karim, K.R., Yamazaki, F., 2003. A simplified method of constructing fragility curves for highway bridges. Earthq. Eng. Struct. Dynam., 32, 1603-1626.

Kárník, V.,1969. Seismicity of the European Area, part. 1. D. Reidel, Dordrecht, Netherlands, 364 pp.
Kárník, V., 1971. Seismicity of the European Area, Part 2. D. Reidel, Dordrecht, Netherlands, 218 pp.
Kárník V., 1996. Seismicity of the Europe and The Mediterranean. Acad. Sc. Czech Rep., Geophys. Inst., 28pp+maps and catalogue.

Karpathios, E.I. 1962. Archion Ieras Mitropoleos Ko Dodekanisou (Archive of the Holly Metropolis of Kos in Dodecanese). 4, 1-165, Athens (in Greek)

Karpathios, E.I. 1968. Ekklisia Ko Dodekanisou (Church of Kos in Dodecanese). 1 (1), 1-516, Athens (in Greek)

Kassaras I, Kapetanidis V, Karakonstantis A., 2016. On the spatial distribution of seismicity and the 3D tectonic stress field in western Greece. Physics and Chemistry of the Earth, 95, 50-72.

Kassaras, I., Kapetanidis, V., Ganas, A., Tzanis, A., Kosma, C., Karakonstantis, A., Valkaniotis, S., Chailas, S., Kouskouna, V., Papadimitriou, P., 2020. The New Seismotectonic Atlas of Greece (v1.0) and Its Implementation. Geosciences, 10, 447, https://doi.org/10.3390/ geosciences10110447

Kaviris, G., Papadimitriou, P., Kravvariti, Ph., Kapetanidis, V., Karakonstantis, A., Voulgaris, N., Makropoulos, K., 2015. A detailed seismic anisotropy study during the 2011-2012 unrest period in the Santorini Volcanic Complex. Phys. Earth. Plan. Inter., 238, 51-88.

Khoury, S. G., Tilford, N. R., Chandra, U., Amick, D., 1983. The effect of multiple events on isoseismal maps of the 1981 earthquakes at the Gulf of Corinth, Greece. Bull. Seismol. Soc. Am., 73 (2): 655–660.

Kijko, A., SelIevoll, M.A., 1989. Estimation of earthquake hazard parameters from incomplete data files. Part I. Utilization of extreme and complete catalogs with different threshold magnitudes. Bull. Seismol. Soc. Am., 79: 645-654.

Kijko, A., Sellevoll, M. A., 1992. Estimation of earthquake hazard parameters from incomplete data files, Part II, incorporation of magnitude heterogeneity. Bull. Seismol. Soc. Am., 82 (1): 120–134.

Kijko, A., Smit, A., 2017. Estimation of the Frequency–Magnitude Gutenberg–Richter b-Value without Making Assumptions on Levels of Completeness. Seismol. Res. Lett., 2017; 88 (2A), 311–318. doi: https://doi.org/10.1785/ 0220160177

Kijko, A., Smit, A., Sellevoll, M. A., 2016. Estimation of earthquake hazard parameters from incomplete data files. Part III. Incorporation of uncertainty of earthquake-occurrence model. Bull. Seismol. Soc. Am., 106(3), 1210–1222. doi:10.1785/0120150252.

Kinna, A., Kostoglou, D., Tourkomanoli, O., Fakkou, M., Chatzinikolaou, K., Sofou, D. ,2002. Istoria tis Ko (A history of Kos). Publication of the Dodecanese Prefecture, 207 pp. (in Greek)

Kiratzi, A.A., 1989. Relations between magnitude scales for earthquakes in the Aegean area. Proc. 1st Scient. Conf. of Geophysics, Geophys. Soc. Greece, April 19-21, 1989, Athens, 658-665.

Kiratzi, A.A., Papazachos, B.C., 1984. Magnitude scales for earthquakes in Greece. Bull. Seism. Soc. Am., 74, 969-985.

Kontopoulos, N., Avramidis, P., 2003. A late Holocene record of environmental changes from the Aliki lagoon, Egion, North Peloponnesus, Greece. Quatern. Internat., 111, 75–90.

Koravos, G.C., Yadav, R.B.S., Tsapanos, T. M., 2015. Evaluation of tsunami potential based on conditional probability for specific zones of the Pacific tsunamigenic rim. Tectonophysics, 658, 159-168, https://doi.org/10.1016/j.tecto.2015.07.018.

Kortekaas, S., Papadopoulos, G.A., Ganas, A., Cundy, A. B., Diakantoni, A., 2011. Geological identification of historical tsunamis in the Gulf of Corinth, Central Greece. Natural Hazards & Earth System Science 11, 2029–2041.
Koukis, G., Rozos, D., 1985. Engineering geological characteristics of the 1981 earthquakes in the eastern corinthian gulf, Greece. Bull. Internat. Ass. Engin. Geol., 32, 91–95, https:// doi.org/ 10.1007/BF02594770.

Koukouvelas, I.K., Doutsos, T., 1996. Implications of structural segmentation during earthquakes: the 1995 Egion earthquake, Gulf of Corinth, Greece. J. Struct. Geol., 18, 1381-1388.

Koukouvelas, I.K., 1998. The Egion fault, earthquake-related and long-term deformation, Gulf of Corinth, Greece. J. Geodynamics, 26, 501–513.

Kouskouna, V., 2001. The (December 28th, 1891) January 9th, 1892 Larissa (Central Greece) earthquake. Bull. Geol. Soc. Greece, 34(4), 1425-1432, doi:org/10.12681/bgsg.17236.

Kouskouna, V., Sakkas, G., 2013. The University of Athens Hellenic Macroseismic Database (HMDB.UoA): historical earthquakes. J. Seismology. 17(4), 1253-1280, DOI 10.1007/s10950-013-9390-3.

Kulikov, E.A., Rabinovich, A.B., Thomson, R.E., 2005. Estimation of tsunami risk for the coasts of Peru and northern Chile. Nat. Hazards, 35,185–209.

Kurt, H., Demirbağ, E., Kuşçu, İ. 1999. Investigation of the submarine active tectonism in the Gulf of Gökova, southwest Anatolia–southeast Aegean Sea, by multi-channel seismic reflection data. Tectonophysics, 305(4), 477-496.

Laigle,M., Sachpazi, M., Hirn, A., 2004. Variation of seismic coupling with slab detachment and upper plate structure along the western Hellenic subduction zone. Tectonophysics, 391 (1-4), 85-95, https://doi.org/10.1016/j.tecto.2004.07.009.

Lario, J., Bardají, T., Silva, P.G., Zazo, C., Goy, J.L. 2016. Improving the coastal record of tsunamis in the ESI-07 scale: Tsunami Environmental Effects Scale (TEE-16 scale). Geologica Acta, 14 (2), 179-193.

Le Pichon, X., Angelier, J., 1979. The Hellenic Arc and Trench System: a key to the neotectonic evolution of the Eastern Mediterranean Area. Tectonophysics. 60, 1-42. 10.1016/0040-1951(79)90131-8.

Le Pichon, X., Şengör, A.M.C., İmren, C., 2019. A new approach to the opening of the eastern Mediterranean Sea and the origin of the Hellenic subduction zone. Part 2: The Hellenic subduction zone. Canadian J. Earth Sciences. 56(11), 1144-1162. https://doi.org/10.1139/cjes-2018-0315.

Lechat, M.F., 1979. Disasters and public health. World Health Organization Bull., 57(1), 11-17.

Leelawat, N., Suppasri, A., Charvet, I., Imamura, F., 2014. Building damage from the 2011 Great East Japan tsunami: quantitative assessment of influential factors. A new perspective on building damage analysis. Nat Hazards, 73, 449–471, doi:10.1007/s11069-014-1081-z.

Lekkas, E., Carydis, P., Mavroulis, S., Gogou, M., Andreadakis, E., Katsetsiadou, K.N., Skourtsos, E., Minos-Minopoulos, D., Bardouli, P., Voulgaris, N., Papadimitriou, P., Kaviris, G.,

Tselentis, G., Karakonstantis, A., Parcharidis, I., Papastergios, A., Tsironi, V., Lalechos, S., Avramea, V., Kleanthi, M., Papaioannou, C., Salonikios, T., Adam, N., Sakellariou, D., 2017. The Mw6.6, July 21, 2017 Kos earthquake-scientific report. Newsletter of Environmental, Disasters & Crises Management Strategies, 1, 57 pp, Athens, https://edcm.edu.gr/images/documents/Presentation_.

Lekkas, E., Kolyva, M., Antonopoulos, G., Kopanas, I., 1997. Oi Sismoi tis Zakynthou. Zakynthos, 78 pp.

Lekkas, E., Kranis, H.D., 1997. Earthquake faulting and human life loss. In: Marinos, Koukis, Tsiambaos & Stournaras (eds): Earthquake Geology & the Environment, 835-840, Balkema, Rotterdam.

Lekkas, E., Mavroulis, S., Gogou, M., Papadopoulos, G.A., Triantafyllou, I., Katsetsiadou, K.-N., Kranis, H., Skourtsos, E., Carydis, P., Voulgaris, N., et al., 2020. The October 30, 2020 Mw6.9 Samos (Greece) earthquake. Newsletter of Environmental, Disaster & Crises Management Strategies; Department of Dynamic, Tectonic & Applied Geology, Faculty of Geology & Geoenvironment, National & Kapodistrian University of Athens: Athens, Greece, 21, 156 pp., ISSN 2653-9454.

Lekkas, E.L., Lozios, S.G., Skourtsos, E.N., Kranis, H.D., 1998. Egio earthquake (15 June 1995): An episode in the neotectonic evolution of Corinthiakos Gulf. J. of Geodynamic, 26 (2–4), 487-499.

Lekkas, L., Andreadakis, E., Kostaki, I., Kapourani, E., 2013. A Proposal for a New Integrated Tsunami Intensity Scale (ITIS-2012). Bull. Seismol. Soc. Am., 103 (2B): 1493–1502. https://doi.org/10.1785/0120120099.

Leone F., Lavigne, F., Paris, R., Denain, J. C., Vinet, F., 2011. A spatial analysis of the December 26th, 2004 tsunami-induced damages: lessons learned for a better risk assessment integrating buildings vulnerability. Appl. Geogr., 31, 363–375.

Leptokaropoulos, K. M., Karakostas, V. G., Papadimitriou, E. E., Adamaki, A. K., Tan, O., İnan, S., 2013. A Homogeneous Earthquake Catalog for Western Turkey and Magnitude of Completeness Determination. Bull. Seism. Soc. Am., 103 (5): 2739–2751. https://doi.org/10.1785/0120120174.

Li, L., Switzer, A.D., Chan, Ch.-H., Wang, Y., Weiss, R., Qiu, Q., 2016. How heterogeneous coseismic slip affects regional probabilistic tsunami hazard assessment: A case study in the South China Sea. J. Geophys. Res., Solid Earth, 121, doi:10.1002/2016JB013111.

Lomnitz, C., 1970. Casualties and behavior of populations during earthquakes. Bull. Seismol. Soc. Am., 60 (4), 1309–1313.

Lorito, S., Tiberti, M. M., Basili, R., Piatanesi, A., Valensise, G., 2007. Earthquake-generated tsunamis in the Mediterranean Sea: Scenarios of potential threats to southern Italy, J. Geophys. Research, 113, B01301, doi: 10.1029/2007JB004943.

Løvholt, F., Griffin, J., Salgado-Gálvez, M., 2015. Tsunami hazard and risk assessment on the global scale, in Encyclopedia of 1480 complexity and systems science, ed. R. A. Meyers (Berlin, Heidelberg: Springer), 1-34. doi:10.1007/978-3-642-27737-5_642-1.

Maggini, M., Caputo, R., 2020. Rheological behavior in continental and oceanic subduction: inferences for the seismotectonics of the Aegean Region. Turkish J. Earth Sci., 29: 381-405, doi:10.3906/yer-1909-4.

Makris, J., 1976. A dynamic model of the Hellenic Arc deduced from geophysical data. Tectonophysics, 36, 339-346.

Makris, J., 1978. The crust and upper mantle of the Aegean region from deep seismic sounding. Tectonophysics, 46, 269-284.

Makropoulos, C., 1978. The Statistics of large Earthquake Magnitude and an Evaluation of Greek Seismicity. Ph. D. Thesis, Univ. of Edinburgh, 193 pp.

Makropoulos, K. C., Burton, P. W., 1981. A catalogue of seismicity in Greece and adjacent areas. Geophys. J. R. astr. Soc, 30, 741-762.

Makropoulos, K. C., Drakopoulos, J. Latoussakis, J., 1989. A revised and extended earthquake catalogue for Greece since 1900. Geophys. J. Int., 99, 305-306.

Makropoulos, K., Kaviris, G., Kouskouna, V., 2012. An updated and extended earthquake catalogue for Greece and adjacent areas since 1900. Nat. Hazards Earth Syst. Sci., 12, 1425–1430, doi:10.5194/nhess-12-1425-2012.

Mallet, R., 1850-1858. First Report on the Facts of Earthquake Phaenomena. Report of the British Association for the Advancement of Science, London, 1850:1-89 1852:1-176,1853:118-212,1854:1-326, 1858:1-136.

Maramai, A., Brizuela, B., Graziani, Laura, 2014. The Euro-Mediterranean Tsunami Catalogue. Annals of Geophysics, 57, S0435; doi:10.4401/ag-6437.

Mariolakos, I., Fountoulis, I., Logos, E., Lozios, S., 1989. Surface faulting caused by the Kalamata (Greece) earthquakes (13.9.1986). Tectonophysics, 163, 197-203.

Martino, S., Prestininzi, A., Romeo, R. W., 2014. Earthquake-induced ground failures in Italy from a reviewed database. Nat. Hazards Earth Syst. Sci. 14, 799–814,vhttps://doi.org/ 10.5194/nhess-14-799-2014.

Matsumura, K., 1986. On Regional Characteristics of Seasonal Variation of Shallow Earthquake Activities in the World. Bull. Disas. Prev. Res. Inst., Kyoto Univ., 36 (2), No. 318, 43-98.

McClusky, S., et al. 2000. Global Positioning System constraints on plate kinematics and dynamics in the eastern Mediterranean and Caucasus. J. Geophys. Res., 105 (B3), 5695– 5719, doi:10.1029/1999JB900351.

McKenzie, D. P., 1970. Plate tectonics of the Mediterranean region. Nature, 226, 239-243.

McKenzie, D., 1972. Active tectonics of the Mediterranean region. Geophys. J. R. astr. Soc, 30 (2), 109-185, 10.1111/j.1365-246X.1972.tb02351.x.

McKenzie, D. P., 1978. Active tectonics of the Alpine-Himalayan belt: the Aegean Sea and and surrounding regions. Geophys. J. R. astr. Soc., 55(1), 217-254, https://doi.org/10.1111/j.1365-246X.1978.tb04759.x

Mignan, A., Chouliaras, G., 2014. Fifty Years of Seismic Network Performance in Greece (1964–2013): Spatiotemporal Evolution of the Completeness Magnitude. Seismol. Res. Lett., 85 (3), 657–667. doi: https://doi.org/10.1785/ 0220130209.
Mignan, A., Woessner, J., 2012. Estimating the magnitude of completeness for earthquake catalogs. In: Community Online Resource for Statistical Seismicity Analysis, doi: 10.5078/ corssa-00180805, available at http://www.corssa.org (last accessed March 2020).

Milne, J., 1912. Catalogue of Destructive Earthquakes. Rep. of the 18th Meeting of the British Association for the Advancement of Science–Portsmouth 1911, Aug. 31-Sept. 7, London, 640-740.

Montandon, F., 1953. Les tremblements de terre destructeurs en Europe, Catalogue par territoirs seismique de l' an 1000 à 1940. Geneve, 195pp.

Montessus de Ballore, F., 1906. Les tremblements de terre: Géographie séismologique. Libr. Armand Colin. Paris, 475 pp.

Mouslopoulou, V., Nicol, A., Begg, J. et al. 2015. Clusters of megaearthquakes on upper plate faults control the Eastern Mediterranean hazard. Geophys. Res. Lett., 42, doi:10.1002/ 2015GL066371.

Murty, T.S., Loomis, H.G., 1980. A new objective tsunami magnitude scale. Marine Geodesy, 4, 267-282.

Nadim, F., Glade, T., 2006. On tsunami risk assessment for the west coast of Thailand. In: Nadim, F., Pöttler, R., Einstein, H., Klapperich, H., Kramer, S. (Eds.), ECI Symposium Series, 7.

Nievas, C.I., Bommer, J.J., Crowley, H. et al., 2020. A database of damaging small-to-medium magnitude earthquakes. J Seismol., https://doi.org/10.1007/s10950-019-09897-0.

Ninkovich, D., Hays, J. D., 1971. Tectonic setting of Mediterranean volcanoes. Acta 1st Int. Sci. Congr. on the Volcano of Thera, 111-113, Athens.

Ninkovich, D., Hays, J. D., 1972. Mediterranean island arcs and origin of high potash volcanoes. Earth and Plan. Sci. Lett., 16, 331-345.

Nocquet, J.M., 2012. Present-day kinematics of the Mediterranean: a comprehensive overview of GPS results. Tectonophysics, 579 (SI), 220-242. ISSN 0040-1951.

Ocakoğlu, N., Nomikou, P., İşcan, Y., Loreto, M.F., Lampridou, D. 2018. Evidence of extensional and strike-slip deformation in the offshore Gökova-Kos area affected by the July 2017 Mw6.6 Bodrum-Kos earthquake, eastern Aegean Sea. Geo-Marine Letters, https://doi.org/ 10.1007/s00367-017-0532-4

Ohta Y., Kagami H., Okada S., Ōhashi H., 1986. Characterization of earthquake disasters in several tens of countries by worldwide earthquake damage data in 1900-1979. Proc. 8th Europ. Conf. Earthq. Engineer., Lisbon.

Oike, K., 1991.A discussion on the relation between magnitude and the number of the dead earthquakes, In: Proc. Inter. Seminar on Earthquake Prediction and Hazard Mitigation Technology, Tsukuba, Japan, 333-341.

Okal, E.A., Titov, V., 2007. MTSU: Recovering seismic moments from tsunameter records. Pure Appl. Geophys., 164, 355-378.

Omira, R., Baptista, M.A., Miranda, J.M., Toto, E., Catita, C., Catalão, J., 2010. Tsunami vulnerability assessment of Casablanca Morocco using numerical modelling and GIS tools, Nat. Hazards Earth Syst. Sci., 54, 75-95.

Orfanogiannaki, K., Papadopoulos, G.A., 2007. Conditional Probability Approach of the Assessment of Tsunami Potential: Application in three Tsunamigenic Regions of the Pacific Ocean. Pure Appl. Geophys., 164, 1-11.

Pagnoni, G., Armigliato, A., Tinti, S., 2015. Scenario-based assessment of buildings' damage and population exposure due to earthquake-induced tsunamis for the town of Alexandria, Egypt. Nat. Hazards Earth Syst. Sci., 15, 2669–2695, doi:10.5194/nhess-15-2669-2015.

Pagnoni, G., Tinti, S., 2016. Application and Comparison of Tsunami Vulnerability and Damage Models for the Town of Siracusa, Sicily, Italy. Pure Appl. Geophys., 173, 3795–3822, DOI:10.1007/s00024-016-1261-8.

Papadimitriou, P., Kapetanidis, V., Karakonstantis, A., Kaviris, G., Voulgaris, N., Makropoulos, K., 2015. The Santorini volcanic complex: a detailed multi-parameter seismological approach with emphasis on the 2011-2012 unrest period. J. Geodyamics, http://doi.org/10.1016/j.jorg.2014.12.004.

Papadopoulos, G. A., 1982. Contribution to the study of the active deep tectonics of the Aegean and surrounding regions. PhD Thesis, Faculty of Physical Sciences, Aristotelian Univ. of Thessaloniki, 176 pp. (in Greek with Engl. summary).

Papadopoulos, G.A., 1988. Statistics of historical earthquakes and associated phenomena in the Aegean and surrounding regions. In: P. Marinos & G. Koukis (Eds.), Proc. Intern. Symp. on Engin. Geology as Related to the Study, Preservation & Protection of Ancient Works, Monuments & Historical Sites, Balkema, Athens, Sept. 1988, 3, 1279-1283.

Papadopoulos, G.A., 1993. The 20 March 1992 South Aegean, Greece, earthquake (M_s=5,3): Possible anomalous effects. Terra Nova, Vol.5, p. 399-404.

Papadopoulos, G. A., 2000. A new catalogue of historical earthquakes in the Corinth Rift, Central Greece, 480 BC-AD 1910. Institute of Geodynamics, National Observatory of Athens, Publ. No 12, Athens, 120 pp.

Papadopoulos, G. A., 2001. Tsunamis in the East Mediterranean: a catalogue for the area of Greece and adjacent seas. Proc. Joint IOC-IUGG Internat. Workshop on Tsunami Risk Assessment Beyond 2000 : Theory, Practice and Plans, Moscow, June 14-16, 2000, 34-42.

Papadopoulos, G.A., 2003. Tsunami Hazard in the Eastern Mediterranean: Strong Earthquakes and Tsunamis in the Corinth Gulf, Central Greece. Natural Hazards 29, 437-464.

Papadopoulos, G. A., 2011. A Seismic History of Crete: Earthquakes and Tsunamis, 2000 B.C.-A.D. 2010. Ocelotos Publ., Athens, 415 pp.

Papadopoulos, G.A., 2012. Kythtira: Oi sismi kai ta tsunami apo tin archaeotita mexri simera. Ocelotos, Athens, 105 pp.

Papadopoulos, G.A., 2014. Rhodes: Oi sismi kai ta tsunami apo tin archaeotita mexri simera. Ocelotos, Athens, 222 pp.

Papadopoulos, G.A., 2015a. Lesvos-Chios-Psara: Oi sismi kai ta tsunami apo tin archaeotita mexri simera. Ocelotos, Athens, 243 pp.

Papadopoulos, G.A., 2015b. Tsunamis in the European-Mediterranean Region: From Historical Record to Risk Mitigation. Elsevier, Amsterdam, 271 pp.

Papadopoulos, G. A., Chalkis, B., 1984. Tsunamis observed in Greece and the surrounding area from antiquity up to the present times. Marine Geology, 56, 309-317.

Papadopoulos, G. A., Daskalaki, E., Fokaefs, A., Giraleas, N., 2007. Tsunami Hazard in the Eastern Mediterranean: Strong Earthquakes and Tsunamis in the East Hellenic Arc and Trench System. Natural Hazards & Earth System Science, 7, 57–64.

Papadopoulos, G. A., Imamura, F., 2001. A proposal for a new tsunami intensity scale. Proc. Internat. Tsunami Symposium, Aug 7-10, 2001, Seattle, 569-577.

Papadopoulos, G. A., Kondopoulou, D., Leventakis, G. A., Pavlides, S., 1986. Seismotectonics of the Aegean region. Tectonophysics, 124, 67-84.

Papadopoulos, G.A., Profis, T., 1990. Macroseismic observations related with the strong shock of October 16th, 1988, in NW Peloponnesus Greece: the important role of the microzonation conditions, J. Geodyn., 12, 217-231

Papadopoulos, G. A., Lefkopoulos, G., 1993. Magnitude-distance relations for liquefaction in soil from earthquakes. Bull. Seismol. Soc. Am., 83, 925–938.

Papadopoulos, G. A., Plessa, A. 2001. Historical earthquakes and tsunamis of the south Ionian Sea occurring from 1591 to 1837. Bull. Geol. Soc. Greece, 34(4), 1547-1554.

Papadopoulos, G. A., Plessa, A., 2000. Magnitude-distance relations for earthquake-induced landslides in Greece. Engin. Geology, 58, 377-386.

Papadopoulos, G.A, Kijko, A., 1991. Maximum likelihood estimation of earthquake hazard parameters in the Aegean area from mixed data, Tectonophysics, Vol. 185, Issues 3–4, 277-294, https://doi.org/10.1016/0040-1951(91)90449-3.

Papadopoulos, G.A., Fountoulis, D., Grivas, K., 1994. The 26 March 1993 earthquake in the area of Pyrgos, NW Peloponnesus, Greece: Earthquake engineering aspects, In: G. Papadopoulos, G.A. and K. Makropoulos (eds), 2nd workshop statistical models and methods in seismology applications on prevention and forcasting of earthquakes, Cephalonia, Greece, 208-235.

Papadopoulos, G.A., Dermentzopoulos, Th., 1998. A Tsunami Risk Management Pilot Study in Heraklion, Crete. Natural Hazards, 18, 91–118.

Papadopoulos, G.A., Ganas, A., Plessa, A., 2002. The Skyros earthquake (M_w 6.5) of 26 July 2001 and precursory seismicity patterns in the North Aegean Sea Bull. Seism. Soc. Am., 92, pp. 1141-1145.

Papadopoulos, G.A., Karastathis, V.K., Kontoes, C., Charalampakis, M., Fokaefs, A. Papoutsis, I., 2010. Crustal deformation associated with East Mediterranean strike-slip earthquakes: The 8 June 2008 Movri (NW Peloponnese), Greece, earthquake (Mw6.4). Tectonophysics, 2010, doi.org/10.1016/j.tecto.2010.06.012.

Papadopoulos, G.A., Gràcia, E., Urgeles, R., Sallares, V., De Martini, P.M., Pantosti, D., González, M., Yalciner, A. C., Mascle, J., Sakellariou, D., Salamon, A., Tinti, S. Karastathis, V., Fokaefs, A., Camerlenghi, A. Novikova, T., Papageorgiou, A. 2014a. Historical and pre-historical tsunamis in the Mediterranean and its connected seas: Geological signatures, generation mechanisms and coastal impacts. Marine Geology, doi: 10.1016/j.margeo.2014.04.014.

Papadopoulos, G. A., Baskoutas, I., Fokaefs, A., 2014b. Historical seismicity of the Kyparissiakos Gulf, western Peloponnese, Greece. Boll. Geof. Teor. Appl., 55, 389-404, DOI 10.4430/bgta0096.

Papadopoulos, G.A., Karastathis, V.K., Ganas, A., Pavlides, S., Fokaefs, A. Orfanogiannaki, K., 2003. The Lefkada, Ionian Sea (Greece), shock (Mw6.2) of 14 August 2003: Evidence for the characteristic earthquake model from seismicity and ground failures. Earth Planets Space, 55, 713-718.

Papadopoulos, G.A., Karastathis, V.K., Koukouvelas, I., Sachpazi, M., Baskoutas, I., Chouliaras, G., Agalos, A., Daskalaki, E., Minadakis, G., Moschou, A., Mouzakiotis, A., Orfanogiannaki, K., Papageorgiou, A., Spanos, D., Triantafyllou, I. 2014c. The Cephalonia, Ionian Sea (Greece), sequence of strong earthquakes of January-February 2014: a first report. Research in Geophysics, DOI: 10.4081/rg.2014.544

Papadopoulos, G.A., Lekkas, E., Katsetsiadou, K.-N., Rovythakis, E., Yahav, A., 2020. Tsunami Alert Efficiency in the Eastern Mediterranean Sea: The 2 May 2020 Earthquake (Mw6.6) and Near-Field Tsunami South of Crete (Greece). GeoHazards, 1, 44-60. https://doi.org/10.3390/geohazards1010005

Papadopoulos, G.A., Imamura, F., Nosov, M., Charalampakis, M., 2020. Tsunami magnitude scales. In: Geological Records of Tsunamis and Other Extreme Waves, 1st ed., Engel, M., Pilarczyk, J., May, S.M., Brill, D., Garrett, E., Eds.; Elsevier: Amsterdam, The Netherlands, 33-45. ISBN 978-0-12-815686-5.

Papaioannou, I., 1999. I sismiki drasi sto Nomo Magnesias kata ton 19o aiona. I Thessalia, 7 Noemvriou 1999 (in Greek).

Papaioannou, I., 2002. Enas megalos sismos sti Larisa to 1892. Eleftheria, 10 Dekemvriou 2002.

Papaioannou, I., 2018. The seismic activity in Thessalia from 1900 to 1950. Thessaliko Imerologio, 73, 289-314 (in Greek).

Papanikolaou, D.J., Royden, L.H., 2007. Disruption of the Hellenic arc: Late Miocene extensional detachment faults and steep Pliocene-Quaternary normal faults—Or what happened at Corinth? Tectonics 26: doi: 10.1029/2006TC002007. issn: 0278-7407

Papastamatiou, D., Mouyiaris, N., 1986. The Sophadhes earthquake occurred on April 30th 1954 - field observations by Yannis Papastamatiou. Geol. & Geoph. Res., Sp. Issue, 341-362

Papathanassiou, G., Pavlides, S., 2007. Using the INQUA scale for the assessment of intensity: Case study of the 2003 Lefkada (Ionian Islands), Greece earthquake. Quaternary International,173-174, 4-14, https://doi.org/10.1016/j.quaint.2006.10.038.

Papathanassiou, G., Pavlides, S., Christaras, B., Pitilakis, K., 2005. Liquefaction case histories and empirical relations of earthquake magnitude versus distance from the broader Aegean Region. Journal of Geodynamics, 40, pp.257-278.

Papathanassiou, G., Valkaniotis, S., Ganas, A., Grendas, N., Kollia, E., 2017. The November 17th, 2015 Lefkada (Greece) strike-slip earthquake: Field mapping of generated failures and assessment of macroseismic intensity ESI-07. Engineering Geology, 220,13-30, https://doi.org/10.1016/j.enggeo.2017.01.019.

Papathoma, M., Dominey-Howes D., 2003. Tsunami vulnerability assessment and its implications for coastal hazard analysis and disaster management planning, Gulf of Corinth, Greece. Nat. Hazards Earth Syst. Sci., 3, 733-747.

Papathoma, M., Dominey-Howes, D., Zong Y., Smith D., 2003. Assessing tsunami vulnerability, an example from Herakleio, Crete. Nat. Hazards Earth Syst. Sci., 3, 377-389.

Papazachos, B.C., 1989. Measures of earthquake size in Greece and surrounding area. Proc. 1st Scient. Conf. of Geophysics, Geophys. Soc. Greece, April 19-21, 1989, Athens, 438-447.

Papazachos, B.C., Comninakis, P.E., 1971. Geophysical and tectonic features of the Aegean arc. J. Geophys. Res., 76, 8517 - 8533.

Papazachos, B.C., Comninakis, P.E., 1972. The seismic activity in the area of Greece during the time period 1911-1971. Manuscript, 60 pp., Athens (in Greek with Engl. abstr.).

Papazachos, B. C., Comninakis, P. E., 1982. A catalogue of earthquakes in Greece and the surrounding area for the period 1901-1980, Publ. Univ. of Thessaloniki, Geophys. Lab., 5, 1-146.

Papazachos, B.C., Comninakis, P.E., Karakaisis, G.F., Karakostas, B.G., Papaioannou, Ch.A., Papazachos, C.B., Scordilis, E.M., 2000. A catalogue of earthquakes in Greece and surrounding area for the period 550BC-1999, Publ. Geophys. Laboratory, University of Thessaloniki, 1, 333pp.

Papazachos, B.C., Comninakis, P.E., Scordilis, E.M., Karakaisis, G.F., Papazachos, C.B.,2010. A catalogue of earthquakes in the Mediterranean and surrounding area for the period 1901-2010,

Publ. Geophys. Laboratory, University of Thessaloniki http://geophysics.geo.auth.gr/ss/station_index_en.html.

Papazachos, B. C., Delibasis, N. D., 1969. Tectonic stress field and seismic faulting in the area of Greece. Tectonophysics, 7, 231-255.

Papazachos, B. C., Koutitas, Ch., Hatzidimitriou P. M., Karakostas, B.M., Papaioannou, Ch. A., 1986. Tsunami hazard in Greece and the surrounding area. Annales Geophysicae, 4, 79-90.

Papazachos, B. C., Papazachou, C., 1989. The Earthquakes of Greece. Ziti Publ., Thessaloniki, 347 pp. (in Greek).

Papazachos, B., Karakostas, V., Kiratzi, A. et al. 2002.Uncertainties in the estimation of earthquake magnitudes in Greece. J. Seismology 6, 557–570, https://doi.org/10.1023/A:1021214126748.

Papazachos, B., Kiratzi, A., Karacostas, B. et al., 1988. Surface fault traces, fault plane solution and spatial distribution of the aftershocks of the September 13, 1986 earthquake of Kalamata (Southern Greece). Pure Appl. Geophys., 126, 55–68, https://doi.org/10.1007/BF00876914

Papazachos, B.C., Papadopoulos, G.A., 1979. Deep tectonic and associated ore deposits in the Aegean area. Proc. 6th. Colloq. Geology Aegean Region, 3, 1071-1080.

Papazachos, B.C., Papazachou, C.B., 1997. Earthquakes of Greece. Editions Ziti, Thessaloniki, 304 pp.

Papazachos, B.C., Papazachou, C.B., 2003. Earthquakes of Greece. Editions Ziti, Thessaloniki, 286 pp. (in Greek).

Papazachos, B.C., Vasilicou, A., 1966. Studies on the magnitude of earthquakes. In: Galanopoulos, A. and Papazachos, B.C. (eds.), Progress Rep. in Seismology & Physics of the Earth's Interior 1964-65, Natl. Obs. Athens, Athens, 17-18.

Papazachos, C., Nolet, G., 1997. P and S deep velocity structure of the Hellenic area obtained by robust nonlinear inversion of travel times, J. Geophys. Res., 102 (B4), 8349-8367, doi:10.1029/96JB03730.

Papazachos, C., Papaioannou, Ch., 1997. The macroseismic field of the Balkan area. J. Seismology, 1, 181-201.

Papazachos, B.C., Kiratzi, A., Karakostas, B., 1997. Toward a homogeneous moment magnitude determination for earthquakes in Greece and the surrounding area. Bull. Seism. Soc. Am., 87, 474-483.

Pararas-Carayannis, G., 1988. Risk assessment of tsunami hazard. In: El-Sabah MI, Murty TS (eds), Natural and man-made hazards. D. Riedel, USA, 183–191.

Paschos, P., Aggelides, Ch., Rontogianni, Th., 1996. Sismi Iouliou-Avgoustou 1996 stin periochi tis Konitsas: macrosismikes kai geotechnikes paratirisis. Technical Report, September 1996, IGME, Athens, 14 pp.

Pavlides, S. B., Zouros, N. C., Chatzipetros, A. A., Kostopoutos, D. S., Mountrakis, D.M., 1995. The 13 May 1995 western Macedonia, Greece (Kozani Grevena) earthquake; preliminary results. Terra Nova 7, 544-549.

Pavlides, S., Papadopoulos, G.A., Ganas, A., 2002. The fault that caused the Athens September 1999 Ms=5.9 earthquake: field observations. Natural Hazards, 27, 61-84

Perrey, A., 1844-1873. Liste de or Note sur les tremblements de terre en (°) avec Suppléments. Long list of publications in C.R. Ac. Sc. Paris, Mém. Acad. Dijon, Bull. Acad. R. Bruxelles, Mém. Acad. R. Sci. Belgique, Annuaire Météorol. De la France, Mém. Cour. Acad. R. Bruxelles.

Perrey, A., 1848. Note sur les tremblements de terre ressentis dans la peninsule Turco-Hellenique et en Syrie. Publ. Academie Royale de Belgique, 73 pp.

Polymenakos, L., 1993. Search for a seasonal trend in earthquake occurrence in the Hellenic Arc. Phys. Earth Plan. Inter., 76, 253-258.

Pomonis, A., 2002. The Mount Parnitha (Athens) Earthquake of September 7, 1999: A Disaster Management Perspective. Natural Hazards, 27, 171-199, https://doi.org/10.1023/A:1019989512220

Pomonis, A., Kappos, A., Karababa, F., Panagopoulos, G., 2009. Seismic Vulnerability and Collapse Probability Assessment of Buildings in Greece. 2nd International Workshop on Disaster Casualties, 15-16 June 2009, University of Cambridge, UK, 18 pp..

Power, W., Wallace, L., Wang, X., Reyners, M., 2012. Tsunami Hazard Posed to New Zealand by the Kermadec and Southern New Hebrides Subduction Margins: An Assessment Based on Plate Boundary Kinematics, Interseismic Coupling, and Historical Seismicity. Pure Appl. Geophys. 169, 1, https://doi.org/10.1007/s00024-011-0299-x.

Qinghai, Z., Adams, W.M., 1988. Tsunami risk analysis for China. Nat Hazards, 1, 181–185. Quaternary International, 173–174, 4-14, https://doi.org/10.1016/j.quaint.2006.10.038.

Rehman, K., Cho, Y.S., 2016. Building Damage Assessment Using Scenario Based Tsunami Numerical Analysis and Fragility Curves. Water, 8, 109, 1-17; doi:10.3390/w8030109.

Reilinger, R., McClusky, S., Paradissis, D., Ergintav, S., Vernant, P. 2010. Geodetic constraints on the tectonic evolution of the Aegean region and strain accumulation along the Hellenic subduction zone. Tectonophysics, 488, 22–30, doi:10.1016/j.tecto. 2009.05.027.

Reilinger, R., McClusky, S., Vernant, Ph., Lawrence, Sh., Ergintav, S., Cakmak, R., Ozener, H., Kadirov, F., Guliev, I., Stepanyan, R., Nadariya, M., Hahubia, G., Mahmoud, S., Sakr, K., ArRajehi, A., Paradissis, D., Al-Aydrus, A., Prilepin, M., Guseva, T., Evren, E., Dmitrotsa, A., Filikov, S. V., Gomez, Fr., Al-Ghazzi, R., Karam, G., 2006. GPS constraints on continental deformation in the Africa-Arabia-Eurasia continental collision zone and implications for the dynamics of plate interactions. J. Geophys. Res., 111, B05411, doi:10.10129/2005JB004051.

Richter, Ch., 1958. Elementary seismology San Francisco: Freeman, 768 pp.

Rikitake, T., Aida, I., 1988. Tsunami hazard probability in Japan. Bull. Seismol. Soc. Am., 78, 1268-1278.

Ross, L.,1852. Reisen nach Kos, Halikarnasos, Rhodos und der Insel Cypern. C. A. Schmetschfe & Sohn, Halle, 216 pp.

Rothé, J.P., 1969. The seismicity of the Earth 1953-1965. UNESCO, 336 pp.
Rotstein, Y., 1985. Tectonics of the Aegean block: rotation, side arc collision on crustal extension. Tectonophysics, 117, 117-137.

Roussos, N., Lyssimachou, T. 1991. Structure of the Central North Aegean Trough: an active strike-slip deformation zone. Basin Research, 3, 39-48.

Sabah, N., Sil, A., 2020. Probabilistic Forecasting of Tsunami Occurrences Across Various Tsunamigenic Zones of the Earth. Pure Appl. Geophys., 177, 2517–2550. https://doi.org/10.1007/s00024-020-02469-1.

Sachpazi, M., Hirn, A., Clément, C., Haslinger, F., Laigle, M., Kissling, E., Charvis, P., Hello, Y. Lépine, J.-C., Sapin, M., Ansorge, J., 2000. Western Hellenic subduction and Cephalonia transform: Local earthquakes and plate transport and strain. Tectonophysics, 319(4), 301-319. https://doi.org/10.1016/S0040-1951(99)00300-5.

Sachpazi, M., Laigle, M., Charalampakis, M., Diaz, J., Kissling, E., Gesret, A., 2016. Segmented Hellenic slab rollback driving Aegean deformation and seismicity. Geophys. Res. Lett., 43, 651–658.

Samardjieva, E., Badal, J., 2002. Estimation of the expected number of casualties caused by strong earthquakes, Bull. Seism. Soc. Am. 92, 2310–2322.

Sato, H., Murakami, H., Kozuki, Y., Yamamoto, N., 2003. Study on a simplified method of tsunami risk assessment. Nat. Hazards, 29, 325-340.

Scawthorn, C., 2011. Disaster casualties-Accounting for economic impacts and diurnal variation. In: R. Spence et al. (eds.), Human casualties in earthquakes, Advances in Natural and Technological Hazards Research, 29, Springer, DOI 10.1007/978-90-481-9455-1_4.

Schmidt, J.F. 1879. Studien über Erdbeben, A.Georgi, Leipzig, 360 pp.

Schoenberg, R., 1997. Constrained Maximum Likelihood. Computational Economics, 10, 251-266, https://doi.org/10.1023/A:1008669208700.

Scordilis, E., 2006. Empirical global relations converting Ms and mb to moment magnitude. J. Seismology, 10, 225-236.

Shaw, B., Jackson, J. 2010. Earthquake mechanisms and active tectonics of the Hellenic subduction zone. Geophys. J. Int., 181, 966-984.

Shebalin, N.V., Kárník V., Hadzievski, D. (Eds), 1974. Catalogue of earthquakes, part II, prior to 1901. UNDP/ UNESCO, Survey of the seismicity of the Balkan region, Skopje, 69 pp.

Shuto, N., 1993. Tsunami intensity and disasters. Advances in Natural and Technological Hazard Research 1, 197-216

Sieberg, A., 1923. Geologische, physicalische und angewandte Erdbebenkunde. Jena, Verlag von G. Fischer.

Sieberg, A., 1927. Geologische einführung in die Geophysik. Jena, Verlag von G. Fischer, 374 pp.

Sieberg, A., 1932. Untersuchungen über Erdbeben und Bruchschollenbau im östlichen Miettelmeersgebiet. Denkschr. Mediz.-Naturwiss. Gesell. Jena, 2, 184-224.

Smit, A., Kijko, A., Stein, A., 2017. Probabilistic Tsunami Hazard Assessment from Incomplete and Uncertain Historical Catalogues with Application to Tsunamigenic Regions in the Pacific Ocean. Pure Appl. Geophys., 174, 3065–3081, https://doi.org/10.1007/s00024-017-1564-4.

Smit, A., Stein, A., Kijko, A., 2019. Bayesian inference in natural hazard analysis for incomplete and uncertain data. Environmetrics, 30:e2566, https://doi.org/10.1002/env.2566.

Smith, K., 1992. Environmental Hazards-Assessing Risk and Reducing Disaster, Routledge, (1st ed.), 324 pp.

So, E., 2014. Introduction to the GEM Earthquake Consequences Database (GEMECD), GEM Technical Report, 2014-14. V1.0.0. 158 P., GEM Foundation, Pavia, Italy. DOI: 10.13117/ GEM.VULN-MOD.TR2014.14, 158 pp.

Sodoudi, F., Kind, R., Hatzfeld, D., Priestley, K., Hanka, W., Wylegalla, K., Stavrakakis, G., Vafidis, A., Harjes, H.-P., Bohnhoff, M., 2006. Lithospheric structure of the Aegean obtained from P and S receiver functions. J. Geophys. Res., 111(B12307), 1-23, doi:10.1029/ 2005JB003932.

Soloviev, S. L., Go, C. N., 1974. Catalog of tsunamis in western coast of the Pacific Ocean. Academy of Sciences, USSR, Izdat. Nauka, 1-130.

Soloviev, S.L., 1970. Recurrence of tsunamis in the Pacific. . In : Adams, W.M., ed. Tsunamis in the Pacific Ocean, Honolulu: East-West Center Press, 149-163.

Sørensen, M.B., Spada, M., Babeyko, A., Wiemer, S., Grünthal, G., 2012. Probabilistic tsunami hazard in the Mediterranean Sea. J. Geophys. Res., 117, B01305, doi:10.1029/2101JB008169.

Spakman, W., Wortel, M. J. R., Vlaar, N. J., 1988. The Hellenic Subduction Zone: A tomographic image and its geodynamic implications. Geophys. Res. Lett., 15 (1), 60-63, https://doi.org/10.1029/GL015i001p00060.

Spence, R., So, E., Jenkins, S., Coburn, A., Ruffle, S., 2011. A global earthquake building damage and casualty database. In: R. Spence et al. (Eds). Human casualties in earthquakes. Advances in Natural and Technological Hazards Research, 29, DOI 10.1007/978-90-481-9455-1_5.

Spyropoulos, P. J., 1997. Chroniko ton Seismon tis Ellados apo tin arcxaiotita mexri simera. Ekdoseis Dodoni, Athens, 453 pp. (in Greek).

Stiros S., Vougioukalakis G., 1996. The 1970, Yali (SE edge of the Aegean volcanic arc) earthquake swarm: surface faulting associated with a small earthquake. Annales Tectonicae, 10:20–30.

Stiros, S., 1995. The 1953 seismic surface fault: Implications for the modeling of the Sousaki (Corinth area, Greece) Geothermal field, J. Geodynamics, 20, 167-180.

Strunz, G., Post, J., Zosseder, K., Wegscheider, S., Mück, M., Riedlinger, T., Mehl, H., Dech, S., Birkmann, J., Gebert, N., Harjono, H., Anwar, H.Z., Khomarudin, R.M., Muhari, A., 2011. Tsunami risk assessment in Indonesia. Nat. Hazards Earth Syst. Sci., 11, 67-82, doi:10.5194/nhess-11-67-2011.

Stucchi, M. et al., 2013. The SHARE European Earthquake Catalogue (SHEEC) 1000–1899. J. Seismology, doi: 10.1007/s10950-012-9335-2.

Suppasri, A., Koshimura, S., Imamura, F., Ruangrassamee, A., Foytong, P., 2013a. A review of tsunami damage assessment methods and building performance in Thailand, J. Earthquake and Tsunami, 7 (5), 1350036.

Suppasri, A., Mas E., Charvet, I., Gunasekera, R., Imai, K., Fukutani, Y., Abe, Y. Imamura, F., 2013b. Building damage characteristics based on surveyed data and fragility curves of the 2011 Great East Japan tsunami. Natural Hazards, 66, 319-341.

Tarbotton, C., Dall'Osso, F., Dominey-Howes, D., Goff, J., 2015. The use of empirical vulnerability functions to assess the response of buildings to tsunami impact: Comparative review and summary of best practice, Earth-Science Reviews, 142, 120-134.

Taxeidis, K., 2003. Study of historical seismicity of the Eastern Aegean Islands, PhD Thesis, National and Kapodistrian University of Athens, 312 pp.

Taymaz, T., Jackson, J., McKenzie, D., 1991. Active tectonics of the north and central Aegean Sea. Geophys. J. Internat., 106 (2), 433–490, https://doi.org/10.1111/j.1365-246X.1991.tb03906.x.

Taymaz, T., Jackson, J., Westaway, R., 1990. Earthquake mechanisms in the Hellenic Trench near Crete. Geophys. J. Internat., 102, 695–731.

Tiedemann, H., 1992. Earthquakes and volcanic eruptions: a handbook on risk assessment. Swiss Reinsurance Company, Zurich, Switzerland, 951 pp.

Tinti S., Armigliato, A., Tonini, R., Maramai, A., Graziani L. 2005. Assessing the hazard related to tsunamis of tectonic origin: A hybrid statistical-deterministic method applied to southern Italy coasts. ISET Journal of Earthquake Technology, 42/4, 189-201.

Tinti S., Bortolucci E., Vannini, C. 1997. A block-based theoretical model suited to gravitational sliding. Nat. Hazards, 16, 1-28.

Tinti, S., Graziani, L., Brizuela, B., Maramai, A., Gallazzi, S., 2012. Applicability of the Decision Matrix of North Eastern Atlantic, Mediterranean and connected seas Tsunami Warning System to

the Italian tsunamis. Nat. Hazards Earth Syst. Sci., 12, 843-857, ,https://doi. org/ 10.5194/nhess-12-843-2012.

Tinti, S., Maramai, A., 1996. Catalogue of tsunamis generated in Italy and in Cote d' Azur, France: a step towards a unified catalogue of tsunamis in Europe. Annali di Geofisica, 39, 1253-1299.

Tonini, R., Armigliato, A., Pagnoni, G., Zaniboni, F., Tinti, S., 2011. Tsunami hazard for the city of Catania, eastern Sicily, Italy, assessed by means of Worst-case Credible Tsunami Scenario Analysis (WCTSA). Nat. Hazards Earth Syst. Sci., 11, 1217-1232, doi:10.5194/nhess-11-1217-2011.

Triantafyllou, I., Gogou, M., Mavroulis, S., Lekkas, E., Papadopoulos, G.A., Thravalos, M., 2021. The Tsunami Caused by the 30 October 2020 Samos (Aegean Sea) Mw7.0 Earthquake: Hydrodynamic Features, Source Properties and Impact Assessment from Post-Event Field Survey and Video Records. J. Mar. Sci. Eng., 9, 68, https://doi.org/10.3390/jmse9010068.

Triantafyllou, I., Novikova, T., Charalampakis, M. et al., 2018. Quantitative Tsunami Risk Assessment in Terms of Building Replacement Cost Based on Tsunami Modelling and GIS Methods: The Case of Crete Isl., Hellenic Arc. Pure Appl. Geophys. 176, 3207–3225, https://doi.org/10.1007/s00024-018-1984-9.

Triantafyllou, I., Papadopoulos, G.A., Lekkas, E., 2020b. Impact on built and natural environment of the strong earthquakes of April 23, 1933, and July 20, 2017, in the southeast Aegean Sea, eastern Mediterranean. Nat Hazards 100, 671–695, https://doi.org/10.1007/s11069-019-03832-9.

Triantafyllou, I., Zaniboni, F., Armigliato, A., Tinti, S., Papadopoulos, G.A., 2020a. The Large Earthquake (~ M7) and Its Associated Tsunami of 8 November 1905 in Mt. Athos, Northern Greece. Pure Appl. Geophys., 177, 1267–1293, https://doi.org/ 10.1007/s00024-019-02363-5.

UNISDR (2009). Terminology on Disaster, Risk Reduction. International Strategy for Disaster Reduction, 35pp., http://www.unisdr.org/eng/library/lib-terminology-eng.htm

Utsu, T., 1990. World catalogue of damaging earthquakes. Tokyo, (in Japanese with Tables in English), 243 pp.

Utsu, T., 2002a. Relationships between magnitude scales. In: W.H.K. Lee et al., International Handbook of Earthquake and Engineering Seismology, Part A, 733-746, Academic Press, Amsterdam.

Utsu, T., 2002b. A list of deadly earthquakes in the World: 1500-2000. In H.K. Lee et al. (eds), International Handbook of Earthquake and Engineering Seismology, IASPEI, Academic Press, Amsterdam, 1, 691-717.

Valencia, N., Gardi, A., Gauraz, A., Leone, F., Guillande, R., 2011. New tsunami damage functions developed in the framework of SCHEMA project: application to European-Mediterranean coasts. Nat. Hazards Earth Syst. Sci., 11, 2835–2846.

Vaněk, J. Zatopek, A., Karnik, V. et al., 1962. Standardization of magnitude scales. Izvest. Akad. Nauk., Ser. Geofiz. (Moscow), 2, 152-158.

Wang, V., Gardoni, P., Murphy, C., Guerrier, S., 2011. Predicting Fatality Rates Due to Earthquakes Accounting for Community Vulnerability. Earthquake Spectra, 35 (2), 513–536, DOI:10.1193/022618EQS046M.

Wegscheider, S., Post, J., Zosseder, K., Mück, M., Strunz, G., Riedlinger, T., Muhari, A. & Anwar, H. Z., 2011. Generating tsunami risk knowledge at community level as a base for planning and implementation of risk reduction strategies. Nat. Hazards Earth Syst. Sci., 11, 249-258, doi:10.5194/nhess-11-249-2011.

Wiemer, S., 2001. A software package to analyze seismicity: ZMAP, Seismol. Res. Lett., 72, 374–383.

Wiemer, S., Wyss, M., 2000. Minimum magnitude of completeness in earthquake catalogs: Examples from Alaska, the Western United States, and Japan. Bull. Seismol. Soc. Am., 90, 859–869.

Wyss, M., A. Hasegawa, S. Wiemer, Umino, N., 1999. Quantitative mapping of precursory seismic quiescence before the 1989, m7.1 off-Sanriku earthquake, Japan. Annali di Geofisica, 42, 851–869.

Wyss, M., Trendafiloski, G., 2009. Trends in the casualty ratio of injured to fatalities in earthquakes, In: 2nd International Workshop on Disaster Casualties, 15-16 June 2009, University of Cambridge, 1-6.

Xinlian, C., 1992. Research on earthquake disasters and countermeasures in China. J. Earthquake Prediction, 1, 127-142.

Yeh, H., Sato, S., Tajima, Y., 2013. The 11 March 2011 East Japan Earthquake and Tsunami: Tsunami Effects on Coastal Infrastructure and Buildings. Pure Appl. Geophys., 170, 1019-1031.

Press Reports consulted

Αθήνα (Athina) 19.10.1843

Πρωινός Κήρυξ (Proinos Kirix) 20.10.1843

Εστία (Estia) 26.02.1926

Appendix

PUBLICATIONS IN THE FRAME OF THIS THESIS

Triantafyllou, I., T. Novikova, A. Fokaefs, M. Charalampakis, G.A. Papadopoulos, 2018. Quantitative tsunami risk assessment in terms of building replacement cost based on tsunami modelling and GIS methods-The case of Crete Isl., Hellenic Arc. Pure & Appl. Geophys.

https://doi.org/10.1007/s00024-018-1984-9.

Triantafyllou, I., Zaniboni, F., Armigliato, A. et al., 2020a. The Large Earthquake (~ M7) and Its Associated Tsunami of 8 November 1905 in Mt. Athos, Northern Greece. Pure Appl. Geophys., 177, 1267-1293.

https://doi.org/10.1007/s00024-019-02363-5.

Triantafyllou, I., G.A. Papadopoulos, E. Lekkas, 2020b. Impact on built and natural environment of the strong earthquakes of April 23, 1933, and July 20, 2017, in the southeast Aegean Sea, eastern Mediterranean. Nat. Hazards, 100, 671–695.

https://doi.org/10.1007/s11069-019-03832-9.

Triantafyllou, I., Gogou, M., Mavroulis, S., Lekkas, E., Papadopoulos, G.A., Thravalos, M., 2021. The Tsunami Caused by the 30 October 2020 Samos (Aegean Sea) Mw7.0 Earthquake: Hydrodynamic Features, Source Properties and Impact Assessment from Post-Event Field Survey and Video Records. J. Mar. Sci. Eng., 9, 68.

https://doi.org/10.3390/jmse9010068.